Acoustically-Responsive Scaffolds: Control of Growth Factor Release for Tissue Regeneration Using Ultrasound

by

Alexander Moncion

A dissertation submitted in partial fulfillment
of the requirements for the degree of
Doctor of Philosophy
(Applied Physics)
in The University of Michigan
2017

Doctoral Committee:

Research Assistant Professor Mario L. Fabiilli, Co-Chair
Professor Andrew J. Putnam, Co-Chair
Professor Charles R. Doering
Professor Renny T. Franceschi
Research Associate Professor Oliver D. Kripfgans

Bondservants, obey in everything those who are your earthly masters, not by way of eye-service, as people-pleasers, but with sincerity of heart, fearing the Lord. Whatever you do, work heartily, as for the Lord and not for men, knowing that from the Lord you will receive the inheritance as your reward. **You are serving the Lord Christ.**

The Holy Bible (ESV), Colossians 3:22-24

Alexander Moncion

ambaez@umich.edu

ORCID iD: 0000-0002-8359-4531

For my parents

ACKNOWLEDGMENTS

Graduate school sets up an interesting relationship between students and their respective research advisor(s). On one hand, these two entities work hand-in-hand to generate knowledge, and on the other is the training component that may one day result in the trainee being the advisor's competition. I am extremely grateful to my doctoral committee Drs. Mario Fabiilli, Andrew Putnam, Oliver Kripfgans, Renny Franceschi, and Charles Doering - for focusing on the generation of knowledge more than the potential of training a future competitor. In particular, my advisor Dr. Fabiilli, is a very special person. Throughout my time as his student, he served many more roles than just a typical research advisor. He provided emotional and moral encouragement during the peak negative times of classwork, scientific writing, and experimentation. He is a master of his craft, who taught me, his apprentice, everything he knew. Most importantly, he served as a role model, someone I look up to and would like to emulate my work ethic after.

There are so many people whom I have met, interacted, and worked with and every one of those people I thank for helping me become the scientist I am today, and thus contributing to this dissertation. On the research side, I've had help, support, and wonderful feedback from Drs. Oliver Kripfgans, Andrew Putnam, Renny Franceschi, Charles Doering, Brian Fowlkes, Douglas Miller, Scott Swanson, Kim Ives, Chunyan Dou, and Xiao Fang Lu. I would like to thank my labmates - Dr. Yiying Zhu, Nneka Richards, Michelle Adan, Rungroj Jintamethasawat, Ben Juliar, Crystal Green, Alex Miller, and Jonah Harmon - for all of the fun times and words of support during our mutual times of struggles. I thank the undergraduate

students - Keith Arlotta, Melissa Lin, Melissa Pilon, Pratik Vadia, Lily Mohr, Eric O'Neill, and Denise Jones - who allowed me to be part of one of their first research experiences. I would also like to extend my gratitude to our wonderful administrative assistants Carol Cribbins, Sharon Karahan, and Sandra Crump for taking care of all the tedious logistical issues that came up. I am extremely thankful to the Applied Physics Program, and the people that make the wheels turn - Dr. Cagliyan Kurdak, Cynthia McNabb, Lauren Seagall, and Charles Sutton - who extended an opportunity for me to attend the University of Michigan and ultimately lead to life changing events. Finally, I would like to thank my family for helping me get through this craziness known as graduate school. I thank my beautiful wife, Ila, who decided to spend the rest of her life with me, and thus put up with all the struggles that came along with having a husband who is a graduate student. I thank my family - Steve, Laura, Collin, and Nikki Myers - who helped keep me grounded, showed endless support and encouragement, as well as served as a model of what is truly important in life. Mostly, I thank my loving parents - Ana and Osvaldo Moncion - who sacrificed so much for me to even have the opportunity to, not only attend graduate school, but immigrate to the United States. I dedicate this dissertation to them.

Although I am wholeheartedly thankful to all of the people I've mentioned above, I am above all thankful to Jesus Christ for always working, and placing those people, in my life. He has blessed me with a wonderful family in Christ, like Dr. Charles and Mrs. Dianne Roeper, who have served as spiritual advisors to me since the Lord placed them in my life. It is in graduate school that I came to know the Lord, and I pray that in the times that are to come I can bring honor and glory to His name through Christ Jesus:

> Each of you should use whatever gift you have received to serve others, as faithful stewards of Gods grace in its various forms. If anyone speaks, they should do so as one who speaks the very words of God. If

anyone serves, they should do so with the strength God provides, so that in all things God may be praised through Jesus Christ. To him be the glory and the power for ever and ever. Amen.[1]

Ann Arbor, Michigan

November 2017

[1]The Holy Bible (NIV), 1 Peter 4:10-13

TABLE OF CONTENTS

LIST OF FIGURES

Figure

LIST OF TABLES

LIST OF APPENDICES

Appendix

ABSTRACT

Administration of exogenous growth factors (GFs) is a proposed method of stimulating tissue regeneration. Conventional administration routes, such as at-site or systemic injections, have yielded problems with efficacy and/or safety, thus hindering the translation of GF-based regenerative techniques. Hydrogel scaffolds are commonly used as biocompatible delivery vehicles for GFs. Yet hydrogels do not afford spatial or temporal control of GF release - two critical parameters for tissue regeneration. Controlled delivery of GFs is critical for angiogenesis, which is a crucial process in tissue engineering that provides oxygen and nutrients to cells within an implanted hydrogel scaffold. Angiogenesis requires multiple GFs that are presented with distinct spatial and temporal profiles. Thus, controlled release of GFs with spatiotemporal modulation would significantly improve tissue regeneration by recapitulating endogenous GF presentation.

In order to achieve this goal, we have developed acoustically-responsive scaffolds (ARSs), which are fibrin hydrogels doped with sonosensitive perfluorocarbon (PFC) emulsions capable of encapsulating various payloads. Focused, mega-Hertz range, ultrasound (US) can modulate the release of a payload non-invasively and in an on-demand manner from ARSs via physical mechanisms termed acoustic droplet vaporization (ADV) and inertial cavitation (IC). This work presents the relationship between the ADV/IC thresholds and various US and hydrogel parameters. These physical mechanisms were used for the controlled release of fluorescent dextran *in*

vitro and *in vivo* to determine the ARS and US parameters that yielded optimal payload release. The optimal ARS and US parameters were used to demonstrate the controlled release of basic fibroblast growth factor from an *in vivo* subcutaneous implant model - leading to enhanced angiogenesis and perfusion. Additionally, different acoustic parameters and PFCs were tested and optimized to demonstrate the controlled release of two encapsulated payloads within an ARS. Overall, ARSs are a promising platform for GF delivery in tissue regeneration applications.

CHAPTER I

Introduction

1.1 The Need for Tissue Engineering

The need and importance of replacement organs is illustrated by the high demand for transplants versus the amount of available donors [1]. The gap widens yearly, as demonstrated by the fact that 28,954 people received transplants in 2013 while 121,272 still awaited them [2]. Tissue engineering aims to restore, maintain, fabricate, and generate viable replacement tissues and organs in order to counteract this trend. The field is driven by the ability of stem cells to differentiate into various specialized types and the recent innovations in fabricating pseudo-tissues [3].

1.1.1 The Approaches to Developing Functional Organs

There are three approaches that have been adopted in developing viable organs: cellular substitution, tissue inducing compounds and substances, and the fabrication of tissue replacing matrices [4]. In recent years, these three strategies have been combined in various ways in order to produce new treatment approaches using hydrogel scaffolds as a foundation [5, 6]. Hydrogel scaffolds are structural materials that can serve as an extracellular matrix (ECM) for cells and a substrate for the encapsulation of biochemical and physiological (i.e., proteins, DNA, drugs, and other macromolecules) stimuli [6]. The goal would be to express these stimuli in such a manner to promote the differentiation of host, or co-encapsulated, cells to the

desired tissue in a manner that mimics the endogenous, spatiotemporally-controlled expression of growth factors (GFs) during tissue regeneration [7]. The control provided by engineered tissue scaffolds, in terms of shape, size, and biochemical components incorporated into the matrix, allows for the fabrication of engineered cartilage, bone, blood vessels, tendons, and bladder among other tissues and organs [8-11].

1.1.2 Why is There a Need for Controlled Release in Time and Space?

Spatiotemporally-controlled release of GF in tissue engineering is desired since during normal (i.e., endogenous) tissue regeneration, GF expression is controlled both spatially and temporally [12, 13]. Angiogenesis, for example, is the formation of new blood vessels and is a very important process in wound healing. Angiogenesis involves the migration, growth, and differentiation of endothelial cells, which line the inside wall of blood vessels, and thus requires multiple GFs (e.g., basic fibroblast growth factor (bFGF), platelet derived growth factor (PDGF-BB), and vascular endothelial growth factor (VEGF)) for vessel formation and subsequent vessel stabilization [12, 13] in a spatially and temporally expressed manner in order to stimulate that migration, growth, and differentiation that is required. Overall, angiogenesis is an important process in tissue engineering, as it is the one of the key mechanisms that must take place in order to ensure oxygen and nutrients can be delivered to tissue implants. Due to the importance and complexity of angiogenesis, in terms of spatiotemporal expression of angiogenic GFs, controlled release of GFs in a tissue implant could greatly improve the efficiency of angiogenesis within the implant. The need for temporal control of GF expression in angiogenesis is further supported by a prior study that demonstrated the improvement that sequential release yielded in angiogenesis [7].

1.1.3 Fibrin Hydrogels, Emulsions, and the Birth of Acoustically-Responsive Scaffolds

Fibrin scaffolds are highly porous hydrogels commonly used in tissue engineering as a substrate for cells and a foundational matrix for tissue fabrication [14-16]. The hydrogel is formed via the enzymatic polymerization of fibrinogen in the presence of thrombin [17]. Fibrin scaffolds have many biological advantages over other hydrogels as fibrin plays a role in natural wound healing, can be derived from a patients own blood for the fabrication of autologous hydrogel scaffolds [18], and is approved by the United States Food and Drug Administration (FDA) as a hemostatic sealant. In addition, being a native protein based scaffold, reabsorption of the hydrogel occurs over time without any inflammatory response. Fibrin scaffolds are typically fabricated in the 5-10 mg/mL fibrin range. This concentration range is on the low-end of the elastic modulus for biomaterials [19] - which also helps promote cellular migration into the scaffold and proliferation from within. In addition to cellular migration, fibrin scaffolds can be seeded with cells as well as other components that aid in tissue engineering. These components may be suspended proteins, drugs, or particles encapsulating drug/protein. However, non-encapsulated compounds exhibit a burst release when dissolved in a conventional fibrin scaffold. Encapsulating particles - such as liposomes, polymeric sphere, or emulsions - can be designed such that release from the particles can be controlled using an externally modulated stimulus - such as light, electricity, magnetic fields, temperature, enzymes, and pH [20-28]. These active scaffolds (i.e., scaffolds that contain stimulus-responsive particles), and means of interacting with them, provide increased control over the biochemical and mechanical environment within the pseudo-tissue. However, previous types of active scaffolds are hindered by clinical translatability due to the inability to focus the triggering stimulus, lack of interaction with deep tissue, and the invasiveness some interactions may require.

1.1.4 Ultrasound Is a Tool That Can be Used to Interact with ARSs

Ultrasound (US), in conjunction with sonosensitive particles, has been studied as a means of interacting with active scaffolds with both spatial and temporal control. US can be applied non-invasively, focused with sub-millimeter precision, and penetrate deep within tissue. US-sensitive fibrin hydrogels can be fabricated by doping them with sonosensitive emulsions, or microbubbles, which have been used clinically for US-based imaging [29, 30]. Sonosensitive emulsions are nano or micron-sized in diameter, and contain a perfluorocarbon (PFC) core while being stabilized by a surfactant shell. In addition, emulsions can be structured such that drugs or proteins, like GFs, are encapsulated within their inner aqueous phase [31-33]. Upon exposure to US, the PFC in the emulsion vaporizes into a gas bubble in a process known as acoustic droplet vaporization (ADV) and can be further enhanced via inertial cavitation [34, 35], thus releasing the encapsulated payload. These US-sensitive hydrogels are termed acoustically-responsive scaffolds (ARSs) and are highly tunable with the ability of modifying the stiffness of the gel, the emulsion formulation, the structure of the emulsion, and the parameters of the US used to interact with the ARS.

Acoustic Droplet Vaporization

ADV occurs when a micron-sized emulsion - such as the perfluorocarbon emulsions previously mentioned - is vaporized due to US exposure. There are various PFCs (i.e., perfluoropentane (C_5F_{12}), perfluorohexane (C_6F_{14}), and perfluoroheptane (C_7F_{16})) that can comprise the PFC component of emulsions, and these class of compounds are inert, hydrophobic, lipophobic, and biocompatible [36]. Post ADV, the vaporization process creates bubbles that are several times bigger than the droplets from which they were generated [37]. The generation of bubbles from ADV has motivated prior work focusing on selectively occluding blood flow to targeted

tissues or organs following the intravascular administration of transcapillary-sized emulsions [37]. However, for our application we will focus on the ability of ADV to vaporize payload containing emulsions in a controlled manner. Another important mechanism that arises from US exposure is acoustic cavitation, which can be defined as the growth and/or collapse of a bubble or cavity within a fluid when the fluid is exposed to an acoustic pressure field [39]. Inertial cavitation (IC), which is a subset of acoustic cavitation, occurs when the bubble diameter grows to at least twice its original diameter, then collapses violently driven by the inertia of the fluid [39]. IC is capable of generating high temperatures, pressures, and velocities that can cause bioeffects. Some of these bioeffects include cellular lysis, molecular degradation, and the formation of free radicals [40, 41]. Within an ARS that contains sonosensitive emulsion, IC occurs at higher pressures than ADV [42], thus payload release is attainable without the bioeffects of IC.

1.1.5 Could ARSs be the Solution for the Need of Controlled Release in Tissue Engineering?

Most hydrogel-based delivery systems do not allow for spatiotemporal control of GF delivery. The tunability of ARSs combined with the spatiotemporal control provided by US yields a tool for the controlled release of the encapsulated payload within the emulsion suspended in the ARS. This could be beneficial in angiogenesis, since this biological process requires spatiotemporal GF expression. The primary goal of a controlled release tool is to deliver a payload with spatiotemporal control in a manner that yields a payload concentration that is not too high to be toxic - or too low to be ineffective - as well as prevent inhibition between GFs as has been demonstrated between bFGF and PDGF-BB [43]. Ideally, a controlled release tool is one that would mimic endogenous angiogenesis. In addition to spatiotemporal control, ARSs can provide control over the amount of payload released by modulating the US exposure time and the concentration of sonosensitive emulsion in the ARS

[29], and have the potential for selective release via custom ARS parameters that respond uniquely to applied US.

1.1.6 What's Ahead?

The work presented in this dissertation looks at four aspects of the ARS and US therapeutic strategy. Chapter 2 looks at how the relationship between the ADV/IC thresholds and various US/hydrogel parameters was determined [42]. Chapter 3 looks at how the physical mechanisms, and the functional relationship between them, were used for the controlled release of Alexa Fluor-labeled dextran *in vitro* and *in vivo* to determine the ARS and US parameters that yielded optimal payload release [44]. In chapter 4, the optimal ARS and US parameters determined via the previously mentioned studies were used to demonstrate the controlled release of bFGF from an *in vivo* subcutaneous implant model [45]. Finally, chapter 5 looks at how different acoustic parameters and PFCs were tested and optimized to demonstrate the controlled release of two encapsulated payloads within an ARS. A preview of these chapters is shown in the following section.

1.2 Characterization of the ARSs-ADV and IC Thresholds

PFC droplets can have a single emulsion structure of PFC-in-water (PFC/W_1) or a double emulsion structure of water-in-PFC-in-water ($W_1/PFC/W_2$). The latter emulsion structure has been used for GF delivery in ARSs with the GF contained within the W_1 phase [29]. PFC emulsions typically contain perfluoropentane (PFP, C_5F_{12}, 29°C boiling point) or perfluorohexane (PFH, C_6F_{14}, 56°C boiling point) as the dispersed phase, are used because of their biocompatibility and inertness, and, for the work presented in Chapter 2, are polydispersed in size. ADV is a non-thermal process initiated by the vaporization of the PFC core of the emulsion by the transmitted US beam [46]. At a typical body temperature of 37°C, larger

diameter PFP droplets are in a superheated state but yet do not vaporize unless perturbed either mechanically, thermally, or chemically. Smaller diameter PFP droplets experience a significant boiling point elevation due to the Laplace pressure. Both superheated and nonsuperheated PFP droplets can vaporize when exposed to US. Upon exposure to US, the decrease in pressure caused by the rarefactional (i.e., expansive) segment of the US wave initiates the vaporization of the PFP and release of the payload contained within the emulsion [47-49]. Another hypothesis behind the vaporization of sonosensitive emulsions is inertial cavitation (IC) in or near the emulsion. In this scenario, a shockwave caused by a cavitating bubble, either generated by ADV or the nucleation of dissolved gas, vaporizes the nearby emulsion [37, 50]. IC has been shown to occur at higher acoustic pressures than ADV [50], and both are dependent on the environment in which the emulsions are dispersed. Thus, ADV (represented in Figure 1) and IC thresholds of ARSs are dependent on acoustic and ARS properties, such as: ARS stiffness, emulsion structure and formulation, and acoustic cycles (i.e., burst length). Thus, controlled release from an ARS is possible since both ADV and IC are threshold-dependent phenomena.

1.2.1 Effects of ADV and IC on Cellular Viability

US capable of generating ADV or IC has the potential to affect the viability of nearby cells. Previously, ADV has been shown to detach nearby adherent cells [51]. However acoustic pressures capable of generating ADV have been shown to have no impact on cellular metabolic activity when encapsulated in an ARS [29]. IC is capable of generating very high temperatures and velocities at the bubble oscillation site, which can ultimately cause bioeffects such as cellular damage and sonoporation [52]. Due to this, IC is capable of reducing the viability of cells co-encapsulated in ARSs when compared to an ARS not exposed to US and an ARS exposed to US that only induces ADV. However, IC has the potential of being a tool for controlled release, and sonoporation, by providing a second acoustically separate mechanism to

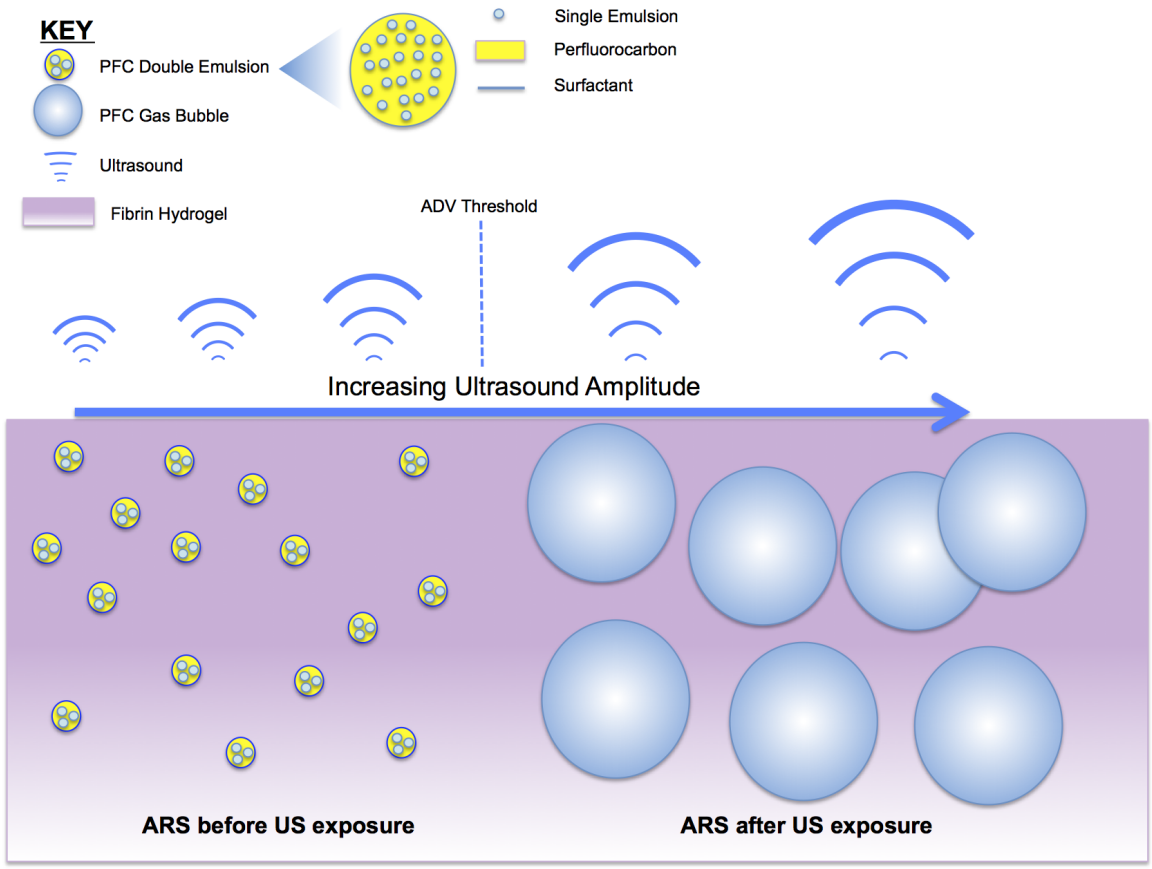

Figure 1.1: Schematic displaying an ARS before and after US exposure. US exposure above the ADV threshold will vaporize the PFC double emulsion into gas bubbles - releasing any payload encapsulated in the emulsion.

ADV for payload release, and therefore important to determine the viability of cells co-encapsulated in an ARS undergoing ADV or IC.

1.2.2 Physical Stability of ARSs

The physical stability of the emulsion in the ARSs is relevant to the stability of the ARS - which is a means of determining how well an ARS can retain it's payload in the absence of US - as a whole and can impact the interaction of US with the ARS itself. Larger PFP droplets are superheated at 37°C and therefore are more prone to spontaneous vaporization and bubble formation due to the decrease in Laplace pressure present with the increase in diameter - thus making the emulsion more sensitive to deformation induced by an applied strain [53]. For spatiotemporally-controlled release of an encapsulated payload within the emulsion, vaporization of the emulsion should occur solely when the ARS is exposed to US; therefore, it is crucial to determine what parameters yield physically stable ARSs with less spontaneous vaporization. ARS stability is crucial for therapies that require prolonged periods of time, like angiogenesis. Thus it is important that ARSs retain their payload in the absence of US.

1.3 Controlled Release of an Encapsulated Surrogate Payload from an ARS

Tissue engineering techniques are highly dependent on the delivery of biochemical and physiological components. Hydrogel scaffolds have been used as a controlled release tool for GFs by means of simply admixing factors within matrices for which they may have some biological affinity and entrapping the GFs within hydrogel networks. Entrapping factors within hydrophobic, degradable polymers that either make up the matrix, binding the GFs to affinity sites that are conjugated to the matrix, or binding the factors directly to the matrix material are also techniques that have been implemented in controlled release [54]. In the prior study, the effects

of ARS stiffness, emulsion structure and formulation, as well as acoustic cycles (i.e. burst length) on the ADV and IC threshold were determined. To maximize the release from ARSs *in vivo*, it is important to determine how these dependencies, as well as the effects of size [35, 55, 56], affect the actual payload release from ARSs. This can be performed more efficiently if done with a surrogate fluorescent payload, like Alexa Fluor 680-labeled dextran - which would allow for the longitudinal and non-invasive monitoring of the *in vivo* release.

1.3.1 Fibrin Degradation

In addition to US-based payload release, payload release from fibrin composites also occurs via endogenous processes such as particle and/or scaffold degradation as well as payload diffusion. Prior work has demonstrated an increase in hydrogel porosity following US exposure [57]. Thus, it is likely that the increased fibrin degradation may also lead to an increase in dextran release caused by changes in the microstructure of the fibrin following US exposure. In order to non-invasively and longitudinally monitor the degradation of the fibrin scaffold *in vivo*, a fluorescent fibrin market (i.e. Alexa Fluor 647-labeled fibrinogen) was used.

1.4 Controlled Release of Growth Factor

GFs have been shown to promote blood vessel formation and restore perfusion in preclinical models of cardiovascular disease [7, 58-61]. However, the clinical use of pro-angiogenic GFs have been disappointing [62-64]. One crucial reason is related to the administration route, dose, and duration of treatment [69-71]. In human studies, basic fibroblast growth factor (bFGF) [62-64] or genes encoding for acidic FGF [72-74], vascular endothelial growth factor (VEGF) [65, 66, 75], or hepatocyte growth factor (HGF) [67, 68] have been administered using intravascular or intramuscular injections. GFs administered using this particular route have short *in vivo* half-lives, slow tissue penetration, and the tendency to cause systemic side

effects (e.g., nephrotoxicity, edema formation) [62, 76].

GF release from the scaffold is dependent on factors such as the growth factor-scaffold affinity as well as the rates of enzymatic and cellular degradation of the scaffold [77]. Scaffold-based GF delivery can extend the *in vivo* half life of the GF [78], localize its actions to the site of implantation [79], and promote cellular processes involved in angiogenesis [80]. Despite these advantages over bolus injections, conventional hydrogels do not enable spatiotemporal control of GF release. In contrast, endogenous growth factors are expressed in spatially- and temporally-regulated patterns during angiogenesis. ARSs can be used for the delivery of payloads such as bFGFs can be controlled non-invasively and in an on-demand manner using focused US [29, 44]. The bFGF was encapsulated in the monodispersed micron-sized, sonosensitive PFC emulsions within the ARSs [37, 46]. Megahertz-range US was used to generate ADV, which causes vaporization of the PFC phase within the emulsion and expulsion of the encapsulated payload [31, 42, 81, 82].

1.4.1 Controlled Release of Multiple Payloads

Controlled release also provides a means of delivering multiple payloads, as described in Figure 1.2, with minimal interaction between them, as well as reducing the amount of payload required for therapeutic effect by localizing the release. For vascularization, both bFGF and PDGF-BB are required for endothelial cellular growth, vessel formation and maturation [58, 59, 83]. However, bFGF and PDGF-BB can inhibit each other if released simultaneously [43, 84]. Therefore, controlled release of bFGF and PDGF-BB with distinct spatiotemporal release profiles could optimize the effect of these GFs on nearby cells. ARSs provide various ways of controlling the release of encapsulated payload and are advantageous over the previously mentioned techniques. Since adjusting fibrin concentration, droplet formulation, and acoustic properties provides means of tuning the acoustic threshold

for vaporization within the ARS, ARSs can be fabricated such that release of the encapsulated payload does not occur in the absence of US; therefore, the benefits of the temporal control of release from ARS is achievable. ARS volume can easily be controlled since the scaffolds can be injected *in vivo* in a liquid state, and thus polymerizing within the host. This makes ARSs versatile in their size as they can be made to any desired volume, which is dependent on the injection site. This coupled with the sub-millimeter focus of mega-Hertz-range US provides great spatial control in the release of encapsulated payload that can be used as gradients to control cell migration and capillary morphogenesis [54, 85].

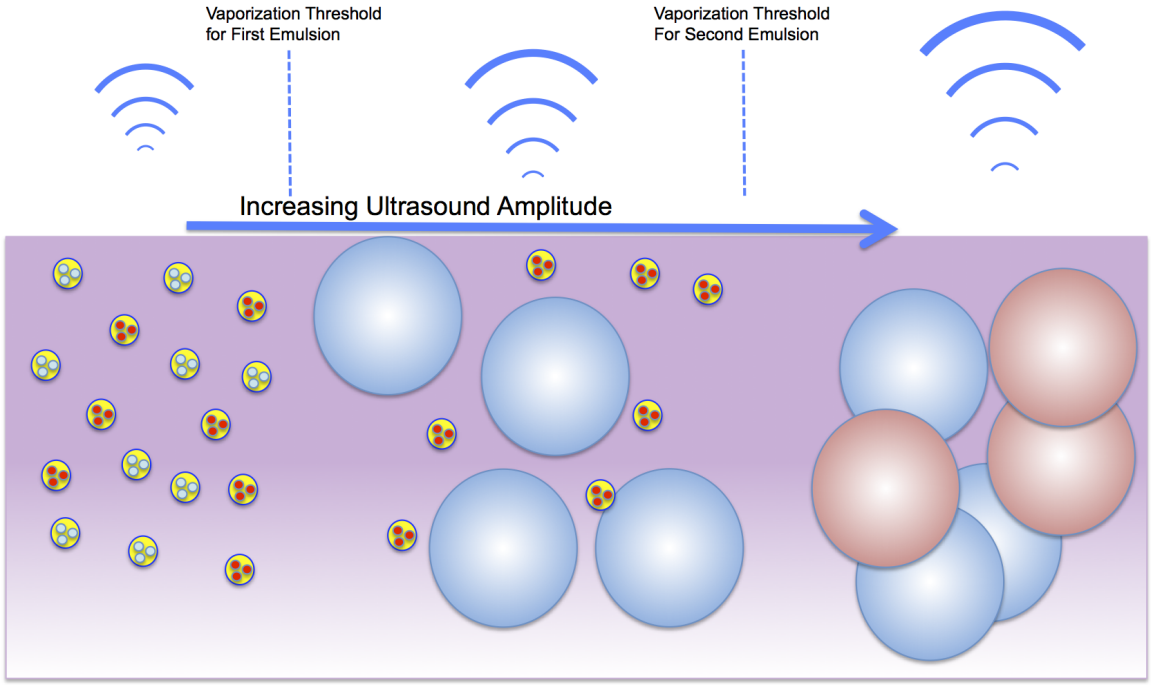

Figure 1.2: Schematic of an ARS doped with two different sonosensitive emulsions containing two different payloads (i.e., payload 1 in blue and payload 2 in red) with unique acoustic thresholds. The emulsions are vaporized independently of each other for controlled release of the encapsulated payloads.

ARSs are capable of holding multiple emulsions with unique vaporization thresholds. Since emulsion thresholds are dependent on the PFC as well as the shell structure, two or more payloads may be incorporated into emulsions with different vaporization thresholds. The two payload holding emulsions can then be vaporized

independently by exposing the dual emulsion holding ARS to low pressure US capable of vaporizing the low threshold emulsion (i.e., blue payload) held within first - shown in Figure 1.2. The second emulsion (i.e., red payload) can then be vaporized, and therefore release the second payload, at a later time point by applying US at a higher pressure than the vaporization threshold of the second emulsion. This can yield the controlled release of two payloads that can be optimized to perform their effects independent of each other.

REFERENCES

[1] Drury, J.L., and Mooney, D.J.: Hydrogels for tissue engineering: scaffold design variables and applications, Biomaterials, 2003, 24, (24), pp. 4337-4351

[2] U.S. Department of Health & Human Services. The Need is Real: Data.

[3] Heath, C.A.: Cells for tissue engineering, Trends in Biotechnology, 2000, 18, (1), pp. 17-19

[4] Langer, R.: Tissue engineering, Molecular therapy : the journal of the American Society of Gene Therapy, 2000, 1, (1), pp. 12-15

[5] Marler, J.J., Upton, J., Langer, R., and Vacanti, J.P.: Transplantation of cells in matrices for tissue regeneration, Advanced Drug Delivery Reviews, 1998, 33, (1-2), pp. 165-182

[6] Thomson, R.C., Wake, M.C., Yaszemski, M.J., and Mikos, A.G.: Biodegradable polymer scaffolds to regenerate organs, Biopolymers Ii, 1995, 122, pp. 245-274

[7] Richardson, T.P., Peters, M.C., Ennett, A.B., and Mooney, D.J.: Polymeric system for dual growth factor delivery, Nat Biotechnol, 2001, 19, (11), pp. 1029-1034

[8] Langer, R., and Vacanti, J.P.: Tissue engineering, Science, 1993, 260, (5110), pp. 920-926

[9] Chamberlain, G., Fox, J., Ashton, B., and Middleton, J.: Concise review: Mesenchymal stem cells: Their phenotype, differentiation capacity, immunological features, and potential for homing, Stem Cells, 2007, 25, (11), pp. 2739-2749

[10] Hutmacher, D.W.: Scaffolds in tissue engineering bone and cartilage, Biomaterials, 2000, 21, (24), pp. 2529-2543

[11] Atala, A., Bauer, S.B., Soker, S., Yoo, J.J., and Retik, A.B.: Tissue-engineered autologous bladders for patients needing cystoplasty, Journal of Urology, 2007, 177, (4), pp. 66-66

[12] Carmeliet, P.: Angiogenesis in life, disease and medicine, Nature, 2005, 438, (7070), pp. 932-936

[13] Risau, W.: Mechanisms of angiogenesis, Nature, 1997, 386, (6626), pp. 671-674

[14] Shaikh, F.M., Callanan, A., Kavanagh, E.G., Burke, P.E., Grace, P.A., and McGloughlin, T.M.: Fibrin: A natural biodegradable scaffold in vascular tissue engineering, Cells Tissues Organs, 2008, 188, (4), pp. 333-346

[15] Dehghani, F., and Annabi, N.: Engineering porous scaffolds using gas-based techniques, Current opinion in biotechnology, 2011, 22, (5), pp. 661-666

[16] Seliktar, D.: Designing Cell-Compatible Hydrogels for Biomedical Applications, Science, 2012, 336, (6085), pp. 1124-1128

[17] Perka, C., Spitzer, R.S., Lindenhayn, K., Sittinger, M., and Schultz, O.: Matrix-mixed culture: New methodology for chondrocyte culture and preparation of cartilage transplants, Journal of Biomedical Materials Research, 2000, 49, (3), pp. 305-311

[18] Lee, K.Y., and Mooney, D.J.: Hydrogels for tissue engineering, Chemical Reviews, 2001, 101, (7), pp. 1869-1879

[19] Markert, C.D., Guo, X.Y., Skardal, A., Wang, Z., Bharadwaj, S., Zhang, Y.Y., Bonin, K., and Guthold, M.: Characterizing the micro-scale elastic modulus of hydrogels for use in regenerative medicine, Journal of the Mechanical Behavior of Biomedical Materials, 2013, 27, pp. 115-127

[20] Matsusaki, M., and Akashi, M.: Novel functional biodegradable polymer IV: pH-Sensitive controlled release of fibroblast growth factor-2 from a poly(gamma-glutamic acid)-sulfonate matrix for tissue engineering, Biomacromolecules, 2005, 6, (6), pp. 3351-3356

[21] Thornton, P.D., McConnell, G., and Ulijn, R.V.: Enzyme responsive polymer hydrogel beads, Chemical Communications, 2005, (47), pp. 5913-5915

[22] Frimpong, R.A., Fraser, S., and Hilt, J.Z.: Synthesis and temperature response analysis of magnetic-hydrogel nanocomposites, Journal of Biomedical Materials Research Part A, 2007, 80A, (1), pp. 1-6

[23] Zhao, X., Kim, J., Cezar, C.A., Huebsch, N., Lee, K., Bouhadir, K., and Mooney, D.J.: Active scaffolds for on-demand drug and cell delivery, Proceedings of the National Academy of Sciences of the United States of America, 2011, 108, (1), pp. 67-72

[24] Kulkarni, R., and Biswanath, S.: Electrically responsive smart hydrogels in drug delivery: a review, Journal of Applied Biomaterials and Biomechanics, 2007, 5, (3), pp. 125-139

[25] Wu, C., Chen, C., Lai, J., Mu, X., Zheng, J., and Zhao, Y.: Molecule-scale controlled-release system based on light-responsive silica nanoparticles, Chemical Communications, 2008, 23, pp. 2662-2664

[26] Lavigne, M.D., Pennadam, S.S., Ellis, J., Yates, L.L., Alexander, C., and Gorecki, D.C.: Enhanced gene expression through temperature profile-induced variations in molecular architecture of thermoresponsive polymer vectors, The Journal of Gene Medicine, 2007, 9, (1), pp. 44-54

[27] Sakiyama-Elbert, S.E., and Hubbell, J.A.: Development of fibrin derivatives for controlled release of heparin-binding growth factors, Journal of Controlled Release, 2000, 65, (3), pp. 389-402

[28] Sakiyama-Elbert, S.E., and Hubbell, J.A.: Controlled release of nerve growth factor from a heparin-containing fibrin-based cell ingrowth matrix, Journal of Controlled Release, 2000, 69, (1), pp. 149-158

[29] Fabiilli, M.L., Wilson, C.G., Padilla, F., Martin-Saavedra, F.M., Fowlkes, J.B., and Franceschi, R.T.: Acoustic droplet-hydrogel composites for spatial and temporal control of growth factor delivery and scaffold stiffness, Acta Biomaterialia, 2013

[30] Epstein-Barash, H., Orbey, G., Polat, B.E., Ewoldt, R.H., Feshitan, J., Langer, R., Borden, M.A., and Kohane, D.S.: A microcomposite hydrogel for repeated on-demand ultrasound-triggered drug delivery, Biomaterials, 2010, 31, (19), pp. 5208-5217

[31] Fabiilli, M.L., Lee, J.A., Kripfgans, O.D., Carson, P.L., and Fowlkes, J.B.: Delivery of water-soluble drugs using acoustically triggered perfluorocarbon double emulsions, Pharmaceutical research, 2010, 27, (12), pp. 2753-2765

[32] Couture, O., Urban, A., Bretagne, A., Martinez, L., Tanter, M., and Tabeling, P.: *In Vivo* targeted delivery of large payloads with an ultrasound clinical scanner, Medical physics, 2012, 39, (8), pp. 5229-5237

[33] Couture, O., Faivre, M., Pannacci, N., Babataheri, A., Servois, V., Tabeling, P., and Tanter, M.: Ultrasound internal tattooing, Medical physics, 2011, 38, (2), pp. 1116-1123

[34] Kripfgans, O.D.: Acoustic droplet vaporization for diagnostic and therapeutic applications, University of Michigan, 2002

[35] Fabiilli, M.L., Haworth, K.J., Fakhri, N.H., Kripfgans, O.D., Carson, P.L., and Fowlkes, J.B.: The Role of Inertial Cavitation in Acoustic Droplet Vaporization, IEEE Transactions on Ultrasonics, Ferroelectrics, and Frequency Control, 2009, 56, (5), pp. 1006-1017

[36] Riess, J.G.: Oxygen Carriers ("Blood Substitutes") - Raison d'Etre, Chemistry, and Some Physiology, Chemical Reviews, 2001, 101, (9), pp. 2797-2919

[37] Kripfgans, O.D., Fowlkes, J.B., Miller, D.L., Eldevik, O.P., and Carson, P.L.: Acoustic droplet vaporization for therapeutic and diagnostic applications, Ultrasound in Medicine and Biology, 2000, 26, (7), pp. 1177-1189

[38] Kripfgans, O.D., Fowlkes, J.B., Woydt, M., Eldevik, O.P., and Carson, P.L.: *In Vivo* Droplet Vaporization for Occlusion Therapy and Phase Aberration Correction, IEEE Transactions on Ultrasonics, Ferroelectrics, and Frequency Control, 2002, 49, (2), pp. 726-738

[39] Neppiras, E.A.: Acoustic Cavitation, Physics Reports, 1980, 61, (3), pp. 159-251

[40] Leighton, T.G.: The Acoustic Bubble (Academic Press Inc., 1994. 1994)

[41] Dalecki, D.: Mechanical Bioeffects of Ultrasound, Annual Review of Biomedical Engineering, 2004, 6, (1), pp. 229-248

[42] Moncion, A., Arlotta, K.J., Kripfgans, O.D., Fowlkes, J.B., Carson, P.L., Putnam, A.J., Franceschi, R.T., and Fabiilli, M.L.: Design and Characterization of Fibrin-Based Acoustically Responsive Scaffolds for Tissue Engineering Applications, Ultrasound in Medicine and Biology, 2016, 42, (1), pp. 257-271

[43] De Marchis, F., Ribatti, D., Giampietri, C., Lentini, A., Faraone, D., Scoccianti, M., Capogrossi, M.C., and Facchiano, A.: Platelet-derived growth factor inhibits basic fibroblast growth factor angiogenic properties *in vitro* and *in vivo* through its alpha receptor, Blood, 2002, 99, (6), pp. 2045-2053

[44] Moncion, A., Arlotta, K.J., O'Neill, E.G., Lin, M., Mohr, L.A., Franceschi, R.T., Kripfgans, O.D., Putnam, A.J., and Fabiilli, M.L.: *In Vitro* and *in vivo* assessment of controlled release and degradation of acoustically responsive scaffolds, Acta Biomaterialia, 2016, 46, pp. 221-233

[45] Moncion, A., Lin, M., O'Neill, E.G., Franceschi, R.T., Kripfgans, O.D., Putnam, A.J., and Fabiilli, M.L.: Controlled release of basic fibroblast growth factor for angiogenesis using acoustically-responsive scaffolds., Biomaterials, 2017, 140, pp. 26-36

[46] Kripfgans, O.D., Fabiilli, M.L., Carson, P.L., and Fowlkes, J.B.: On the acoustic vaporization of micrometer-sized droplets, The Journal of the Acoustical Society of America, 2004, 116, (1), pp. 272-281

[47] Sheeran, P.S., Matsunaga, T.O., and Dayton, P.A.: Phase-transition thresholds and vaporization phenomena for ultrasound phase-change nanoemulsions assessed via high-speed optical microscopy, Physics in Medicine and Biology, 2013, 58, (13), pp. 4513-4534

[48] Li, D.S., Kripfgans, O.D., Fabiilli, M.L., Fowlkes, J.B., and Bull, J.L.: Initial nucleation site formation due to acoustic droplet vaporization, Applied Physics Letters, 2014, 104, (6)

[49] Shpak, O., Stricker, L., Kokhuis, T., Luan, Y., Fowlkes, B., Fabiilli, M., Lohse, D., de Jong, N., and Versluis, M.: Ultrafast dynamics of the acoustic vaporization of phase-change microdroplets, The Journal of the Acoustical Society of America, 2013, 133, (5), pp. 3586

[50] Fabiilli, M.L., Haworth, K.J., Fakhri, N.H., Kripfgans, O.D., Carson, P.L., and Fowlkes, J.B.: The role of inertial cavitation in acoustic droplet vaporization, IEEE Trans Ultrason Ferroelectr Freq Control, 2009, 56, (5), pp. 1006-1017

[51] Ohl, C.D., Arora, M., Ikink, R., de Jong, N., Versluis, M., Delius, M., and Lohse, D.: Sonoporation from jetting cavitation bubbles, Biophysical Journal, 2006, 91, (11), pp. 4285-4295

[52] Ferrara, K.W., Pollard, R., and Borden, M.A.: Ultrasound microbubble contrast agents: fundamentals and application to gene and drug delivery, Annual Review of Biomedical Engineering, 2007, 9, pp. 425-447

[53] Mason, T.G., Bibette, J., and Weitz, D.A.: ELASTICITY OF COMPRESSED EMULSIONS, Physical Review Letters, 1995, 75, (10), pp. 2051-2054

[54] Hubbell, J.: Controlled release strategies in tissue engineering (2008. 2008)

[55] Schad, K.C., and Hynynen, K.: *In Vitro* characterization of perfluorocarbon droplets for focused ultrasound therapy, Physics in Medicine and Biology, 2010, 55, (17), pp. 4933-4947

[56] Sheeran, P.S., Wong, V.P., Luois, S., McFarland, R.J., Ross, W.D., Feingold, S., Matsunaga, T.O., and Dayton, P.A.: Decafluorobutane as a Phase-Change Contrast Agent for Low-Energy Extravascular Ultrasonic Imaging, Ultrasound in Medicine and Biology, 2011, 37, (9), pp. 1518-1530

[57] Cuignet, O.Y., Baele, P.M., and Van Obbergh, L.J.: A second-generation blood substitute (perflubron emulsion) increases the blood solubility of modern volatile anesthetics *in vitro*, Anesthesia and Analgesia, 2002, 95, (2), pp. 368-372

[58] Cao, R.H., Brakenhielm, E., Pawliuk, R., Wariaro, D., Post, M.J., Wahlberg, E., Leboulch, P., and Cao, Y.H.: Angiogenic synergism, vascular stability and improvement of hind-limb ischemia by a combination of PDGF-BB and FGF-2, Nat Med, 2003, 9, (5), pp. 604-613

[59] Li, J., Wei, Y.Q., Liu, K., Yuan, C., Tang, Y.J., Quan, Q.L., Chen, P., Wang, W., Hu, H.Z., and Yang, L.: Synergistic effects of FGF-2 and PDGF-BB on angiogenesis and muscle regeneration in rabbit hindlimb ischemia model, Microvasc Res, 2010, 80, (1), pp. 10-17

[60] Awada, H.K., Johnson, N.R., and Wang, Y.D.: Sequential delivery of angiogenic growth factors improves revascularization and heart function after myocardial infarction, Journal of Controlled Release, 2015, 207, pp. 7-17

[61] Phelps, E.A., Landazuri, N., Thule, P.M., Taylor, W.R., and Garcia, A.J.: Bioartificial matrices for therapeutic vascularization, Proceedings of the National Academy of Sciences of the United States of America, 2010, 107, (8), pp. 3323-3328

[62] Lederman, R.J., Mendelsohn, F.O., Anderson, R.D., Saucedo, J.F., Tenaglia, A.N., Hermiller, J.B., Hillegass, W.B., Rocha-Singh, K., Moon, T.E., Whitehouse, M.J., Annex, B.H., and Investigators, T.: Therapeutic angiogenesis with recombinant fibroblast growth factor-2 for intermittent claudication (the TRAFFIC study): a randomised trial, Lancet, 2002, 359, (9323), pp. 2053-2058

[63] Lazarous, D.F., Unger, E.F., Epstein, S.E., Stine, A., Arevalo, J.L., Chew, E.Y., and Quyyumi, A.A.: Basic fibroblast growth factor in patients with intermittent claudication: Results of a phase I trial, J Am Coll Cardiol, 2000, 36, (4), pp. 1239-1244

[64] Cooper, L.T., Hiatt, W.R., Creager, M.A., Regensteiner, J.G., Casscells, W., Isner, J.M., Cooke, J.P., and Hirsch, A.T.: Proteinuria in a placebo-controlled study of basic fibroblast growth factor for intermittent claudication, Vasc Med, 2001, 6, (4), pp. 235-239

[65] Makinen, K., Manninen, H., Hedman, M., Matsi, P., Mussalo, H., Alhava, E., and Yla-Herttuala, S.: Increased vascularity detected by digital subtraction angiography after VEGF gene transfer to human lower limb artery: a randomized, placebo-controlled, double-blinded phase II study, Molecular therapy : the journal of the American Society of Gene Therapy, 2002, 6, (1), pp. 127-133

[66] Rajagopalan, S., Mohler, E.R., Lederman, R.J., Mendelsohn, F.O., Saucedo, J.F., Goldman, C.K., Blebea, J., Macko, J., Kessler, P.D., Rasmussen, H.S., and Annex, B.H.: Regional angiogenesis with vascular endothelial growth factor in peripheral arterial disease - A phase II randomized, double-blind, controlled study of adenoviral delivery of vascular endothelial growth factor 121 in patients with disabling intermittent claudication, Circulation, 2003, 108, (16), pp. 1933-1938

[67] Powell, R.J., Simons, M., Mendelsohn, F.O., Daniel, G., Henry, T.D., Koga, M., Morishita, R., and Annex, B.H.: Results of a double-blind, placebo-controlled Study to Assess the Safety of Intramuscular Injection of Hepatocyte Growth Factor Plasmid to Improve Limb Perfusion in Patients with Critical Limb Ischemia, Circulation, 2008, 118, (1), pp. 58-65

[68] Morishita, R., Aoki, M., Hashiya, N., Makino, H., Yamasaki, K., Azuma, J., Sawa, Y., Matsuda, H., Kaneda, Y., and Ogihara, T.: Safety evaluation of clinical gene therapy using hepatocyte growth factor to treat peripheral arterial disease, Hypertension, 2004, 44, (2), pp. 203-209

[69] Grochot-Przeczek, A., Dulak, J., and Jozkowicz, A.: Therapeutic angiogenesis for revascularization in peripheral artery disease, Gene, 2013, 525, (2), pp. 220-228

[70] Blatchley, M.R., and Gerecht, S.: Acellular implantable and injectable hydrogels for vascular regeneration, Biomed Mater, 2015, 10, (3)

[71] Briquez, P.S., Clegg, L.E., Martino, M.M., Mac Gabhann, F., and Hubbell, J.A.: Design principles for therapeutic angiogenic materials, Nat Rev Mater, 2016, 1, (1)

[72] Comerota, A.J., Throm, R.C., Miller, K.A., Henry, T., Chronos, N., Laird, J., Sequeira, R., Kent, C.K., Bacchetta, M., Goldman, C., Salenius, J.P., Schmieder, F.A., and Pilsudski, R.: Naked plasmid DNA encoding fibroblast growth factor type I for the treatment of end-stage unreconstructible lower extremity ischemia: Preliminary results of a phase I trial, J Vasc Surg, 2002, 35, (5), pp. 930-936

[73] Nikol, S., Baumgartner, I., Van Belle, E., Diehm, C., Visona, A., Capogrossi, M.C., Ferreira-Maldent, N., Gallino, A., Wyatt, M.G., Wijesinghe, L.D., Fusari, M., Stephan, D., Emmerich, J., Pompilio, G., Vermassen, F., Pham, E., Grek, V., Coleman, M., and Meyer, F.: Therapeutic angiogenesis with intramuscular NV1FGF improves amputation-free survival in patients with critical limb ischemia, Molecular Therapy, 2008, 16, (5), pp. 972-978

[74] Belch, J., Hiatt, W.R., Baumgartner, I., Driver, I.V., Nikol, S., Norgren, L., Van Belle, E., and Investigators, T.C.: Effect of fibroblast growth factor NV1FGF on amputation and death: a randomised placebo-controlled trial of gene therapy in critical limb ischaemia, Lancet, 2011, 377, (9781), pp. 1929-1937

[75] Kusumanto, Y.H., van Weel, V., Mulder, N.H., Smit, A.J., van den Dungen, J.J., Hooymans, J.M., Sluiter, W.J., Tio, R.A., Quax, P.H., Gans, R.O., Dullaart, R.P., and Hospers, G.A.: Treatment with intramuscular vascular endothelial growth factor gene compared with placebo for patients with diabetes mellitus and critical limb ischemia: a double-blind randomized trial, Hum Gene Ther, 2006, 17, (6), pp. 683-691

[76] Baumgartner, I., Pieczek, A., Manor, O., Blair, R., Kearney, M., Walsh, K., and Isner, J.M.: Constitutive expression of phVEGF165 after intramuscular gene transfer promotes collateral vessel development in patients with critical limb ischemia, Circulation, 1998, 97, (12), pp. 1114-1123

[77] Lei, P., Padmashali, R.M., and Andreadis, S.T.: Cell-controlled and spatially arrayed gene delivery from fibrin hydrogels, Biomaterials, 2009, 30, (22), pp. 3790-3799

[78] Yang, H.S., Bhang, S.H., Hwang, J.W., Kim, D.I., and Kim, B.S.: Delivery of Basic Fibroblast Growth Factor Using Heparin-Conjugated Fibrin for Therapeutic Angiogenesis, Tissue Eng Pt A, 2010, 16, (6), pp. 2113-2119

[79] Losi, P., Briganti, E., Errico, C., Lisella, A., Sanguinetti, E., Chiellini, F., and Soldani, G.: Fibrin-based scaffold incorporating VEGF- and bFGF-loaded nanoparticles stimulates wound healing in diabetic mice, Acta Biomaterialia, 2013, 9, (8), pp. 7814-7821

[80] Kniazeva, E., Kachgal, S., and Putnam, A.J.: Effects of Extracellular Matrix Density and Mesenchymal Stem Cells on Neovascularization *In Vivo*, Tissue Eng Pt A, 2011, 17, (7-8), pp. 905-914

[81] Fabiilli, M.L., Haworth, K.J., Sebastian, I.E., Kripfgans, O.D., Carson, P.L., and Fowlkes, J.B.: Delivery of chlorambucil using an acoustically-triggered perfluoropentane emulsion, Ultrasound in Medicine and Biology, 2010, 36, (8), pp. 1364-1375

[82] Fabiilli, M.L., Lee, J.A., Kripfgans, O.D., Carson, P.L., and Fowlkes, J.B.: The release of thrombin, using acoustic droplet vaporization (ADV), from perfluoropentane double emulsions, IEEE International Ultrasonics Symposium, 2010

[83] Saik, J.E., Gould, D.J., Watkins, E.M., Dickinson, M.E., and West, J.L.: Covalently immobilized platelet-derived growth factor-BB promotes antiogenesis in biomirnetic poly(ethylene glycol) hydrogels, Acta Biomaterialia, 2011, 7, (1), pp. 133-143

[84] Tengood, J.E., Ridenour, R., Brodsky, R., Russell, A.J., and Little, S.R.: Sequential Delivery of Basic Fibroblast Growth Factor and Platelet-Derived Growth Factor for Angiogenesis, Tissue Eng Pt A, 2011, 17, (9-10), pp. 1181-1189

[85] Helm, C.L.E., Fleury, M.E., Zisch, A.H., Boschetti, F., and Swartz, M.A.: Synergy between interstitial flow and VEGF directs capillary morphogenesis *in vitro* through a gradient amplification mechanism, Proceedings of the National Academy of Sciences of the United States of America, 2005, 102, (44), pp. 15779-15784

CHAPTER II

Design and Characterization of Fibrin-Based Acoustically Responsive Scaffolds for Tissue Engineering Applications

2.1 Introduction

Fibrin scaffolds are highly porous, protein-based hydrogels frequently used in regenerative medicine as a substrate for cells and for encapsulation of proteins such as growth factors (GFs) [1–3]. Similar to other hydrogels, the release of a bioactive molecule (i.e., payload) from a conventional fibrin scaffold as well as degradation of the scaffold are dominated by processes such as molecular diffusion, material degradation, and cell migration. Thus the rate that biochemical (e.g., GFs) or mechanical (e.g., microporosity) cues are presented in a conventional fibrin scaffold cannot be externally controlled spatially or temporally, especially after the scaffold is implanted *in vivo*. It is well documented that spatial and temporal patterns of GF signaling are critically important in regenerative processes [4; 5]; additionally, cellular processes are influenced by the mechanical properties of the local scaffold microenvironment [6–10]. Alternatively, scaffolds have been designed to respond to environmental or externally applied stimuli - such as light, electricity, magnetic fields, temperature, enzymes, and pH in order to obtain spatiotemporal control of payload release or to modify scaffold architecture after implantation [11–19]. Despite their promising potential in controlling both biochemical and mechanical

cues, further development of responsive scaffolds is limited in part by the clinical translatability of the modulating stimulus, especially in terms of focusing the stimulus or targeting deeply located scaffolds. Ultrasound (US) has been explored as a stimulus for achieving spatial and temporal control with responsive scaffolds due to its potential for translatability. Unlike other stimuli, US can be applied non-invasively, focused with submillimeter precision, and penetrate deep within the body. Broadly, US can be used to generate mechanical and/or thermal effects within a scaffold to achieve on-demand control. In many instances, US-responsive scaffolds contain sonosensitive particles such as emulsions or microbubbles, thus making the scaffold more responsive to US [20; 21]. However, it has been demonstrated using low frequency US that payload release can be modulated from scaffolds in the absence of sonosensitive particles [22]. Sonosensitive particles are usually administered intravascularly for US-based imaging or therapy, with microbubbles used clinically as US contrast agents. These particles are typically micron-size in diameter, contain a perfluorocarbon (PFC) dispersed (i.e., core) phase, and are stabilized by a surfactant shell. Microbubbles, which contain a gaseous PFC core, have been used to indirectly facilitate payload delivery from an in situ cross-linking hydrogel containing liposomes co-encapsulated with the microbubbles [21]. In the absence of US, microbubbles have also been used to create on-demand, microporous agarose hydrogels [23] or to simultaneously act as a porogen and GF carrier within poly(lactic-co-glycolic-acid) scaffolds [24].

The presented studies build upon previous work where we demonstrated the utility of fibrin scaffolds doped with sonosensitive PFC emulsions, termed here acoustically responsive scaffolds (ARSs). US was used to modulate GF release from the ARS as well as induce drastic changes in architecture and shear stiffness of the ARS [20]. Fibrin was chosen as the hydrogel in the ARS due to its widespread use within the field of tissue engineering as a delivery system for GFs, cells, drugs,

and genes [25]. Sonosensitive PFC emulsions, with single or double structures, have been used as on-demand contrast agents and delivery vehicles for bioactive payloads, respectively [20; 26–29]. The PFC within these emulsions transitions from a liquid into a gas when the emulsion is exposed to US above a specific acoustic amplitude. This phase transition is termed acoustic droplet vaporization (ADV) [30] and occurs in a microsecond time frame [31; 32]. PFCs such as perfluoropentane (PFP, C_5F_{12}, 29°C boiling point) and perfluorohexane (PFH, C_6F_{14}, 56°C boiling point) are typically used in sonosensitive emulsions because of their biocompatibility and inertness. The emulsification process (i.e., formation of droplets) prevents low boiling point PFCs, like PFP, from vaporizing at homeostatic body temperature (37°C) due to an increase in Laplace pressure, which causes an elevation of the PFC boiling point within the droplets [33; 34]. Sonosensitive emulsions can possess both single and double emulsion structures. With single emulsions of the form PFC-in-water (PFC/W), the PFC is dispersed within an aqueous continuous phase. For delivery of payloads such as GFs, a secondary dispersed phase is added since PFCs are extremely hydrophobic and lipophobic. Thus double emulsions of the form water-in-PFC-in-water (W_1/PFC/W_2) have been used for GF delivery in ARSs whereby the GF is contained within the W_1 phase [20].

For responsive scaffolds, the physicochemical properties of the scaffold are related to the manner in which the scaffold will respond to a stimulus. Conversely, the properties of the stimulus (e.g., intensity, duration, or directionality) impact the response of the scaffold. Thus, elucidating the mechanisms that occur when an ARS is exposed to US is critical in not only achieving optimal payload release from the scaffold, but also relevant for facilitating regenerative processes that could occur within or adjacent to the ARS. In addition to ADV, inertial cavitation (IC) has been observed when sonosensitive emulsions undergo a phase shift [31]. IC can occur when a bubble, either generated by ADV or the nucleation of dissolved gas, rapidly

expands and collapses due to US exposure. This violent behavior by the bubble can generate very high temperatures and velocities at the bubble site, which can ultimately cause bioeffects such as cellular damage and sonoporation [36].

The presented *in vitro* work on a fibrin-based ARS is divided into three main parts. First, the ADV and IC thresholds were measured for ARSs of varying composition. Parameters such as fibrin density, emulsion formulation (including stabilizing shell, PFC core, and emulsion structure), and acoustic cycles were explored. Second, the viability of cells encapsulated in the ARS was evaluated across the different regimes of ADV and IC. Third, the physical stabilities of the ARSs, including non-selective (i.e., without US exposure) release profiles, were measured over the course of 7 days.

2.2 Materials and Methods

2.2.1 Single Emulsion Preparation and Characterization

Four different formulations of single emulsions (PFC/W) were made by combining 25% (v/v) PFP (CAS#: 678-26-2, Strem Chemicals, Newburyport, MA USA) or PFH (CAS#: 355-42-0, Strem Chemicals) and 75% (v/v) of an aqueous emulsifying agent. The aqueous phase consisted of either a lipid blend of 6.67 mg/mL 1,2-dipalmitoyl-sn-glycero-3-phosphocholine (DPPC, CAS#: 63-89-8 Avanti Polar Lipids, Inc., Alabaster, AL USA) and 0.27 mg/mL 1,2-dipalmitoyl-sn-glycero-3-phosphate monosodium salt (DPPA, CAS#: 169051-60-9, Avanti Polar Lipids, Inc) dissolved in a solution of propylene glycol (CAS#: 57-55-6, Sigma-Aldrich, St. Louis, MO USA), normal saline (Baxter Healthcare, Deerfield, IL USA), and glycerol (CAS#: 56-81-5, Sigma-Aldrich); 4 mg/mL bovine serum albumin (BSA) (CAS#: 9048-46-8, Sigma-Aldrich) dissolved in Dulbeccos phosphate buffered saline (DPBS, Life Technologies, Grand Island, NY USA); or 4 mg/mL Pluronic F68 (CAS#: 9003-11-6, Sigma-Aldrich) dissolved in DPBS. The fluids were shaken with

an amalgamator (Wig-L-Bug, Sigma-Aldrich) at 4800 rpm for 90 seconds [35]. The resulting emulsions were stored at 5°C for 30 minutes and then subsequently washed with normal saline to remove excess emulsifier. The emulsions were characterized with a Coulter Counter (Multisizer 4, Beckman Coulter, Inc., Indianapolis, IN USA) in the range of 1-30 μm. All single emulsion formulations are listed in Table 1.1.

2.2.2 Double Emulsion Preparation and Characterization

Double emulsions (W_1/PFC/W_2) were prepared with PFP or PFH as the PFC phase by modifying a previous method (Fabiilli et al. 2010). A triblock fluorosurfactant, consisting of Krytox 157FSH (CAS# 51798-33-5, DuPont, Wilmington, DE, USA) and polyoxyethylene glycol (MW: 1000, CAS#: 24991-53-5, Alfa Aeser, Ward Hill, MA USA), was dissolved in 1g of PFC at 2% (w/w). The PFC solution was then combined with an aqueous solution of fluorescein sodium salt (FSS, CAS#: 518-47-8, Sigma-Aldrich), reconstituted at 1 mg/mL in DPBS, in a volumetric ratio of 2.1:1. The phases were sonicated (CL-188, QSonica, LLC, Newton, CT USA) for 30 seconds while on ice. The resulting primary emulsion (W_1/PFC) was added drop wise to a solution of 50 mg/mL Pluronic F68 in DPBS and stirred with a magnetic stir bar at 700 rpm for 2 minutes while on ice. The particle size of the resulting coarse double emulsion (W_1/PFC/W_2) was reduced using a homogenizer (T10, IKA Works Inc., Wilmington, NC USA). The resulting emulsion had a FSS encapsulation efficiency of 89.7% and 92.3% for the PFP and PFH formulations, respectively. Emulsions were stored at 5C for 30 minutes and characterized with a Coulter Counter in the range of 1-30 μm. All double emulsion formulations are listed in Table 1.1.

2.2.3 ARS Fabrication

ARSs were prepared using 3, 5, or 10 mg/mL clottable protein by first combining bovine fibrinogen (Sigma-Aldrich), dissolved in degassed (40% O2 saturation)

Table 2.1: Structure and composition of emulsions used to dope the acoustically responsive scaffolds.

Structure	PFC	Shell	Mean Diameter (μm)	Droplet Concentration (#/mL)	Percentage > 6 μm
Single	PFP	Lipid	2.34 ± 0.08	6.27E+09 ± 1.84E+09	5.99 ± 1.93
Single	PFH	Lipid	2.27 ± 0.04	6.54E+09 ± 1.56E+09	5.78 ± 1.23
Single	PFH	BSA	1.60 ± 0.01	1.98E+10 ± 2.41E+09	1.02 ± 0.05
Single	PFH	Pluronic F68	2.12 ± 0.14	1.03E+10 ± 2.99E+09	1.25 ± 0.18
Double	PFP	Fluorosurfactant/Pluronic F68	4.95 ± 0.59	5.15E+08 ± 9.67E+07	27.99 ± 2.98
Double	PFH	Fluorosurfactant/Pluronic F68	4.00 ± 0.22	9.90E+08 ± 3.17E+08	13.03 ± 3.72

Dulbeccos modified Eagles medium (DMEM, Life Technologies), with bovine thrombin (2 U/mL, Thrombin-JMI, King Pharmaceuticals, Bristol, TN, USA), and 1% (v/v) emulsion. The mixture was injected into an OptiCell (Thermo Fisher Scientific Inc., Waltham, MA USA) and allowed to polymerize for 30 min at room temperature. Hydrogels without emulsions were prepared as a sham condition.

2.2.4 Ultrasound Exposure

OptiCells containing the ARSs were fixed vertically in a tank of degassed water (30-36% O_2 saturation) at 37°C, as shown in Figure 2.1A. A calibrated, single element US transducer (2.5 MHz, H108, Sonic Concepts, Inc., Bothell, WA USA) was positioned such that the focus of the transducer was located equidistant from the OptiCell windows, which are 75 μm thick and spaced 2 mm apart. This single element transducer (f-number = 0.83, focal length = 50 mm) was used to generate ADV and IC within the ARS. The ARS was exposed to 100 pulses of US that were 3, 6, or 13 acoustic cycles in length with a pulse repetition frequency (PRF) of 10 Hz and amplitudes ranging from 0.8 - 8 MPa peak rarefactional pressure. Waveforms were generated using a dual channel function generator (33500B, Agilent Technologies, Santa Clara, CA USA) and amplified by a gated radio frequency (RF) amplifier (GA-2500A Ritec Inc, Warwick, RI USA). Gating was realized using the second channel of the function generator. During exposure, broadband noise indicative of IC [37; 38] - was detected by a calibrated hydrophone (1-50 MHz, Onda Corporation, Sunnyvale, CA USA) that was coupled to the single element

transducer and positioned 6 cm from the OptiCell. Hydrophone waveforms were digitized by an oscilloscope (HDO4034, Teledyne Lecroy, Chestnut Ridge, NY USA) at a sampling rate of 100 MHz. In order to detect bubble formation, B-mode US images were acquired before and after exposures from the single element transducer using a clinical US scanner (10 MHz US linear imaging array, 10L, GE Vivid 7, GE Healthcare, Waukesha, WI USA). To prevent the linear US array from generating ADV and/or IC within the ARS, a mechanical index (MI) of 0.03 was used, which is significantly lower than the MI required to cause cavitation [39]. It was confirmed that this low MI caused no increase in echogenicity, and hence no ADV, in the ARS. Each acoustic exposure was spatially separated within the OptiCell.

All acoustic data (i.e., B-mode images and hydrophone data) were analyzed in MATLAB (The Mathworks Inc., Natick, MA USA). The B-mode images, before and after US exposure from the single element transducer, were subtracted and the mean echo power (MEP) was calculated for the subtracted image as done previously [35]. The ADV threshold was defined as P_n, where P_n was the first acoustic pressure that satisfied Equation 1.1,

$$MEP_n > (\sum_{i=1}^{n-1} MEP_i)/(n-1) + 3\sigma \tag{2.1}$$

where MEP_n was the MEP of the nth pressure exposure, MEP_i was the MEP of the ith pressure exposure, and σ was the standard deviation of MEP_1, MEP_2, MEP_3,...MEP_{n-1}. At each acoustic exposure condition, the RF signals collected using the hydrophone consisted of 100 segments, one for each of the 100 pulses fired by the single element transducer. A Hanning window was applied to each segment to time gate physical window reflections from the OptiCell and the direct path transmit signal from the single element transducer. Then the fast Fourier transform (FFT) of each segment was computed. Fundamental as well as second and third harmonics of the transmit US frequency were filtered out by excluding spectral amplitudes that

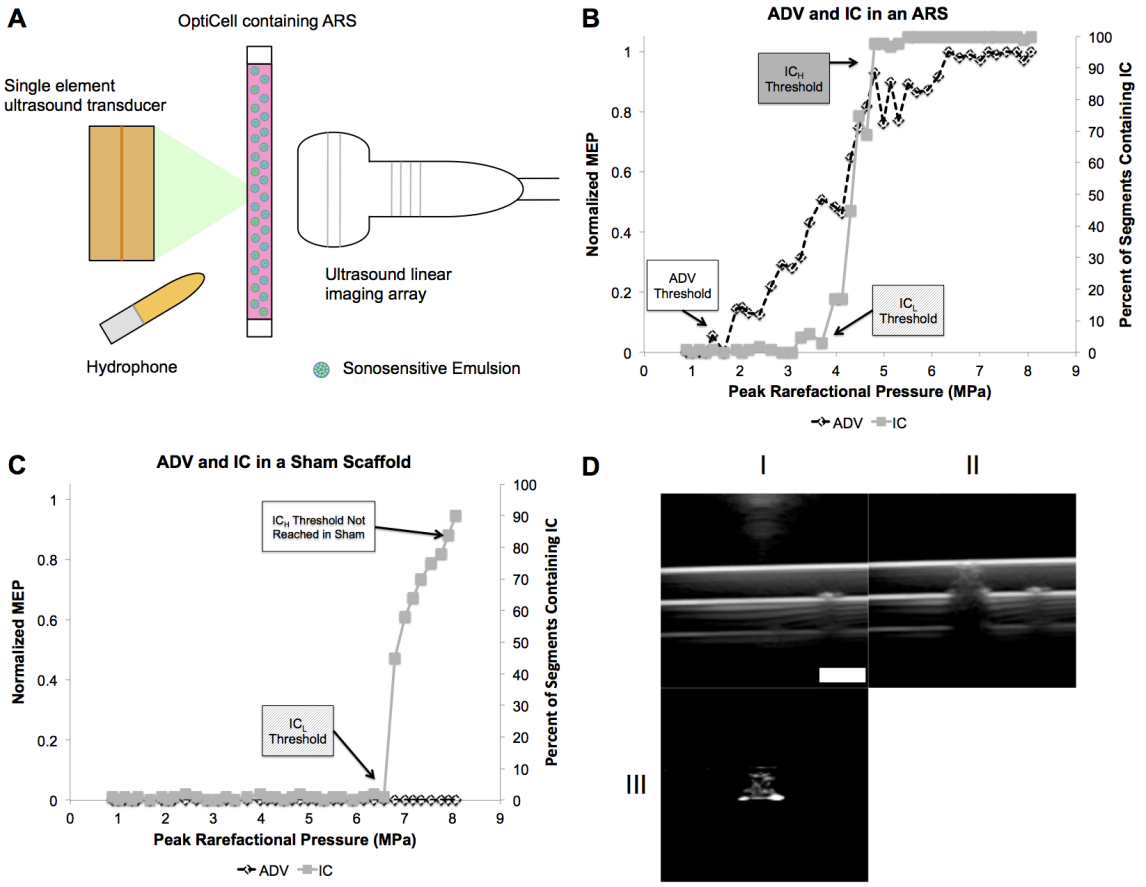

Figure 2.1: (A) Experimental setup used to expose ARSs to US. Representative plots showcasing the behavior of ADV, measured via enhanced brightness in the B-mode US images (i.e., MEP), and IC, measured via enhanced broadband noise, for an ARS (B) and a sham scaffold (C, without droplets). The ADV and IC_L thresholds were defined as the first acoustic pressure data point that met the criteria in Equations 1 and 2, respectively. The threshold for persistent cavitation, IC_H, was defined as the first acoustic pressure data point where all 100 segments contained at least one IC event. For the sham scaffold (C), there was no detectable ADV since there were no droplets and also no enhanced brightness due to persistent bubbles generated by IC. Additionally, IC_L occurred at a higher acoustic pressure relative to the ARS with the same fibrin concentration. IC_H was not measured in the sham scaffold across the range of acoustic pressures interrogated in this work (i.e., 0 8.07 MPa). B-mode US images of the cross-section of an Opticell containing an ARS (D). Images were taken before (DI) and after (DII) the ARS was exposed to high amplitude acoustic pulses generated by the single element US transducer. The subtracted image of DII DI (DIII) clearly shows the bubbles generated by ADV in the ARS, which was used for ADV threshold analysis (i.e., MEP). Scale bar = 2 mm.

were within 3 dB with respect to the maximum amplitude at each harmonic. The integrated power spectrum was then calculated across the entire detected frequency range (1-50 MHz) although the majority of the signal was in the 1-10 MHz range and then compared to the mean (across all segments) of the integrated FFT of the sham condition (i.e., an ARS without emulsion). Two thresholds related to IC were then calculated. First, the *initiation* of inertial cavitation (IC_L) was defined as the first pressure for which at least one of the 100 segments contained an IC event, which is defined in Equation 1.2,

$$S_n(P_{i,ARS}) > \sum_{n}^{N} S_n(P_{i,sham})/N + 3\sigma \tag{2.2}$$

where $S_n(P_{i,ARS})$ is the nth segment in the sequence $P_{i,ARS}$ for an ARS exposed to pressure P_i, $S_n(P_{i,sham})$ is the nth segment in the sequence $P_{i,sham}$ for a sham exposed to pressure P_i, N is the total number of segments, and σ is the standard deviation of the mean of the sham. Second, persistent cavitation (IC_H) was defined as the first pressure at which an IC event was detected in all 100 segments, and thus each segment passed the criterion in Equation 1.2.

2.2.5 Ultrasound Exposure

ARSs were prepared as previously described except that 5.0×10^4 cells/mL of the mouse multipotent line C3H10T1/2, clone 8 (CCL-226, ATCC, Manassas, VA, USA) were encapsulated along with 1% (v/v) PFP double emulsion in 5 mg/mL fibrin. Prior to casting the ARS, OptiCell windows were blocked with a 10 mg/mL solution of BSA. The acoustic exposures (13 cycles and 10 Hz PRF) were completed as previously described except that the single element transducer was rastered across the OptiCell in a paintbrush format to create large regions exposed to the same acoustic condition (rather than a single point as section 2.4). Immediately after US exposure, the ARS was biopsied with an 8 mm biopsy punch (Miltex, Plainsboro, NJ

USA) and each biopsied sample was placed in 0.05% trypsin-EDTA (Gibco, Grand Island, NY USA) to degrade the hydrogel. Following complete degradation of the ARS sample, the remaining cells were isolated via centrifugation, resuspended in DMEM, and then stained with 16.2 μM Hoechst 33342 (Invitrogen, Grand Island, NY USA), 5 μM calcein AM (Live stain, Invitrogen), and 15 μM propidium iodide (PI, Dead stain, Invitrogen). The labeled cells were imaged with a Leica DM IL microscope (Leica Microsystems Inc., Buffalo Groove, IL USA) using a 10x objective.

2.2.6 Physical Stability of ARSs

For stability studies, 0.5 mL ARSs were cast in 24 well plates (Corning Life Sciences, Tewksbury, MA USA) with 1% (v/v) emulsion either single or double and 5 mg/mL fibrin. Double emulsions contained 1 mg/mL FSS in the W1 phase. After polymerization at room temperature, each ARS was covered with DMEM and placed in a standard tissue culture incubator at 37°C. At each time point, the overlying media was removed and the ARS was degraded with 0.05% trypsin-EDTA. Following complete degradation of the ARS, the resulting sample was centrifuged and the remaining emulsion was sized using a Coulter Counter as previously described. It was experimentally confirmed that incubation of the emulsion in trypsin did not alter the size distribution or number density of the emulsion. For studies with double emulsions, the concentration of FSS in the overlying media was determined using a plate reader (Molecular Devices Spectramax M2e, Sunnyvale, CA USA, 494 nm EX/ 521 nm EM). Measurements were taken twice on the first day at t = 0 h and t = 2 h, then every 24 h from t = 0 h for 144 h. The stability of the emulsions, not contained within ARSs, was also measured using aforementioned methods. Light microscopy (10x objective, Leica DM IL) images of ARSs containing single PFP and PFH emulsions were taken at t = 0 and t = 72 h to depict differences in physical stability.

2.2.7 Statistics

The data are expressed as the mean ± standard deviation of measured quantities. All n-values are listed below each corresponding figure. The TukeyKramer method, evaluated in MATLAB, was used to determine statistically significant differences between multiple groups for acoustic data (i.e., ADV and IC thresholds), with differences deemed significant for $p < 0.05$. The 95% confidence interval of slopes is listed in the following format: S [S_L, S_H], where S is the slope, S_L is the lower bound slope and S_H is the upper bound slope). Statistically significant differences of all other data sets were determined with a Students t-test with differences deemed significant for $p < 0.05$.

2.3 Results

2.3.1 Characterization of Emulsions

Table 1.1 displays the sizing characteristics of the single and double emulsions used in the ARSs. For lipid shell single emulsions, no statistical differences in the mean diameter, droplet concentration, and number percent greater than 6 μm were observed between PFP and PFH emulsions. However, a smaller mean diameter, larger droplet concentration, and a smaller number percent greater than 6 μm were measured when the single PFH emulsions were stabilized with BSA or Pluronic F68 versus lipid. Double emulsion droplets were larger than single emulsions. Additionally, no differences in mean diameter were observed between double emulsions made with PFP and PFH, however PFP double emulsions had a smaller droplet concentration and larger percentage of droplets greater than 6 μm than PFH double emulsions.

2.3.2 ADV and IC Thresholds

Figure 2.1B-C display the characteristic trends in ADV and IC of ARSs and sham fibrin scaffolds. At low acoustic pressures, neither bubbles (i.e., ADV) nor IC was detected in the ARS or the sham. As the acoustic pressure was increased, the ADV threshold was reached and the droplets in the ARS started to vaporize, generating echogenic bubbles that increased the MEP in the recorded B-mode images (Figure 2.1D). Thus, any acoustic pressure greater than the ADV threshold triggered ADV. A further increase in the acoustic pressure caused the first detectable IC event (i.e., the IC_L threshold), where both IC and ADV occurred. Eventually, at an acoustic pressure higher than the IC_L threshold, persistent IC was detected (i.e., all recorded segments contained at least one IC event). This pressure was the ICH threshold for an ARS. The acoustic pressure range where IC_H occurred also contained ADV due to detectable bubble formation with B-mode imaging. Sham scaffolds (i.e., fibrin scaffolds without emulsion) did not display an ADV threshold and IC_L occurred at a higher acoustic pressure than the IC_L threshold of an ARS with the same fibrin concentration and exposed to the same number of acoustic cycles. Furthermore IC_H was not detected in any of the sham scaffolds - containing 3, 5, or 10 mg/mL fibrin. Figure 2.1D shows a B-mode image of an OptiCell containing an ARS. Figure 2.1D-I and Figure 2.1D-II shows the ARS before and after US exposure from the single element transducer, respectively. The change in echogenicity (i.e., brightness) post US exposure can be observed, and Figure 2.1D-III shows an image subtraction of Figure 2.1C-I and 1C-II displaying clear persistent bubble formation and the appearance of the back OptiCell window produced by its shadowing in Figure 2.1D-II due to the bubble production.

The ADV, IC_L and IC_H ($IC_{L/H}$) thresholds for an ARS with 5 mg/mL fibrin and doped with varying single emulsion cores (PFP vs. PFH) stabilized by a lipid shell were quantified (Figure 2.2A). Qualitatively, all thresholds tended to decrease

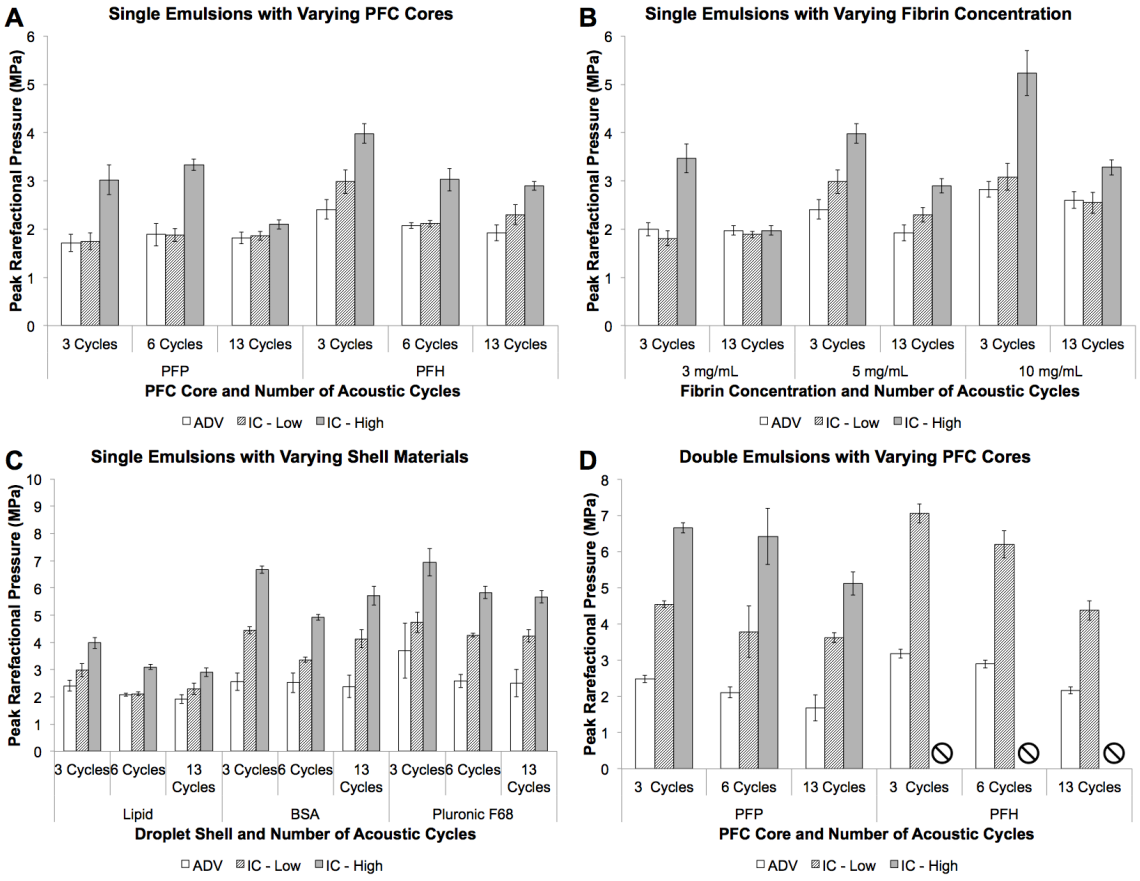

Figure 2.2: ADV and IC thresholds of ARSs containing varying (A) droplet formulations (i.e., different PFC cores), (B) fibrin concentration, (C) droplet shell material, and (D) emulsion structures. For each parameter set, the number of acoustic cycles was varied. In (B) and (C), the ARSs were doped with a PFH single emulsion. A fibrin concentration of 5 mg/mL fibrin was used in ARSs in (A), (C), and (D). A lipid shell was used in (A) and (B). For certain conditions in (D), IC_H was not detected in the range of acoustic pressures interrogated in this work (i.e, 0 - 8.0 MPa); these conditions are denoted by a circle-backslash symbol. Data are shown as mean standard deviation for n = 5 and all ARSs were prepared the day of acoustic measurement. Statistically significant differences within each subfigure are detailed in Tables 2.2-2.5.

Table 2.2: Result of Tukey-Kramer test for Figure 2.2A.

Group	Single-Emulsion PFC	Number of Cycles	Parameter	Pressure (MPa)	Statistically Diff. Groups (t-test)
1	PFP	3	ADV	1.71 ± 0.18	3
2	PFP	3	IC_L	1.75 ± 0.18	3, 11
3	PFP	3	IC_H	3.02 ± 0.31	1, 2
4	PFP	6	ADV	1.89 ± 0.24	6
5	PFP	6	IC_L	1.88 ± 0.14	6
6	PFP	6	IC_H	3.34 ± 0.12	4, 5
7	PFP	13	ADV	1.82 ± 0.13	
8	PFP	13	IC_L	1.86 ± 0.09	
9	PFP	13	IC_H	2.10 ± 0.10	
10	PFH	3	ADV	2.41 ± 0.20	12, 16
11	PFH	3	IC_L	2.98 ± 0.24	2, 12
12	PFH	3	IC_H	3.98 ± 0.20	10, 11
13	PFH	6	ADV	2.08 ± 0.06	15
14	PFH	6	IC_L	2.11 ± 0.07	15
15	PFH	6	IC_H	3.03 ± 0.24	13, 14
16	PFH	13	ADV	1.92 ± 0.16	10, 18
17	PFH	13	IC_L	2.30 ± 0.21	18
18	PFH	13	IC_H	2.89 ± 0.09	16, 17

Table 2.3: Result of Tukey-Kramer test for Figure 2.2B.

Group	Fibrin Concentration (mg/mL)	Number of Cycles	Parameter	Pressure (MPa)	Statistically Diff. Groups (t-test)
1	3	3	ADV	2.00 ± 0.14	3
2	3 3	IC_L	1.81 ± 0.15	3	
3	3	3	IC_H	3.47 ± 0.30	1, 2
4	3	13	ADV	1.97 ± 0.10	16
5	3	13	IC_L	1.89 ± 0.07	11, 17
6	3	13	IC_H	1.97 ± 0.10	
7	5	3	ADV	2.41 ± 0.20	9
8	5	3	IC_L	2.98 ± 0.24	9
9	5	3	IC_H	3.98 ± 0.20	7, 8
10	5	13	ADV	1.92 ± 0.17	12
11	5	13	IC_L	2.30 ± 0.15	5
12	5	13	IC_H	2.90 ± 0.15	10
13	10	3	ADV	2.83 ± 0.16	15
14	10	3	IC_L	3.08 ± 0.28	15
15	10	3	IC_H	5.24 ± 0.47	13, 14
16	10	13	ADV	2.60 ± 0.18	4, 18
17	10	13	IC_L	2.55 ± 0.22	5, 18
18	10	13	IC_H	3.28 ± 0.16	16, 17

as the number of acoustic cycles increased, with a statistically significant difference between 3 and 13 cycles for PFH droplets. All thresholds were higher for PFH than PFP at 3 cycles. There were no differences between ADV and ICL for any acoustic condition in Fig 2-A. However, IC_H was larger than ADV and IC_L for both PFP and PFH at 3 and 6 cycles; at 13 cycles, no differences were observed with the ADV and ICL/H thresholds.

Figure 2.2B shows the ADV and $IC_{L/H}$ thresholds for ARSs containing either 3, 5, or 10 mg/mL fibrin and doped with a lipid stabilized, PFH single emulsion. Qualitatively, the ADV and $IC_{L/H}$ thresholds directly correlated with fibrin concentration, with statistically larger ADV and IC_L thresholds at 10 mg/mL versus 3 mg/mL for all acoustic cycles. Similar to the data in Figure 2.2A, the ADV and $IC_{L/H}$ thresholds decreased as the number of acoustic cycles increased for 5 and 10 mg/mL fibrin. The IC_H threshold was higher than the ADV and IC_L thresholds for

Table 2.4: Result of Tukey-Kramer test for Figure 2.2C.

Group	Shell Material	Number of Cycles	Parameter	Pressure (MPa)	Statistically Diff. Groups (t-test)
1	Lipid	3	ADV	2.41 ± 0.20	3
2	Lipid	3	IC_L	2.98 ± 0.24	3, 11, 20
3	Lipid	3	IC_H	3.98 ± 0.20	1, 2
4	Lipid	6	ADV	2.08 ± 0.06	6, 22
5	Lipid	6	IC_L	2.11 ± 0.07	6, 14, 23
6	Lipid	6	IC_H	3.10 ± 0.09	4, 5
7	Lipid	13	ADV	1.92 ± 0.16	9
8	Lipid	13	IC_L	2.30 ± 0.21	17, 26
9	Lipid	13	IC_H	2.90 ± 0.15	7
10	BSA	3	ADV	2.55 ± 0.32	11, 12
11	BSA	3	IC_L	4.44 ± 0.13	2, 10, 12, 14
12	BSA	3	IC_H	6.68 ± 0.14	10, 11
13	BSA	6	ADV	2.52 ± 0.37	15
14	BSA	6	IC_L	3.36 ± 0.09	5, 11, 15, 23
15	BSA	6	IC_H	4.92 ± 0.11	13, 14
16	BSA	13	ADV	2.38 ± 0.41	17, 18
17	BSA	13	IC_L	4.13 ± 0.33	8, 16
18	BSA	13	IC_H	5.71 ± 0.35	16, 17
19	Pluronic F68	3	ADV	3.70 ± 1.01	21
20	Pluronic F68	3	IC_L	4.73 ± 0.37	2, 21
21	Pluronic F68	3	IC_H	6.95 ± 0.51	19, 20
22	Pluronic F68	6	ADV	2.58 ± 0.25	4, 23, 24
23	Pluronic F68	6	IC_L	4.27 ± 0.07	5, 14, 22, 24
24	Pluronic F68	6	IC_H	5.83 ± 0.23	22, 23
25	Pluronic F68	13	ADV	2.51 ± 0.50	26, 27
26	Pluronic F68	13	IC_L	4.24 ± 0.22	8, 25, 27
27	Pluronic F68	13	IC_H	5.67 ± 0.23	25, 26

Table 2.5: Result of Tukey-Kramer test for Figure 2.2D.

Group	Double Emulsion PFC	Number of Cycles	Parameter	Pressure (MPa)	Statistically Diff. Groups (t-test)
1	PFP	3	ADV	2.48 ± 0.10	2, 3, 10
2	PFP	3	IC_L	4.55 ± 0.09	1, 3, 11
3	PFP	3	IC_H	6.66 ± 0.15	1, 2
4	PFP	6	ADV	2.11 ± 0.15	5, 6, 13
5	PFP	6	IC_L	3.78 ± 0.71	4, 6, 14
6	PFP	6	IC_H	6.42 ± 0.78	4, 5
7	PFP	13	ADV	1.68 ± 0.36	8, 9
8	PFP	13	IC_L	3.63 ± 0.14	7, 9, 17
9	PFP	13	IC_H	5.11 ± 0.32	7, 8
10	PFH	3	ADV	3.18 ± 0.12	1, 11, 16
11	PFH	3	IC_L	7.05 ± 0.26	2, 10
12	PFH	3	IC_H		
13	PFH	6	ADV	2.90 ± 0.11	4, 14
14	PFH	6	IC_L	6.20 ± 0.37	5, 13
15	PFH	6	IC_H		
16	PFH	13	ADV	2.17 ± 0.10	10, 17
17	PFH	13	IC_L	4.38 ± 0.27	8, 16
18	PFH	13	IC_H		

all acoustic conditions and fibrin concentrations except 13 cycles at 3 mg/mL.

The ADV and $IC_{L/H}$ thresholds for ARSs containing 5 mg/mL fibrin and doped with single PFH emulsions of varying droplet shell composition are displayed in Figure 2.2C. ARSs doped with lipid shelled emulsions had a lower IC_L threshold compared to the protein based BSA shell and the polymer based Pluronic F68 shell emulsions at all acoustic cycles, with the largest difference occurring between lipid and Pluronic F68 emulsions. A higher ADV threshold was observed with Pluronic F68 shell emulsions versus lipid shell emulsions at 6 acoustic cycles. For all cases, the IC_H threshold occurred at a higher acoustic pressure than the ADV and IC_L thresholds. Increasing the number of acoustic cycles yielded lower IC_H thresholds for all three shell materials when comparing 3 versus 13 acoustic cycles.

In Figure 2.2-D, the ADV and $IC_{L/H}$ thresholds for ARSs containing 5 mg/mL fibrin and doped with either PFP or PFH double emulsions are shown. Similar to the trend observed in Figure 2.2-A, PFH emulsions had higher ADV and IC_L thresholds than PFP emulsions when comparing 3 and 6 acoustic cycles. The IC_H threshold was higher than the ADV and IC_L thresholds within all acoustic conditions for PFP emulsions. The IC_L threshold for ARSs doped with PFH double emulsion was equivalent to that observed in the sham. IC_H was not detected with PFH emulsions in the range of acoustic pressures tested.

2.3.3 Cell Viability

The viability of C3H10T1/2 cells encapsulated in an ARS containing 5 mg/mL fibrin and doped with PFP double emulsion was quantified (Figure 2.3). This ARS was identical in composition to the ARS in Figure 2.2D, with the addition of cells. In Figure 2.2D, the ADV, IC_L, and IC_H thresholds occurred approximately at 2, 3.8, and 5 MPa, respectively. The percentage of live cells (i.e., calcein+) correlated inversely with acoustic pressure, with a linear regression of the entire data yielding a slope of -3.2 [-4.7, -1.7]. Conversely, the percentage of dead cells (i.e., PI+) was

directly correlated with acoustic pressure, with a linear regression of the entire data yielding a slope of 3.7 [2.2, 5.3]. In the region before ADV and IC (i.e., 0 2 MPa), regressions of the live and dead data yield slopes whose 95% confidence intervals are nearly centered at zero (live: -0.1 [-25.8, 25.6], dead: 0.6 [-21.6, 22.8]), thus indicating no change in cell viability. In the region from 0 to 4 MPa, regressions of the live and dead data yield a slope of -0.9 [-5.5, 3.7] for live and 1.6 [-2.9, 6.1] for dead. In the region between 4 and 8 MPa, regressions of the live and dead data yield a slope of -5.7 [-9.5, -1.9] for live and 5.2 [0.3, 10.0] for dead.

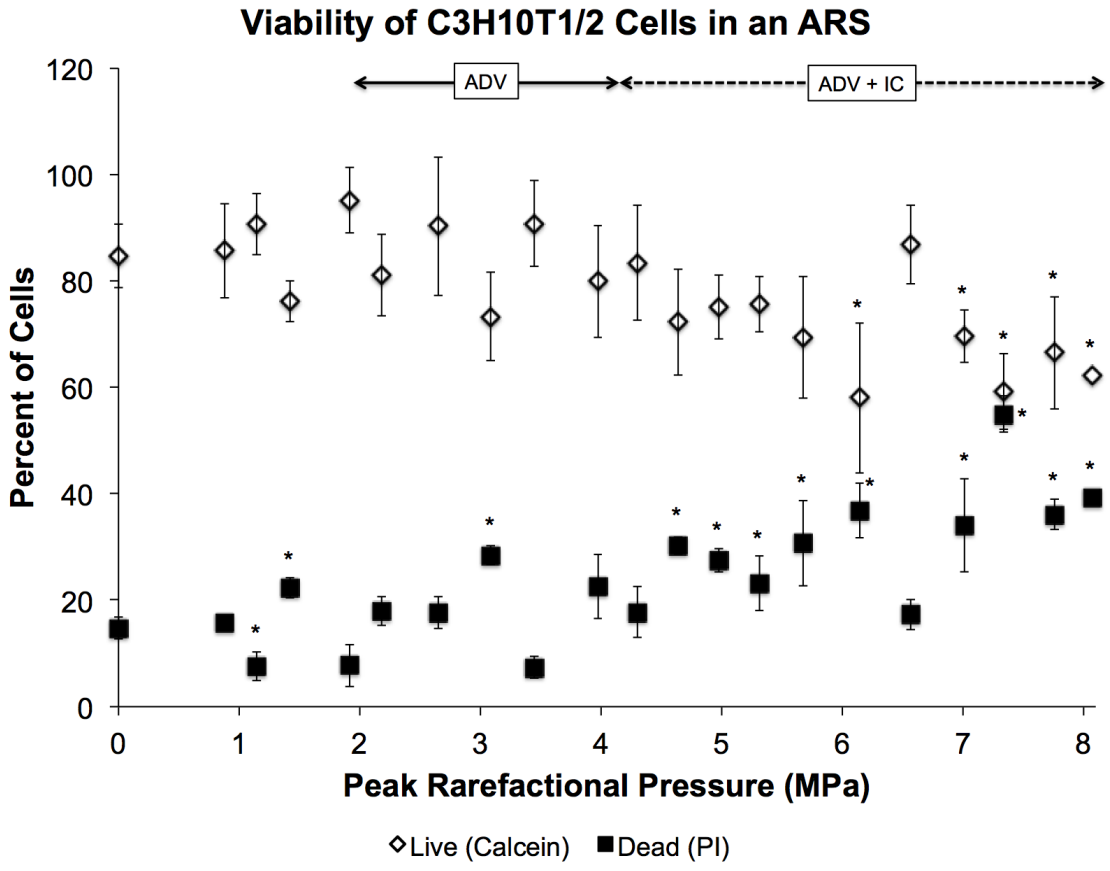

Figure 2.3: Viability of C3H10T1/2 cells in an ARS containing 5 mg/mL fibrin, 1% (v/v) PFP double emulsion, and 50,000 cells/mL after exposure to US at 13 cycles and 10 Hz PRF. Viability was determined with calcein for live staining, propidium iodide for dead staining, and Hoechst for total number of cells. The sham condition (i.e., 0 MPa) underwent the same experimental steps and exposure to environmental conditions as the non-sham conditions. Data are shown as mean ± standard deviation for n = 9. *$p < 0.05$ vs. no US condition.

2.3.4 Physical Stability of ARSs

Light microscopy images of ARSs containing 5 mg/mL fibrin and doped with PFP or PFH double emulsions immediately after and 72 h after polymerization are shown in Figure 2.4. These ARSs were not exposed to US and were placed in a standard tissue culture incubator at 37C between imaging sessions. At 0 h both ARSs contained no bubbles. However after 72 h of incubation, the ARS doped with PFP emulsion contained significantly more bubbles than the ARS doped with PFH emulsion.

Quantification of the physical stability of ARSs containing 5 mg/mL fibrin and doped with single or double emulsions is presented in Figure 2.5A-B. The stability is displayed in terms of droplet concentration (i.e., number density per volume of ARS) and volume percentage of droplets remaining. Note that the ARSs initially contained 1% (v/v) emulsion. Figure 2.5-A shows the physical stability of ARSs doped with PFP or PFH single emulsions. After 2h, ARSs doped with PFH single emulsion exhibited a 10% decrease in droplet concentration. After 144 h, a 40% decrease in droplet concentration, relative to 0 h, was observed for the ARS with PFH emulsion. The volume percentage increased to 1.4% after 2 h of incubation and decreased to 1.2% after 144 h of incubation. For ARSs with PFP single emulsions there was a statistically significant decrease in both droplet concentration and volume percentage beginning 24 h after incubation, relative to 0 h, with further decreases in both metrics over time. At 144h, the droplet concentration and volume percentage decreased by 97% and 94%, respectively, compared to 0 h. No statistically significant differences in mean diameter or number percent greater than 6 μm was observed for ARSs with single PFP or PFH emulsions (data not shown). As a comparison, Figure 2.6A shows the stability of the same single emulsion formulations in DMEM, at the same concentration used in the ARSs (i.e., 1% (v/)). Overall, droplet concentration and volume percentage of emulsions did not change at 144 h relative to 0 h for PFP

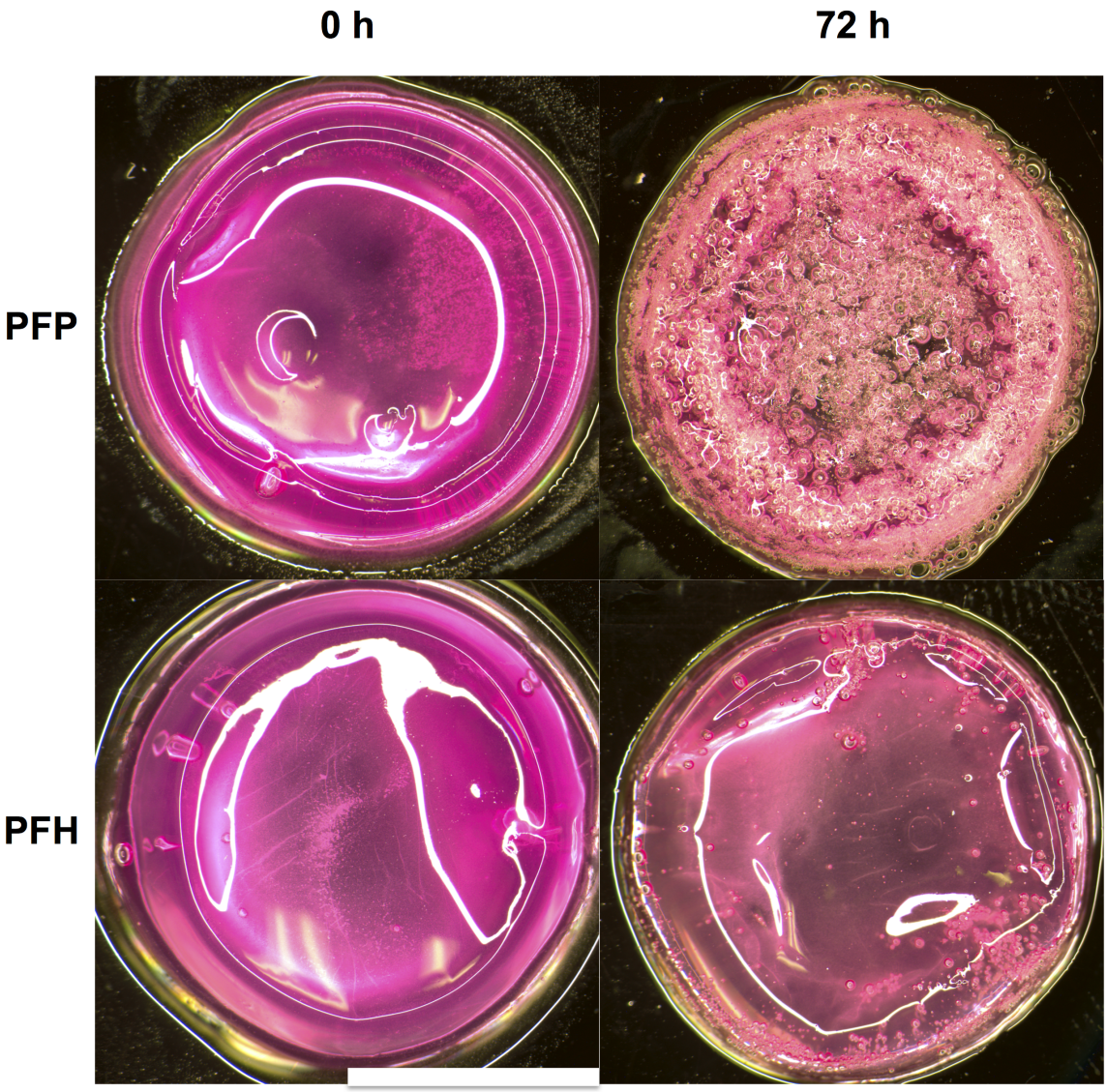

Figure 2.4: Light microscopy images of ARSs doped with 1% (v/v) PFP or PFH emulsions at 0 h and 72 h after polymerization. Between imaging, the ARSs were placed in a standard tissue culture incubator at 37°C and were not exposed to US. Scale bar = 7.8 mm.

and PFH emulsions.

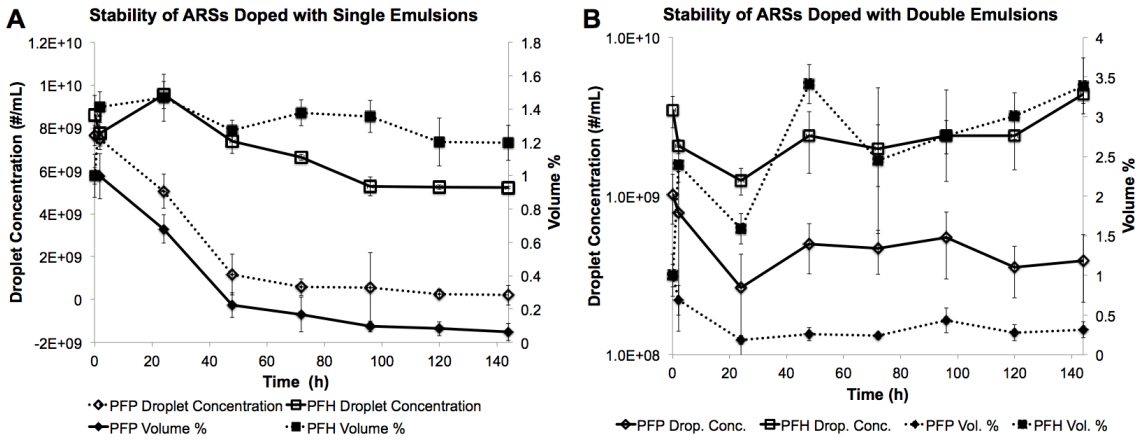

Figure 2.5: Physical stability of ARSs doped with single (A) and double (B) emulsions. The ARSs were degraded with 0.05% trypsin and the remaining emulsion was sized with a Coulter Counter. Data are shown as mean ± standard deviation for n = 5.

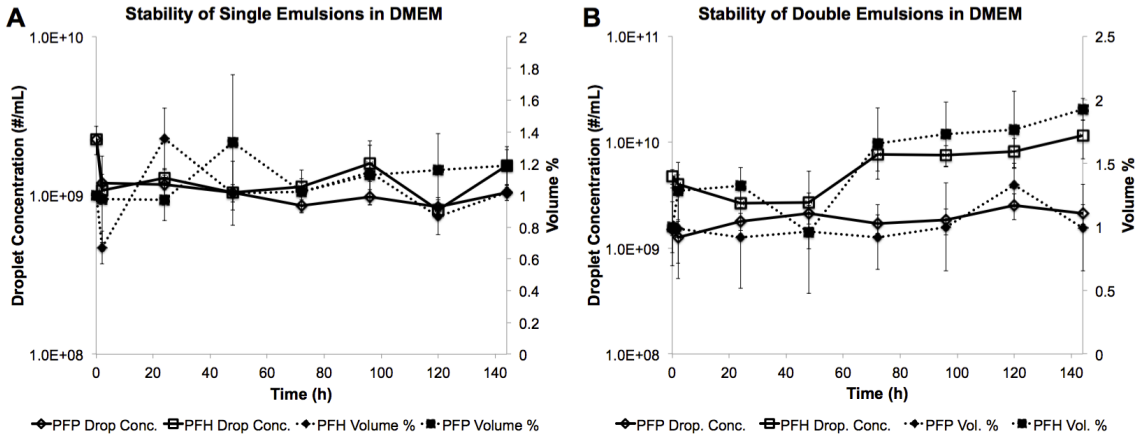

Figure 2.6: Physical stability of single (a) and double (b) emulsions in DMEM. The emulsions were fabricated, and incubated, in the exact same manner as the emulsions contained in acoustically responsive scaffolds. Sizing was done with a Coulter counter. Data are means standard deviations for n = 5.

Figure 2.5B show that ARSs containing PFP double emulsion exhibited a 50% decrease in droplet concentration 24 hours after polymerization. The concentration then remained relatively unchanged through the remainder of the experiment, with a linear regression of the PFP droplet concentration data yielding a slope roughly centered at zero $[-2.8 \times 10^6\ ,\ 3.5 \times 10^6]$. A 61% decrease in droplet concentration was observed when comparing 0 h versus 144 h. The volume percentage also decreased

after 24 hours and remained relatively constant at 0.5%, with a linear regression through the data yielding a slope of 0.001 [-0.001, 0.003]. A 68% decrease in volume percentage was observed when comparing 0 h versus 144 h. This is similar to the results observed in Figure 2.5-A where the ARSs doped with PFP single emulsion exhibited a statistically significant decrease in both volume percentage and droplet concentration at 144 h relative to 0 h. For ARS with PFH double emulsion, both the droplet concentration and volume percentage of droplets increased with time. A 27% increase in droplet concentration and a 238% increase in volume percentage was seen when comparing data at 0 h and 144 h. No statistically significant differences in mean diameter or number percent greater than 6 μm was observed for ARSs with double PFP or PFH emulsions (data not shown). Figure 2.6B shows the stability of double emulsions in DMEM. Similar to single emulsions in DMEM, the droplet concentration and volume percent of emulsions did not decrease at t = 144 h relative to t = 0 h for PFP or PFH emulsions. For PFH double emulsions, the volume percentage increased to 2% (v/v).

2.3.5 Non-Selective Payload Release

The release of FSS from ARSs containing 5 mg/mL fibrin and doped with PFP or PFH double emulsions is shown in Figure 2.7. The FSS was initially encapsulated within the W_1 phase of each emulsion. The data in Figure 2.7 was acquired in the same experiment as the stability data in Figure 2.5. As a control, the release profile of FSS, not encapsulated in a double emulsion but incorporated directly into the fibrin scaffold, is also shown. After 144 h, less than 3% of the initially loaded FSS is released from the ARSs with either the PFP or PFH emulsions. Comparatively, 62% of the initially loaded FSS was released from the control scaffold after 144h.

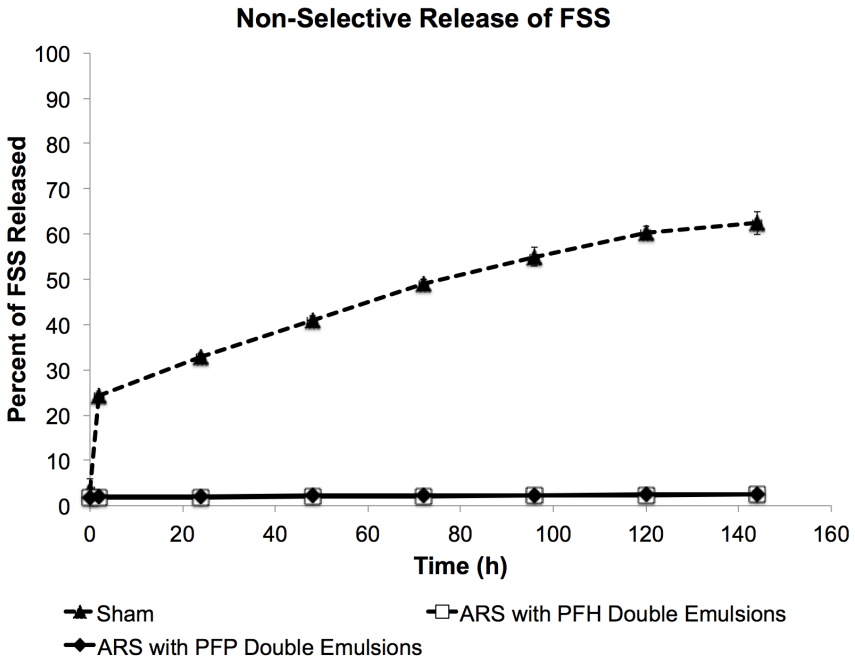

Figure 2.7: Non-selective (i.e., without US exposure) release of a small molecular weight surrogate payload, FSS, from ARSs containing PFP or PFH double emulsions. The FSS was encapsulated within the W1 phases of the respective emulsions. The ARSs were placed in a standard tissue culture incubator at 37°C. The release profile of non-emulsified FSS, doped within a sham fibrin scaffold (i.e., without emulsion) is also shown. Data are shown as mean standard deviation for n = 5.

2.4 Discussion

Recently, we demonstrated that US can be used to actively control GF release, architecture, and stiffness in a fibrin scaffold doped with sonosensitive emulsion [20]. Here we characterize the acoustic response of fibrin-based ARSs with a surrogate payload and relate it to cell viability within the scaffold, while also focusing on the stability of the ARSs. By design, an ARS is more responsive to US than a conventional fibrin scaffold. The results demonstrated that stable bubbles were created via ADV in all tested compositions of ARSs. For acoustic measurements, all ARSs and sham hydrogels were formulated with degassed DMEM and placed in a degassed water tank, which decreased the amount of dissolved gas present and thus likelihood for bubble generation and persistence within the scaffolds. Bubble formation was not detected in the sham scaffolds (i.e., no droplets) using B-mode US. Additionally, IC_L, and IC_H thresholds were lower in the ARSs, compared to the sham scaffold, except in the case of ARS doped with PFH double emulsions at 3 and 6 cycle pulses (Fig 2D). This is consistent with previous studies, where the IC threshold of a solution containing microbubbles or high concentrations of dissolved gas was lower than the IC threshold in the same solution without microbubbles or a low concentration of dissolved gas [35]. During IC, the rapid collapse of cavitation nuclei typically results in various remnant fragments [40–42]. These daughter nuclei last from milliseconds to full seconds [21; 42; 43], and may serve as cavitation nuclei for following US pulses. However in degassed media, more aggressive acoustic conditions are required to form cavitation nuclei and any subsequent daughter nuclei. *in vitro* and *in vivo* bioeffects related to IC have been found to correlate with the IC dose, which is the magnitude of IC activity over time [37; 45]. Thus, for delivery of large molecules such as GFs that have higher order structure, avoidance of acoustic pressures that generate persistent IC may be beneficial in retaining GF bioactivity [46].

A trend observed in prior work was that the ADV threshold occurred at a lower acoustic pressure than the IC_L threshold, where the bubbles generated by ADV were hypothesized to undergo IC [35; 47]. These previous studies measured the acoustic thresholds of sonosensitive emulsions in flowing saline, thus emulating the presence of intravascularly administered emulsion in blood flow. Depending on the flow velocity and acoustic parameters, bubbles generated by ADV may not be insonified by multiple pulses of US. However, bubbles formed in the ARSs are stationary and thus are exposed to multiple acoustic pulses. Therefore, given that 100 pulses were fired at one location within the ARS (Fig 2), a bubble formed by ADV within the first 99 pulses fired by the single element transducer has the potential to undergo IC during the remaining pulse, at a given acoustic pressure.

ARSs doped with PFH double emulsions displayed higher ADV and $IC_{L/H}$ thresholds than ARSs doped with PFP double emulsions (Fig 2A versus Fig 2D). Interestingly, ARSs doped with PFP or PFH single emulsions displayed similar thresholds. Previous studies have demonstrated that the acoustic pressure required to vaporize a PFC emulsion was related to the boiling point of the PFC [34; 35; 48]. However another study showed that the IC thresholds of PFC emulsions was independent of the boiling point of the dispersed PFC phase [49]. Gases are very soluble in PFCs, especially oxygen, with the solubility inversely correlated to PFC molecular weight [50–52]. It is hypothesized that the interaction of US with the dissolved gases within a PFC droplet causes the vaporization of high boiling point PFCs, such as perfluoro-15-crown-5-ether (boiling point: 146°C) [33] or yields similar IC threshold for PFCs with different molecular weights [49]. Thus, the similar ADV thresholds in ARSs with single PFP and PFH emulsions may potentially be attributed in part to high gas solubility within both PFCs.

For the same number of acoustic cycles, ARSs doped with double emulsions generally displayed higher ADV and $IC_{L/H}$ thresholds than ARSs doped with

single emulsions (Fig 2A versus Fig 2D). These acoustic differences could be due to variations in the outer shell stabilizing the emulsion droplets, droplet diameter, or emulsion morphology. The outer shells of the single and double emulsions were lipid and Pluronic F68, respectively. It can be seen in Fig 2C that ARSs containing single emulsions with Pluronic F68 shells had higher acoustic thresholds than ARSs with single emulsions with lipid shells. Since the ADV threshold is inversely related to droplet size [34; 35; 47], it was expected that the ADV threshold of ARSs with double emulsions would have been lower than single emulsions since the double emulsions were larger in size (Table 1.1). Thus, it is hypothesized that the mechanism governing the initiation of ADV for double emulsions is different than that of single emulsions. In addition, the fraction of PFC within a double emulsion droplet is smaller than in a single emulsion droplet, which may diminish the probability for an appropriate nucleation site and therefore increase the pressure needed to trigger ADV in a double emulsion. Prior work has also shown that the expansion rate of double emulsions is slower than that of single emulsions during ADV [54]. Thus more acoustic energy may be required to displace the viscous hydrogel media surrounding the double emulsion droplet while also preventing recondensation of the PFC during the relatively slow expansion.

For ARSs with single emulsions, the effects of shell material and droplet size on ADV and $IC_{L/H}$ thresholds cannot be completely decoupled since different shells yielded differently sized emulsions. As stated previously, higher thresholds were observed with Pluronic F68 emulsions versus lipid shell emulsions (Fig 2C). Microbubbles with a soft-shell surfactant, such as lipid, can undergo net radial fluctuations of at least 15%, while stiffer albumin-shelled microbubbles demonstrate constrained expansion and contraction when exposed to US [55]. In addition, microbubbles with stiffer polymer based shells have higher fragmentation thresholds than lipid-based microbubbles [43]. Lipid shell emulsions also displayed the largest

mean diameter and highest percentage of droplets greater than 6 μm, which could also lead to a lower ADV and $IC_{L/H}$ thresholds. Within an ARS, the interaction between a droplet and the surrounding fibrin could be affected by the physiochemical properties of the shell stabilizing the droplet. For example, Pluronic F68 can alter the arrangement of fibrin fibers, which could ultimately impact the acoustic response of the ARS [57]. Such interactions would also explain the apparent instability of the PFP droplets in the ARSs in comparison to that found in aqueous solutions.

Higher ADV and IC thresholds were observed as the fibrin concentration of the ARS increased. The inertia of the surrounding media, large Laplace pressure, and viscosity may delay the startup of bubble nucleation during ADV or growth during ADV/IC. If the time delay caused by these factors comprise a significant portion of the acoustic period, then a much higher acoustic pressure could be required to initiate the growth of the bubble from the emulsion or to cause the generated bubble to undergo IC [20; 35; 58; 59]. Overall, ADV and IC thresholds generally decreased as the number of acoustic cycles increased. Previous research has demonstrated an inverse correlation between the IC threshold and the number of acoustic cycles, especially in the range of 1 to 10 cycles [60–62].

Since the ADV and IC thresholds can be modulated by altering the composition of the ARS, this opens the possibility of expanding the GF delivery capabilities of an ARS beyond what has been previously demonstrated [20]. Release of two distinct payloads could be achieved by formulating an ARS with two droplet formulations. For example, as seen in Figure 2.2-D, the ADV thresholds in an ARS containing PFP or PFH double emulsion is 2.5 MPa and 3 MPa, respectively, at 3 cycles. Therefore one payload could be released first at the lower acoustic threshold while a second payload could be released at a higher acoustic threshold thus enabling temporal control of multiple payload release. Though not investigated in this work, the use of different US frequencies could also be used to tune different release thresholds

[47; 63; 64]. Other modifications to the droplet formulations including differential size distributions could further increase the separation in threshold for temporal control. Spatial control of ADV/IC and payload release is also an inherent feature of an ARS due to the use of focused US as the means to interact with the sonosensitive emulsion, compared to studies where unfocused US has been used to facilitate drug release [22]. The use of megahertz frequency US to trigger ADV enables patterning at submillimeter resolution within an ARS. Additionally, ADV thresholds of the ARSs ranged from approximately 1.5 to 3 MPa peak rarefactional pressure, which is within the output range of clinical diagnostic US scanners (i.e., at 2.5 MHz, 3 MPa is equivalent to a mechanical index of 1.9 which is the current upper limit set by the United States Food and Drug Administration).

Cell adherence and viability can be impacted by US capable of generating ADV and IC. ADV adjacent to adherent cells can cause detachment [65] while an 80% decrease in cell number was observed for cells in the presence of bubbles undergoing IC [**?**]. It was previously demonstrated that the metabolic activity of cells encapsulated in an ARS was not impacted by high amplitude US used to generate ADV within an ARS [20]. However, this prior study used only one acoustic condition (i.e., 6 MPa peak rarefactional pressure at 3.5 MHz) and the presence of IC was not detected. In this work, the viability of cells contained in the ARS was not affected by acoustic pressures up to 2 MPa but decreased to 60% when exposed to an acoustic pressure of 8 MPa, which generated sustained IC. As seen in Fig 2, some of the ADV thresholds occurred at a pressure less than 2 MPa. Additionally, the use of higher frequency US could reduce the acoustic bioeffects stemming from IC, though at the expense of depth penetration. Beyond viability, the impact of ADV and IC on cellular proliferation and differentiation as well as cytokine production in an ARS are also critically important, but were outside of the scope of this work.

The physical stability of the emulsion used to dope an ARS is relevant to

the stability of the ARS as a whole and can impact the ability of US to interact with the ARS. ARSs doped with PFH emulsions displayed less spontaneous (i.e., in the absence of US) bubble formation than ARSs doped with PFP emulsions. The millimeter size bubbles formed in the ARS doped with PFP likely formed via coalescence of multiple smaller bubbles. Also, subsequent in-gassing may have occurred as the ARS, which was prepared with degassed fluids, was placed into a cell culture incubator at atmospheric gas saturation with 5% carbon dioxide. Additional nucleation of dissolved gas within the PFC could also have occurred as the ARS warmed from room temperature to 37^{circ}C. It is hypothesized that the higher boiling point of PFH versus PFP imparts greater stability. Previous studies with PFP emulsions indicate that these droplets are stable at 37°C [20], though few if any studies explored the stability at 37°C for one week or in a matrix like a fibrin scaffold. Additionally, as seen when comparing Fig 5 to Figure 2.6B, PFP emulsions displayed greater stability in DMEM versus in an ARS. Within an ARS, the fibrin surrounding each droplet may be exerting tension on the droplet, or effectively lowering the interfacial tension, which would destabilize the PFC droplet.

Encapsulation of FSS within the W_1 phase of the emulsion hindered its release from the ARS when compared to non-emulsified FSS (Figure 2.7). However, despite exhibiting greater stability, the retention of FSS was similar for ARSs doped with PFP and PFH double emulsions. The higher bubble density within ARSs doped with PFP double emulsion could impact the diffusivity of FSS through the ARS. Overall, the greater stability of the ARS with PFH double emulsion makes this composition better suited for controlled release or *in vivo* implantation since any spontaneously formed bubbles would prevent US from penetrating the ARS. In additional to spontaneous vaporization, the population of PFC droplets may be shifting toward larger sizes, due to droplet coalescence or Ostwald ripening. This would cause sub-micron size droplets that are initially below the sizing range of

the Coulter Counter to enter the detectable range (i.e., 1-30 μm), thus causing an increase in the droplet concentration and volume percentage. The osmotic imbalance between the W_1 phase, which contained FSS at 1 mg/mL, and the surrounding environment (i.e., the fibrin scaffold and overlying DMEM), could have contributed to the increase in volume percentage of the emulsion within the ARS doped with PFH double emulsion.

2.5 Conclusions

In this study, we characterized the interactions of US with droplets and associated bubbles occurring in sonosensitive hydrogels. ADV and IC thresholds were modulated by modifying ARS parameters such as fibrin concentration, emulsion shell material, PFC core, emulsion structure, and the number of acoustic cycles. ADV occurred within an ARS without significant effects on cell viability. ARSs doped with PFH emulsions displayed better physical stability and less spontaneous bubble formation than ARSs doped with PFP emulsions. Non-selective payload release was minimal for both ARS compositions tested. These data can be used in selecting an ARS composition and associated acoustic parameters for future studies that evaluate regenerative processes within ARSs or for delivery of multiple payloads/GFs.

2.6 Acknowledgments

This work was supported by NIH grant R21AR065010 (MLF) and the Basic Radiological Sciences Innovative Research Award (MLF). AM is supported by the National Science Foundation Graduate Student Research Fellowship (Grant No. DGE 1256260).

REFERENCES

[1] Shaikh, F.M., Callanan, A., Kavanagh, E.G., Burke, P.E., Grace, P.A., and McGloughlin, T.M.: Fibrin: A natural biodegradable scaffold in vascular tissue engineering, Cells Tissues Organs, 2008, 188, (4), pp. 333-346

[2] Dehghani, F., and Annabi, N.: Engineering porous scaffolds using gas-based techniques, Current opinion in biotechnology, 2011, 22, (5), pp. 661-666

[3] Seliktar, D.: Designing Cell-Compatible Hydrogels for Biomedical Applications, Science, 2012, 336, (6085), pp. 1124-1128

[4] Sojo, K., Sawaki, Y., Hattori, H., Mizutani, H., and Ueda, M.: Immunohistochemical study of vascular endothelial growth factor (VEGF) and bone morphogenetic protein-2,-4 (BMP-2,-4) on lengthened rat femurs, Journal of Cranio-Maxillofacial Surgery, 2005, 33, (4), pp. 238-245

[5] Bos, P.K., van Osch, G.J.V.M., Frenz, D.A., Verhaar, J.A.N., and Verwoerd-Verhoef, H.L.: Growth factor expression in cartilage wound healing: temporal and spatial immunolocalization in a rabbit auricular cartilage wound model, Osteoarthritis and Cartilage, 2001, 9, (4), pp. 382-389

[6] Barthes, J., Ozcelik, H., Hindie, M., Ndreu-Halili, A., Hasan, A., and Vrana, N.E.: Cell Microenvironment Engineering and Monitoring for Tissue Engineering and Regenerative Medicine: The Recent Advances, Biomed Research International, 2014

[7] Satyam, A., Kumar, P., Fan, X.L., Gorelov, A., Rochev, Y., Joshi, L., Peinado, H., Lyden, D., Thomas, B., Rodriguez, B., Raghunath, M., Pandit, A., and Zeugolis, D.: Macromolecular Crowding Meets Tissue Engineering by Self-Assembly: A Paradigm Shift in Regenerative Medicine, Advanced Materials, 2014, 26, (19), pp. 3024-3034

[8] Fujie, T., Mori, Y., Ito, S., Nishizawa, M., Bae, H., Nagai, N., Onami, H., Abe, T., Khademhosseini, A., and Kaji, H.: Micropatterned Polymeric Nanosheets for Local Delivery of an Engineered Epithelial Monolayer, Advanced Materials, 2014, 26, (11), pp. 1699-1705

[9] Tse, H.T.K., Weaver, W.M., and Di Carlo, D.: Increased Asymmetric and Multi-Daughter Cell Division in Mechanically Confined Microenvironments, Plos One, 2012, 7, (6)

[10] Metallo, C.M., Mohr, J.C., Detzel, C.J., de Pablo, J.J., Van Wie, B.J., and Palecek, S.P.: Engineering the stem cell microenvironment, Biotechnology Progress, 2007, 23, (1), pp. 18-23

[11] Matsusaki, M., and Akashi, M.: Novel functional biodegradable polymer IV: pH-Sensitive controlled release of fibroblast growth factor-2 from a poly(gamma-glutamic acid)-sulfonate matrix for tissue engineering, Biomacromolecules, 2005, 6, (6), pp. 3351-3356

[12] Thornton, P.D., McConnell, G., and Ulijn, R.V.: Enzyme responsive polymer hydrogel beads, Chemical Communications, 2005, (47), pp. 5913-5915

[13] Frimpong, R.A., Fraser, S., and Hilt, J.Z.: Synthesis and temperature response analysis of magnetic-hydrogel nanocomposites, Journal of Biomedical Materials Research Part A, 2007, 80A, (1), pp. 1-6

[14] Zhao, X., Kim, J., Cezar, C.A., Huebsch, N., Lee, K., Bouhadir, K., and Mooney, D.J.: Active scaffolds for on-demand drug and cell delivery, Proceedings of the National Academy of Sciences of the United States of America, 2011, 108, (1), pp. 67-72

[15] Kulkarni, R., and Biswanath, S.: Electrically responsive smart hydrogels in drug delivery: a review, Journal of Applied Biomaterials and Biomechanics, 2007, 5, (3), pp. 125-139

[16] Wu, C., Chen, C., Lai, J., Mu, X., Zheng, J., and Zhao, Y.: Molecule-scale controlled-release system based on light-responsive silica nanoparticles, Chemical Communications, 2008, 23, pp. 2662-2664

[17] Lavigne, M.D., Pennadam, S.S., Ellis, J., Yates, L.L., Alexander, C., and Gorecki, D.C.: Enhanced gene expression through temperature profile-induced variations in molecular architecture of thermoresponsive polymer vectors, The Journal of Gene Medicine, 2007, 9, (1), pp. 44-54

[18] Sakiyama-Elbert, S.E., and Hubbell, J.A.: Development of fibrin derivatives for controlled release of heparin-binding growth factors, Journal of Controlled Release, 2000, 65, (3), pp. 389-402

[19] Sakiyama-Elbert, S.E., and Hubbell, J.A.: Controlled release of nerve growth factor from a heparin-containing fibrin-based cell ingrowth matrix, Journal of Controlled Release, 2000, 69, (1), pp. 149-158

[20] Fabiilli, M.L., Wilson, C.G., Padilla, F., Martin-Saavedra, F.M., Fowlkes, J.B., and Franceschi, R.T.: Acoustic droplet-hydrogel composites for spatial and temporal control of growth factor delivery and scaffold stiffness, Acta Biomaterialia, 2013

[21] Epstein-Barash, H., Orbey, G., Polat, B.E., Ewoldt, R.H., Feshitan, J., Langer, R., Borden, M.A., and Kohane, D.S.: A microcomposite hydrogel for repeated on-demand ultrasound-triggered drug delivery, Biomaterials, 2010, 31, (19), pp. 5208-5217

[22] Huebsch, N., Kearney, C.J., Zhao, X.H., Kim, J., Cezar, C.A., Suo, Z.G., and Mooney, D.J.: Ultrasound-triggered disruption and self-healing of reversibly cross-linked hydrogels for drug delivery and enhanced chemotherapy, Proceedings of the National Academy of Sciences of the United States of America, 2014, 111, (27), pp. 9762-9767

[23] Lima, E.G., Durney, K.M., Sirsi, S.R., Nover, A.B., Ateshian, G.A., Borden, M.A., and Hung, C.T.: Microbubbles as biocompatible porogens for hydrogel scaffolds, Acta Biomaterialia, 2012, (in press), (http://dx.doi.org/10.1016/j.actbio.2012.07.007)

[24] Nair, A., Thevenot, P., Dey, J., Shen, J.H., Sun, M.W., Yang, J., and Tang, L.P.: Novel Polymeric Scaffolds Using Protein Microbubbles as Porogen and Growth Factor Carriers, Tissue Eng Part C-Me, 2010, 16, (1), pp. 23-32

[25] Whelan, D., Caplice, N.M., and Clover, A.J.P.: Fibrin as a delivery system in wound healing tissue engineering applications, Journal of Controlled Release, 2014, 196, pp. 1-8

[26] Kripfgans, O.D., Fowlkes, J.B., Miller, D.L., Eldevik, O.P., and Carson, P.L.: Acoustic droplet vaporization for therapeutic and diagnostic applications, Ultrasound in Medicine and Biology, 2000, 26, (7), pp. 1177-1189

[27] Unger, E.C., Porter, T., Culp, W., LaBell, R., Matsunaga, T., and Zutshi, R.: Therapeutic applications of lipid-coated microbubbles, Advanced Drug Delivery Reviews, 2004, 56, (9), pp. 1291-1314

[28] Diaz-Lopez, R., Tsapis, N., and Fattal, E.: Liquid perfluorocarbons as contrast agents for ultrasonography and 19F-MRI, Pharmaceutical Research, 2010, 27, (1), pp. 1-16

[29] Buil-Bruna, N., Lopez-Picazo, J.M., Martin-Algarra, S., and Troconiz, I.F.: Bringing Model-Based Prediction to Oncology Clinical Practice: A Review of Pharmacometrics Principles and Applications, Oncologist, 2016, 21, (2), pp. 220-232

[30] Kripfgans, O.D., Fabiilli, M.L., Carson, P.L., and Fowlkes, J.B.: On the acoustic vaporization of micrometer-sized droplets, The Journal of the Acoustical Society of America, 2004, 116, (1), pp. 272-281

[31] Fabiilli, M.L., Lee, J.A., Kripfgans, O.D., Carson, P.L., and Fowlkes, J.B.: Delivery of water-soluble drugs using acoustically triggered perfluorocarbon double emulsions, Pharmaceutical research, 2010, 27, (12), pp. 2753-2765

[32] Wong, Z.Z., Kripfgans, O.D., Qamar, A., Fowlkes, J.B., and Bull, J.L.: Bubble evolution in acoustic droplet vaporization at physiological temperature via ultra-high speed imaging, Soft Matter, 2011, 7, (8), pp. 4009-4016

[33] Rapoport, N.Y., Kennedy, A.M., Shea, J.E., Scaife, C.L., and Nam, K.-H.: Controlled and targeted tumor chemotherapy by ultrasound-activated nanoemulsions/microbubbles, Journal of Controlled Release, 2009, 138, (2), pp. 268-276

[34] Sheeran, P.S., Wong, V.P., Luois, S., McFarland, R.J., Ross, W.D., Feingold, S., Matsunaga, T.O., and Dayton, P.A.: Decafluorobutane as a Phase-Change Contrast Agent for Low-Energy Extravascular Ultrasonic Imaging, Ultrasound in Medicine and Biology, 2011, 37, (9), pp. 1518-1530

[35] Fabiilli, M.L., Haworth, K.J., Fakhri, N.H., Kripfgans, O.D., Carson, P.L., and Fowlkes, J.B.: The role of inertial cavitation in acoustic droplet vaporization, IEEE Trans Ultrason Ferroelectr Freq Control, 2009, 56, (5), pp. 1006-1017

[36] Ferrara, K.W., Pollard, R., and Borden, M.A.: Ultrasound microbubble contrast agents: fundamentals and application to gene and drug delivery, Annual Review of Biomedical Engineering, 2007, 9, pp. 425-447

[37] Hwang, J.H., Tu, J., Brayman, A.A., Matula, T.J., and Crum, L.A.: Correlation between inertial cavitation dose and endothelial cell damage *in vivo*, Ultrasound in Medicine and Biology, 2006, 32, (10), pp. 1611-1619

[38] Madanshetty, S.I., and Apfel, R.E.: ACOUSTIC MICROCAVITATION - ENHANCEMENT AND APPLICATIONS, Journal of the Acoustical Society of America, 1991, 90, (3), pp. 1508-1514

[39] Apfel, R.E., and Holland, C.K.: Gauging the likelihood of cavitation from short-pulse, low-duty cycle diagnostic ultrasound, Ultrasound in Medicine and Biology, 1991, 17, (2), pp. 179-185

[40] Flynn, H.G., and Church, C.C.: A MECHANISM FOR THE GENERATION OF CAVITATION MAXIMA BY PULSED ULTRASOUND, Journal of the Acoustical Society of America, 1984, 76, (2), pp. 505-512

[41] Brennen, C.E.: Fission of collapsing cavitation bubbles, Journal of Fluid Mechanics, 2002, 472, pp. 153-166

[42] Pishchalnikov, Y.A., McAteer, J.A., Pishchalnikova, I.V., Williams, J.C., Bailey, M.R., and Sapozhnikov, O.A.: Bubble proliferation in shock wave lithotripsy occurs during inertial collapse, in Enflo, B.O., Hedberg, C.M., and Kari, L. (Eds.): Nonlinear Acoustics Fundamentals and Applications (2008), pp. 460-463

[43] Chen, W.S., Matula, T.J., and Crum, L.A.: The disappearance of ultrasound contrast bubbles: Observations of bubble dissolution and cavitation nucleation, Ultrasound Med Biol, 2002, 28, (6), pp. 793-803

[44] Epstein, P.S., and Plesset, M.S.: On the stability of gas bubbles in liquid-gas solutions, Journal of Chemical Physics, 1950, 18, (11), pp. 1505-1509

[45] Hallow, D.M., Mahajan, A.D., McCutchen, T.E., and Prausnitz, M.R.: Measurement and correlation of acoustic cavitation with cellular bioeffects, Ultrasound in Medicine and Biology, 2006, 32, (7), pp. 1111-1122

[46] Marchioni, C., Riccardi, E., Spinelli, S., dell'Unto, F., Grimaldi, P., Bedini, A., Giliberti, C., Giuliani, L., Palomba, R., and Castellano, A.C.: Structural changes induced in proteins by therapeutic ultrasounds, Ultrasonics, 2009, 49, (6-7), pp. 569-576

[47] Schad, K.C., and Hynynen, K.: *In vitro* characterization of perfluorocarbon droplets for focused ultrasound therapy, Physics in Medicine and Biology, 2010, 55, (17), pp. 4933-4947

[48] Kawabata, K.-I., Sugita, N., Yoshikawa, H., Azuma, T., and Umemura, S.-I.: Nanoparticles with Multiple Perfluorocarbons for Controllable Ultrasonically Induced Phase Shifting, Japanese Journal of Applied Physics, 2005, 44, (6B), pp. 4548-4552

[49] Giesecke, T., and Hynynen, K.: Ultrasound-mediated cavitation thresholds of liquid perfluorocarbon Droplets '*in vitro*, Ultrasound in Medicine and Biology, 2003, 29, (9), pp. 1359-1365

[50] Riess, J.G.: Oxygen Carriers ("Blood Substitutes") - Raison d'Etre, Chemistry, and Some Physiology, Chemical Reviews, 2001, 101, (9), pp. 2797-2919

[51] Johnson, J.L.H., Dolezal, M.C., Kerschen, A., Matsunaga, T.O., and Unger, E.C.: *In vitro* comparison of dodecafluoropentane (DDFP), perfluorodecalin (PFD), and perfluoroctylbromide (PFOB) in the facilitation of oxygen exchange, Artificial cells, blood substitutes, and biotechnology, 2009, 37, (4), pp. 156-162

[52] Dias, A.M.A., Freire, M., Coutinho, J.A.P., and Marrucho, I.M.: Solubility of oxygen in liquid perfluorocarbons, Fluid Phase Equilibria, 2004, 222, pp. 325-330

[53] Rapoport, N., Nam, K.H., Gupta, R., Gao, Z.G., Mohan, P., Payne, A., Todd, N., Liu, X., Kim, T., Shea, J., Scaife, C., Parker, D.L., Jeong, E.K., and Kennedy, A.M.: Ultrasound-mediated tumor imaging and nanotherapy using drug loaded, block copolymer stabilized perfluorocarbon nanoemulsions, Journal of Controlled Release, 2011, 153, (1), pp. 4-15

[54] Shpak, O., Stricker, L., Kokhuis, T., Luan, Y., Fowlkes, B., Fabiilli, M., Lohse, D., de Jong, N., and Versluis, M.: Ultrafast dynamics of the acoustic vaporization of phase-change microdroplets, The Journal of the Acoustical Society of America, 2013, 133, (5), pp. 3586

[55] Dayton, P.A., Morgan, K.E., Klibanov, A.L., Brandenburger, G.H., and Ferrara, K.W.: Optical and acoustical observations of the effects of ultrasound on contrast agents, Ieee Transactions on Ultrasonics Ferroelectrics and Frequency Control, 1999, 46, (1), pp. 220-232

[56] Chen, W.S., Matula, T.J., Brayman, A.A., and Crum, L.A.: A comparison of the fragmentation thresholds and inertial cavitation doses of different ultrasound contrast agents, Journal of the Acoustical Society of America, 2003, 113, (1), pp. 643-651

[57] Vangelder, J.M., Nair, C.H., and Dhall, D.P.: EFFECTS OF POLOXAMER-188 ON FIBRIN NETWORK STRUCTURE, WHOLE-BLOOD CLOT PERMEABILITY AND FIBRINOLYSIS, Thrombosis Research, 1993, 71, (5), pp. 361-376

[58] Holland, C.K., and Apfel, R.E.: An improved theory for the prediction of microcavitation thresholds, IEEE Transactions on Ultrasonics, Ferroelectrics, and Frequency Control, 1989, 36, (2), pp. 204-208

[59] Apfel, R.E.: POSSIBILITY OF MICROCAVITATION FROM DIAGNOSTIC ULTRASOUND, Ieee Transactions on Ultrasonics Ferroelectrics and Frequency Control, 1986, 33, (2), pp. 139-142

[60] Atchley, A.A., Frizzell, L.A., Apfel, R.E., Holland, C.K., Madanshetty, S., and Roy, R.A.: Thresholds for Cavitation Produced in Water by Pulsed Ultrasound, Ultrasonics, 1988, 26, (5), pp. 280-285

[61] Fowlkes, J.B., and Crum, L.A.: CAVITATION THRESHOLD MEASUREMENTS FOR MICROSECOND LENGTH PULSES OF ULTRASOUND, Journal of the Acoustical Society of America, 1988, 83, (6), pp. 2190-2201

[62] Ammi, A.Y., Cleveland, R.O., Mamou, J., Wang, G.I., Bridal, S.L., and O'Brien, W.D.: Ultrasonic contrast agent shell rupture detected by inertial cavitation and rebound signals, Ieee Transactions on Ultrasonics Ferroelectrics and Frequency Control, 2006, 53, (1), pp. 126-136

[63] Kripfgans, O.D.: Acoustic droplet vaporization for diagnostic and therapeutic applications, University of Michigan, 2002

[64] Martz, T.D., Sheeran, P.S., Bardin, D., Lee, A.P., and Dayton, P.A.: Precision Manufacture of Phase-Change Perfluorocarbon Droplets Using Microfluidics, Ultrasound in Medicine and Biology, 2011, 37, (11), pp. 1952-1957

[65] Ohl, C.-D., Arora, M., Ikink, R., de Jong, N., Versluis, M., Delius, M., and Lohse, D.: Sonoporation from jetting cavitation bubbles, Biophysical Journal, 2006, 91, (11), pp. 4285-4295

[66] Ward, M., Wu, J.R., and Chiu, J.F.: Ultrasound-induced cell lysis and sonoporation enhanced by contrast agents, Journal of the Acoustical Society of America, 1999, 105, (5), pp. 2951-2957

CHAPTER III

In Vitro and *In Vivo* Assessment of Controlled Release and Degradation of Acoustically-Responsive Scaffolds

3.1 Introduction

Fibrin hydrogels are biomaterials that are commonly used in tissue engineering as a foundational matrix for tissue fabrication [1–3]. These hydrogels are formed via the enzymatic polymerization of fibrinogen in the presence of thrombin [4] and have many biological advantages versus other hydrogels. Fibrin plays a role in natural wound healing and can be derived from a patients own blood for the fabrication of autologous hydrogel scaffolds [5]. In addition, being a native protein based biomaterial, enzymatic degradation of fibrin hydrogels occur over time with minimal inflammatory response. The viscoelastic properties of fibrin based implants are relatively low compared to other biomaterials [6], which helps facilitate cellular migration and proliferation into the hydrogel.

Fibrin hydrogels can be seeded with cells and/or other molecular payloads such as proteins, genes, or drugs - that aid in tissue regeneration [7]. In a conventional fibrin matrix, passive diffusion of the entrapped payload yields a burst release [8]. This limits the ability to sustain release of the payload, unless the payload-scaffold affinity is increased (e.g., modification of fibrin using bioactive peptides [9]) or the payload diffusivity is decreased (e.g., incorporation of heparin [10-12], alteration

of crosslinking [13, 14]). Another method of limiting payload diffusivity is by encapsulating the payload into colloidal particles - such as liposomes, polymeric spheres, or emulsions which are then incorporated into fibrin [15]. However, payload release from these fibrin-colloid composites is still dominated by endogenous processes such as particle and/or scaffold degradation as well as payload diffusion.

During endogenous tissue regeneration, expression of bioactive molecules (e.g., growth factors (GFs)) is regulated both spatially and temporally [16, 17]. This has motivated the development of scaffolds where payload release can be modulated spatiotemporally. Control of payload release has been realized by designing particles that release payload in response to an externally modulated stimulus such as light, electricity, magnetic fields, temperature or microenvironmental factors like pH and enzymatic activity [10, 11, 18-24]. These active scaffolds (e.g., hydrogels that contain stimulus-responsive particles) and the means of interacting with them (i.e., modulating stimulus) provide increased control over the biochemical and mechanical microenvironment within the hydrogel. However, clinical translation of these active scaffolds has been hindered by issues related to biocompatibility, biodegradability, spatiotemporal targeting of the modulating stimulus, or penetration of the stimulus into the body [25, 26].

Ultrasound (US), in conjunction with sonosensitive particles, has been studied as a means of interacting with active scaffolds to achieve both spatial and temporal control exogenously [27, 28]. US can be applied non-invasively, focused with sub-millimeter precision, and reach deeply located implants. US-sensitive hydrogels can be fabricated by doping the scaffold with sonosensitive emulsions or microbubbles, the latter of which are used clinically for contrast enhanced US imaging [27, 29]. Possessing greater stability than microbubbles, sonosensitive emulsions are composed of nano- or micron-sized droplets, contain a liquid perfluorocarbon (PFC) core, and are stabilized by a surfactant shell. PFC emulsions typically contain

perfluoropentane (C_5F_{12}, 29°C boiling point) or perfluorohexane (C_6F_{14}, 56C boiling point) as the dispersed phase and are used because of their biocompatibility and inertness, a general characteristic of PFCs. In addition, sonosensitive emulsions can be formulated as double emulsions such that a payload, like a GF, is encapsulated within their inner aqueous phase [30-32]. Upon exposure to US, the PFC phase within each droplet of the emulsion vaporizes into a gas bubble in a process known as acoustic droplet vaporization (ADV) [33], thus releasing the encapsulated payload to the surrounding environment. Acoustically-responsive scaffolds (ARSs), comprising fibrin scaffolds doped with sonosensitive emulsion, are highly tunable since emulsion (e.g., structure, size), scaffold (e.g., density, geometry), and US properties (e.g., frequency, amplitude) can be easily modified [34]. Compared to approaches using unfocused, low-frequency (i.e., 20 kHz) US [35, 36], the use of focused, high frequency (i.e., $>$ 1 MHz) US to trigger ADV and payload release from an ARS could enable higher spatial resolution, even within deeply-located implants.

We have previously characterized the acoustic mechanisms occurring in ARSs and demonstrated, in a proof-of-concept *in vitro* study, that US can control the release of GF (i.e., basic fibroblast growth factor) contained in an ARS [27]. This work builds upon these previous publications and focuses on the impact of ARS and US properties on the controlled release of a surrogate payload (i.e., dextran) using *in vitro* and *in vivo* models. In addition, scaffold degradation of the ARSs is also characterized *in vitro* and *in vivo*, as well as scaffold morphology and vascular in-growth for ARSs.

3.2 Materials and Methods

3.2.1 Double Emulsion Preparation and Characterization

Double emulsions with a water-in-PFC-in-water (W_1/PFC/W_2) structure were prepared by modifying a previous method [30]. Briefly, a triblock fluorosurfactant,

consisting of Krytox 157FSH (CAS# 51798-33-5, DuPont, Wilmington, DE, USA) and polyethylene glycol (MW: 1000, CAS#: 24991-53-5, Alfa Aeser, Ward Hill, MA USA), was dissolved in 1g of perfluorocarbon (PFC) at 2% (w/w). The PFC phase consisted of perfluoropentane (subsequently referred to as C_5, CAS#: 678-26-2, Strem Chemicals, Newburyport, MA USA), perfluorohexane (subsequently referred to as C_6, CAS#: 355-42-0, Strem Chemicals), or a 1:1 (w/w) C_5:C_6 admixture. The PFC solution was then combined, in a 2:1 volumetric ratio, with an aqueous solution of Alexa Fluor 680-labeled dextran (MW: 10,000 Da, Life Technologies, Grand Island, NY USA) reconstituted at 0.625 mg/mL in Dulbecco's Phosphate-Buffered Saline (DPBS, Life Technologies). This concentration of dextran was chosen to prevent self-quenching of the fluorophore. The phases were sonicated (CL-188, QSonica, LLC, Newton, CT USA) for 30 seconds while on ice. The resulting primary emulsion, with a water-in-PFC (W_1/PFC) structure, was added drop wise to a solution of 50 mg/mL Pluronic F68 (CAS# 9003-11-6, Sigma-Aldrich, St. Louis, MO USA) in DPBS and stirred with a magnetic stir bar at 700 RPM for 2 minutes while on ice. The particle size of the resulting coarse double emulsion (W_1/PFC/W_2) was reduced using a homogenizer (T10, IKA Works Inc., Wilmington, NC USA). Emulsions with large and small droplet distributions were processed at 7.9 kRPM and 29.9 kRPM, respectively. Blank emulsions were prepared as described above with only DPBS as the W1 phase.

Emulsions were stored at 5°C for 30 minutes and characterized with a Coulter Counter (Multisizer 4, Beckman Coulter, Brea, CA USA) in the range of 1-30 μm. The encapsulation efficiency of the emulsions, defined as the amount of dextran encapsulated in the emulsion divided by the amount of dextran initially loaded into the emulsion, was determined by breaking diluted emulsion in a vacuum oven (23^{circ}C, Isotemp Vacuum Oven Model 282A, Pittsburgh, PA USA). The ADV threshold of each emulsion formulation was determined using a previously described

method [34]. The structure, composition, and physical parameters of all double emulsion formulations used in this study are listed in Table 1.

3.2.2 ARS Fabrication

ARSs were prepared using 10 mg/mL clottable protein by first combining bovine fibrinogen (Sigma-Aldrich, 75% total protein, 96% clottable protein) - dissolved in degassed (36% O^2 saturation) Dulbeccos modified Eagles medium (DMEM, Life Technologies) - with bovine thrombin (20 U/mL, Thrombin-JMI, King Pharmaceuticals, Bristol, TN, USA), 0.025 U/mL aprotinin (Sigma-Aldrich), and 1% (v/v) emulsion. For *in vitro* studies, 0.5 mL aliquots of the ARS mixture were added into each well of a 24 well BioFlex plate (Flexcell International, Burlington, NC, USA) and allowed to polymerize for 30 min at room temperature. Each ARS was then covered with 0.5 mL of overlying media, consisting of DMEM supplemented with 100 U/mL penicillin and 100 μg/mL streptomycin. The ARSs were placed in a humidified incubator at 37C with 5% carbon dioxide between US exposures.

Table 3.1: Physical parameters of emulsions used to dope the acoustically responsive scaffolds (SEM: standard error of the mean).

PFC	Distribution Size	Payload	Number Weighted Mean Diameter (μm)	Volume Weighted Droplet Concentration (#/mL)	Droplet Concentration (#/mL)	ADV Threshold (MPa)	Encapsulation Efficiency (%)
100% PFP	Large	AF680	3.5 ± 0.1	21.2 ± 0.5	1.0E+10 ± 2.2E+08	1.7 ± 0.2	82.5 ± 7.8
	Small	AF680	3.0 ± 0.1	11.8 ± 0.2	7.4E+10 ± 8.2E+08	1.9 ± 0.1	50.1 ± 9.9
1:1 PFP:PFH	Large	AF680	3.4 ± 0.1	20.8 ± 0.4	1.5E+10 ± 2.2E+08	2.1 ± 0.1	72.7 ± 5.1
	Small	AF680	2.9 ± 0.1	10.7 ± 0.1	1.1E+11 ± 6.6E+08	2.3 ± 0.1	67.4 ± 3.7
100% PFH	Large	AF680	3.5 ± 0.1	21.5 ± 0.9	2.3E+10 ± 2.2E+09	2.5 ± 0.1	75.9 ± 2.0
	Small	AF680/DPBS	2.8 ± 0.1	10.6 ± 0.1	1.0E+11 ± 6.3E+08	2.7 ± 0.1	70.0 ± 8.6

3.2.3 US Exposure

All acoustic exposures were conducted using the following setup. A calibrated transducer (2.5 MHz, H108, f-number = 0.83, focal length = 50 mm, Sonic Concepts, Inc., Bothell, WA USA) was driven by pulsed waveforms generated using a dual channel function generator (33500B, Agilent Technologies, Santa Clara, CA USA),

amplified by a gated radio frequency amplifier (GA-2500A Ritec Inc, Warwick, RI USA), and passed through a matching circuit (H108_3MN, Sonic Concepts) to reduce impedance between the transducer and amplifier (Figure 3.1 (a-I)). Waveform gating was realized using the second channel of the function generator. All generated and amplified signals were monitored with an oscilloscope (HDO4034, Teledyne LeCroy, Chestnut Ridge, NY USA). All acoustic exposures were done with the following parameters unless otherwise stated: 8 MPa peak rarefactional pressure, 13 acoustic cycles, and 100 Hz pulse repetition frequency (PRF).

3.2.4 *In Vitro* Controlled Release of Dextran

For controlled release experiments, the BioFlex plate containing the ARSs was placed in a tank of degassed water (30-36% O^2 saturation) at 37°C such that only the bottom half of the plate was submerged, as shown in Figure 3.1 (a). The single element US transducer was positioned under the plate such that the axial focus was located at mid-height of the ARS. The bottom of each well in the plate consisted of a silicone elastomer membrane, which based on a thickness of 1 mm, attenuates the US by less than 2% [37]. During US exposure, the transducer was rastered across the entire ARS for 2 min. Three US exposure conditions were explored: no US, a single US exposure one day after polymerization, and daily US for a period of 6 days beginning one day after polymerization. To quantify the amount of dextran released, 50% of the overlying media was collected and replaced with an equal volume of fresh media immediately after every US exposure. The concentration of dextran in the media was measured with a fluorometer (Molecular Devices Spectramax M2e, Sunnyvale, CA USA, 679 nm EX/ 702 nm EM). As a comparison, the release of dextran incorporated directly in fibrin scaffolds with and without any blank emulsion - was also measured.

3.2.5 *In Vitro* Fibrin Degradation

ARSs were prepared in 24-well BioFlex plates as described previously except with blank C_6 emulsion and Alexa Fluor 647-labeled fibrinogen (Molecular Probes). The final concentration of labeled fibrinogen in each ARS was 0.125 mg/mL; this concentration was chosen to prevent self-quenching of the labeled fibrinogen. The ARSs were exposed to US (as described in Section 2.4) and incubated between US exposures. To quantify the amount of fibrin degradation 50% of the media was collected and replaced with fresh media after every US exposure. The concentration of labeled fibrinogen in the media was measured with a fluorometer (650 nm EX/ 668 nm EM). As a control, fibrin scaffolds without emulsion but with labeled fibrinogen were prepared, and their degradation was quantified similarly.

3.2.6 *In Vivo* Controlled Release of Dextran

This *in vivo* research was conducted with approval of the Institutional Animal Care & Use Committee at the University of Michigan. Female BALB/c mice (n = 22, 18-21 g, Charles River Laboratories, Wilmington, MA, USA) were anesthetized with isoflurane (5% for induction and 1.5% for maintenance). The lower dorsal hair was removed by shaving and depilatory cream (Nair, Church & Dwight Co, Ewing, NJ USA); the skin was sterilized with betadine surgical scrub (Purdue Products L.P., Stamford, CT USA). The ARS mixture (0.25 mL per implant) was then injected subcutaneously using a 20 gauge needle (Becton Dickinson, Franklin Lakes, NJ, USA) at two locations with the dorsal region and allowed to polymerize for 2 minutes prior to removal of the needle. The ARS mixture contained 1% (v/v) dextran-loaded emulsion with either 1:1 C_5:C_6 or C_6 as the PFC phase. The mice were allowed to recover following implantation. Fibrin scaffolds without emulsion, but containing dextran, were injected as control implants. Blank scaffolds (i.e., without emulsion and dextran) were injected as sham controls.

Figure 3.1(b) shows the experimental setup used for all *in vivo* studies. Each mouse was anesthetized with isoflurane and placed in a prone position. US coupling gel (MediChoice, Owens & Minor, Mechanicsville, VA USA) was applied to the implant region. A coupling cone (C106, Sonic Concepts) was placed on the US transducer, filled with degassed water (30-36% O^2 saturation), and the water was sealed in by Tegaderm film (3M Health Care, St. Paul, MN USA). The transducer was rastered across the implant for 2 min. For each mouse, US was applied daily to only one scaffold beginning one day after implantation for a period of 10 days. The scaffolds receiving US treatment (i.e., left or right implant) were randomized for all mice.

3.2.7 *In Vivo* Fibrin Degradation

ARSs containing 1% (v/v) blank emulsion, with C_6 as the PFC phase, and labeled fibrinogen (0.125 mg/mL) were prepared, injected into female BALB/c mice (n = 10), and exposed to US as described in sections 2.5 and 2.6. Fibrin scaffolds without emulsion, but containing labeled fibrinogen, were injected as control implants. Blank scaffolds (i.e., without emulsion and labeled fibrinogen) were injected as sham controls.

3.2.8 IVIS Imaging

The mice were anesthetized with isoflurane and imaged with an IVIS Spectrum Preclinical *In Vivo* Imaging System (Perkin Elmer, Houston, TX USA) at the University of Michigan Center for Molecular Imaging to quantify the fraction of dextran or fibrinogen released from the implants [38]. The mice were imaged on day 0 (i.e., the day of implantation), 1 (i.e., the first day of US exposure), 2, 3, 4, 7, and 10. On days 1-10, the mice were imaged after US exposure. For the dextran release study, the fluorophore signal was collected using an excitation filter of 675 nm and emission filters ranging from 720 to 780 nm. To account for autofluorescence, a

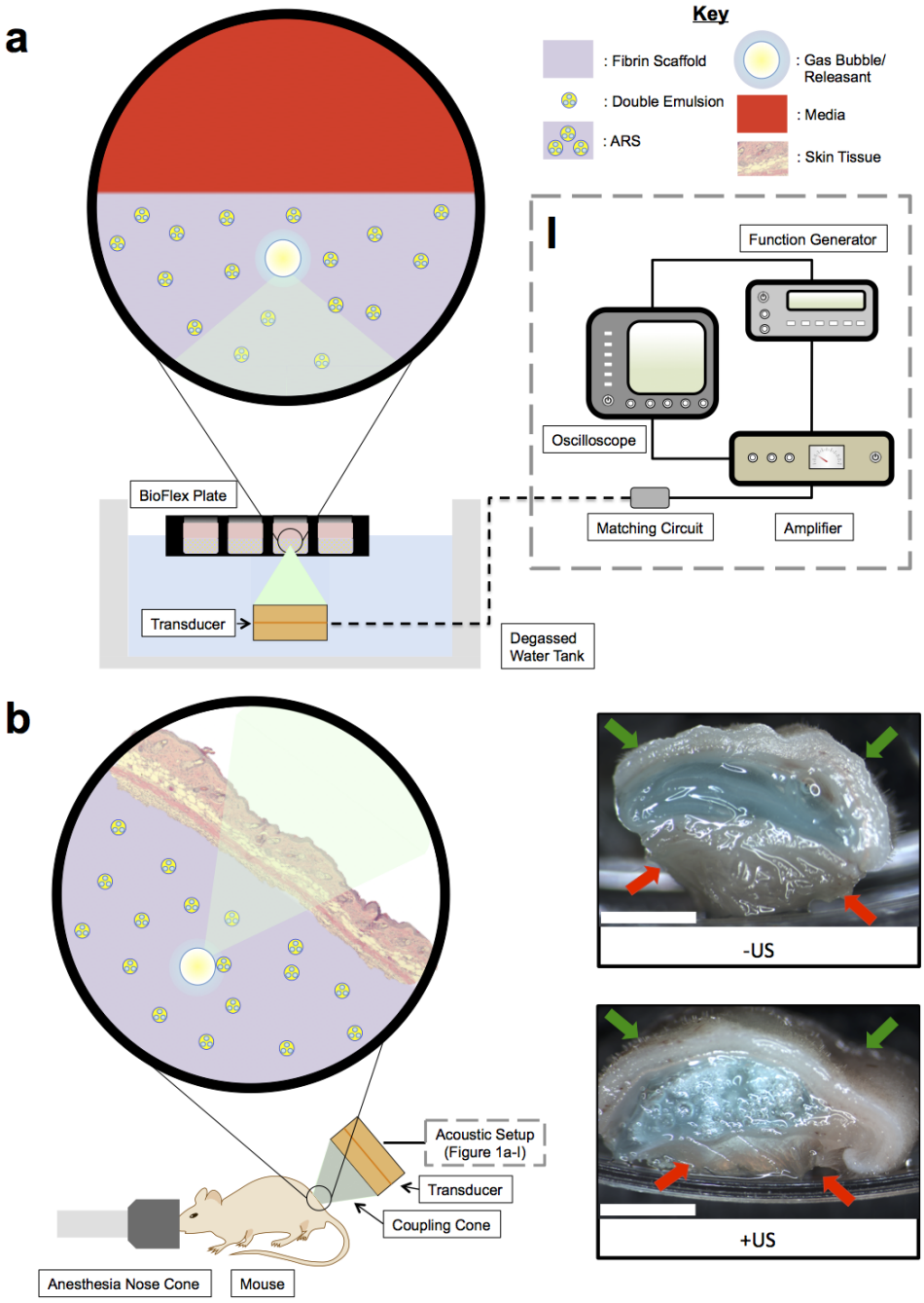

Figure 3.1: *In vitro* and (b) *in vivo* setups for US exposure. The equipment used to drive the transducer is depicted in (a-I). (b) Right: Macroscopic images of ARSs containing blank C6 emulsion and AF647-labeled fibrinogen (blue). The ARSs were harvested 3 days after subcutaneous implantation. Gas bubbles, produced when the US vaporizes the emulsion within the ARS, is evident for the +US condition. The skin surface and underlying muscle are indicated by the green and red arrows, respectively. Scale bar = 0.5 cm.

sequence of background signals was collected using an excitation filter of 605 nm and emission filters ranging from 660 to 780 nm. For the fibrin degradation study, the fluorophore signal was collected using an excitation filter of 640 nm and emission filters ranging from 680 to 740 nm. To account for autofluorescence, a sequence of background signals was collected using an excitation filter of 570 nm and emission filters ranging from 620 to 740 nm. Spectral unmixing was performed on the dextran and fibrinogen data sets in Living Image software (Perkin Elmer), according to the manufacturers instructions, using the fluorophore and autofluorescence (background) images. Following unmixing, equally sized regions of interest (ROIs, 1.25 cm diameter) corresponding to each implant, were drawn and the average radiant efficiency ([photons/s/cm^2/sr]/[μW/cm^2]) was calculated. For each implant, the average radiant efficiency on days 1-10 was normalized by the day 0 measurement, thus accounting for any differences in the amount of fluorophore initially loaded.

3.2.9 Histology

For the *in vivo* fibrin degradation study, mice were euthanized on day 3 and day 10 post implantation. ARSs were retrieved and fixed overnight in aqueous buffered zinc formalin (CAS# 50-00-0, Formalde-Fresh, Fisher Scientific). Implants were then transferred to 70% ethanol until they were processed and embedded in paraffin at the University of Michigan Microscopy & Image Analysis Laboratory. The paraffin-embedded tissues were cut into 5 μm thick serial sections and placed on pre-cleaned glass slides (Fisherbrand Superfrost Plus, Fisher Scientific) for histological analysis. Tissue sections were stained with Modified Harris Formulation hematoxylin (Ricca Chemical Company, Arlington, TX USA) and aqueous eosin Y solution (0.25% (w/v) in 57% (v/v) alcohol, Sigma-Aldrich) (H&E) to visualize the overall tissue morphology. Immunostaining of mice-derived blood vessels was performed using a rabbit anti-mouse CD31 primary antibody (ab28364, Abcam, Cambridge, MA USA) combined with a goat anti-rabbit secondary labeled polymer-horseradish peroxidase

conjugate (Envision+ System-HRP (DAB), Dako North America, Inc., Carpinteria, CA USA), as described previously [39, 40]. Negative controls, involving staining with a rabbit IgG polyclonal isotype control (ab27478, Abcam) as the primary antibody or staining with the secondary antibody only, confirmed the specificity of the CD31 staining. Tissue sections were visualized and photographed with a Leica DMRB light microscope (Leica Microsystems, Inc., Buffalo Grove, IL USA). Three tissue sections from each implant - with five images per tissue section - were analyzed manually for blood vessel formation per unit area. Blood vessel counting was done, in a blinded manner, by three separate individuals. Blood vessels were identified in CD31-stained tissues at 20x magnification by defined lumens and complete enclosure of the lumen.

3.2.10 Statistics

All statistical analyses were performed using GraphPad Prism software (GraphPad Software, Inc., La Jolla, CA USA). All data is expressed as the mean ± standard error of the mean of measured quantities. All n-values are listed below each corresponding figure. The 95% confidence intervals of slopes are listed in the format S [S_L, S_H], where S is the average slope, S_L is the lower bound slope, and S_H is the upper bound slope. Statistically significant differences of all other data sets were determined with a Students t-test corrected for multiple comparisons using the Holm-Sidak method, with differences deemed significant for $p < 0.05$.

3.3 Results

3.3.1 Emulsion Properties

As listed in Table 1, each large emulsion displayed a larger mean droplet diameter and smaller number concentration compared to the small emulsion for a given PFC core. A higher ADV threshold was observed for the small C_6 emulsion when compared to the large C_6 emulsion, while the large C_5 emulsion had a higher payload

encapsulation efficiency compared to the small C_5 emulsion. The droplet number concentration and ADV threshold correlated with the fraction of C_6 in the PFC core while the mean droplet diameter correlated inversely. Example droplet distributions, comparing small and large emulsions, are shown in Figure 3.2(a).

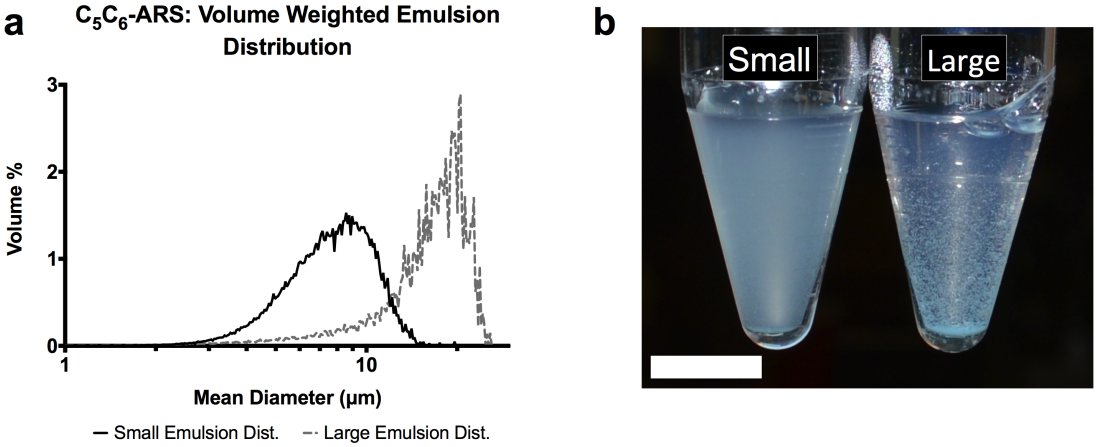

Figure 3.2: (a) The volume weighted size distributions of two C_6 emulsion populations small and large. The different size distributions were obtained by varying the rotational speed of the homogenizer following the second emulsification step. (b) Image of C_6-ARSs with small (left) and large (right) emulsions 1 min after polymerization. The small emulsion is evenly dispersed in the ARS while some settling is observed for the large emulsion. Scale bar = 1 cm.

3.3.2 *In Vitro* Controlled Release of Dextran from ARSs

With US applied daily beginning on day 1, Figure 3.3(a,b) shows that the amount of dextran released from a C_5/C_6-ARS with large emulsion correlated with acoustic pressure and PRF. The acoustic condition that yielded the greatest release was 8 MPa and 100 Hz PRF (40.0 ± 0.8% released by day 6). This acoustic condition was used for all subsequent studies. Comparatively, US exposures at 3 MPa and 100 Hz PRF or 8 MPa and 10 Hz PRF yielded 13.2 ± 0.7% and 29.6 ± 0.7% release by day 6, respectively. The negative control (i.e., -US) exhibited 3.8 ± 0.7% payload release by day 6.

The release profiles of ARSs with varying emulsion formulations (i.e., C_5-ARS, C_5/C_6-ARS, and C_6-ARS) and emulsion sizes (i.e., large and small) are shown in

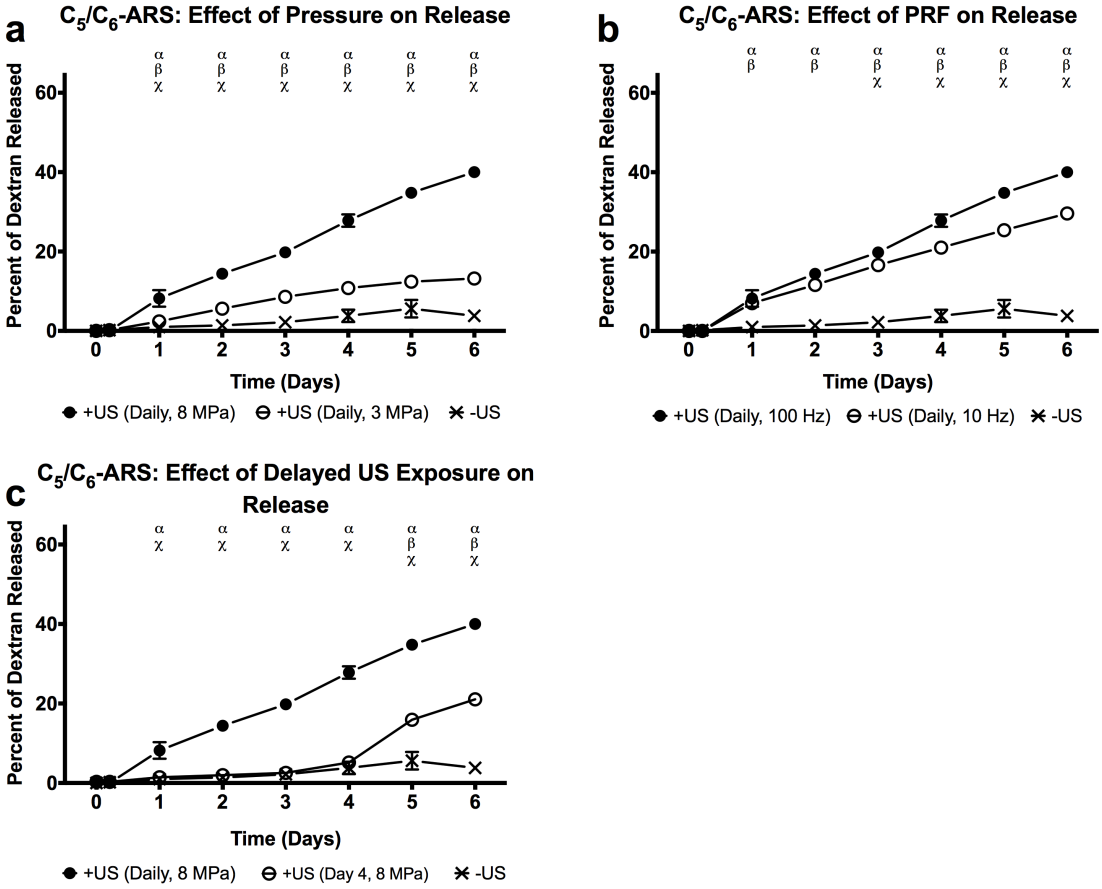

Figure 3.3: Effect of acoustic pressure (a) and PRF (b) on the release profiles of a C_5/C_6-ARS. US exposure was done at 2.5 MHz and 13 acoustic cycles for a period of 2-min/scaffold. For (a), the PRF was 100 Hz and for (b) the pressure was 8 MPa. All data is represented as mean ± standard error of the mean for n = 5 scaffolds. Statistically significant differences (p ¡ 0.05) are denoted as follows. α: +US (daily, 8 MPa) vs. US; β: +US (daily, 3 MPa) versus US; χ: +US (daily, 8 MPa) versus +US (daily, 3 MPa).

Figure 3.4(a-b) and Figure 3.5(a-d). Three acoustic exposures were explored: -US, +US (day 1 only), and +US (daily beginning on day 1). Without US exposure, no statistically significant differences were observed between ARSs with small and large emulsions (for the same PFC type) by day 6. However the release from C_5-ARSs was statistically higher than both C_5/C_6-ARS, and C6-ARS on day 6 in the absence of US.

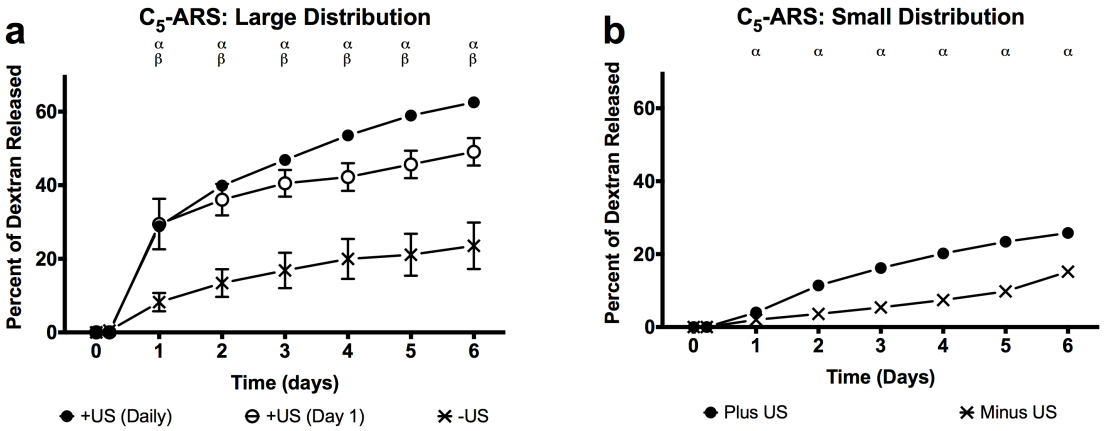

Figure 3.4: *In vitro* release profiles for C_5-ARSs with (a) large and (b) small emulsions. All ARSs contained emulsified dextran and were exposed to one of the following acoustic conditions: -US, +US (day 1 only), and +US (daily beginning on day 1). For all experimental conditions, US exposure was done with the same setup/parameters described in Methods. All ARSs had a fibrin concentration of 10 mg/mL and a volume of 0.5 mL. All data is represented as mean ± standard error of the mean for n = 5 scaffolds. Statistically significant differences (p ¡ 0.05) are denoted as follows. α: +US (daily) vs. US; β: +US (day 1) vs. US; χ: +US (daily) vs. +US (day 1).

In the presence of US, the amount of dextran released correlated inversely with the amount of C_6 in the PFC core of the emulsion and directly with the number of US exposures. With the large emulsion, a single US exposure (i.e., +US on day 1) produced 20.1 ± 1.5% and 12.1 ± 1.5% dextran release for C_5/C_6-ARS and C_6-ARS by day 6, respectively, while daily US exposure yielded 38.6 ± 1.6% and 22.2 ± 1.3% dextran release by day 6, respectively. For the small emulsion, daily US exposure produced 23.0 ± 1.8% and 14.8 ± 0.4% dextran release for C_5/C_6-ARS and C_6-ARS, respectively. For C_5/C_6-ARS and C_6-ARS with large emulsions, both +US

conditions were statistically different from US starting on day 1, while differences between the two +US exposure conditions began on day 2. For the small emulsions, there were significant differences between +US (daily) and US starting on day 1 for C_5/C_6-ARS and day 2 for C_6-ARS. The greatest release was observed with C_5-ARS with 15.2 ± 1.0% and 23.5 ± 6.3% release by day 6 for small and large emulsions, respectively. Significant differences between each distributions ±US conditions started on day 1.

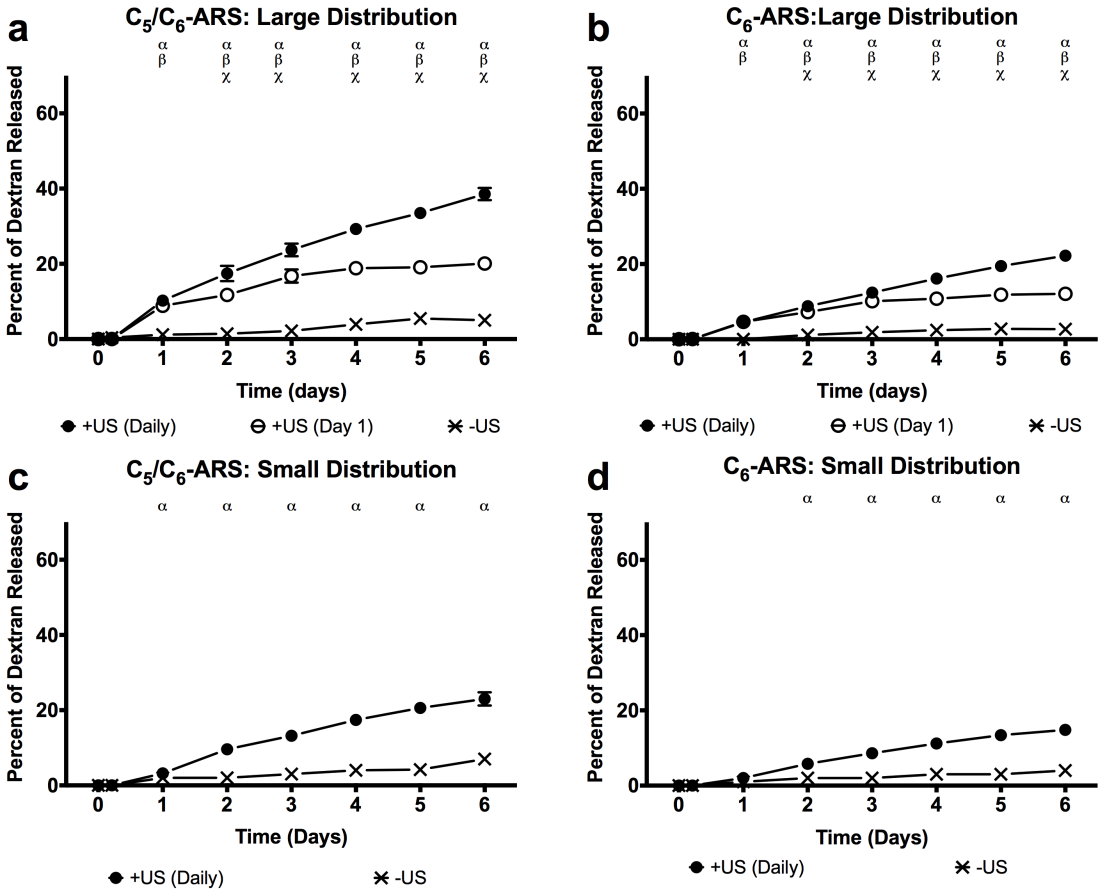

Figure 3.5: *In vitro* release profiles for (a) C_5/C_6-ARSs and (b) C_6-ARSs with large emulsions as well as (c) C_5/C_6-ARSs and (d) C_6-ARSs with a small emulsions. All ARSs contained emulsified dextran and were exposed to one of the following acoustic conditions: US, +US (day 1 only), and +US (daily beginning on day 1). For all experimental conditions, US exposure was done with the same setup/parameters described in Section 2.3. All data is represented as mean ± standard error of the mean for n = 5 scaffolds. Statistically significant differences ($p < 0.05$) are denoted as follows. α: +US (daily) vs. US; β: +US (day 1) vs. US; χ: +US (daily) vs. +US (day 1).

3.3.3 *In vitro* Enhanced Release of Dextran from Fibrin

Figure 3.6(a) shows that US increased the release of non-encapsulated dextran from a conventional fibrin gel (i.e., without emulsion). Burst release of the dextran was clearly observed on day 1 (i.e., 1 day after polymerization) with 64.0 ± 1.8, 72.0 ± 0.7, and 72.2 ± 0.5% released for US, +US (day 1 only), +US (daily), respectively). Thus, exposure to US generates an additional 8.3 ± 0.1% (absolute) release of dextran for both +US conditions relative to US. By day 6, the maximum amount of dextran released for the three conditions was 88.2 ± 1.2% (-US), 96.6 ± 1.1 (+US day 1 only), and 99.9 ± 0.1 (+US daily). Both +US conditions were statistically different from the -US case starting on day 1 and were different from each other starting on day 2.

3.3.4 Effect of US on *In Vitro* Fibrin Degradation of Fibrin and ARSs

The rate of fibrin degradation in the ARSs was also measured (Figure 3.6(b)). By day 6, 44.3 ± 0.8% of the C6-ARS was degraded for the +US condition while 38.4 ± 0.3% of the C_6-ARS was degraded for the - US condition. Significant differences were observed between ±US for ARSs starting on day 1. By comparison, for fibrin gels (i.e., without emulsion), 37.0 ± 0.3% and 34.8 ± 0.7% degradation was observed by day 6 for the US and +US conditions, respectively, with significant differences observed starting on day 2 (data not shown).

3.3.5 *In Vivo* Controlled Release of Dextran and Fibrin Degradation from ARSs

For *in vivo* studies, dextran release from the subcutaneously implanted scaffolds was monitored longitudinally with whole body fluorescence imaging. We hypothesize that upon release of the dextran from the scaffold, the dextran diffused into the local microvasculature and lymphatic vessels [41] and then was ultimately cleared

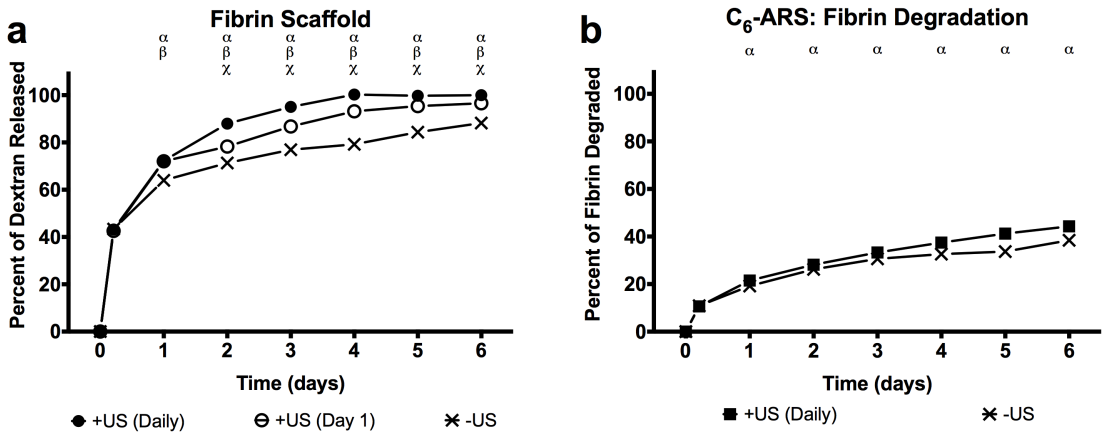

Figure 3.6: (a) *In vitro* release profiles of non-encapsulated dextran in a fibrin scaffold exposed to one of the following acoustic conditions: US, +US (day 1 only), and +US (daily beginning on day 1). (b) Fibrin degradation of ARSs with and without US (daily beginning on day 1). For all experimental conditions, US exposure was done with the same setup/parameters described in Section 2.3. All data is represented as mean ± standard error of the mean for n = 5 scaffolds. Statistically significant differences (p ¡ 0.05) are denoted as follows. α: +US (daily) vs. US; β: +US (day 1) vs. US; χ: +US (daily) vs. +US (day 1).

by the systemic circulation. The clearance caused a decrease in fluorescence signal within the ARS, which was quantified via imaging. Figure 3.7 shows longitudinal photographs and fluorescence images of mice with implanted C_5/C_6- and C_6-ARSs. Over the 10 day study, the ARSs exhibited a slight volumetric expansion, which was more clearly evident for the C_5/C_6-ARSs. Additionally, the fluorescence signal within the ARS exposed to US decreased qualitatively faster than the sham (i.e., -US) ARS, thus indicating greater dextran release from the +US condition.

Using ROIs corresponding to each implant, the fluorescence images were quantified to obtain the *in vivo* release profiles for C_5/C_6-ARS and C_6-ARS (Figure 3.8(a,b)). Since *in vitro* results demonstrated that daily US exposure yielded greater dextran release than a single US exposure, two acoustic conditions were evaluated *in vivo*: -US and +US (daily beginning on day 1). Figure 3.8(a) shows that a large fraction of the dextran payload was released from the C_5/C_6-ARSs on day 1 for the +US condition (74.1 ± 2.2%); comparatively, 55.1 ± 1.5% was released on day 1 for

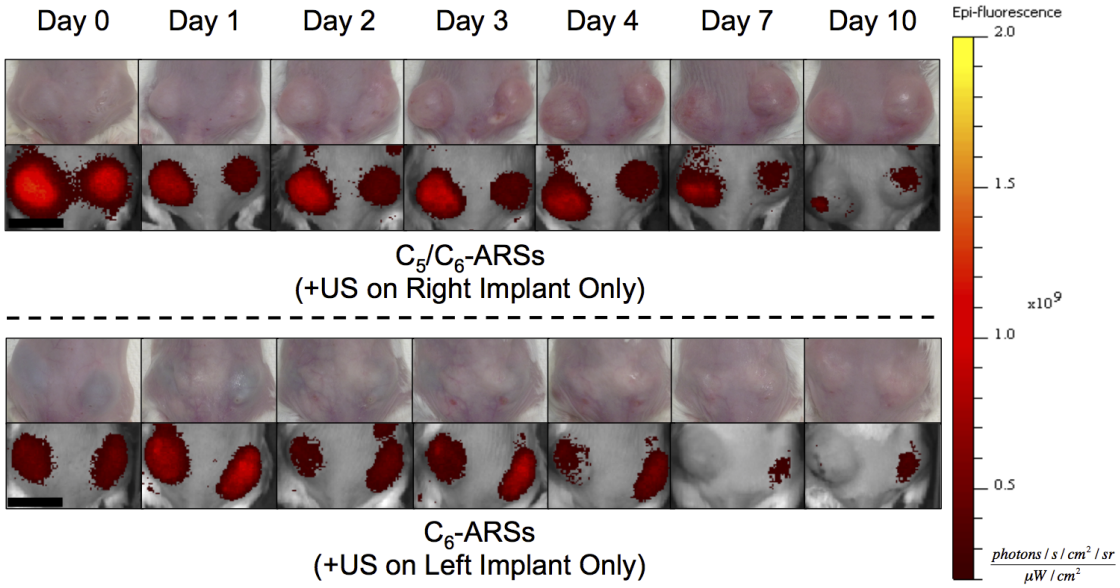

Figure 3.7: Longitudinal images, visible and fluorescence, of two mice each with two subcutaneously implanted ARSs (top: C_5/C_6-ARSs, bottom: C_6-ARSs). The ARSs were implanted on day 0 and US applied daily starting on day 1 to the right (C_5/C_6-ARSs) or left (C_6-ARSs) implant. The colormap is quantitatively indicative of the dextran concentration remaining in the ARS. Scale bar = 1 cm.

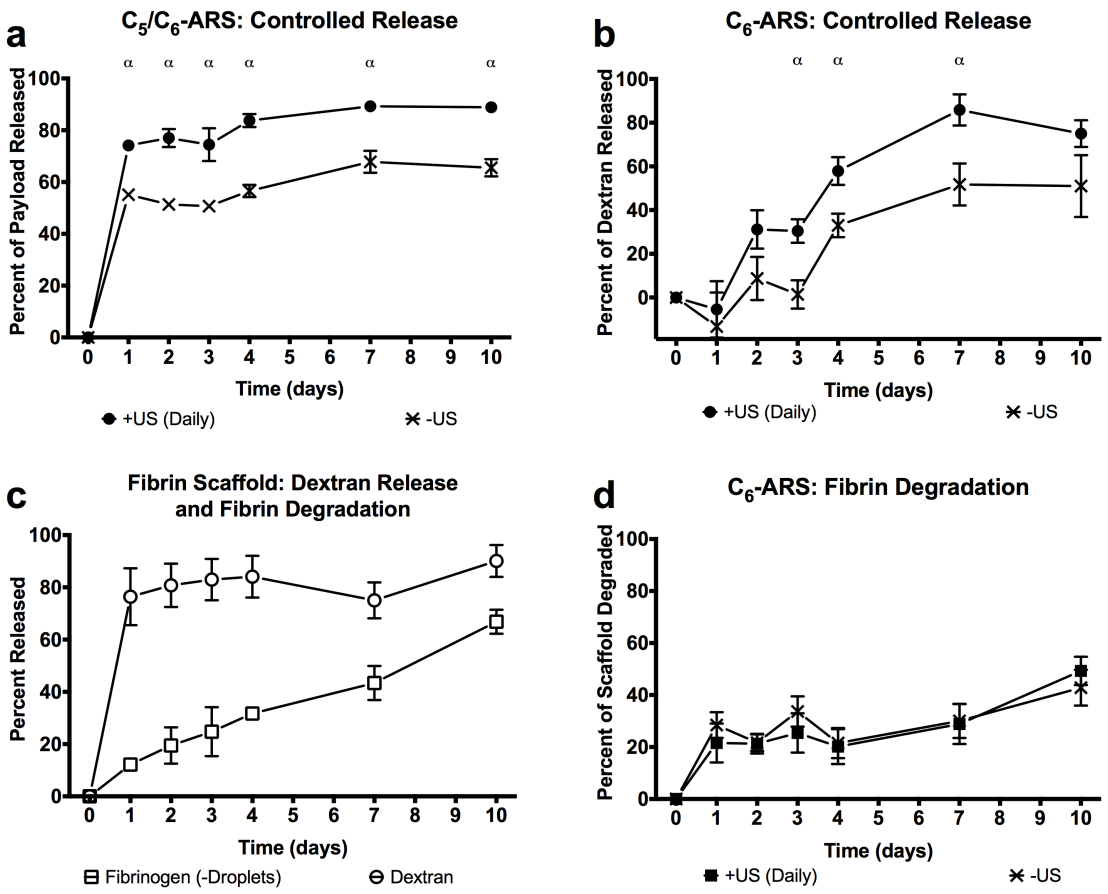

Figure 3.8: *In vivo* release profiles of dextran from (a) C_5/C_6-ARSs with a small emulsion, (b) C_6-ARSs with a small emulsion, or (c) fibrin scaffolds. The scaffolds contained emulsified (a, b) or non-emulsified (c) dextran. *In vivo* fibrin degradation of (c) fibrin and (d) ARSs with blank C_6 emulsion. ARSs were exposed to +US (daily beginning on day 1) or US using the same setup/parameters described in Section 2.3. All ARSs had a fibrin concentration of 10 mg/mL, were implanted one day prior to the first acoustic exposure, and had a volume of 0.25 mL. All data is represented as mean ± standard error of the mean for n = 11 (a, b), n = 4 (c), and n = 10 (d) implants/condition. Statistically significant differences (p ¡ 0.05) are denoted as follows. α: +US (daily) vs. US.

the -US condition. By day 10, the total dextran released was 88.9 ± 0.8% and 65.5 ± 3.3% for +US and US, respectively. For C_6-ARSs (Figure 3.8(b)), significant dextran release in response to US was first observed on day 2 (31.1 ± 8.8%), with greater release for +US versus US occurring between days 3 and 7. Unlike the C_5/C_6-ARSs, a burst release was not observed for US on day 1. Between days 0 and 3, release from the US was not statistically different than zero (p = 0.6, slope: 2.6 [-17.4, 22.7]). By day 4, non-selective (i.e., -US) payload release started to occur, with US and +US conditions yielding 33.0 ± 5.4% and 57.9 ± 6.4% released, respectively. By day 10, 51 ± 14.2 and 75.0 ± 6.1% release was observed for the US and +US conditions, respectively.

The release profile of non-encapsulated dextran, contained within fibrin scaffolds, is displayed in Figure 3.8(c). Similar to the *in vitro* results with non-encapsulated dextran (Figure 3.6(a)), significant burst release occurred within the first day after in situ polymerization (76.4 ± 5.4%). This *in vivo* burst release was greater than that observed *in vitro* for all tested conditions. The total amount of payload released by day 10 was 90.1 ± 3.1%, which was less than that observed *in vitro* for all tested conditions on day 6.

The degradation rate for the implanted fibrin scaffolds, evaluated using fluorescence imaging, is also shown in Figure 3.8(c). In the absence of US, 66.8 ± 2.3% degradation was observed by day 10. Comparatively, the degradation rate for C_6-ARSs is displayed in Figure 3.8(d). No differences were observed between US and +US in terms of degradation rate (p = 0.4, slope of US: 2.8 [-0.1, 5.7], slope of +US: 3.6 [1.5, 5.8]) or the amount of ARS degraded at any time point. By day 10, the fraction of degradation was 42.8 ± 6.9% and 49.3 ± 5.4% for US and +US, respectively. Thus, at 10 days after implantation, ARSs were less degraded than fibrin scaffolds of equal fibrin concentration.

3.3.6 Morphology and Vascularization of Implanted ARSs

H&E images of fibrin and C_6-ARS implants are displayed in Figure 3.9. All implants appeared similar on day 0, with no cell invasion and implant degradation. Cellular infiltration was observed on days 3 and 10 for both fibrin and ARSs. For ARSs, there was a difference in morphology between the ±US conditions 3 days after implantation. The +US ARS had large ruptures within the scaffold, presumably caused by droplet vaporization induced by the US exposures beginning on day 1. The morphology of the US ARS condition began to approach that of the +US ARS condition 10 days after implantation, as is seen with the gas pocket observed in the H&E section (Figure 3.9, Day 10-II). This finding was consistent with the release observed for the -US condition for C_6-ARS (Figure 3.8(b)) and the measured fibrin degradation (Figure 3.8(d)).

As seen in Figure 3.10, blood vessel in-growth into the fibrin and ARS implants was evaluated immunohistochemically. As expected, no blood vessels were observed in any scaffold on day 0. Blood vessels were observed in the scaffolds beginning on day 3, with a higher density and larger vessels evident by day 10. Blood vessel density (i.e., number of blood vessels per area) within each scaffold is quantified in Figure 3.11. Blood vessel density increased from day 3 (1.3 ± 0.5, 8.4 ± 7.1, and 16.9 ± 8.8 vessels/mm^2) to day 10 (25.5 ± 4.5, 62.1 ± 12.3, and 73.8 ± 7.1 vessels/mm^2) for fibrin, -US ARSs, and +US ARSs, respectively. On day 10, the blood vessel density within an ARS exposed to US was significantly higher than in a fibrin scaffold. Although not statistically significant ($p = 0.057$), blood vessel density in the US ARSs was trending higher than in fibrin.

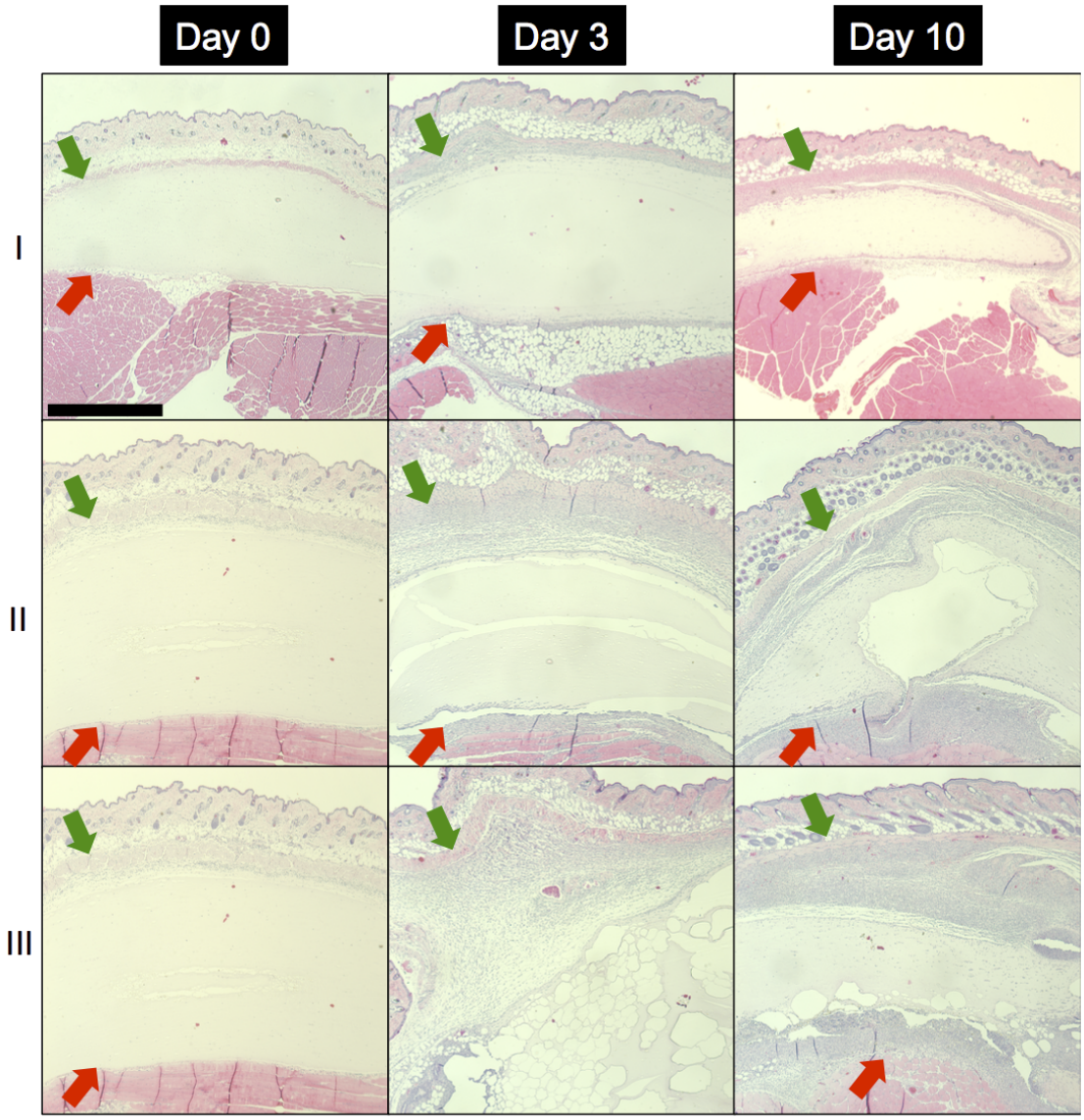

Figure 3.9: H&E images of implanted (I) fibrin scaffolds, (II) ARS not exposed to US (i.e., US), and (III) ARS exposed to daily US beginning on day 1 (i.e., +US) on days 0, 3, and 10 at 5 magnification. The ±US images of the ARSs are from contralateral implants within the same mouse. The green and red arrows denote the skin/implant interface and implant/(adipose or muscle) interface, respectively. Scale bar = 1 mm.

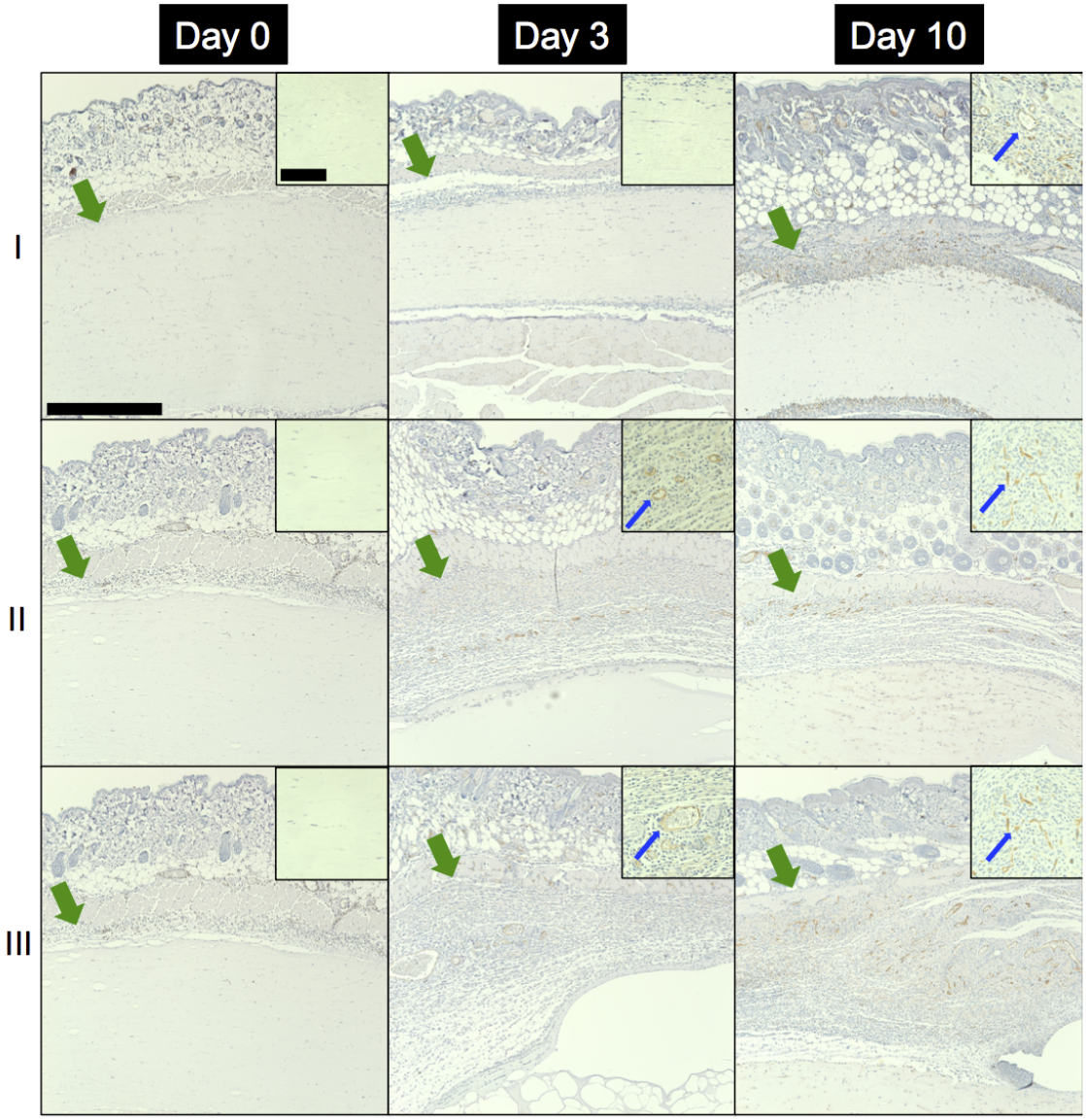

Figure 3.10: CD31 images with hematoxylin counterstain of implanted (I) fibrin scaffolds, (II) C_6-ARSs not exposed to US (i.e., US), and (III) C_6-ARSs exposed to daily US (beginning on day 1 (i.e., +US)) on days 0, 3, and 10 at 10x magnification. The ±US images of the ARSs are from contralateral implants within the same mouse. Inset images (63x magnification) are zoomed in within the implant to highlight blood vessel invasion, or lack thereof. The green arrows denote the skin/implant interface while the blue arrows denote blood vessels. Large scale bar = 0.5 mm and the small scale bar = 0.1 mm.

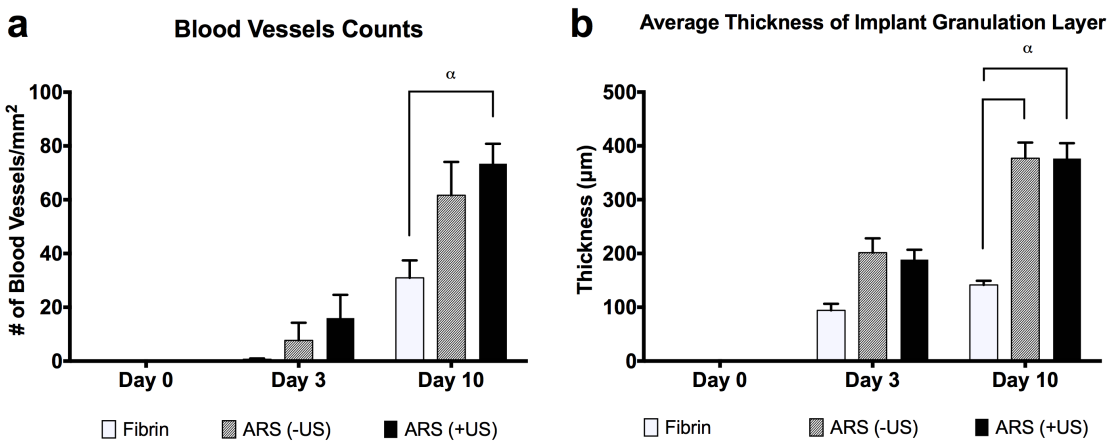

Figure 3.11: Quantification of (a) blood vessel density from CD31-stained images and (b) granulation layer thickness from H&E stained images of fibrin scaffolds, C_6-ARSs not exposed to US (i.e., US), and C_6-ARSs exposed to daily US beginning on day 1 (i.e., +US). All data is represented as mean ± standard error of the mean for n = 9. a denotes statistically significant differences ($p < 0.05$).

3.4 Discussion

We have demonstrated how US can be used to modulate the release of a surrogate payload (i.e., dextran) encapsulated within an ARS. Various acoustic parameters have been shown to affect the ADV threshold (i.e., the lowest acoustic pressure at which ADV begins to occur) and efficiency (i.e., the fraction of droplets that vaporize at a given acoustic pressure) of sonosensitive emulsions and ARSs [34]. For example, ADV thresholds correlate inversely with US pulse duration, insonation frequency, and PRF [33, 34] while ADV efficiency correlates with acoustic pressure [32, 42]. Figure 3.3 and Figure 3.5 show that payload release which is directly related to ADV efficiency - correlated with acoustic pressure, PRF, and number of US exposures for both small and large emulsions.

The tunable responsiveness of ARSs is enhanced further when ARS parameters (e.g., matrix stiffness, emulsion surfactant, emulsion size, composition of the PFC core) are modified [34]. We previously demonstrated that the ADV threshold correlated with fibrin density and the bulk boiling point of the PFC core in the

emulsion [34] while ADV efficiency correlated inversely with fibrin density for a fixed acoustic amplitude [27]. In this study, the ADV thresholds of the ARSs (Table 1) correlated with the fraction of C_6 in the PFC core and correlated inversely with droplet diameter (for C_6 only). The acoustic pressure used for all release experiments (except Figure 3.3a) was 8 MPa, which was significantly higher than the measured ADV thresholds. However complete payload release in response to US was not observed for any of the ARSs, either *in vitro* or *in vivo*, despite complete exposure of the ARSs to US. This is likely a consequence of the polydisperse size distribution of the emulsions used in the ARSs (Figure 3.2a). Since the ADV threshold correlates inversely with droplet diameter [43-45], larger droplets are more likely to undergo ADV, which can decrease the ADV efficiency generated by subsequent US exposures due to the increase in attenuation caused by the formed bubbles. The use of monodispersed emulsions, which have the same ADV threshold [46, 47], and tighter spatial control of US application could increase the maximum release achievable.

Retention of payload within the ARS (i.e., in the absence of US) is crucial in order to achieve on-demand, controlled release using US. In the absence of US, all ARS formulations displayed significantly better payload retention than non-emulsified dextran contained within fibrin (Figure 3.6(a), Figure 3.8(c)). Payload retention in ARSs correlated with the fraction of C_6 in the emulsion for both *in vitro* and *in vivo* results; for a given PFC core, droplet size did not affect payload retention. The emulsification process minimizes the spontaneous vaporization of low boiling point PFCs, like C_5 (29°C bulk boiling point), at homeostatic body temperature (37°C) because of an increase in Laplace pressure which increases the effective boiling point of the PFC within each droplet [45, 48]. However, C_5-ARSs were not used for *in vivo* studies since they displayed the lowest payload retention in the absence of US (Figure 3.4). This finding was consistent with our previous demonstration that droplet destabilization occurs within a C_5-ARS [34].

Conversely, payload release in response to US correlated inversely with the fraction of C_6 in the emulsion for both *in vitro* and *in vivo* results. Additionally, greater overall release was observed for large emulsions compared to small. However, the small emulsions yielded ARSs with better homogeneity (Figure 3.2(b)), and thus were selected for the *in vivo* studies. These differences in payload release are likely related to the effective boiling point of the PFC within the emulsions, which is dependent on both the droplet diameter and bulk PFC boiling point. For example, the bubble point of a 1:1 (w/w) C_5/C_6 ad-mixture is approximately 39°C, which is in between the boiling points of C_5 or C_6. Thus, recondensation of the gas nucleus formed by ADV within a droplet is more likely as the fraction of C_6 increases, especially if the US pulse duration is short [49, 50], since vaporized C_6 exists as a supercooled gas at 37°C.

The stability of the fibrin matrix is also critical for controlling release from the ARS. Studies have shown that fibrin degradation occurs even in the presence of a protease inhibitor like aprotinin [38, 51], which was used in the preparation of the ARSs. Fibrin degradation was observed *in vitro*, presumably due to protease impurities in the starting fibrinogen material [52], and further enhanced with US (Figure 3.6(b)). C_6-ARSs displayed better payload retention than C_5/C_6-ARSs both *in vitro* and *in vivo*. However, various factors present *in vivo* that were mitigated or absent *in vitro* could affect payload retention in the ARS. During *in vitro* fibrin degradation, emulsion released from the fibrin matrix of the ARS accumulated at the bottom of each well. During *in vivo* fibrin degradation, however, non-vaporized emulsion released from the fibrin matrix was exposed to the subcutaneous microenvironment. This could lead to emulsion destabilization and non-selective payload release via enzymatic or cellular pathways as well as uptake and clearance by blood and lymphatic vessels [53]. In addition, cellular migration into the ARS could destabilize the emulsion due to the degradation of the

fibrin surrounding each droplet, which could alter the interfacial tension between the emulsion and the fibrin. For example, the fraction of dextran released in the absence of US (i.e., 51 ± 8.2%) for C_6-ARSs at day 10 is similar to the fraction of scaffold degraded (i.e., 42.8 ± 2.6%). With C_5/C_6-ARSs in the absence of US, a burst release was observed *in vivo* on day 1 that was not observed *in vitro*. At this early time point, scaffold degradation is likely not the cause of this burst release. However, the reshaping of the scaffold and forces exerted on the scaffold in the *in vivo* setting (e.g., caused by animal movement) could have caused destabilization of the C_5/C_6-ARSs. Alternatively, the solubilization of the isoflurane anesthetic in the PFC could have also contributed to destabilization [54].

US enhanced *in vitro* dextran release and fibrin degradation in fibrin scaffolds (Figure 3.6), which was consistent with a previous study that demonstrated an increase in hydrogel porosity following US exposure [55]. Thus, it is likely that the increase in dextran release was due to changes in the microstructure of the fibrin following US exposure. Changes in fibrin macroporosity were visible *in vivo* in the ARS in response to US at day 3 (Figure 3.9, Figure 3.10), though overall ARS degradation by day 10 was less than fibrin scaffolds. Unlike the monotonically increasing degradation observed with fibrin (Figure 3.8(c)), the rate (i.e., slope) of fibrin degradation for the C_6-ARSs was not statistically different than zero between days 1-7. Previously, we demonstrated that ARS stiffness increases following US exposure [27, 34], which could reduce cellular infiltration and associated fibrin degradation [56, 57]. Additionally, the bubbles formed in the ARS could reduce the rate of cellular infiltration via the formation of a physical boundary (i.e., fibrin-gas) that cells must circumvent.

Greater blood vessel formation was observed in ARSs versus fibrin by day 10 (Figure 3.11), which suggests that vascularization was enhanced by the presence of C_6 emulsion in the fibrin matrix. PFCs are known for having high gas

solubility, especially oxygen, with lower boiling point PFCs exhibiting higher oxygen solubilization [58-60]. As such, cells co-encapsulated in hydrogel scaffolds with PFC display higher viability than cells encapsulated without PFC [61, 62]. The PFC within the ARS may be serving as oxygen depots that could attract cells into the ARS. This effect may be further enhanced by the use of an oxygen gas carrier for the isoflurane anesthesia, would which render transient hyperoxia in the mice. Since hyperoxia has been shown to increase angiogenesis and cell survival [63, 64], it is possible that the inclusion of PFC in the ARS prolongs local hyperoxia relative to fibrin alone. In addition, the generation of macropores by US within the ARS may have facilitated cell invasion into the ARS without the need for cell-based degradation of the fibrin. This is demonstrated by H&E images of tissue samples taken on day 3 (Figure 3.9), where greater cell invasion is seen in ARSs versus fibrin implants. Overall, the finding that ARSs increase vascularization is interesting, given that no growth factors were released in these experiments, and potentially useful in future studies involving angiogenesis.

3.5 Conclusions

In this study, we demonstrated controlled release of encapsulated dextran from fibrin-based scaffolds using focused, 2.5 MHz US. The release profiles were dependent on ARS (e.g., emulsion size, PFC core) and US (e.g., amplitude, PRF, number of exposures) parameters. Payload retention in the absence of US and payload release due to US correlated directly and inversely with the fraction of C_6 in the ARS. US also increased the release of non-encapsulated dextran from fibrin, which was linked to increased fibrin degradation. Within ARSs, US induced morphological changes associated with the formation of gas bubbles produced by ADV. Greater (i.e., up to 2.9-fold) blood vessel formation occurred in ARSs compared to fibrin scaffolds. Overall, ARSs provide a biocompatible, minimally invasive approach for on-demand,

controlled payload release using US, and have potential for use in tissue engineering applications.

3.6 Acknowledgements

This work was supported by NIH grant R21AR065010 (MLF) and the Basic Radiological Sciences Innovative Research Award (MLF). AM was supported by the National Science Foundation Graduate Student Research Fellowship (Grant No. DGE 1256260). EGO and ML were supported by funds from the Undergraduate Research Opportunity Program.

REFERENCES

[1] Shaikh, F.M., Callanan, A., Kavanagh, E.G., Burke, P.E., Grace, P.A., and McGloughlin, T.M.: Fibrin: A natural biodegradable scaffold in vascular tissue engineering, Cells Tissues Organs, 2008, 188, (4), pp. 333-346

[2] Dehghani, F., and Annabi, N.: Engineering porous scaffolds using gas-based techniques, Current opinion in biotechnology, 2011, 22, (5), pp. 661-666

[3] Seliktar, D.: Designing Cell-Compatible Hydrogels for Biomedical Applications, Science, 2012, 336, (6085), pp. 1124-1128

[4] Vatnitsky, S., Rosenblatt, E., and International Atomic Energy Agency.: Transition from 2-D radiotherapy to 3-D conformal and intensity modulated radiotherapy (International Atomic Energy Agency, 2008. 2008)

[5] Valicenti, R.K., Dicker, A.P., and Jaffray, D.A.: Image-guided radiation therapy of prostate cancer (Informa Healthcare, 2008. 2008)

[6] Szpalski, M., and Gunzburg, R.: Vertebral tumors (Lippincott Williams and Wilkins, 2008. 2008)

[7] Petkar, I., Rooney, K., Roe, J.W., Patterson, J.M., Bernstein, D., Tyler, J.M., Emson, M.A., Morden, J.P., Mertens, K., Miles, E., Beasley, M., Roques, T., Bhide, S.A., Newbold, K.L., Harrington, K.J., Hall, E., and Nutting, C.M.: DARS: a phase III randomised multicentre study of dysphagia- optimised intensity- modulated radiotherapy (Do-IMRT) versus standard intensity-modulated radiotherapy (S-IMRT) in head and neck cancer, BMC cancer, 2016, 16, (1), pp. 770

[8] Chen, X., Lei, H., Liang, Z., Li, L., Qu, S., and Zhu, X.: Intensity-modulated radiotherapy controls nasopharyngeal carcinoma distant metastasis and improves survival of patients, SpringerPlus, 2016, 5, (1), pp. 1459

[9] Spatola, C., Militello, C., Tocco, A., Salamone, V., Raffaele, L., Migliore, M., Pagana, A., Milazzotto, R., Chillura, I., Pergolizzi, S., and Privitera, G.: Intensity-modulated radiotherapy for relapsed malignant pleural mesothelioma, Future oncology, 2016, 12, (23s), pp. 67-71

[10] Sakiyama-Elbert, S.E., and Hubbell, J.A.: Development of fibrin derivatives for controlled release of heparin-binding growth factors, Journal of Controlled Release, 2000, 65, (3), pp. 389-402

[11] Sakiyama-Elbert, S.E., and Hubbell, J.A.: Controlled release of nerve growth factor from a heparin-containing fibrin-based cell ingrowth matrix, Journal of Controlled Release, 2000, 69, (1), pp. 149-158

[12] Chen, K.H., Zhu, X.D., Li, L., Qu, S., Liang, Z.Q., Liang, X., Pan, X.B., Liang, Z.G., and Jiang, Y.M.: Comparison of the efficacy between concurrent chemoradiotherapy with or without adjuvant chemotherapy and intensity-modulated radiotherapy alone for stage II nasopharyngeal carcinoma, Oncotarget, 2016

[13] Estabrook, N.C., Bartlett, G.K., Compton, J.J., Cardenes, H.R., and Das, I.J.: Role of belly board device in the age of intensity modulated radiotherapy for pelvic irradiation, Medical dosimetry : official journal of the American Association of Medical Dosimetrists, 2016, 41, (4), pp. 300-304

[14] Kong, F., Ying, H., Zhai, R., Du, C., Huang, S., Zhou, J., He, X., Hu, C., Wang, Z., Sun, T., and Ji, Q.: Clinical outcome of intensity modulated radiotherapy for carcinoma showing thymus-like differentiation, Oncotarget, 2016

[15] Fabiilli, M.L., Haworth, K.J., Sebastian, I.E., Kripfgans, O.D., Carson, P.L., and Fowlkes, J.B.: Delivery of chlorambucil using an acoustically-triggered perfluoropentane emulsion, Ultrasound in Medicine and Biology, 2010, 36, (8), pp. 1364-1375

[16] Carmeliet, P.: Angiogenesis in life, disease and medicine, Nature, 2005, 438, (7070), pp. 932-936

[17] Risau, W.: Mechanisms of angiogenesis, Nature, 1997, 386, (6626), pp. 671-674

[18] Matsusaki, M., and Akashi, M.: Novel functional biodegradable polymer IV: pH-Sensitive controlled release of fibroblast growth factor-2 from a poly(gamma-glutamic acid)-sulfonate matrix for tissue engineering, Biomacromolecules, 2005, 6, (6), pp. 3351-3356

[19] Thornton, P.D., McConnell, G., and Ulijn, R.V.: Enzyme responsive polymer hydrogel beads, Chemical Communications, 2005, (47), pp. 5913-5915

[20] Frimpong, R.A., Fraser, S., and Hilt, J.Z.: Synthesis and temperature response analysis of magnetic-hydrogel nanocomposites, Journal of Biomedical Materials Research Part A, 2007, 80A, (1), pp. 1-6

[21] Zhao, X., Kim, J., Cezar, C.A., Huebsch, N., Lee, K., Bouhadir, K., and Mooney, D.J.: Active scaffolds for on-demand drug and cell delivery, Proceedings of the National Academy of Sciences of the United States of America, 2011, 108, (1), pp. 67-72

[22] Kulkarni, R., and Biswanath, S.: Electrically responsive smart hydrogels in drug delivery: a review, Journal of Applied Biomaterials and Biomechanics, 2007, 5, (3), pp. 125-139

[23] Wu, C., Chen, C., Lai, J., Mu, X., Zheng, J., and Zhao, Y.: Molecule-scale controlled-release system based on light-responsive silica nanoparticles, Chemical Communications, 2008, 23, pp. 2662-2664

[24] Lavigne, M.D., Pennadam, S.S., Ellis, J., Yates, L.L., Alexander, C., and Gorecki, D.C.: Enhanced gene expression through temperature profile-induced variations in molecular architecture of thermoresponsive polymer vectors, The Journal of Gene Medicine, 2007, 9, (1), pp. 44-54

[25] He, Y.X., Wang, Y., Cao, P.F., Shen, L., Zhao, Y.J., Zhang, Z.J., Chen, D.M., Yang, T.B., Huang, X.Q., Qin, Z., Dai, Y.Y., and Shen, L.F.: Prognostic value and predictive threshold of tumor volume for patients with locally advanced nasopharyngeal carcinoma receiving intensity-modulated radiotherapy, Chinese journal of cancer, 2016, 35, (1), pp. 96

[26] Boisselier, P., Racadot, S., Thariat, J., Graff, P., and Pointreau, Y.: [Intensity-modulated radiotherapy of head and neck cancers. Dose constraint for spinal cord and brachial plexus], Cancer radiotherapie : journal de la Societe francaise de radiotherapie oncologique, 2016, 20, (6-7), pp. 459-466

[27] Fabiilli, M.L., Wilson, C.G., Padilla, F., Martin-Saavedra, F.M., Fowlkes, J.B., and Franceschi, R.T.: Acoustic droplet-hydrogel composites for spatial and temporal control of growth factor delivery and scaffold stiffness, Acta Biomaterialia, 2013

[28] Kripfgans, O.D., Zhang, M., Fabiilli, M.L., Carson, P.L., Padilla, F., Swanson, S.D., Mougenot, C., Fowlkes, J.B., and Mougenot, C.: Acceleration of ultrasound thermal therapy by patterned acoustic droplet vaporization, The Journal of the Acoustical Society of America, 2014, 135, (1), pp. 537-544

[29] Epstein-Barash, H., Orbey, G., Polat, B.E., Ewoldt, R.H., Feshitan, J., Langer, R., Borden, M.A., and Kohane, D.S.: A microcomposite hydrogel for repeated on-demand ultrasound-triggered drug delivery, Biomaterials, 2010, 31, (19), pp. 5208-5217

[30] Fabiilli, M.L., Lee, J.A., Kripfgans, O.D., Carson, P.L., and Fowlkes, J.B.: Delivery of water-soluble drugs using acoustically triggered perfluorocarbon double emulsions, Pharmaceutical research, 2010, 27, (12), pp. 2753-2765

[31] Couture, O., Urban, A., Bretagne, A., Martinez, L., Tanter, M., and Tabeling, P.: *In vivo* targeted delivery of large payloads with an ultrasound clinical scanner, Medical physics, 2012, 39, (8), pp. 5229-5237

[32] Couture, O., Faivre, M., Pannacci, N., Babataheri, A., Servois, V., Tabeling, P., and Tanter, M.: Ultrasound internal tattooing, Medical physics, 2011, 38, (2), pp. 1116-1123

[33] Kripfgans, O.D.: Acoustic droplet vaporization for diagnostic and therapeutic applications, University of Michigan, 2002

[34] Lin, C.G., Xu, S.K., Yao, W.Y., Wu, Y.Q., Fang, J.L., and Wu, V.W.: Comparison of set up accuracy among three common immobilisation systems for intensity modulated radiotherapy of nasopharyngeal carcinoma patients, Journal of medical radiation sciences, 2016

[35] Luo, Y., Qin, Y., and Lang, J.: Effect of adaptive replanning in patients with locally advanced nasopharyngeal carcinoma treated by intensity-modulated radiotherapy: a propensity score matched analysis, Clinical & translational oncology : official publication of the Federation of Spanish Oncology Societies and of the National Cancer Institute of Mexico, 2016

[36] Lu, Y., Gu, W., Deng, J., Yang, H., and Yang, W.: A phase I study of nedaplatin, pemetrexed and thoracic intensity-modulated radiotherapy for inoperable stage III lung adenocarcinoma, BMC cancer, 2016, 16, (1), pp. 775

[37] Garvin, K.A., Hocking, D.C., and Dalecki, D.: Controlling the Spatial Organization of Cells and Extracellular Matrix Proteins in Engineered Tissues Using Ultrasound Standing Wave Fields, Ultrasound in Medicine and Biology, 2010, 36, (11), pp. 1919-1932

[38] Tang, C., Wu, F., Wang, R., Lu, H., Li, G., Liu, M., Zhu, H., Zhu, J., Zhang, Y., and Hu, K.: Comparison between nedaplatin and cisplatin plus docetaxel combined with intensity-modulated radiotherapy for locoregionally advanced nasopharyngeal carcinoma: a multicenter randomized phase II clinical trial, American journal of cancer research, 2016, 6, (9), pp. 2064-2075

[39] Huang, C.M., Huang, M.Y., Tsai, H.L., Huang, C.W., Ma, C.J., Lin, C.H., Huang, C.J., and Wang, J.Y.: A retrospective comparison of outcome and toxicity of preoperative image-guided intensity-modulated radiotherapy versus conventional pelvic radiotherapy for locally advanced rectal carcinoma, Journal of radiation research, 2016

[40] Wood, M., Fonseca, A., Sampson, D., Kovendy, A., Westhuyzen, J., Shakespeare, T., and Turnbull, K.: Prostate intensity-modulated radiotherapy planning in seven mouse clicks: Development of a class solution for cancer, Reports of practical oncology and radiotherapy : journal of Greatpoland Cancer Center in Poznan and Polish Society of Radiation Oncology, 2016, 21, (6), pp. 567-570

[41] Fang, F.M., Chuang, H.C., Chou, S.Y., Huang, T.L., Wang, C.J., Lin, Y.T., Chiu, T.J., Lin, W.C., Li, S.H., Su, Y.Y., and Chien, C.Y.: The Therapeutic

Benefit of Radical Resection for T4b Oral Cavity Squamous Cell Carcinoma with Partial or Complete Response After Radical Chemo-Intensity-Modulated Radiotherapy (IMRT), Annals of surgical oncology, 2016

[42] Cao, C., Luo, J., Gao, L., Yi, J., Huang, X., Li, S., Xiao, J., Zhang, Z., and Xu, G.: Magnetic Resonance Imaging-Detected Intracranial Extension in the T4 Classification Nasopharyngeal Carcinoma with Intensity-modulated Radiotherapy, Cancer research and treatment : official journal of Korean Cancer Association, 2016

[43] Fabiilli, M.L., Haworth, K.J., Fakhri, N.H., Kripfgans, O.D., Carson, P.L., and Fowlkes, J.B.: The role of inertial cavitation in acoustic droplet vaporization, IEEE Trans Ultrason Ferroelectr Freq Control, 2009, 56, (5), pp. 1006-1017

[44] Schad, K.C., and Hynynen, K.: *In vitro* characterization of perfluorocarbon droplets for focused ultrasound therapy, Physics in Medicine and Biology, 2010, 55, (17), pp. 4933-4947

[45] Sheeran, P.S., Wong, V.P., Luois, S., McFarland, R.J., Ross, W.D., Feingold, S., Matsunaga, T.O., and Dayton, P.A.: Decafluorobutane as a Phase-Change Contrast Agent for Low-Energy Extravascular Ultrasonic Imaging, Ultrasound in Medicine and Biology, 2011, 37, (9), pp. 1518-1530

[46] Shakespeare, T.P., Chin, S., Manuel, L., Wen, S., Hoffman, M., Wilcox, S.W., and Aherne, N.J.: Long-term decision regret after post-prostatectomy image-guided intensity-modulated radiotherapy, Journal of medical imaging and radiation oncology, 2016

[47] Martz, T.D., Sheeran, P.S., Bardin, D., Lee, A.P., and Dayton, P.A.: Precision Manufacture of Phase-Change Perfluorocarbon Droplets Using Microfluidics, Ultrasound in Medicine and Biology, 2011, 37, (11), pp. 1952-1957

[48] Rapoport, N.Y., Kennedy, A.M., Shea, J.E., Scaife, C.L., and Nam, K.-H.: Controlled and targeted tumor chemotherapy by ultrasound-activated nanoemulsions/microbubbles, Journal of Controlled Release, 2009, 138, (2), pp. 268-276

[49] Chi, A., Wen, S., Monga, M., Almubarak, M., He, X., Rojanasakul, Y., Tse, W., and Remick, S.C.: Definitive Upfront Stereotactic Ablative Radiotherapy Combined with Image-Guided, Intensity Modulated Radiotherapy (IG-IMRT) or IG-IMRT Alone for Locally Advanced Non-Small Cell Lung Cancer, PloS one, 2016, 11, (9), pp. e0162453

[50] Rapoport, N., Nam, K.H., Gupta, R., Gao, Z.G., Mohan, P., Payne, A., Todd, N., Liu, X., Kim, T., Shea, J., Scaife, C., Parker, D.L., Jeong, E.K., and Kennedy, A.M.: Ultrasound-mediated tumor imaging and nanotherapy using drug loaded, block copolymer stabilized perfluorocarbon nanoemulsions, Journal of Controlled Release, 2011, 153, (1), pp. 4-15

[51] Pointreau, Y., Lizee, T., Bensadoun, R.J., Boisselier, P., Racadot, S., Thariat, J., and Graff, P.: [Intensity-modulated radiotherapy for head and neck cancer. Dose constraint for salivary gland and mandible], Cancer radiotherapie : journal de la Societe francaise de radiotherapie oncologique, 2016, 20, (6-7), pp. 445-451

[52] Sun, Z., Adam, M.A., Kim, J., Czito, B., Mantyh, C., and Migaly, J.: Intensity-Modulated Radiation Therapy Is Not Associated with Perioperative or Survival Benefit over 3D-Conformal Radiotherapy for Rectal Cancer, Journal of gastrointestinal surgery : official journal of the Society for Surgery of the Alimentary Tract, 2016

[53] Kapoor, R., Bansal, A., Kumar, N., and Oinam, A.S.: Dosimetric correlation of acute and late toxicities in high-risk prostate cancer patients treated with three-dimensional conformal radiotherapy followed by intensity modulated radiotherapy boost, Indian journal of urology : IJU : journal of the Urological Society of India, 2016, 32, (3), pp. 210-215

[54] Ooishi, M., Motegi, A., Kawashima, M., Arahira, S., Zenda, S., Nakamura, N., Ariji, T., Tokumaru, S., Sakuraba, M., Tahara, M., Hayashi, R., and Akimoto, T.: Patterns of failure after postoperative intensity-modulated radiotherapy for locally advanced and recurrent head and neck cancer, Japanese journal of clinical oncology, 2016, 46, (10), pp. 919-927

[55] Thariat, J., Racadot, S., Pointreau, Y., Boisselier, P., Grange, J.D., Graff, P., and Weber, D.C.: [Intensity-modulated radiotherapy of head and neck cancers: Dose effects on the ocular, orbital and eyelid structures], Cancer radiotherapie : journal de la Societe francaise de radiotherapie oncologique, 2016, 20, (6-7), pp. 467-474

[56] Ghajar, C.M., Chen, X., Harris, J.W., Suresh, V., Hughes, C.C.W., Jeon, N.L., Putnam, A.J., and George, S.C.: The effect of matrix density on the regulation of 3-D capillary morphogenesis, Biophysical Journal, 2008, 94, (5), pp. 1930-1941

[57] Wu, V.W., Leung, W.S., Wong, K.L., Chan, Y.K., Law, W.L., Leung, W.K., and Yu, Y.L.: The impact of positron emission tomography on primary tumour delineation and dosimetric outcome in intensity modulated radiotherapy of early T-stage nasopharyngeal carcinoma, Radiation oncology, 2016, 11, (1), pp. 109

[58] Johnson, J.L.H., Dolezal, M.C., Kerschen, A., Matsunaga, T.O., and Unger, E.C.: *In vitro* comparison of dodecafluoropentane (DDFP), perfluorodecalin (PFD), and perfluoroctylbromide (PFOB) in the facilitation of oxygen exchange, Artificial cells, blood substitutes, and biotechnology, 2009, 37, (4), pp. 156-162

[59] Riess, J.G.: Oxygen Carriers ("Blood Substitutes") - Raison d'Etre, Chemistry, and Some Physiology, Chemical Reviews, 2001, 101, (9), pp. 2797-2919

[60] Dias, A.M.A., Freire, M., Coutinho, J.A.P., and Marrucho, I.M.: Solubility of oxygen in liquid perfluorocarbons, Fluid Phase Equilibria, 2004, 222, pp. 325-330

[61] Chin, K., Khattak, S.F., Bhatia, S.R., and Roberts, S.C.: Hydrogel-perfluorocarbon composite scaffold promotes oxygen transport to immobilized cells, Biotechnol Progr, 2008, 24, (2), pp. 358-366

[62] Maillard, E., Juszczak, M.T., Clark, A., Hughes, S.J., Gray, D.R.W., and Johnson, P.R.V.: Perfluorodecalin-enriched fibrin matrix for human islet culture, Biomaterials, 2011, 32, (35), pp. 9282-9289

[63] OuYang, P.Y., Bi, Z.F., Zhang, L.N., You, K.Y., Xiao, Y., Lan, X.W., Tang, J., Wang, X.C., Deng, W., and Xie, F.Y.: Outcomes of Induction Chemotherapy Plus Intensity-Modulated Radiotherapy (IMRT) Versus IMRT Plus Concurrent Chemotherapy for Locoregionally Advanced Nasopharyngeal Carcinoma: A Propensity Matched Study, Translational oncology, 2016, 9, (4), pp. 329-335

[64] Yahya, S., Benghiat, H., Nightingale, P., Tiffany, M., Sanghera, P., and Hartley, A.: Does Dose to an Oral Mucosa Organ at Risk Predict the Duration of Grade 3 Mucositis after Intensity-modulated Radiotherapy for Oropharyngeal Cancer?, Clinical oncology, 2016, 28, (12), pp. e216-e219

CHAPTER IV

Controlled Release of Basic Fibroblast Growth Factor for Angiogenesis Using Acoustically-Responsive Scaffolds

4.1 Introduction

Exogenous, pro-angiogenic growth factors can stimulate blood vessel formation and restore perfusion in preclinical models of cardiovascular disease [1-5]. However, the clinical use of pro-angiogenic growth factors for treating conditions, such as coronary artery and peripheral artery diseases, has been disappointing [6-12]. Retrospective analysis of these studies revealed many potential shortcomings in the preclinical to clinical transition of therapeutic angiogenesis. One crucial reason is related to the route of the growth factor including variables such as the administration route, dose, and duration of treatment [13-15]. In human studies, basic fibroblast growth factor (bFGF) [6-8] or genes encoding for acidic FGF [16-18], vascular endothelial growth factor (VEGF) [9, 10, 19], or hepatocyte growth factor (HGF) [11, 12] were administered using intravascular or intramuscular injections. Growth factors administered using these routes have short *in vivo* half-lives, slow tissue penetration, and the tendency to cause systemic side effects (e.g., nephrotoxicity, edema formation) [6, 20].

The paradigm of acellular (i.e., inductive) tissue engineering has been to incorporate angiogenic growth factors within a hydrogel scaffold, which is then

implanted at or adjacent to the site of intended vascularization. Growth factor release from the scaffold is dependent on factors such as the growth factor-scaffold affinity as well as the rates of enzymatic and cellular degradation of the scaffold [21]. This approach can extend the *in vivo* half life of the growth factor [22], localize its actions to the site of implantation [23], and promote cellular processes involved in angiogenesis [24]. Despite these advantages over bolus injections, conventional hydrogels do not enable spatiotemporal control of growth factor release. In contrast, endogenous growth factors are expressed in spatially- and temporally-regulated patterns during angiogenesis. Taking VEGF-A as an example, the spatial gradient of the growth factor impacts the directionality of blood vessel growth while differences in temporal gradients influence vessel density [25, 26].

Several approaches have been used to impart spatiotemporally-controlled release from hydrogels. By altering material properties, temporally-controlled release (e.g., burst, sustained, or delayed) of bFGF, VEGF, and platelet derived growth factor (PDGF) has been achieved with collagen [27], alginate [28, 29], and poly(lactide-co-glycolide) (PLG) [30] based scaffolds. Anisotropic (e.g., bi-layer) scaffolds composed of collagen or PLG enable spatially-controlled delivery of bFGF, VEGF, and PDGF [27, 31]. By definition, however, these a priori approaches do not provide the ability to modulate the spatiotemporal gradients or released dose of growth factor once the scaffold is fabricated and implanted *in vivo*. This is potentially problematic when trying to personalize pro-angiogenic growth factor therapy based on the patient response during treatment. Thus, a scaffold where growth factor delivery can be actively modulated could facilitate the understanding of how variations in growth factor presentation impact angiogenesis.

We have developed fibrin-based hydrogels where the delivery of payloads such as growth factors can be controlled non-invasively and in an on-demand manner using focused ultrasound (US) [32, 33]. These acoustically-responsive scaffolds

(ARSs) contain a fibrin matrix doped with micron-sized, sonosensitive emulsions. Payloads, which are contained within the perfluorocarbon (PFC) emulsion, are released from the ARS through a non-thermal mechanism termed acoustic droplet vaporization (ADV) [34, 35]. Megahertz-range US is used to generate ADV, which causes vaporization of the PFC phase within the emulsion and expulsion of the encapsulated payload [36-39].

Previously, we demonstrated that release from the ARS is a threshold-based phenomenon that is dependent on characteristics of the emulsion, scaffold, and US [39]. Additionally, we showed in an *in vivo* proof-of-concept study that US can modulate release of a surrogate payload (i.e., dextran) from an ARS [32, 33]. In the current study, we focus on the *in vitro* and *in vivo* delivery of bFGF using ARSs (Figure 4.1). bFGF-loaded emulsions were generated using a microfluidic device, which yielded monodispersed particles having more consistent release kinetics than the heterogeneous particles used in our prior work [32, 33, 39]. We characterized the *in vitro* release of bFGF from ARSs, including bioactivity of the released bFGF and we evaluated the angiogenic response of subcutaneously-implanted ARSs. Overall, as will be shown, ARSs yield a robust angiogenic response that is controlled by focused non-invasive US.

4.2 Materials and Methods

4.2.1 Preparation and Characterization of the Double Emulsion

Double emulsions with a water-in-PFC-in-water (W_1/PFC/W_2) structure were prepared as previously described [32, 38]. Briefly, a triblock fluorosurfactant, consisting of Krytox 157FSH (CAS# 51798-33-5, DuPont, Wilmington, DE, USA) and polyethylene glycol (MW: 1000, CAS#: 24991-53-5, Alfa Aesar, Ward Hill, MA USA), was dissolved at 2% (w/w) in 1 g of perfluorohexane (PFH, C_6F_14, boiling

point: 56°C, CAS#: 355-42-0, Strem Chemicals, Newburyport, MA USA). The PFC solution was combined at 2:1 (v/v) with a W_1 phase containing 1 mg/mL basic fibroblast growth factor (bFGF, Cat#: GF003AF, EMD Millipore, Temecula, CA USA), 7.5 mg/mL bovine serum albumin (Sigma-Aldrich, St. Louis, MO USA), and 7.5 μg/mL heparin (Cat #: 375095, Calbiochem, San Diego, CA, USA) in phosphate-buffered saline (PBS, Life Technologies, Grand Island, NY USA). The PFC and W_1 phases were sonicated (Q55, QSonica, Newton, CT USA) for 30 seconds while on ice. The resulting primary emulsion, with a water-in-PFC (W_1/PFC) structure and mean diameter of approximately 2 μm [40], was pumped at 0.5 μL/min into the inner channel of a quartz microfluidic chip (Cat#: 3200146, junction: 14 x 17 μm, hydrophilic coating, Dolomite, Royston, United Kingdom) using a syringe pump (KDS-410, kd Scientific, Holliston, MA USA). Simultaneously, 50 mg/mL Pluronic F68 (CAS# 9003-11-6, Sigma-Aldrich) in PBS was pumped at 2.5 μL/min into the outer channels of the chip using a second syringe pump (78-0388, kd Scientific).

Blank or fluorescently-labeled emulsions were prepared as described above with either PBS or 0.1 mg/mL Alexa Fluor 488-labeled dextran (MW: 10 kDa, Life Technologies) as the W_1 phases, respectively. Emulsions were characterized with a Coulter Counter (Multisizer 4, Beckman Coulter, Brea, CA USA) in the range of 1-30 μm. To confirm emulsion morphology, the dextran-loaded emulsion was imaged using an inverted confocal microscope (SP5X, Leica Microsystems, Inc., Buffalo Grove, IL USA) at the University of Michigan Microscopy & Image Analysis Laboratory. The encapsulation efficiency of bFGF in the emulsion was determined by first allowing the emulsion to settle from the supernatant, which contained non-encapsulated bFGF. Next, an aliquot of the emulsion pellet was broken, as done previously [32], and the bFGF concentration was measured using an enzyme-linked immunosorbent assay (ELISA) (Cat#: DY233, R&D Systems, Minneapolis, MN

USA). The encapsulation efficiency was determined by comparing the measured bFGF concentration with the theoretical concentration initially loaded into the emulsion. For all experiments, ARSs were prepared using emulsion pellet, which minimized the carryover of non-encapsulated bFGF.

4.2.2 Fabrication and Characterization of the ARS

ARSs were prepared using 10 mg/mL clottable protein by first combining bovine fibrinogen (Sigma-Aldrich) dissolved in degassed (36% O^2 saturation) Dulbeccos modified Eagles medium (DMEM, Life Technologies), with 10% (v/v) bovine thrombin (20 U/mL, Thrombin-JMI, King Pharmaceuticals, Bristol, TN, USA), 0.025 U/mL aprotinin (Sigma-Aldrich), and 1% (v/v) emulsion. ARSs used for *in vivo* experiments contained 0.125 mg/mL Alexa Fluor 647-labeled fibrinogen (Cat#: F35200, Molecular Probes, Eugene, OR USA) for non-invasive monitoring of fibrin degradation.

The ADV and inertial cavitation (IC) thresholds of the ARSs were determined using previously described methods [39]. Briefly, 0.5 mL ARSs were cast in 24-well Bioflex plates (Flexcell International, Burlington, NC, USA) by aliquoting the ARS mixture into each well and allowing it to polymerize for 30 min at room temperature. The ARSs were exposed to focused US generated by a calibrated, single-element transducer (2.5 MHz, H108, f-number = 0.83, focal length = 50 mm, Sonic Concepts, Inc., Bothell, WA USA) in the range of 0 to 8.0 MPa peak rarefactional pressure. The complete acoustic setup is described in section 2.3. A calibrated hydrophone (HGL-0085, dynamic range = 1-50 MHz, Onda, Sunnyvale, CA USA) was placed 6 cm away from the focus of the transducer to detect backscattered acoustic signals generated in the ARS during the US exposure. The radiofrequency signals collected with the hydrophone and digitized by an oscilloscope (sampling rate = 100 MHz) were analyzed in MATLAB (The MathWorks, Natick, MA, USA) using the fast Fourier transform. The ADV threshold was determined by analyzing the

fundamental frequency since bubbles formed in the ARS due to ADV significantly increase the scattered, fundamental signal [41, 42]. The ADV threshold was defined as the lowest acoustic pressure at which the increase in fundamental signal was observed. The IC threshold was computed using the broadband signal from the acquired radiofrequency waveforms using identical methods as described previously [39].

Using a prior method [39], the physical stability of the ARSs was determined by casting 0.5 mL ARSs in 24-well plates (Corning Life Sciences, Tewksbury, MA, USA) with 1% (v/v) blank emulsion. After polymerization at room temperature, each ARS was covered with 0.5 mL of DMEM and placed in a standard tissue culture incubator (37°C, 5% carbon dioxide). At each time point (i.e., days 0, 1, 3, and 7), the overlying medium was removed and replaced with 0.05% trypsinEDTA (Life Technologies). After complete degradation of the fibrin component of the ARS, the resulting sample was centrifuged to isolate the emulsion, and the emulsion was sized using a Coulter Counter. It was experimentally confirmed that incubation of the emulsion in trypsin did not alter the size distribution or number density of the emulsion.

4.2.3 US Exposure

All acoustic exposures were conducted using the following setup. The single-element transducer was driven by pulsed waveforms generated using a dual channel function generator (33500B, Agilent Technologies, Santa Clara, CA USA), amplified by a gated radiofrequency amplifier (GA-2500A Ritec Inc, Warwick, RI USA), and passed through a matching circuit (H108_3MN, Sonic Concepts) to reduce impedance between the transducer and amplifier. Gating of the carrier waveform was realized using the second channel of the function generator, resulting in a pulsed signal. All generated and amplified signals were monitored with an oscilloscope (HDO4034, Teledyne LeCroy, Chestnut Ridge, NY USA). All acoustic exposures were done with

the following parameters unless otherwise stated: 2, 4, 6, or 8 MPa peak rarefactional pressure, 13 acoustic cycles, and 100 Hz pulse repetition frequency (PRF). All US pressures are listed as peak rarefactional pressures.

4.2.4 *In Vitro* Controlled Release of bFGF

For *in vitro* studies, 0.5 mL aliquots of the ARS mixture were added into each well of a 24 well BioFlex plate and allowed to polymerize for 30 min at room temperature. Each ARS was then covered with 0.5 mL of overlying media, consisting of DMEM supplemented with 100 U/mL penicillin and 100 μg/mL streptomycin. The ARSs were placed in a tissue culture incubator between US exposures. For controlled release experiments, the BioFlex plate containing the ARSs was placed in a tank of degassed water (30-36% O^2 saturation) at 37°C such that only the bottom half of the plate was submerged. The single element US transducer was positioned under the plate such that the axial focus was located at mid-height of the ARS. The bottom of each well in the plate consisted of a silicone elastomer membrane, which based on a thickness of 1 mm, attenuated the US by less than 2% [43]. During US exposure, the transducer was rastered across the entire ARS for 2 min. Five US exposure conditions were explored: no US; daily US for 6 days beginning one day after polymerization at 2, 4, or 8 MPa; and daily US beginning 4 days after polymerization at 8 MPa.

The overlying media was sampled daily by collecting half of the media and replacing the sampled volume with an equal volume of fresh media. On days with US exposure, the media was sampled immediately after US exposure. The concentration of bFGF in the media, subsequently referred to as releasate, was measured by ELISA. The bioactivity of the released bFGF was assessed using NR-6-R murine fibroblasts [44], kindly provided by Dr. Angie Rizzino at the University of Nebraska Medical Center, and modifying a previously published method [45]. Briefly, the cells were initially cultured in DMEM with 10% bovine calf serum (BCS, Thermo

Fisher Scientific Inc, Waltham, MA USA) and then passaged into DMEM/F12 media (Thermo Fisher Scientific Inc) supplemented with 10% BCS three days prior to the start of the bioactivity assay. The cells were seeded in a 96 well plate at 5000 cells/well in serum free media containing DMEM/F12 supplemented with ITS liquid media supplement (10 μg/mL insulin, 5.5 μg/mL transferrin, and 5 ng/mL selenium, Sigma-Aldrich), 100 μg/mL ovalbumin (Sigma-Aldrich), 1 μM dexamethasone (Sigma-Aldrich), and 5 μg/mL fibronectin (Sigma-Aldrich). The cells were then incubated with either freshly prepared bFGF standards or releasate for 44 hours. Cell proliferation was quantified using the CellTiter 96 AQueous One Solution Cell proliferation Assay (Promega, Madison, WI USA), according to the manufacturers instructions.

4.2.5 *In Vivo* Controlled Release of bFGF

This *in vivo* research was conducted with approval of the Institutional Animal Care & Use Committee at the University of Michigan. Female BALB/c mice (n = 16, 18-21 g, Charles River Laboratories, Wilmington, MA, USA) were anesthetized with isoflurane (5% for induction and 1.5% for maintenance). The lower dorsal hair was removed by shaving and applying depilatory cream (Nair, Church & Dwight Co, Ewing, NJ USA); the skin was sterilized with betadine surgical scrub (Purdue Products L.P., Stamford, CT USA). The ARS mixture (0.3 mL per implant) was then injected subcutaneously using a 20-gauge needle (Becton Dickinson, Franklin Lakes, NJ, USA) at two locations with the dorsal region and allowed to polymerize for 2 minutes prior to removal of the needle. The ARS mixture contained 1% (v/v) bFGF-loaded emulsion, which yielded 1 μg bFGF per ARS. The mice were allowed to recover following implantation. Scaffolds containing 10 mg/mL fibrin or 10 mg/mL fibrin with unencapsulated bFGF (1 μg per scaffold) were injected as negative and positive control implants, respectively.

US was applied using previously published methods [32]. Briefly, each mouse

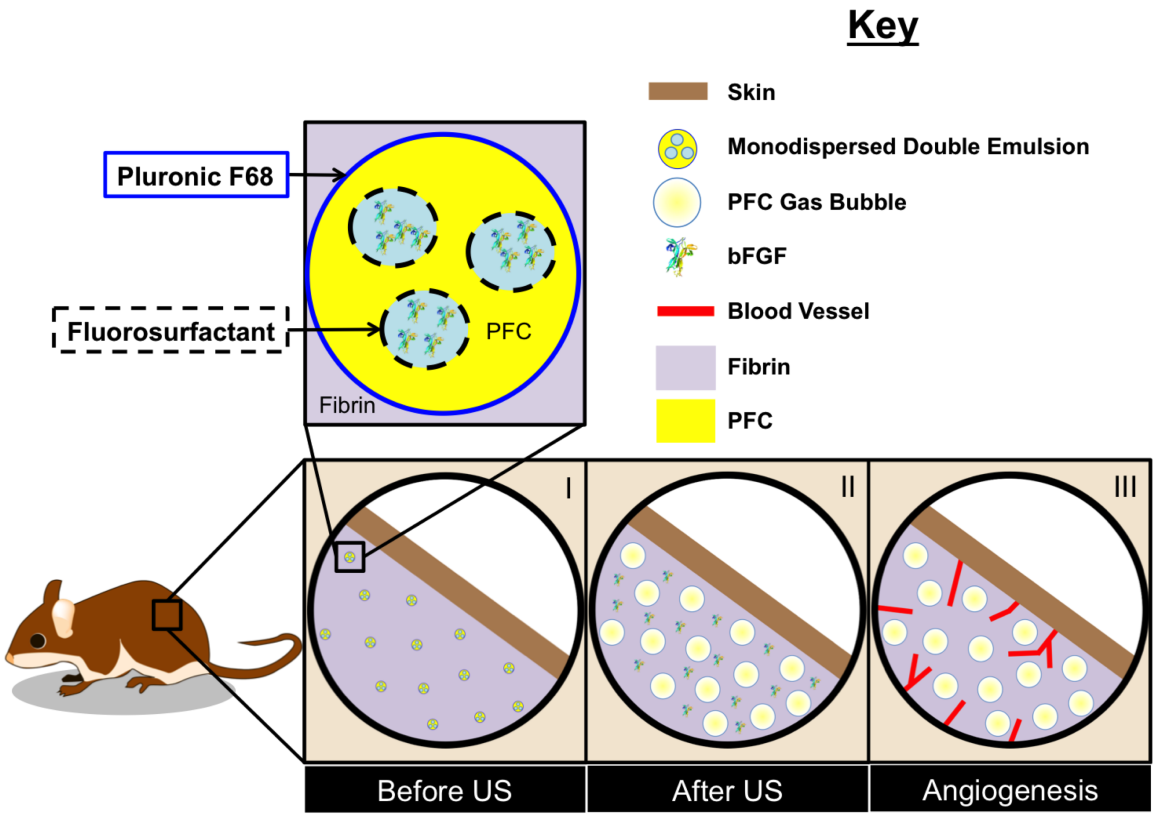

Figure 4.1: Control of angiogenesis using an ARS. (I) ARSs were polymerized in situ in the subcutaneous space. The fibrin-based ARSs contained bFGF encapsulated within a monodispersed double emulsion. (II) During US exposure, the PFC within the emulsion transitioned from a liquid into a gas, thereby releasing the encapsulated bFGF. (III) The released bFGF stimulated blood vessel growth into the ARS.

was anesthetized with isoflurane and placed in a prone position. US coupling gel (MediChoice, Owens & Minor, Mechanicsville, VA USA) was applied to the implant region. A coupling cone (C106, Sonic Concepts) was placed on the US transducer, filled with degassed water (30-36% O^2 saturation), and the water was sealed in by Tegaderm film (3M Health Care, St. Paul, MN USA). The transducer was rastered across the implant for 2 min. For each mouse, US was applied daily to only one ARS per mouse beginning 1 day after implantation for a period of 7 or 14 days. The scaffolds receiving US treatment (i.e., left or right implant) were randomized for all mice.

4.2.6 Perfusion Imaging

The mice were anesthetized with isoflurane and imaged with a PeriCam PSI HR (Perimed, Ardmore, PA USA) laser speckle contrast analysis (LASCA) system to quantify the relative perfusion within the implant region. The mice were imaged on day 0 (i.e., immediately after implantation), 1 (i.e., the first day of US exposure), 3, 7, 10, and 14. All images were acquired with a 10 cm distance between the scanner and implant, resulting in a resolution of 20 μm/pixel. Pimsoft software (Perimed) was used for image acquisition and processing. A total of 30 images per implant per time point were acquired at a rate of 0.096 images/s with a field of view of 2.0 x 2.8 cm. Every 6 images were averaged to create a total of five averaged images per implant per time point. Three of the five averaged images were used for perfusion analysis, whereby the average relative perfusion was computed within circular regions of interest (ROIs, 0.9 cm diameter) encompassing each implant.

4.2.7 Imaging Scaffold Degradation

The mice were anesthetized with isoflurane and imaged with an IVIS Spectrum Preclinical *In Vivo* Imaging System (Perkin Elmer, Houston, TX USA) at the University of Michigan Center for Molecular Imaging to quantify the fraction of

Alexa Fluor 647-labeled fibrinogen remaining in the ARS implants. The mice were imaged on day 0 (i.e., the day of implantation), 1 (i.e., the first day of US exposure), 7, and 14. The signal from the Alexa Fluor 647-labeled fibrinogen was collected using an excitation filter of 640 nm and emission filters ranging from 680 to 740 nm. To account for autofluorescence, a sequence of background signals was collected using an excitation filter of 570 nm and emission filters ranging from 620 to 740 nm. Spectral unmixing was performed on the data sets in Living Image software (Perkin Elmer), according to the manufacturers instructions, using the fluorophore and autofluorescence (background) images. Following unmixing, equally sized ROIs (0.9 cm diameter), were drawn to encompass each implant and the average radiant efficiency ([photons/s/cm^2/sr]/[μW/cm^2]) was calculated. For each implant, the average radiant efficiency on days 1, 7, and 14 was normalized by the day 0 measurement, thus accounting for any differences in the amount of fluorophore initially loaded.

4.2.8 Histology

Mice were euthanized on days 7 and 14 post implantation. ARSs or fibrin implants were retrieved and fixed overnight in aqueous buffered zinc formalin (CAS# 50-00-0, Formalde-Fresh, Fisher Scientific, Waltham, MA USA). Implants were then transferred to 70% ethanol until they were processed and embedded in paraffin at the University of Michigan Microscopy & Image Analysis Laboratory. The paraffin-embedded tissues were cut into 5 μm thick serial sections and placed on pre-cleaned glass slides (Fisherbrand Superfrost Plus, Fisher Scientific) for histological analysis. Immunostaining of mice-derived blood vessels was performed using a rabbit anti-mouse CD31 primary antibody (ab28364, Abcam, Cambridge, MA USA) combined with a goat anti-rabbit secondary labeled polymer-horseradish peroxidase conjugate (Envision+ System-HRP (DAB), Dako North America, Inc., Carpinteria, CA USA), as described previously [46, 47]. Negative controls, involving

staining with a rabbit IgG polyclonal isotype control (ab27478, Abcam) as the primary antibody or staining with the secondary antibody only, confirmed the specificity of the CD31 staining. Tissue sections were visualized and photographed with a Leica DMRB light microscope (Leica Microsystems). Three tissue sections from each implant with six images per tissue section were analyzed manually for blood vessel formation per unit area. Blood vessel counting was done, in a blinded manner, by three separate individuals. Blood vessels were identified in CD31-stained tissues at 20x magnification by defined lumens and complete enclosure of the lumen.

4.2.9 Statistics

All statistical analyses were performed using GraphPad Prism software (GraphPad Software, Inc., La Jolla, CA USA). All data is expressed as the mean ± standard error of the mean of measured quantities. All n-values are listed below each corresponding figure. Statistically significant differences of all data sets were determined with a Students t-test corrected for multiple comparisons using the Holm-Sidak method, with differences deemed significant for $p < 0.05$.

4.3 Results

4.3.1 Emulsion and ARS Properties

Figure 4.2A shows the flow focusing geometry of the microfluidic device used to produce the double emulsion. The primary emulsion (W_1/PFC), containing bFGF in the W_1 phase and stabilized by fluorosurfactant, was pumped through the inner channel (yellow arrow). The primary emulsion was generated offline via sonication. The flow from the inner channel converged at the junction with two lateral flow channels (green arrows) of an aqueous solution of Pluronic F68, the W_2 phase. Double emulsions were formed at the junction and exited the device through the bottom channel into a collection vial. To confirm morphology of the generated

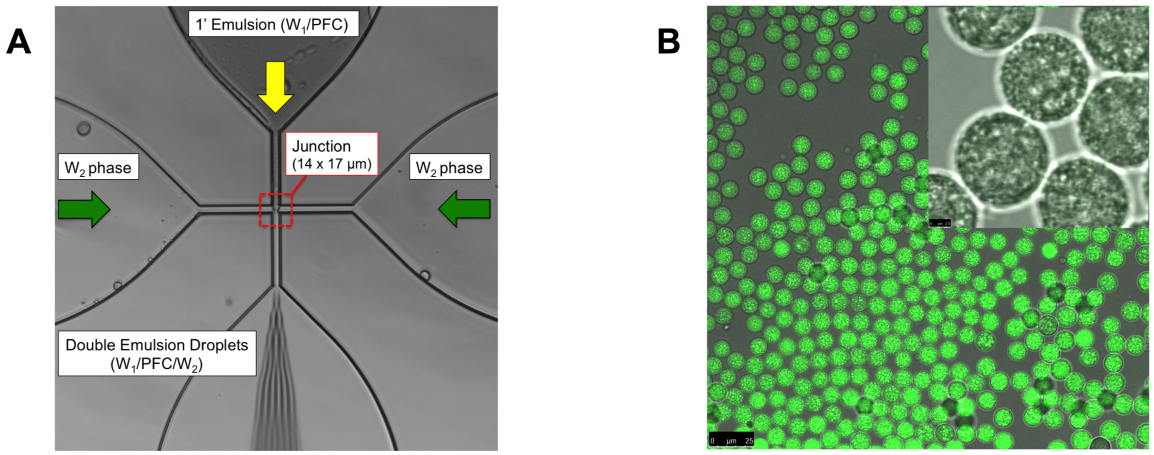

Figure 4.2: (A) An image highlighting the flow focusing geometry of the microfluidic device, including the 14 x 17 μm junction where the monodispersed double emulsions were formed. (B) Confocal microscopy images of the resulting double emulsion at 40x and 100x magnification for the large and inset images, respectively. The images show emulsions that are visually uniform in size. Scale bars: 25 μm (large image) and 2.5 μm (inset).

double emulsion, the emulsions were imaged using confocal microscopy. Images of a double emulsion with Alexa Fluor 488-labeled dextran in the W_1 phase are displayed in Figure 4.2B. The double emulsion droplets appeared uniform in size and the W1 droplets were submicron in diameter. Identical morphology was observed for double emulsions containing bFGF (images not shown). The size distribution of the emulsion, measured with a Coulter counter, is shown in Figure 4.3A. The emulsions had a mean diameter of 13.9 $\pm$ 0.04 μm and a coefficient of variance (CV) of 4.5%. The encapsulation efficiency of bFGF in the emulsions was 99.3 $\pm$ 1.6%.

The ADV and IC thresholds of the ARS were determined by passively detecting the scattered fundamental and broadband acoustic signals, respectively. Figure 4.3B shows the frequency spectrum from ARSs exposed to US that was either below (black) or above (red) the ADV threshold. The presented spectrum accounts for background subtraction of a fibrin gel without emulsion. The frequency spectra appeared qualitatively similar to the black signal until the ADV threshold was reached. Following ADV, bubbles formed in the ARS lead to an increase in the

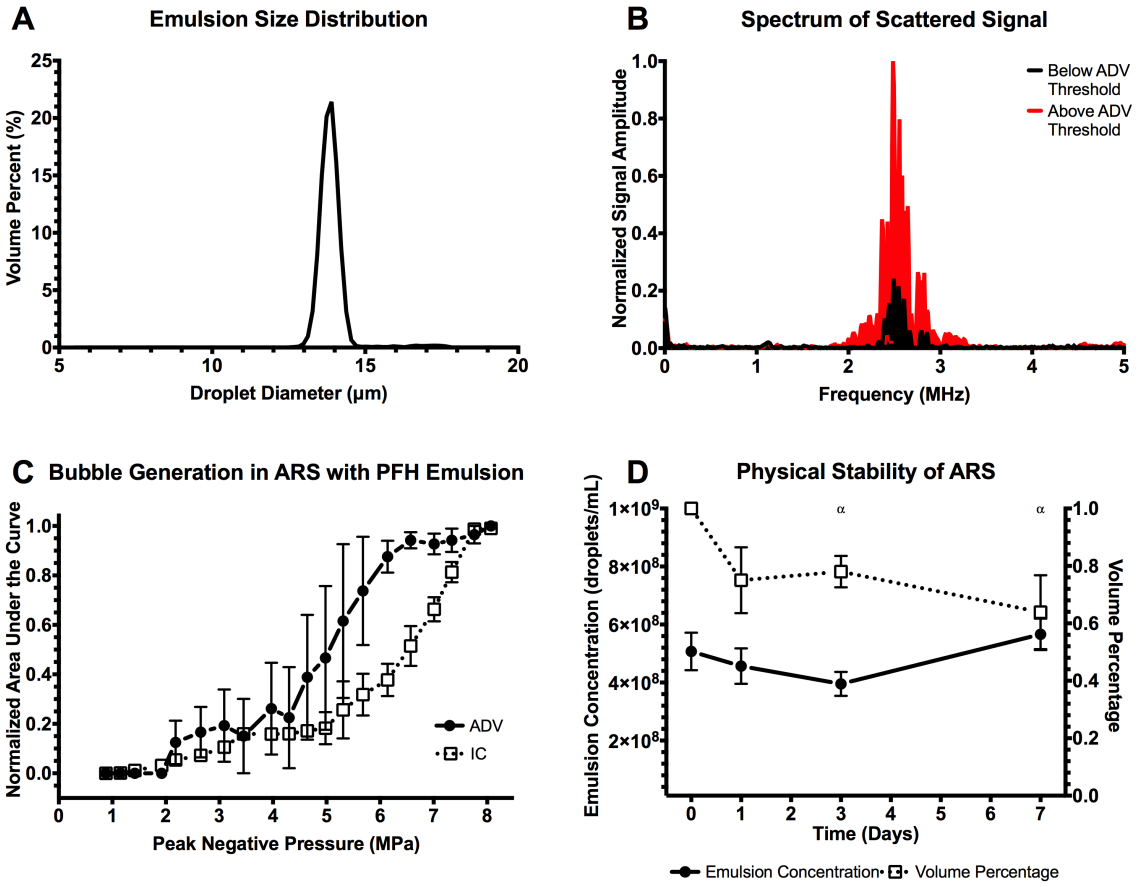

Figure 4.3: (A) Volume-weighted size distribution of the monodispersed double emulsion. The mean diameter and coefficient of variance of the emulsion was 13.9 ± 0.04 μm and 4.5%, respectively. (B) The scattered, fundamental frequency (i.e., 2.5 MHz) was passively recorded and used as an indicator of ADV, specifically the presence of bubbles generated in the ARS. (C) At pressures above the ADV threshold, 2.2 μ 0.2 MPa, bubble formation was evident. Additionally, the scattered broadband noise was also recorded and used as an indicator of IC, caused by rapid expansion and collapse of the bubbles formed through ADV at high pressures. The IC threshold was 4.8 μ 1.5 MPa (n=3 for both ADV and IC measurements). (D) Stability of the ARS, specifically the emulsions within the ARS, when placed in a cell culture incubator at 37°C (n=5). Statistically significant differences ($p < 0.05$) relative to day 0 for n=5 samples are denoted by α.

intensity of the scattered signal (red). The relationship between the fundamental signal, broadband signal, and acoustic pressure is shown in Figure 4.3C. The ADV threshold of the ARS was 2.2 ± 0.2 MPa and the IC threshold was 4.8 ± 1.5 MPa. At subthreshold pressures, bubble formation, characterized by the integrated fundamental signal, was negligible. At superthreshold pressures, bubble formation and IC correlated with acoustic pressure. Figure 4.3D shows the *in vitro* physical stability of the emulsion within the ARSs as a function of time. There were no statistically significant changes in emulsion concentration. However, there were significant decreases in the volume percent of emulsion in the ARS on days 3 and 7. As displayed in Figure 4.4, the mean diameter and CV decreased and increased, respectively, over time.

4.3.2 *In Vitro* Release of bFGF from the ARSs

Figure 4.5 shows macroscopic images of ARSs exposed to various US conditions. ARSs not exposed to US or exposed to US at a subthreshold pressure (i.e., 2 MPa), have minimal bubble formation, which is indicative of the absence of ADV. ARSs exposed to US at superthreshold pressures (i.e., 4 and 8 MPa) contain bubbles from ADV. The bubbles in the ARSs on day 2 are larger than those on day 1 (the day of US exposure). Figure 4.7A shows that release of bFGF from ARSs correlated with acoustic pressure. By day 7, the cumulative percentage of bFGF released when the ARSs were exposed to 0 (i.e. US), 2, 4, and 8 MPa was 1.4 ± 0.4%, 1.9 ± 0.7%, 8.4 ± 2.9%, and 17.9 ± 4.5%, respectively. bFGF release at 4 and 8 MPa was statistically different from the US condition on days 2-7. No significant differences in bFGF release were observed at any time point when comparing 0 and 2 MPa, which was expected since 2 MPa is subthreshold. A delayed release experiment was performed where the initial US exposure was done on day 4, rather than day 1. This experimental condition, which used 8 MPa, yielded 6.6 ± 0.6% bFGF release by day 7, which was 3 days after the initial US exposure. Significant bFGF release was

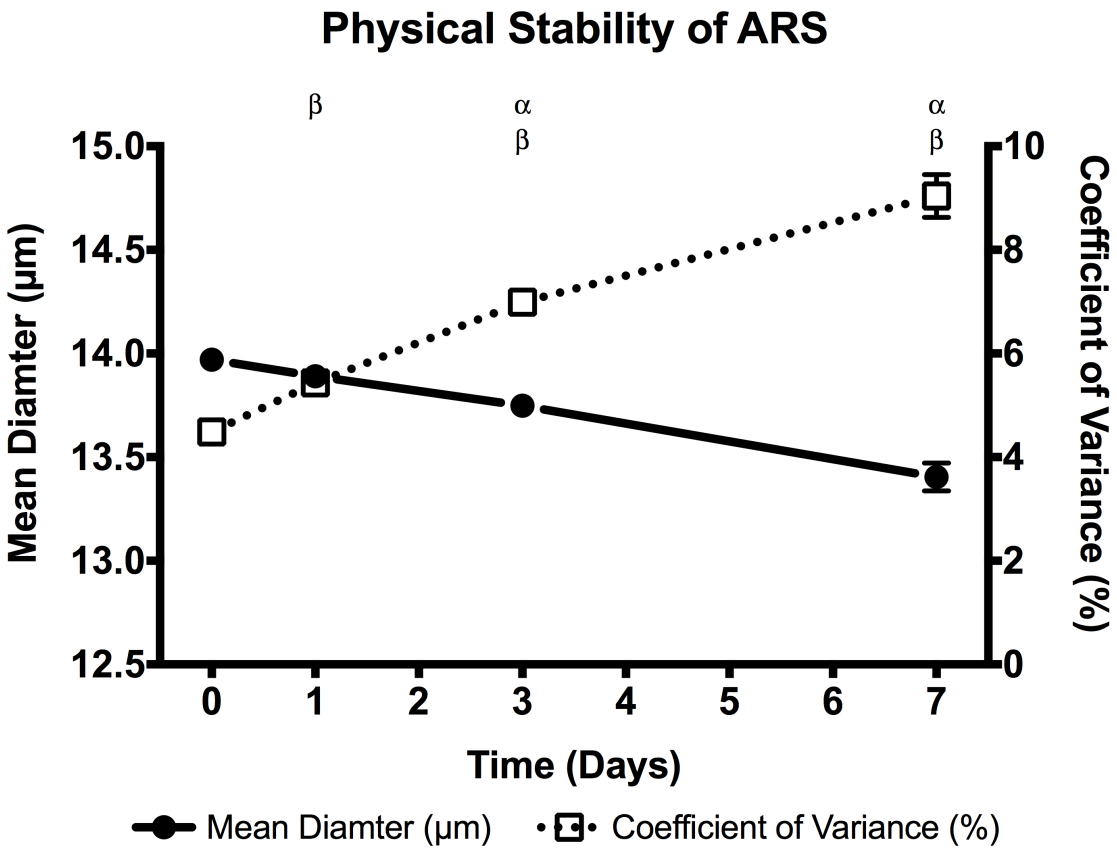

Figure 4.4: Stability of the ARS (n=5), specifically the emulsions within the ARS, when placed in a cell culture incubator at 37°C. Statistically significant differences (p ¡ 0.05) relative to day 0 for n=5 gels are denoted by α for mean diameter and β for coefficient of variance.

observed for this delayed experiment on days 5-7, demonstrating temporal control of bFGF release.

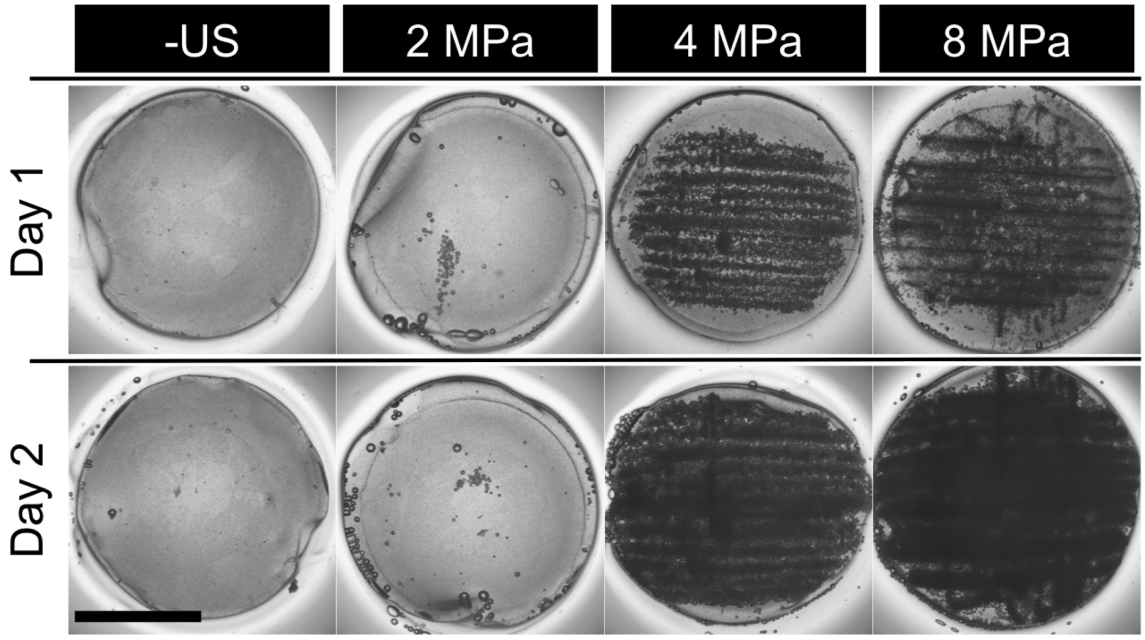

Figure 4.5: Images of ARSs after exposure to various US pressures on day 1. ARSs exposed to superthreshold US (i.e. $>$ 2.2 MPa) show bubble formation on day 1, while subthreshold US (i.e. $<$ 2.2 MPa) exposures yield no bubble formation. Scale bar: 8 mm. The generated bubbles increase in size by day 2 due to in-gassing.

In Figure 4.7B, the bioactivity of bFGF released from an ARS at 4 and 8 MPa, as well as from a fibrin gel, is displayed. The presented values are calculated relative to cells incubated with freshly prepared bFGF standards (see Figure 4.6). At 4 MPa, the bioactivity was 113.3 $\pm$ 9.4% and 100.9 $\pm$ 11.6% for releasates collected on days 2 and 6, respectively, while at 8 MPa exposure the bioactivity was 118.1 $\pm$ 8.0% and 90.0 $\pm$ 16.6%, respectively. For a fibrin gel with non-encapsulated bFGF (i.e., fibrin + bFGF), the bioactivity was 157.4 $\pm$ 9.4% and 135.0 $\pm$ 6.9% for days 2 and 6, respectively. Within an experimental group, there were no significant differences in bioactivity between time points. However, both ARS conditions tested lower than fibrin + bFGF on each day. The concentration of bFGF released at 0 or 2 MPa was too low to induce cell proliferation.

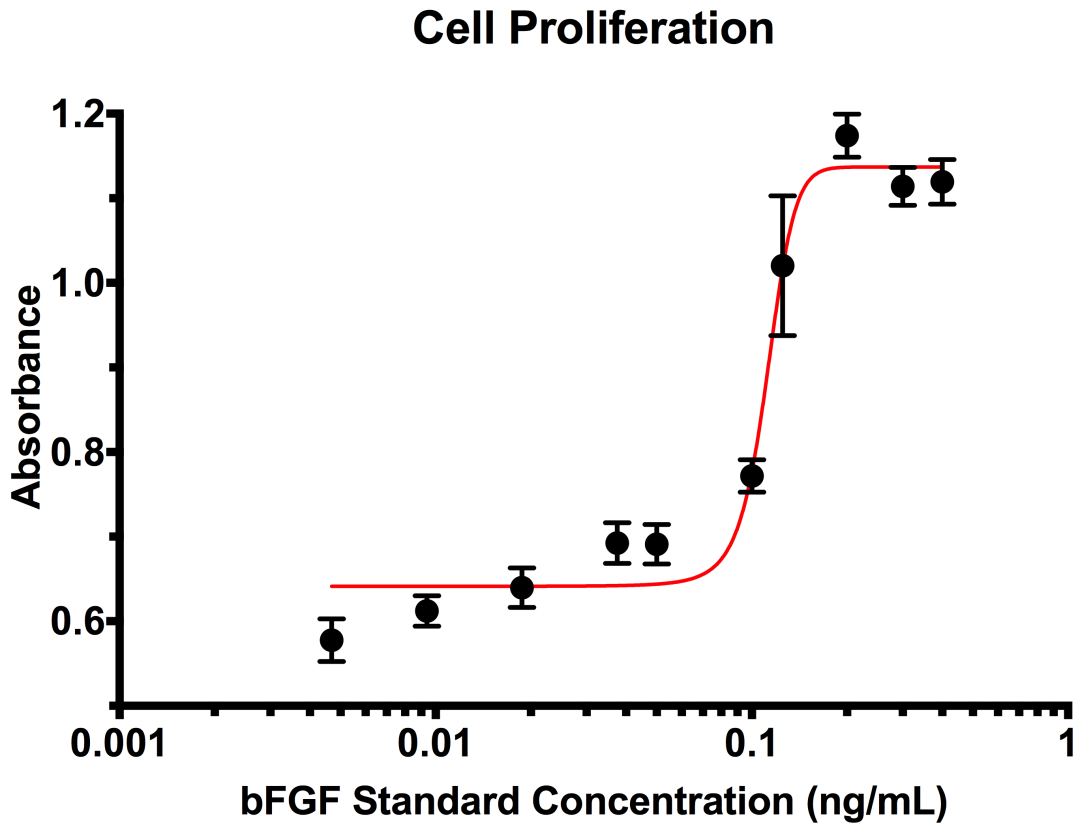

Figure 4.6: The proliferation of NR-6-R cells when incubated with increasing concentrations of freshly prepared bFGF. Proliferation was assessed after 44 hours using the CellTiter 96 assay for n=10 wells/bFGF concentration.

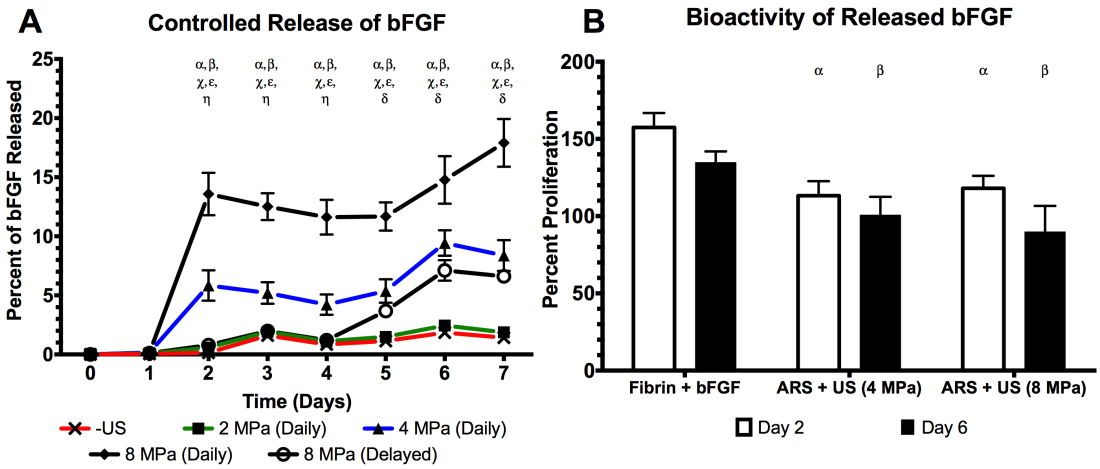

Figure 4.7: US was used to control the release of bioactive, bFGF from an ARS (A) The percent of bFGF released as a function of acoustic pressure where Daily indicates US exposure on days 1-7. A delayed release experiment was also performed (i.e., Delayed) where US was applied on days 4-7. (B) The bioactivity of the released growth factor was determined by incubating NR-6-R fibroblasts with releasate. Cell proliferation was measured after 44 hours. Releasates obtained at 0 or 2 MPa did not contain enough bFGF to induce cell proliferation. All data is represented as mean ± standard error of the mean for n = 5 ARSs. For (A), statistically significant differences ($p < 0.05$) are denoted as follows. α: 8 MPa (daily) vs. US; β: 4 MPa (daily) vs. US; χ: 8 MPa (daily) vs. 4 MPa (daily); ϵ: 8 MPa (daily) vs. 8 MPa (delayed); η: 4 MPa (daily) vs. 8 MPa (delayed); δ: 8 MPa (delayed) vs. -US. For (B), statistically significant differences (p ¡ 0.05) are denoted as follows. α: vs. fibrin+bFGF on day 2, β: vs. fibrin+bFGF on day 6.

4.3.3 *In Vivo* Release of bFGF from the ARSs

LASCA imaging was used to non-invasively and longitudinally monitor perfusion in and around the subcutaneous implants placed in the lower dorsal region. Figure 4.8 shows a representative set of images used to quantify relative perfusion. Qualitatively, the images show that greater perfusion was observed with the ARS exposed to US (i.e., ARS+US, red circle) versus the ARS not exposed to US (i.e., ARS, black circle). The fibrin implants containing bFGF yielded more perfusion than the fibrin control, and overall less perfusion than either ARS condition. Figure 4.9A displays a quantitative analysis of the images, based on ROIs. The perfusion for both ARS and ARS+US increased up to day 7, with the greatest change in perfusion relative to day 0 observed on day 7 (i.e., 54.0 ± 13.1 and 97.0 ± 14.8% for ARS and ARS+US, respectively). After day 7, the change in perfusion decreased, with a difference of 12.7 ± 6.7 and 25.8 ± 6.3% on day 14 for ARS and ARS+US, respectively. The greatest changes in perfusion induced by fibrin or fibrin+bFGF was observed on day 3 (7.7 ± 5.0 and 20.9 ± 7.0% for fibrin and fibrin+bFGF, respectively). There were significant differences between ARS and ARS+US on days 7 and 10, and no differences between fibrin and fibrin+bFGF at any time point. The ARS condition yielded greater relative perfusion than fibrin on day 7, and ARS+US yielded a greater perfusion than both fibrin and fibrin+bFGF on days 7 and 10.

Figure 4.9B shows the blood vessel density within the ARSs and fibrin implants, based on CD31-staining. On day 7, greater blood vessel density was observed in ARS+US versus ARS (126.8 ± 23.8 and ± 73.1 *pm* 21.2 vessels/mm^2, respectively). All three groups containing bFGF displayed more blood vessels than the fibrin control on day 7. On day 14, greater vascularization was still observed in ARS+US versus ARS. However, blood vessel density regressed in the fibrin + bFGF group.

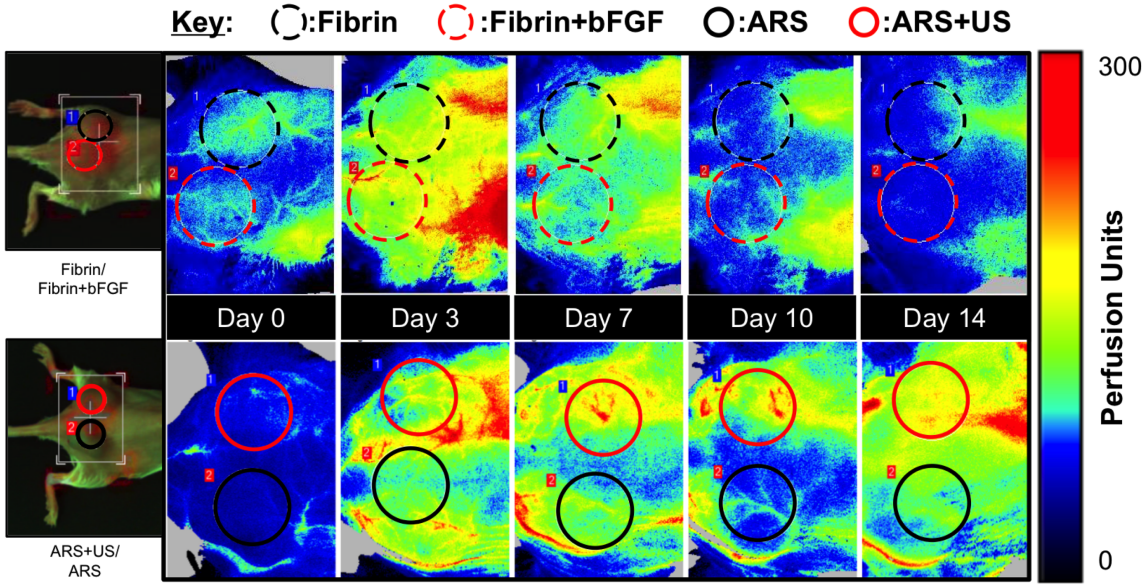

Figure 4.8: Longitudinal LASCA images of two mice, each with two implants. The regions of interests (ROIs) were chosen based on the physical location of the implants, and are denoted by colored circles. The left most images are visible images of the mice. For all images, the caudal direction is left. ROI diameter: 0.9 cm.

4.3.4 Degradation of the ARSs *In Vivo*

The degradation of ARS and ARS+US is shown in Figure 4.10. At 14 days after implantation there was 36.3 ± 9.0 and 39.0 ± 9.1% remaining of the ARS and ARS+US, respectively. There were no significant differences between ARS and ARS+US at any time point.

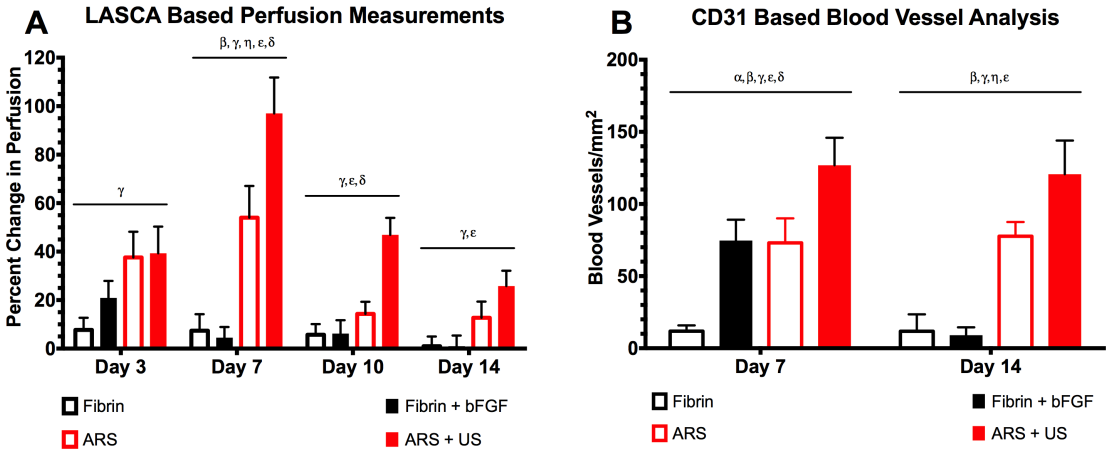

Figure 4.9: US increased perfusion and blood vessel growth in the bFGF-loaded ARSs (A) Quantification of LASCA images using ROIs. The greatest change in perfusion was observed on day 7, with ARS+US exhibiting greater perfusion than ARS. The differences between ARS and ARS+US were significant on days 7 and 10. All data is represented as mean ± standard error of the mean for n = 8 ARSs (days 1-7) and n = 4 ARSs (days 10 and 14). Statistically significant differences ($p < 0.05$) are denoted as follows. β: Fibrin vs. ARS; γ: Fibrin vs. ARS+US; η: Fibrin+bFGF vs. ARS; ϵ: Fibrin+bFGF vs. ARS+US; δ: ARS vs. ARS+US. (B) Blood vessels were identified using CD31 staining. On both days 7 and 14, the greatest blood vessel density was observed for ARS + US. All data is represented as mean ± standard error of the mean for n = 8 ARSs (days 1-7) and n = 4 ARSs (days 10 and 14). Statistically significant differences ($p < 0.05$) are denoted as follows. α: Fibrin vs. Fibrin+bFGF; β: Fibrin vs. ARS; γ: Fibrin vs. ARS+US; η: Fibrin+bFGF vs. ARS; ϵ: Fibrin+bFGF vs. ARS+US; δ: ARS vs. ARS+US.

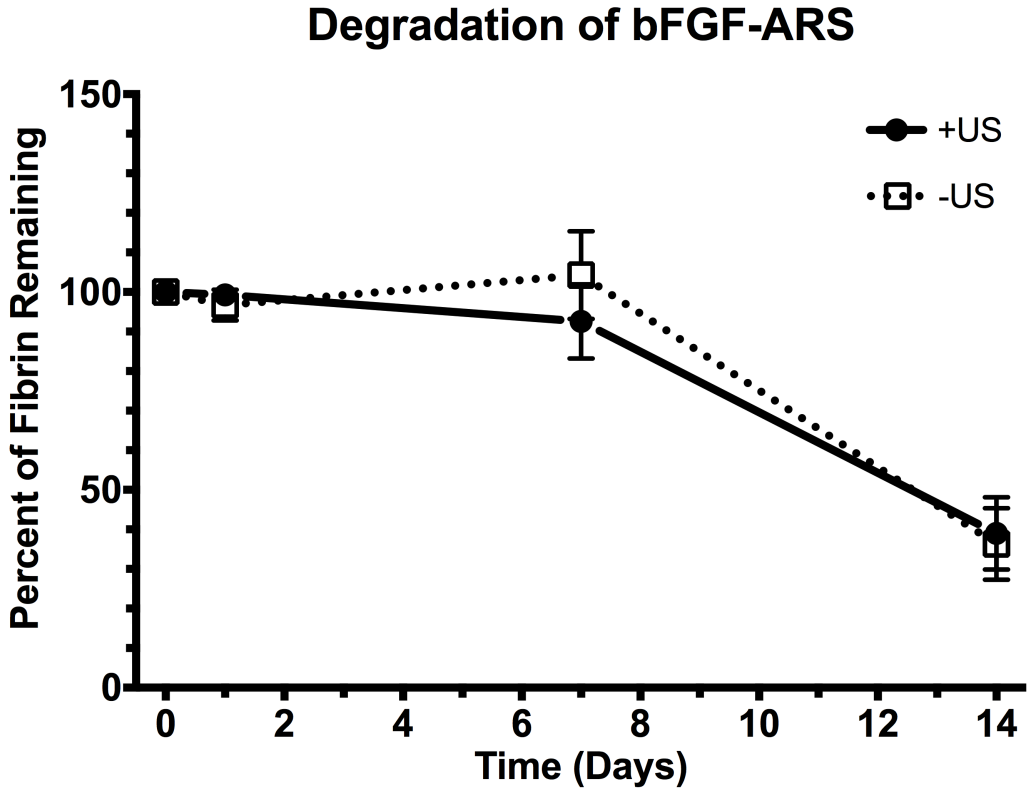

Figure 4.10: Degradation of the subcutaneously-implanted ARSs, which contained Alexa Fluor 647-labeled fibrinogen, was longitudinally monitored using a fluorescence, *in vivo* imaging system. All data is represented as mean ± standard error of the mean for n = 8 ARSs (days 1-7) and n = 4 ARSs (day 14).

4.4 Discussion

Many approaches have been used to obtain spatiotemporally-controlled delivery of growth factors from implantable scaffolds. In this work, US was shown to increase perfusion and angiogenesis via the controlled release of bFGF from an ARS. bFGF release was triggered by focused, megahertz range US, which can be applied non-invasively and in a spatiotemporally-defined manner. Unlike passive approaches, the ARS provides a method of actively modulating growth factor release after polymerization and implantation of the scaffold. The highly versatile nature of the ARS - including the ability to modulate properties of the emulsion, scaffold, and US [39] - suggests that the ARS could be beneficial in both basic and applied studies of therapeutic angiogenesis. This is the first study to use monodispersed emulsions in ARSs. Previous studies have demonstrated several advantages of using monodispersed, sonosensitive emulsions including uniform ADV thresholds and improved stability during storage [48, 49]. Our prior publication showed that the droplet concentration and volume in an ARS with polydispersed PFH emulsions increased over time [39], likely due to a difference in the chemical potential of the material within the emulsions as defined by the Ostwald ripening phenomena [50]. A polydispersed emulsion is non-ideal for achieving spatiotemporally-controlled release from an ARS since ADV thresholds are inversely correlated with droplet size [51, 52] and larger emulsions have a higher probability of spontaneous vaporization at lower temperatures [41, 53]. ARSs with monodispersed PFH emulsion displayed greater stability (Figure 4.3D) with no significant change in concentration over time. We did observe a decrease in droplet volume that was associated with an increased CV (Figure 4.4), which suggests that the W1 phase slowly leaked out of the double emulsion. This hypothesis is further supported by the non-zero release of bFGF in the absence of US or at subthreshold pressures (Figure 4.7A).

Figure 4.7A shows that the amount of bFGF released correlated with acoustic

pressure for superthreshold pressures while little release was observed with subthreshold pressures. Relative to the US exposure at 8 MPa, less than 8% of bFGF was released in the absence of US by day 7, thus demonstrating stable payload retention for the US condition. These release profiles are consistent with Figure 4.3C, which displays an ADV threshold of 2.2 ± 0.2 MPa. The majority of the bFGF release for superthreshold pressures occurred one day after US exposure. This is due to the lack of attenuating bubbles in the ARS prior to US exposure, which is identical to the US condition shown in Figure 4.5. Subsequent US exposures on day 2 and onward did ultimately cause additional bFGF release, which is consistent with our previous study that demonstrated the benefit of daily US exposures [32]. The impact of bubble attenuation could be mitigated by formulating the ARS with a higher boiling point PFC that is more likely to recondense after ADV [54, 55] or by using US to dislodge bubbles from the ARS by enhancing fibrin degradation [32]. bFGF is known to bind fibrin irreversibly with nanomolar affinity via heparin-binding domains [56]. Therefore, a fraction of the bFGF released from the emulsion binds to fibrin within the ARS, thus hindering its release. The mechanisms by which US interacts with bFGF in the ARS were outside of the scope of the current study, but warrant further investigation. For example, we previously demonstrated that US can increase both the release of unencapsulated dextran from a conventional fibrin hydrogel and the degradation rate of an ARS [32]. Therefore, US could facilitate diffusion of bFGF in the ARS, though it is important to note that unlike dextran, bFGF displays a high affinity for fibrin [57].

As seen in Figure 4.5, the gas bubbles generated by ADV persisted within the ARS. The following mechanisms can potentially explain this observation. The bulk boiling point of PFH, the sonosensitive phase within the ARS, is 56°C. When formulated as droplets, the boiling point of PFH is higher due to the Laplace pressure [51, 52]. Therefore, it is expected that PFH should form transient bubbles

that ultimately recondense, unless PFH existed as a supercooled gas. Alternatively, the persistent bubbles could consist of gas, which was initially dissolved in the liquid PFH due to its high gas solubility [58-60], and that nucleated following ADV. As shown in our prior study [33]. the consolidation of the fibrin surrounding each bubble could also facilitate the persistence of the bubbles in the ARS. As shown macroscopically in Figure 4.5, the bubbles generated in the ARSs due to ADV increase in size from day 1 (i.e., the first day of US exposure) to day 2. This is due to diffusion of dissolved gases within the media overlying the ARS into the PFH bubbles [35]. This gas modulating capacity of the ARS could potentially explain why ARSs have been shown to increase angiogenesis even in the absence of angiogenic growth factors in the W1 phase of the emulsion [32]. However, the angiogenic response induced following release of bFGF from the ARS (Figure 4.9B) is significantly greater than without bFGF.

The bioactivity of the bFGF released in the *in vitro* experiments was assessed by measuring the proliferation of NR-6-R cells following incubation with releasates of known bFGF concentration. Proliferation was normalized relative to that obtained with freshly prepared bFGF standards in serum free media (Figure 4.6). In most cases, proliferation was greater than 100% (Figure 4.7B). We have shown *in vitro* that fibrin gels and ARSs degrade over time, both in the presence and absence of US [32]. Thus, the releasate added to the NR-6-R cells contained some soluble components from this degradation. Prior studies demonstrated that fibrin promotes the proliferation of various types of cells [61-63], which could explain the enhanced proliferation observed in Figure 4.7B.

The bioactivity measured for both ARS conditions was lower than a fibrin gel containing non-encapsulated bFGF. There are two possible explanations for this: 1) acoustic mechanisms (i.e., ADV and/or IC) and 2) the method by which the primary emulsion was prepared. Figure 4.3C shows that the IC threshold was 4.8 $\pm$ 1.5 MPa.

Thus, there are instances of IC at 4 MPa and sustained IC at 8 MPa. The rapid expansion and collapse of a bubble during IC can generate very high temperatures and velocities at the bubble site, which can lead to molecular degradation, cellular damage, and sonoporation [64]. Given that there was no significant difference in bioactivity between 4 and 8 MPa, IC is not likely the main mechanism. ADV can also generate high fluid velocities as the PFC within the droplet transitions from a liquid into a gas [34], which can lead to cellular deplating [36, 65] and sonoporation [66]. Both 4 and 8 MPa are superthreshold for ADV, so ADV itself could be impacting the bioactivity of bFGF. A reduction in the pulse length or pulse repetition frequency could reduce the impact of ADV. Another possibility is that the bioactivity of the bFGF was affected by sonication at 20 kHz, the method used to produce the primary emulsion (W_1/PFC). The use of a microfluidic device that enables the formation of the double emulsion using two sequential junctions would obviate the need for sonication, which has been shown to impact protein structure and cause protein aggregation [67].

Significantly greater perfusion and angiogenesis were observed for ARS + US versus ARS. Both ARS conditions yielded more sustained increases in perfusion and angiogenesis compared to delivery using a conventional fibrin scaffold (Figure 4.9). Burst release of bFGF occurs when the growth factor is incorporated directly into a conventional fibrin scaffold [68, 69]. This burst release, coupled with the lack of physiologic demand of vascularization in a subcutaneous implantation model, lead to a transient increase in both perfusion and blood vessel growth for fibrin + bFGF. Vessel regression could explain why the fibrin + bFGF group displayed lower perfusion than ARS and ARS + US groups on day 7 yet had the same blood vessel density, based on CD31 staining, as the ARS group. Since vessels lacking perfusion are prone to regression [70, 71], it is possible that vessels in the fibrin + bFGF group did not mature enough to acquire a substantial blood flow. Additionally, it

is also important to consider that perfusion was monitored using a LASCA system, which relies on speckle contrast generated by moving erythrocytes. This technique inherently lacks axial (i.e., in plane) spatial resolution due to its two-dimensional nature. Thus, unlike blood vessel counting via tissue sectioning, the perfusion measurements were not restricted to the axial location of the implant and thereby included effects within the implant and in overlying tissue layers. Additionally, the perfusion measurements could include effects related to both angiogenesis and arteriogenesis, the latter of which would not change the number of vessels. On day 14, the trends observed with both the perfusion and immunohistochemical data were consistent for the experimental groups, with blood vessels regressing in fibrin + bFGF to a level similar to that found with fibrin only. The degradation of ARSs is an important component of the controlled release process that may affect the uncontrolled release of the bFGF. The degradation may be due to factors within the ARS or the subcutaneous environment such as protease impurities in the starting fibrinogen [72], uptake and clearance by blood and lymphatic vessels [73], and US exposure [32]. Prior studies have shown that US exposure can disrupt hydrogel crosslinking as well as enhance diffusion through the creation of micropores [74, 75]. The results in Figure 4.10 are consistent with our prior work conducted with Alexa-Fluor 680 dextran loaded emulsions [32], where US did not impact the *in vivo* degradation rate of ARSs. In the current study, a slower degradation rate over the first 7 days was observed compared with our prior study. This difference could be due to the use of monodispersed versus polydispersed emulsions.

4.5 Conclusion

Here we show that controlled release of bioactive bFGF is possible using ARSs with monodispersed emulsions in conjunction with non-invasive, focused ultrasound. Monodispersed, double emulsions were made in a two-step approach by first

sonicating the primary emulsion followed by generating a double emulsion using a microfluidic device with a flow focusing geometry. *In vitro* studies showed that the amount of bFGF released was dependent on the acoustic pressure of the US exposure, and that bFGF release could be delayed by postponing the initial US exposure. In addition, the bioactivity of the released bFGF was independent of the acoustic pressure used for US exposure as well as the time at which it was measured. Although the bioactivity of the bFGF released from the ARS was somewhat lower than unencapsulated bFGF, overall, ARSs with monodispered emulsions displayed better stability than was previously observed with polydispersed emulsions. *In vivo* studies demonstrated that controlled release of bFGF from an ARS exposed to US increased perfusion and blood vessel formation compared to an ARS without US. Both ARS conditions yielded greater perfusion and blood vessel formation than fibrin alone or a conventional fibrin scaffold doped with bFGF. US exposure did not affect the *in vivo* degradation of the ARS. These results show that ARSs can be used for *in vivo* controlled release of pro-angiogenic growth factors for both basic science and applied studies of therapeutic angiogenesis. Future work will focus on improving the bioactivity of the bFGF from the ARS as well as establishing proof-of-concept in an animal model of ischemia.

4.6 Acknowledgements

This work was supported by NIH grant R21AR065010 (MLF) and the Basic Radiological Sciences Innovative Research Award (MLF). AM was supported by the National Science Foundation Graduate Student Research Fellowship (Grant No. DGE 1256260). EGO and ML were supported by funds from the Undergraduate Research Opportunity Program. Special thanks to Dr. Allen F. Brooks for aiding in the synthesis of the fluorosurfactant used to formulate the double emulsions.

REFERENCES

[1] Cao, R.H., Brakenhielm, E., Pawliuk, R., Wariaro, D., Post, M.J., Wahlberg, E., Leboulch, P., and Cao, Y.H.: Angiogenic synergism, vascular stability and improvement of hind-limb ischemia by a combination of PDGF-BB and FGF-2, Nat Med, 2003, 9, (5), pp. 604-613

[2] Li, J., Wei, Y.Q., Liu, K., Yuan, C., Tang, Y.J., Quan, Q.L., Chen, P., Wang, W., Hu, H.Z., and Yang, L.: Synergistic effects of FGF-2 and PDGF-BB on angiogenesis and muscle regeneration in rabbit hindlimb ischemia model, Microvasc Res, 2010, 80, (1), pp. 10-17

[3] Awada, H.K., Johnson, N.R., and Wang, Y.D.: Sequential delivery of angiogenic growth factors improves revascularization and heart function after myocardial infarction, Journal of Controlled Release, 2015, 207, pp. 7-17

[4] Richardson, T.P., Peters, M.C., Ennett, A.B., and Mooney, D.J.: Polymeric system for dual growth factor delivery, Nat Biotechnol, 2001, 19, (11), pp. 1029-1034

[5] Phelps, E.A., Landazuri, N., Thule, P.M., Taylor, W.R., and Garcia, A.J.: Bioartificial matrices for therapeutic vascularization, Proceedings of the National Academy of Sciences of the United States of America, 2010, 107, (8), pp. 3323-3328

[6] Lederman, R.J., Mendelsohn, F.O., Anderson, R.D., Saucedo, J.F., Tenaglia, A.N., Hermiller, J.B., Hillegass, W.B., Rocha-Singh, K., Moon, T.E., Whitehouse, M.J., Annex, B.H., and Investigators, T.: Therapeutic angiogenesis with recombinant fibroblast growth factor-2 for intermittent claudication (the TRAFFIC study): a randomised trial, Lancet, 2002, 359, (9323), pp. 2053-2058

[7] Lazarous, D.F., Unger, E.F., Epstein, S.E., Stine, A., Arevalo, J.L., Chew, E.Y., and Quyyumi, A.A.: Basic fibroblast growth factor in patients with intermittent claudication: Results of a phase I trial, J Am Coll Cardiol, 2000, 36, (4), pp. 1239-1244

[8] Cooper, L.T., Hiatt, W.R., Creager, M.A., Regensteiner, J.G., Casscells, W., Isner, J.M., Cooke, J.P., and Hirsch, A.T.: Proteinuria in a placebo-controlled

study of basic fibroblast growth factor for intermittent claudication, Vasc Med, 2001, 6, (4), pp. 235-239

[9] Makinen, K., Manninen, H., Hedman, M., Matsi, P., Mussalo, H., Alhava, E., and Yla-Herttuala, S.: Increased vascularity detected by digital subtraction angiography after VEGF gene transfer to human lower limb artery: a randomized, placebo-controlled, double-blinded phase II study, Molecular therapy : the journal of the American Society of Gene Therapy, 2002, 6, (1), pp. 127-133

[10] Rajagopalan, S., Mohler, E.R., Lederman, R.J., Mendelsohn, F.O., Saucedo, J.F., Goldman, C.K., Blebea, J., Macko, J., Kessler, P.D., Rasmussen, H.S., and Annex, B.H.: Regional angiogenesis with vascular endothelial growth factor in peripheral arterial disease - A phase II randomized, double-blind, controlled study of adenoviral delivery of vascular endothelial growth factor 121 in patients with disabling intermittent claudication, Circulation, 2003, 108, (16), pp. 1933-1938

[11] Powell, R.J., Simons, M., Mendelsohn, F.O., Daniel, G., Henry, T.D., Koga, M., Morishita, R., and Annex, B.H.: Results of a double-blind, placebo-controlled Study to Assess the Safety of Intramuscular Injection of Hepatocyte Growth Factor Plasmid to Improve Limb Perfusion in Patients with Critical Limb Ischemia, Circulation, 2008, 118, (1), pp. 58-65

[12] Morishita, R., Aoki, M., Hashiya, N., Makino, H., Yamasaki, K., Azuma, J., Sawa, Y., Matsuda, H., Kaneda, Y., and Ogihara, T.: Safety evaluation of clinical gene therapy using hepatocyte growth factor to treat peripheral arterial disease, Hypertension, 2004, 44, (2), pp. 203-209

[13] Grochot-Przeczek, A., Dulak, J., and Jozkowicz, A.: Therapeutic angiogenesis for revascularization in peripheral artery disease, Gene, 2013, 525, (2), pp. 220-228

[14] Blatchley, M.R., and Gerecht, S.: Acellular implantable and injectable hydrogels for vascular regeneration, Biomed Mater, 2015, 10, (3)

[15] Briquez, P.S., Clegg, L.E., Martino, M.M., Mac Gabhann, F., and Hubbell, J.A.: Design principles for therapeutic angiogenic materials, Nat Rev Mater, 2016, 1, (1)

[16] Comerota, A.J., Throm, R.C., Miller, K.A., Henry, T., Chronos, N., Laird, J., Sequeira, R., Kent, C.K., Bacchetta, M., Goldman, C., Salenius, J.P., Schmieder, F.A., and Pilsudski, R.: Naked plasmid DNA encoding fibroblast growth factor type I for the treatment of end-stage unreconstructible lower extremity ischemia: Preliminary results of a phase I trial, J Vasc Surg, 2002, 35, (5), pp. 930-936

[17] Nikol, S., Baumgartner, I., Van Belle, E., Diehm, C., Visona, A., Capogrossi, M.C., Ferreira-Maldent, N., Gallino, A., Wyatt, M.G., Wijesinghe, L.D., Fusari, M., Stephan, D., Emmerich, J., Pompilio, G., Vermassen, F., Pham, E., Grek, V., Coleman, M., and Meyer, F.: Therapeutic angiogenesis with intramuscular NV1FGF improves amputation-free survival in patients with critical limb ischemia, Molecular Therapy, 2008, 16, (5), pp. 972-978

[18] Belch, J., Hiatt, W.R., Baumgartner, I., Driver, I.V., Nikol, S., Norgren, L., Van Belle, E., and Investigators, T.C.: Effect of fibroblast growth factor NV1FGF on amputation and death: a randomised placebo-controlled trial of gene therapy in critical limb ischaemia, Lancet, 2011, 377, (9781), pp. 1929-1937

[19] Kusumanto, Y.H., van Weel, V., Mulder, N.H., Smit, A.J., van den Dungen, J.J., Hooymans, J.M., Sluiter, W.J., Tio, R.A., Quax, P.H., Gans, R.O., Dullaart, R.P., and Hospers, G.A.: Treatment with intramuscular vascular endothelial growth factor gene compared with placebo for patients with diabetes mellitus and critical limb ischemia: a double-blind randomized trial, Hum Gene Ther, 2006, 17, (6), pp. 683-691

[20] Baumgartner, I., Pieczek, A., Manor, O., Blair, R., Kearney, M., Walsh, K., and Isner, J.M.: Constitutive expression of phVEGF165 after intramuscular gene transfer promotes collateral vessel development in patients with critical limb ischemia, Circulation, 1998, 97, (12), pp. 1114-1123

[21] Lei, P., Padmashali, R.M., and Andreadis, S.T.: Cell-controlled and spatially arrayed gene delivery from fibrin hydrogels, Biomaterials, 2009, 30, (22), pp. 3790-3799

[22] Yang, H.S., Bhang, S.H., Hwang, J.W., Kim, D.I., and Kim, B.S.: Delivery of Basic Fibroblast Growth Factor Using Heparin-Conjugated Fibrin for Therapeutic Angiogenesis, Tissue Eng Pt A, 2010, 16, (6), pp. 2113-2119

[23] Losi, P., Briganti, E., Errico, C., Lisella, A., Sanguinetti, E., Chiellini, F., and Soldani, G.: Fibrin-based scaffold incorporating VEGF- and bFGF-loaded nanoparticles stimulates wound healing in diabetic mice, Acta Biomaterialia, 2013, 9, (8), pp. 7814-7821

[24] Kniazeva, E., Kachgal, S., and Putnam, A.J.: Effects of Extracellular Matrix Density and Mesenchymal Stem Cells on Neovascularization *In Vivo*, Tissue Eng Pt A, 2011, 17, (7-8), pp. 905-914

[25] Ruhrberg, C., Gerhardt, H., Golding, M., Watson, R., Ioannidou, S., Fujisawa, H., Betsholtz, C., and Shima, D.T.: Spatially restricted patterning cues provided by heparin-binding VEGF-A control blood vessel branching morphogenesis, Genes & development, 2002, 16, (20), pp. 2684-2698

[26] Abe, Y., Ozaki, Y., Kasuya, J., Yamamoto, K., Ando, J., Sudo, R., Ikeda, M., and Tanishita, K.: Endothelial progenitor cells promote directional three-dimensional endothelial network formation by secreting vascular endothelial growth factor, PloS one, 2013, 8, (12), pp. e82085

[27] Li, X.M., Wang, J.H., Su, G.H., Zhou, Z.M., Shi, J.W., Liu, L.R., Guan, M., and Zhang, Q.Q.: Spatiotemporal control over growth factor delivery from collagen-based membrane, Journal of Biomedical Materials Research Part A, 2012, 100A, (2), pp. 396-405

[28] Silva, E.A., and Mooney, D.J.: Spatiotemporal control of vascular endothelial growth factor delivery from injectable hydrogels enhances angiogenesis, Journal of thrombosis and haemostasis : JTH, 2007, 5, (3), pp. 590-598

[29] Silva, E.A., and Mooney, D.J.: Effects of VEGF temporal and spatial presentation on angiogenesis, Biomaterials, 2010, 31, (6), pp. 1235-1241

[30] Brudno, Y., Ennett-Shepard, A.B., Chen, R.R., Aizenberg, M., and Mooney, D.J.: Enhancing microvascular formation and vessel maturation through temporal control over multiple pro-angiogenic and pro-maturation factors, Biomaterials, 2013, 34, (36), pp. 9201-9209

[31] Chen, R.R., Silva, E.A., Yuen, W.W., and Mooney, D.J.: Spatio-temporal VEGF and PDGF delivery patterns blood vessel formation and maturation, Pharmaceutical research, 2007, 24, (2), pp. 258-264

[32] Moncion, A., Arlotta, K.J., O'Neill, E.G., Lin, M., Mohr, L.A., Franceschi, R.T., Kripfgans, O.D., Putnam, A.J., and Fabiilli, M.L.: *In vitro* and *in vivo* assessment of controlled release and degradation of acoustically responsive scaffolds, Acta Biomaterialia, 2016, 46, pp. 221-233

[33] Fabiilli, M.L., Wilson, C.G., Padilla, F., Martin-Saavedra, F.M., Fowlkes, J.B., and Franceschi, R.T.: Acoustic droplet-hydrogel composites for spatial and temporal control of growth factor delivery and scaffold stiffness, Acta Biomaterialia, 2013

[34] Kripfgans, O.D., Fabiilli, M.L., Carson, P.L., and Fowlkes, J.B.: On the acoustic vaporization of micrometer-sized droplets, The Journal of the Acoustical Society of America, 2004, 116, (1), pp. 272-281

[35] Kripfgans, O.D., Fowlkes, J.B., Miller, D.L., Eldevik, O.P., and Carson, P.L.: Acoustic droplet vaporization for therapeutic and diagnostic applications, Ultrasound in Medicine and Biology, 2000, 26, (7), pp. 1177-1189

[36] Fabiilli, M.L., Haworth, K.J., Sebastian, I.E., Kripfgans, O.D., Carson, P.L., and Fowlkes, J.B.: Delivery of chlorambucil using an acoustically-triggered perfluoropentane emulsion, Ultrasound in Medicine and Biology, 2010, 36, (8), pp. 1364-1375

[37] Fabiilli, M.L., Lee, J.A., Kripfgans, O.D., Carson, P.L., and Fowlkes, J.B.: The release of thrombin, using acoustic droplet vaporization (ADV), from perfluoropentane double emulsions, IEEE International Ultrasonics Symposium, 2010

[38] Fabiilli, M.L., Lee, J.A., Kripfgans, O.D., Carson, P.L., and Fowlkes, J.B.: Delivery of water-soluble drugs using acoustically triggered perfluorocarbon double emulsions, Pharmaceutical research, 2010, 27, (12), pp. 2753-2765

[39] Moncion, A., Arlotta, K.J., Kripfgans, O.D., Fowlkes, J.B., Carson, P.L., Putnam, A.J., Franceschi, R.T., and Fabiilli, M.L.: Design and Characterization of Fibrin-Based Acoustically Responsive Scaffolds for Tissue Engineering Applications, Ultrasound in Medicine and Biology, 2016, 42, (1), pp. 257-271

[40] Orizondo, R.A., Babcock, C.I., Fabiilli, M.L., Pavlovsky, L., Fowlkes, J.B., Younger, J.G., and Cook, K.E.: Characterization of a reverse-phase perfluorocarbon emulsion for the pulmonary delivery of tobramycin, Journal of aerosol medicine and pulmonary drug delivery, 2014, 27, (5), pp. 392-399

[41] Schad, K.C., and Hynynen, K.: *In vitro* characterization of perfluorocarbon droplets for focused ultrasound therapy, Physics in Medicine and Biology, 2010, 55, (17), pp. 4933-4947

[42] Reznik, N., Williams, R., and Burns, P.N.: Investigation of Vaporized Submicron Perfluorocarbon Droplets as an Ultrasound Contrast Agent, Ultrasound in Medicine and Biology, 2011, 37, (8), pp. 1271-1279

[43] Garvin, K.A., Hocking, D.C., and Dalecki, D.: Controlling the Spatial Organization of Cells and Extracellular Matrix Proteins in Engineered Tissues Using Ultrasound Standing Wave Fields, Ultrasound in Medicine and Biology, 2010, 36, (11), pp. 1919-1932

[44] Rizzino, A., and Ruff, E.: Fibroblast growth factor induces the soft agar growth of two non-transformed cell, *In Vitro* Cell Dev Biol. 1986 Dec;22(12):749-55., (0883-8364 (Print))

[45] Promega: CellTiter 96® AQueous One Solution Cell Proliferation Assay, in Editor (Ed.)ˆ(Eds.): Book CellTiter 96 AQueous One Solution Cell Proliferation Assay (2012, edn.), pp.

[46] Vigen, M., Ceccarelli, J., and Putnam, A.J.: Protease-Sensitive PEG Hydrogels Regulate Vascularization *In Vitro* and *In Vivo*, Macromol Biosci, 2014, 14, (10), pp. 1368-1379

[47] Nor, J.E., Peters, M.C., Christensen, J.B., Sutorik, M.M., Linn, S., Khan, M.K., Addison, C.L., Mooney, D.J., and Polverini, P.J.: Engineering and characterization of functional human microvessels in immunodeficient mice, Laboratory Investigation, 2001, 81, (4), pp. 453-463

[48] Martz, T.D., Sheeran, P.S., Bardin, D., Lee, A.P., and Dayton, P.A.: Precision Manufacture of Phase-Change Perfluorocarbon Droplets Using Microfluidics, Ultrasound Med Biol, 2011, 37, (11), pp. 1952-1957

[49] Bardin, D., Martz, T.D., Sheeran, P.S., Shih, R., Dayton, P.A., and Lee, A.P.: High-speed, clinical-scale microfluidic generation of stable phase-change droplets for gas embolotherapy, Lab on a Chip, 2011, 11, (23), pp. 3990-3998

[50] Taylor, P.: Ostwald ripening in emulsions, Advances in Colloid and Interface Science, 1998, 75, (2), pp. 107-163

[51] Rapoport, N.Y., Kennedy, A.M., Shea, J.E., Scaife, C.L., and Nam, K.-H.: Controlled and targeted tumor chemotherapy by ultrasound-activated nanoemulsions/microbubbles, Journal of Controlled Release, 2009, 138, (2), pp. 268-276

[52] Sheeran, P.S., Wong, V.P., Luois, S., McFarland, R.J., Ross, W.D., Feingold, S., Matsunaga, T.O., and Dayton, P.A.: Decafluorobutane as a Phase-Change Contrast Agent for Low-Energy Extravascular Ultrasonic Imaging, Ultrasound Med Biol, 2011, 37, (9), pp. 1518-1530

[53] Fabiilli, M.L., Haworth, K.J., Fakhri, N.H., Kripfgans, O.D., Carson, P.L., and Fowlkes, J.B.: The Role of Inertial Cavitation in Acoustic Droplet Vaporization, IEEE Transactions on Ultrasonics, Ferroelectrics, and Frequency Control, 2009, 56, (5), pp. 1006-1017

[54] Rapoport, N., Nam, K.H., Gupta, R., Gao, Z., Mohan, P., Payne, A., Todd, N., Liu, X., Kim, T., Shea, J., Scaife, C., Parker, D.L., Jeong, E.K., and Kennedy, A.M.: Ultrasound-mediated tumor imaging and nanotherapy using drug loaded, block copolymer stabilized perfluorocarbon nanoemulsions, Journal of controlled release : official journal of the Controlled Release Society, 2011, 153, (1), pp. 4-15

[55] Reznik, N., Shpak, O., Gelderblom, E.C., Williams, R., de Jong, N., Versluis, M., and Burns, P.N.: The efficiency and stability of bubble formation by acoustic vaporization of submicron perfluorocarbon droplets, Ultrasonics, 2013, 53, (7), pp. 1368-1376

[56] Sahni, A., Odrljin, T., and Francis, C.W.: Binding of basic fibroblast growth factor to fibrinogen and fibrin, J Biol Chem, 1998, 273, (13), pp. 7554-7559

[57] Martino, M.M., Briquez, P.S., Ranga, A., Lutolf, M.P., and Hubbell, J.A.: Heparin-binding domain of fibrin(ogen) binds growth factors and promotes tissue repair when incorporated within a synthetic matrix, Proceedings of the National Academy of Sciences of the United States of America, 2013, 110, (12), pp. 4563-4568

[58] Johnson, J.L.H., Dolezal, M.C., Kerschen, A., Matsunaga, T.O., and Unger, E.C.: *In vitro* comparison of dodecafluoropentane (DDFP), perfluorodecalin (PFD), and perfluoroctylbromide (PFOB) in the facilitation of oxygen exchange, Artificial cells, blood substitutes, and biotechnology, 2009, 37, (4), pp. 156-162

[59] Riess, J.G.: Oxygen Carriers ("Blood Substitutes") - Raison d'Etre, Chemistry, and Some Physiology, Chemical Reviews, 2001, 101, (9), pp. 2797-2919

[60] Dias, A.M.A., Freire, M., Coutinho, J.A.P., and Marrucho, I.M.: Solubility of oxygen in liquid perfluorocarbons, Fluid Phase Equilibria, 2004, 222, pp. 325-330

[61] Sha'ban, M., Yoon, S.J., Ko, Y.K., Ha, H.J., Kim, S.H., So, J.W., Idrus, R.B.H., and Khang, G.: Fibrin promotes proliferation and matrix production of intervertebral disc cells cultured in three-dimensional poly(lactic-co-glycolic acid) scaffold, Journal of Biomaterials Science-Polymer Edition, 2008, 19, (9), pp. 1219-1237

[62] Yamamoto, M., Yanaga, H., Nishina, H., Watabe, S., and Mamba, K.: Fibrin stimulates the proliferation of human keratinocytes through the autocrine mechanism of transforming growth factor-alpha and epidermal growth factor receptor, Tohoku Journal of Experimental Medicine, 2005, 207, (1), pp. 33-40

[63] Pawelec, K.M., Best, S.M., Cameron, R.E., and Wardale, R.J.: Scaffold architecture and fibrin gels promote meniscal cell proliferation, APL Materials, 2015, 3, (1)

[64] Ferrara, K.W., Pollard, R., and Borden, M.A.: Ultrasound microbubble contrast agents: fundamentals and application to gene and drug delivery, Annual Review of Biomedical Engineering, 2007, 9, pp. 425-447

[65] Seda, R., Li, D.S., Fowlkes, J.B., and Bull, J.L.: Characterization of Bioeffects on Endothelial Cells under Acoustic Droplet Vaporization, Ultrasound in medicine & biology, 2015, 41, (12), pp. 3241-3252

[66] Fix, S.M., Novell, A., Yun, Y., Dayton, P.A., and Arena, C.B.: An evaluation of the sonoporation potential of low-boiling point phase-change ultrasound contrast agents *in vitro*, Journal of Therapeutic Ultrasound, 2017, 5, pp. 1-11

[67] Stathopulos, P.B., Scholz, G.A., Hwang, Y.M., Rumfeldt, J.A.O., Lepock, J.R., and Meiering, E.M.: Sonication of proteins causes formation of aggregates that resemble amyloid, Protein Science, 2004, 13, (11), pp. 3017-3027

[68] Jeon, O., Kang, S.W., Lim, H.W., Chung, J.H., and Kim, B.S.: Long-term and zero-order release of basic fibroblast growth factor from heparin-conjugated poly(L-lactide-co-glycolide) nanospheres and fibrin gel, Biomaterials, 2006, 27, (8), pp. 1598-1607

[69] Jeon, O., Ryu, S.H., Chung, J.H., and Kim, B.S.: Control of basic fibroblast growth factor release from fibrin gel with heparin and concentrations of fibrinogen and thrombin, Journal of Controlled Release, 2005, 105, (3), pp. 249-259

[70] Ando, J., and Yamamoto, K.: Vascular Mechanobiology - Endothelial Cell Responses to Fluid Shear Stress, Circulation Journal, 2009, 73, (11), pp. 1983-1992

[71] Kom, C., and Augustin, H.G.: Mechanisms of Vessel Pruning and Regression, Developmental Cell, 2015, 34, (1), pp. 5-17

[72] Lucas, M.A., Fretto, L.J., and McKee, P.A.: The binding of human-plasminogen to fibrin and fibrinogen, J Biol Chem, 1983, 258, (7), pp. 4249-4256

[73] Ikomi, F., Hanna, G.K., and Schmid-Schonbein, G.W.: Size- and surface-dependent uptake of colloid particles into the lymphatic system, Lymphology, 1999, 32, (3), pp. 90-102

[74] Huebsch, N., Kearney, C.J., Zhao, X., Kim, J., Cezar, C.A., Suo, Z., and Mooney, D.J.: Ultrasound-triggered disruption and self-healing of reversibly cross-linked hydrogels for drug delivery and enhanced chemotherapy, Proc Natl Acad Sci U S A, 2014, 111, (27), pp. 9762-9767

[75] Cuignet, O.Y., Baele, P.M., and Van Obbergh, L.J.: A second-generation blood substitute (perflubron emulsion) increases the blood solubility of modern volatile anesthetics *in vitro*, Anesthesia and Analgesia, 2002, 95, (2), pp. 368-372

CHAPTER V

Sequential Payload Release from Acoustically-Responsive Scaffolds Using Focused Ultrasound

5.1 Introduction

Tissue regeneration is driven by the spatiotemporally-controlled expression and regulation of multiple growth factors (GFs). For example, during blood vessel growth, pro-angiogenic GFs such as vascular endothelial growth factor (VEGF) and fibroblast growth factor (FGF) stimulate endothelial cell migration, mitogenesis, and sprouting [1-6]. The newly sprouting vessels are then stabilized by pericytes, which are recruited by platelet derived growth factor (PDGF). During the healing of a bone fracture, bone morphogenetic protein 2 (BMP2) initially stimulates callus formation during the inflammation stage. Later, VEGF causes vascular in-growth from the periosteum. Reviews more fully highlight the complex, temporal orchestration of GF signaling involved in the multiple stages of angiogenesis and osteogenesis [7, 8].

Hydrogel scaffold-based delivery systems can provide sequential delivery of multiple GFs to enhance tissue regeneration. The motivation for generating these scaffolds is that sequential delivery of GFs can mimic critical aspects of endogenous GF signaling more closely. Additionally, certain GFs (e.g., bFGF and PDGF) are mutually antagonistic when present simultaneously [9], thus further highlighting the need for sequential delivery. Sequential delivery of two GFs (e.g., GF1, GF2) has

been obtained by designing a composite scaffold using one of two general strategies. First, GF1 is incorporated into a scaffold while GF2 is pre-encapsulated into particles which are then incorporated into the scaffold [10]. This therapeutic approach typically results in GF1 being released at a faster rate than GF2. Second, GF1 and GF2 are pre-encapsulated into separate particles, which are then incorporated into a scaffold [11]. In both strategies, the release kinetics of the GFs are dependent on the material properties of both the scaffold and particles such as crosslinking density, pore size, GF affinity, and charge. Sequential delivery of VEGF/PDGF [12], bFGF/BMP-2 [13], BMP-2/BMP-7 [11], VEGF/BMP-2 [14], and BMP-2/insulin-like growth factor (IGF-1) [15] has been demonstrated using the previously mentioned techniques.

A critical limitation of the previous sequential delivery strategies is that the release kinetics of GF1 and GF2 are designed a priori. Therefore, after the scaffold is implanted at, or adjacent to, the site of intended tissue regeneration the release kinetics including the initial timing of release of GF1 and GF2 cannot be altered. From a clinical perspective, this is potentially problematic since the release kinetics of the multiple encapsulated GFs cannot be adjusted based on the actual progress of tissue regeneration within a patient. Thus, scaffold-based delivery systems that enable active modulation of sequential release would be beneficial. We have a developed a scaffold-based delivery system where release of a bioactive payload is controlled non-invasively and in an on-demand manner using focused, megahertz-range ultrasound (US). These acoustically-responsive scaffolds (ARSs) consist of a fibrin hydrogel doped with a micron-sized, perfluorocarbon (PFC) double emulsion [16, 17]. Fibrin was chosen as the hydrogel due to its biocompatibility, ability to degrade with minimal inflammatory response, potential for autologous sourcing, and low viscoelastic properties that help facilitate cell migration [18, 19]. A water-soluble payload is encapsulated within the PFC double emulsion having

a water-in-PFC-in-water (W_1/PFC/W_2) structure. When exposed to pulsed (i.e., non-thermal) US above a certain pressure, the PFC phase within the emulsion vaporizes in a process known as acoustic droplet vaporization (ADV), which causes release of the encapsulated payload [20-22].

We demonstrated that release of a single payload from an ARS is a threshold based phenomenon, which is dependent on properties of the emulsion and the fibrin scaffold [16]. Recently, we have shown, both in vitro and in vivo, that US can modulate the release of bFGF from an ARS, with a potential application in therapeutic angiogenesis [17]. In the current in vitro study, we demonstrate for the first time that US can control the sequential release of two surrogate payloads, AlexaFluor 488-labelled dextran and Alexa Fluor 594-labelled dextran, from an ARS. These payloads were chosen for this proof-of-concept study since they can be spectrally differentiated. To achieve sequential release, we formulate ARSs containing two separate emulsion populations, each containing a different PFC. This strategy was inspired by previous publications demonstrating the inverse relationship between the minimum acoustic pressure required for ADV (i.e., the ADV threshold) and the boiling point of the dispersed PFC phase within the emulsion [21, 23, 24].

5.2 Materials and Methods

5.2.1 Preparation and Characterization of the Double Emulsion

Double emulsions with a water-in-PFC-in-water (W_1/PFC/W_2) structure were prepared using a previous method [17]. Briefly, a triblock fluorosurfactant, consisting of Krytox 157FSH (CAS# 51798-33-5, DuPont, Wilmington, DE, USA) and polyethylene glycol (MW: 1000, CAS#: 24991-53-5, Alfa Aesar, Ward Hill, MA USA), was dissolved at 2% (w/w) in 1 g of perfluoropentane (PFP, CAS# 678-26-2, Strem Chemicals, Newburyport, MA USA), perfluorohexane (PFH, CAS# 355-42-0,

Strem Chemicals), or perfluoroheptane (PFHep, CAS#: 335-57-9, Sigma-Aldrich, St. Louis, MO USA). For PFP and PFH emulsions, the PFC solution was combined at 2:1 (v/v) with a W_1 phase containing 1.66 mg/mL Alexa Fluor 488-labeled dextran (AF488, MW: 10,000 Da, Life Technologies, Grand Island, NY USA) in phosphate-buffered saline (PBS, Life Technologies). For PFHep emulsions, the PFC solution was combined with a 3.32 mg/mL solution of Alexa Fluor 594-labeled dextran (AF594, MW: 10,000 Da, Life Technologies) in PBS. The PFC and W_1 phases were emulsified using a probe sonicator (Q55, QSonica, Newton, CT USA) for 30 seconds while on ice. The resulting primary emulsion, with a water-in-PFC (W_1/PFC) structure, was pumped at 0.5 μL/min through an in-line filter (0.5 μm stainless steel frit, Cat#: 24993, Restek, Bellefonte, PA, USA) and then into the inner channel of a quartz microfluidic chip (Cat#: 3200146, junction: 14 x 17 μm, hydrophilic coating, Dolomite, Royston, United Kingdom) using a syringe pump (KDS-410, kd Scientific, Holliston, MA USA). Simultaneously, 50 mg/mL Pluronic F68 (CAS# 9003-11-6, Sigma-Aldrich) in PBS was pumped at 2.5 μL/min though an in-line filter and then into the outer channels of the chip using a second syringe pump (78-0388, kd Scientific). The chip was mounted on an inverted microscope (DMIL, Leica Microsystems, Buffalo Grove, IL USA) which enabled visualization of emulsion production. Emulsion was collected following equilibration of the chip and then stored at 5C until use.

Emulsions were characterized with a Coulter Counter (Multisizer 4, Beckman Coulter, Brea, CA USA) in the range of 1-30 μm. To confirm emulsion morphology, the emulsion was imaged using an inverted confocal microscope (SP5X, Leica Microsystems, Inc., Buffalo Grove, IL USA) at the University of Michigan Microscopy & Image Analysis Laboratory. One day after production of the emulsion, the concentration of dextran in the W_2 phase was measured with a plate reader (Molecular Devices, SpextraMax M2e, Sunnyvale, CA USA). The encapsulation

efficiency of dextran in the emulsion was calculated via a mass balance. Using the PFP and PFH emulsions, we determined that this technique was equivalent to our previous method of measuring encapsulation efficiency via breaking the emulsion pellet [16].

5.2.2 Fabrication of ARSs for Acoustic Characterization

ARSs were prepared using 10 mg/mL clottable protein by first combining bovine fibrinogen (Sigma-Aldrich) dissolved in degassed (36% O^2 saturation) FluoroBrite Dulbeccos modified Eagles medium (DMEM, Life Technologies), with 10% (v/v) bovine thrombin (20 U/mL, Thrombin-JMI, King Pharmaceuticals, Bristol, TN, USA), 0.025 U/mL aprotinin (Sigma-Aldrich), and 1.0% (v/v) of PFP, PFH, or PFHep emulsion. The ADV and inertial cavitation (IC) thresholds of the ARSs were determined using previously described methods [22]. Briefly, 0.5 mL ARSs (height: 0.28 cm) were cast in 24-well Bioflex plates (Flexcell International, Burlington, NC, USA) by aliquoting the ARS mixture into each well and allowing it to polymerize for 30 min at room temperature. The ARSs were exposed to focused US generated by a calibrated, single-element transducer (2.5 MHz, H108, f-number = 0.83, focal length = 50 mm, Sonic Concepts, Inc., Bothell, WA USA) in the range of 0 to 8.0 MPa peak rarefactional pressure. The bottom of each well in the plate consisted of a silicone elastomer membrane, which based on a thickness of 1 mm, attenuated the US by less than 2% [25]. The complete acoustic setup is described in section 2.3. A calibrated hydrophone (HGL-0085, dynamic range = 1-50 MHz, Onda, Sunnyvale, CA USA) was placed 6 cm away from the focus of the transducer to detect backscattered acoustic signals generated in the ARS during the US exposure. The radiofrequency signals collected with the hydrophone and digitized by an oscilloscope (sampling rate = 100 MHz) were analyzed in MATLAB (The MathWorks, Natick, MA, USA). The ADV threshold was determined by analyzing the fundamental frequency since bubbles formed in the ARS due to ADV significantly increase the scattered,

fundamental signal [26, 27]. The ADV threshold was defined as the lowest acoustic pressure at which the increase in fundamental signal over background was observed. The IC threshold was computed using the broadband signal from the acquired radiofrequency waveforms using identical methods as described previously [22].

5.2.3 US Exposure

All acoustic exposures were conducted using the following setup [16]. The single-element transducer was driven by pulsed waveforms generated using a dual channel function generator (33500B, Agilent Technologies, Santa Clara, CA USA), amplified by a gated radiofrequency amplifier (GA-2500A Ritec Inc, Warwick, RI USA), and passed through a matching circuit (H108_3MN, Sonic Concepts) to reduce impedance between the transducer and amplifier. Gating of the carrier waveform was realized using the second channel of the function generator, resulting in a pulsed signal. All generated and amplified signals were monitored with an oscilloscope (HDO4034, Teledyne LeCroy, Chestnut Ridge, NY USA). All acoustic exposures were done with the following parameters unless otherwise stated: 2.5 MHz fundamental frequency, 0.8 to 8.0 MPa peak rarefactional pressure, 13 acoustic cycles, and 100 Hz pulse repetition frequency (PRF). All US pressures are listed as peak rarefactional pressures.

To localize the axial focus of the US transducer with respect to the ARS, a pulse echo technique was used. Briefly, the single element transducer was driven by a pulser-receiver (5077PR, Olympus, Center Valley, PA US) that generated a low energy signal at 100 Hz PRF. The reflected signal was visualized on an oscilloscope, and maximized in amplitude by modifying the distance between the transducer and ARS. Using this technique, the axial focus of the transducer was positioned at mid-height of the ARS.

5.2.4 Single Payload Release

The goal of this experiment was to characterize single payload release as a function of acoustic pressure. As seen in Table 1, four ARSs compositions were interrogated for the single payload release studies. ARSs were fabricated with either 0.33 or 0.67% (v/v) emulsion in a modified 48-well plate (Thermo Fisher Scientific, Waltham, MA, USA) in which the plate bottom was drilled out and replaced with a Tegaderm film (3M Health Care, St. Paul, MN, USA). The ARSs, 0.3 mL volume per well (height: 0.32 cm), were allowed to polymerize for 30 min at room temperature. Each ARS was then covered with 0.3 mL of overlying media, consisting of FluoroBrite DMEM supplemented with 100 U/mL penicillin and 100 μg/mL streptomycin. The ARSs were placed in a standard tissue culture incubator (37°oC, 5% carbon dioxide), except during the US exposure.

Table 5.1: List of all ARSs used in the presented experiments, as well as the ultrasound pressures interrogated and the days of exposure.

	Emulsion 1			Emulsion 2				
PFC Composition	**PFC**	**Payload**	**Volume %**	**PFC**	**Payload**	**Volume %**	**US Pressure (MPa)**	**Day of US Exposure**
PFP	PFP	AF488	0.33	-	-	-	0-8	1
PFP/PFHep	PFP	AF488	0.33	PFHep	AF680	0.67	0-8 2 or 8 2 and 8	1 1 1 and 3
PFH	PFH	AF488	0.67	-	-	-	0-8	1
PFH/PFHep	PFH	AF488	0.67	PFHep	AF680	0.33	0-8 2 or 8 2 and 8	1 1 1 and 3
PFHep	PFHep	AF680	0.67	-	-	-	0-8	1
PFHep	PFHep	AF680	0.33	-	-	-	0-8	1

One day after polymerization, the plate containing the ARSs was placed in a tank of degassed water (30-36% O^2 saturation) at 37°C such that only the bottom half of the plate was submerged. Using pulse-echo, the single element US transducer was positioned under the plate such that the axial focus was located at mid-height of the ARS. During US exposure, the transducer was rastered across the entire ARS until the entire surface area was exposed to US. The overlying media was sampled daily for three days by collecting half of the media and replacing the sampled volume

with an equal volume of fresh media. On the day of US exposure, the media was sampled immediately after exposure. The concentration of dextran released into the sampled media was measured using a plate reader (Molecular Devices). As a comparison, the release of unencapsulated dextran, incorporated directly into the fibrin scaffold, was also measured.

5.2.5 Dual Payload Release

Figure 5.1A schematically shows the strategy used to obtain sequential dual payload release from ARSs. As seen in Table 1, two different ARSs compositions, PFP/PFHep-ARSs or PFH/PFHep-ARSs, were interrogated for the dual payload release studies. The acoustic pressures used for exposure were selected based on results obtained from the acoustic characterization (section 2.2) and single payload release studies (section 2.4). Two different exposure schemes were used. For single US exposure, PFP/PFHep-ARSs were exposed to US at 2 or 8 MPa one day after polymerization, while PFH/PFHep-ARSs were exposed to US at 2.6 or 8 MPa one day after polymerization. For sequential US exposures, PFP/PFHep-ARSs were exposed to US at 2 and 8 MPa one day and three days after polymerization, respectively. Similarly, PFH/PFHep-ARSs were exposed to US at 2.6 and 8 MPa one and three days after polymerization, respectively. Similar to the single payload experiments, the overlying media was sampled daily for three days by collecting half of the media and replacing the sampled volume with an equal volume of fresh media. For the initial US exposure, the media was sampled immediately after US exposure. For samples that had US exposure on day three, the media was sampled immediately before and after US exposure. The concentration of each dextran in the sampled media was measured using a plate reader.

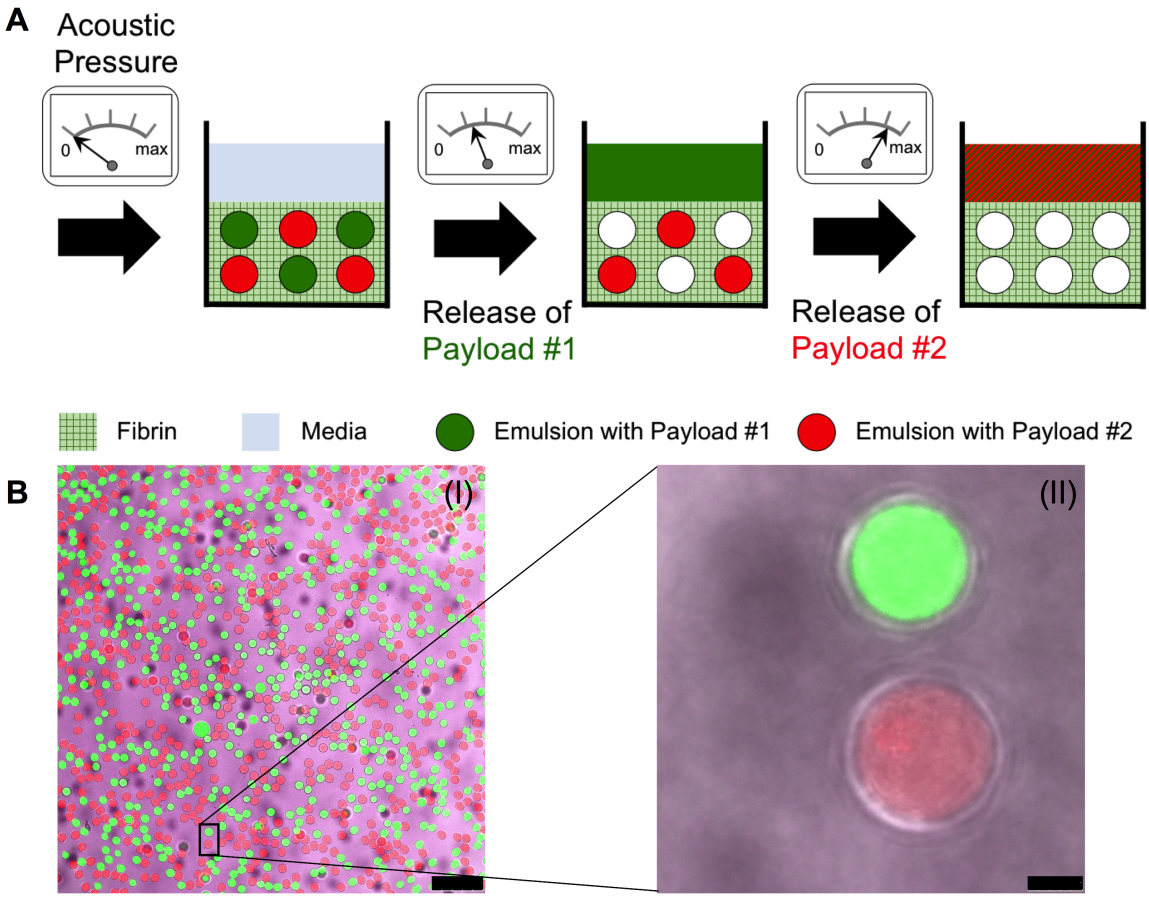

Figure 5.1: (A) Sequential release of two payloads using an ARS. Two similarly-sized emulsions, each containing a different PFC and payload, are incorporated into an ARS. For release of payload #1, the ARS is exposed to US at an acoustic pressure above the ADV threshold of the emulsion with payload #1, but below the threshold of the emulsion containing payload #2. At a later time point, the same ARS is exposed to US at an acoustic pressure above the ADV threshold of the emulsion with payload #2, thus releasing payload #2. (B) Confocal microscopy images of an ARS with two payloads at 25x (I) and 100x (II) magnification. The ARS contained 0.67% (v/v) PFH emulsion with AF488-labelled dextran in the W_1 phase (green), 0.33% (v/v) PFHep emulsion with AF594-labelled dextran in the W_1 phase (red), and AF647-labelled fibrinogen (magenta) in the fibrin matrix. Scale bar equals 75 μm and 5 μm for B(I) and B(II), respectively.

5.2.6 Statistics

All statistical analyses were performed using GraphPad Prism software (GraphPad Software, Inc., La Jolla, CA USA). All data is expressed as the mean ± the standard deviation of measured quantities. All n-values are listed below each corresponding figure. Payload release data, collected as a function of acoustic pressure, was fit to a four parameter sigmoid function where the following parameters are reported: maximum payload release (R_{max}), minimum payload release ($R_{min)}$, and the acoustic pressure at which half of maximum payload release was observed (P50). The 95% confidence intervals of R_{max}, R_{min}, and P50 are listed in the format S [S_L, S_H], where S is the average value, S_L is the lower bound value, and S_H is the upper bound value. Statistically significant differences of all data sets were determined with a Students t-test corrected for multiple comparisons using the Holm-Sidak method, with differences deemed significant for $p < 0.05$.

5.3 Results

5.3.1 Emulsion and ARS Properties

Table 2 displays the characteristics of the double emulsions used in the ARSs. No statistically significant differences in the encapsulation efficiency, mean diameter, and droplet concentration were observed between any of the emulsion formulations. The PFP emulsion had a greater coefficient of variance than either the PFH or PFHep emulsion. The ADV thresholds of ARSs with PFH emulsion (i.e., PFH-ARSs) or PFHep emulsion (PFHep-ARSs) was lower than their respective IC thresholds. Additionally, ARSs with PFP emulsion (i.e., PFP-ARSs) had a significantly lower ADV threshold than PFH- and PFHep-ARSs, while no differences were observed between the ADV thresholds of PFH- and PFHep-ARSs. The IC threshold of PFHep-ARSs was higher than the IC threshold in PFP-ARSs. Confocal microscopy images of a dual payload containing ARS in shown in Figure 5.1B. The two

emulsions, containing AF488 (green) or AF594 (red) in the W1 phase, were dispersed within the fibrin scaffold containing Alexa Fluor 647-labeled fibrinogen (magenta). The double emulsion droplets appeared uniform in size and the W1 droplets were submicron in diameter.

Table 5.2: Physiochemical and acoustic characteristics of the double emulsions used in the ARSs. The ADV and IC thresholds are for ARSs with a single emulsion type.

Perfluorocarbon in Emulsion	Boiling Point (°C)	Encapsulation Efficiency (%)	Mean Diameter (μm)	Coefficient of Variance (%)	Concentration (#/mL)	ADV Threshold (MPa)	IC Threshold (MPa)
PFP (C_5F_{12}	29	95.90 ± 4.42	12.56 ± 0.65	5.08 ± 1.81	4.50E+8 ± 1.41E+8	1.42 ± 0.14	2.84 ± 1.45
PFH (C_6F_{14}	56	99.60 ± 0.51	12.92 ± 0.17	3.42 ± 0.65	4.02E+8 ± 1.01E+8	1.92 ± 0.37	3.77 ± 0.16
PFHep (C_7F_{16}	84	99.70 ± 0.23	13.09 ± 0.21	3.19 ± 0.20	4.290E+8 ± 4.93E+7	2.18 ± 0.37	4.10 ± 0.10

5.3.2 Dextran Release from a Conventional Fibrin Scaffold

Release of the unencapsulated dextrans, which were incorporated directly into a conventional fibrin matrix, is shown in Figure 5.2. There was significant release of both dextrans one day after the scaffold was formulated, resulting in 44.01 ± 1.00% and 40.13 ± 0.62% release of AF488 and AF594, respectively. On day 7 there was 73.98 ± 1.61% and 71.34 ± 1.21% release of AF488 and AF594, respectively, with statistically significant differences between the two conditions occurring on days 1-5.

5.3.3 Pressure Dependent Dextran Release from Single Payload-Containing ARSs

Figure 5.3(A-D) shows the release of a single payload from different ARS formulations as function of acoustic pressure and time. The release from PFH- and PFHep-ARSs had a sigmoidal profile on days 2 and 3, with more release observed at acoustic pressures above, and near, the ADV threshold while being asymptotic at the highest pressures interrogated in this work. On day 1, there were no differences in payload release across the range of acoustic pressures. In addition, all ARS formulations yielded more payload release on day 3 compared to days 1 and 2. PFP-ARSs had the most payload release in the absence of US (i.e., 0 MPa), with

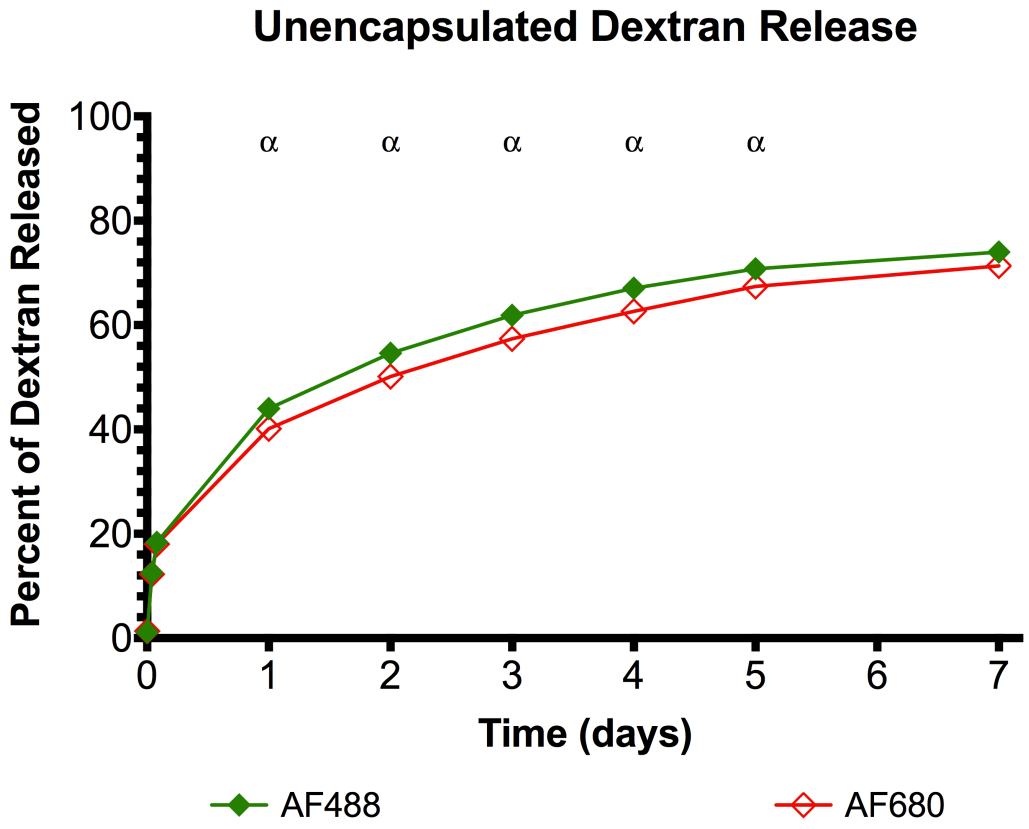

Figure 5.2: Dextrans, incorporated directly into a conventional fibrin scaffold without any encapsulation, are released quickly. Statistically significant differences ($p < 0.05$) between AF488 and AF594 dextrans are denoted by for n=5 samples.

8.75 ± 0.77% released on day 3, compared to 1.54 ± 0.22, 0.78 ± 0.11, and 1.65 ± 0.23% payload release for ARSs with 0.67% (v/v) PFH, 0.67% (v/v) PFHep, and 0.33% (v/v) PFHep emulsions, respectively, at the same time point. The most payload release was observed from ARSs with 0.33% (v/v) PFHep emulsion, with 18.07 ± 2.25% release at 8 MPa. Conversely, ARSs with 0.33% (v/v) PFP, 0.67% (v/v) PFH, 0.67% (v/v) PFHep emulsions had 15.35 ± 0.93, 10.66 ± 0.41, and 5.30 ± 0.88% released, respectively, at the same pressure and time point.

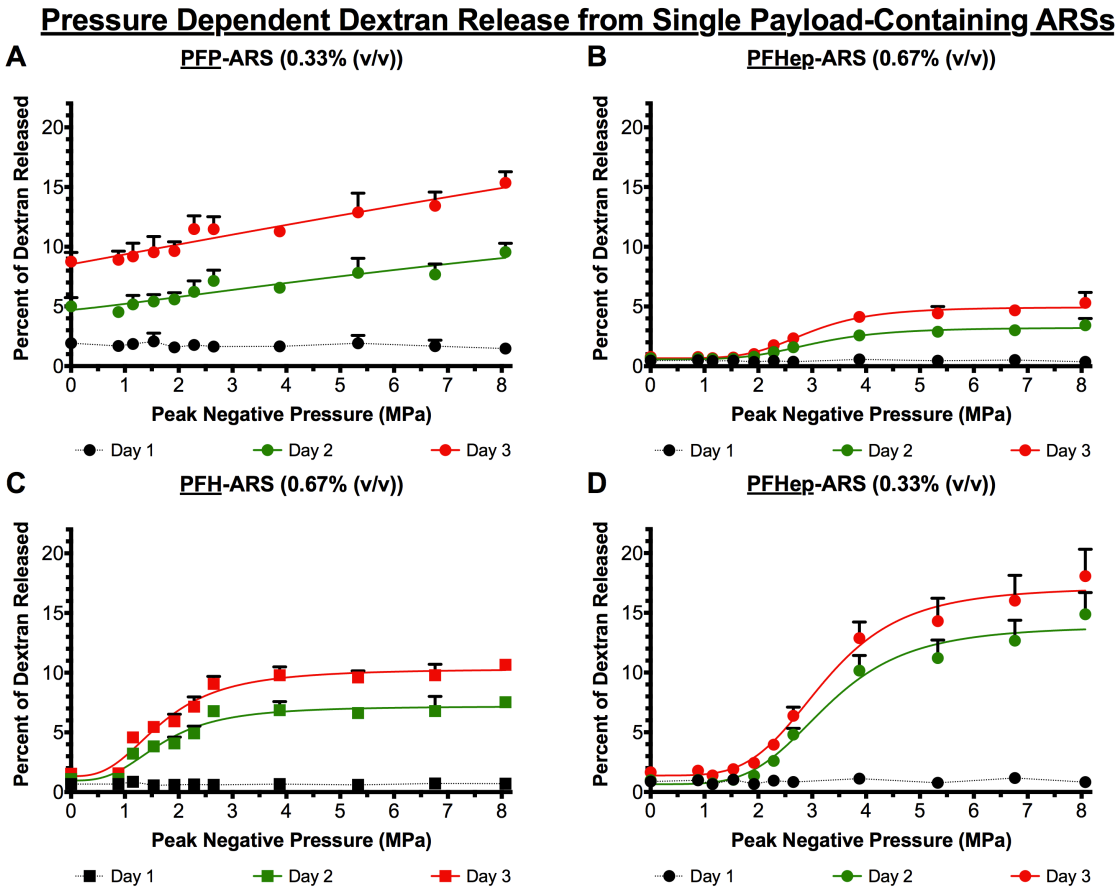

Figure 5.3: The release of dextran was longitudinally measured as a function of acoustic pressure from ARSs containing (A) 0.33% (v/v) PFP emulsion (B) 0.67% (v/v) PFHep emulsion (C) 0.67% (v/v) PFH emulsion, and (D) 0.33% (v/v) PFHep emulsion. PFP and PFH emulsions contained AF488 dextran while PFHep emulsion contained AF594 dextran. In all cases, the dextran was incorporated into the W1 phase of the emulsion and US exposure occurred one day after polymerization of the ARS. Statistics are based on n=5 measurements per condition. Curve fits are based on a 4 parameter sigmoidal model.

5.3.4 Pressure Dependent Dextran Release from Dual Payload-Containing ARSs

Release of two payloads from an ARS following a single US exposure is shown in Figure 5.4(A-D). Similar to single emulsion-containing ARSs, all dual payload ARS conditions displayed a sigmoidal release profile on days 2 and 3. Similar to PFP-ARSs, the most payload release in the absence of US was observed from the PFP emulsion within PFP/PFHep-ARSs (Figure 5.4A), resulting in statistically different releases of 1.46 ± 0.21%, 5.21 ± 0.58%, and 7.73 ± 0.54% on days 1, 2, and 3, respectively. Contrastingly, within the same PFP/PFHep-ARS, the PFHep emulsions had 0.70 ± 0.21%, 1.07 ± 0.31%, and 1.45 ± 0.37% payload release on days 1, 2, and 3 in the absence of US. The highest overall release among the conditions tested was observed from the PFH emulsion within the PFH/PFHep-ARS; on day 3, 9.82 ± 0.65% release was observed following exposure to 8 MPa. The lowest release, 3.14 ± 0.39%, measured on day 3 following exposure to 8 MPa US was from the PFHep emulsion in the PFH/PFHep-ARS (Figure 5.4D). With PFP/PFHep-ARSs (Figure 5.4A-B), US exposure at 8 MPa yielded greater release on day 3 from the PFP emulsion (7.73 ± 0.54%) versus the PFHep emulsion (6.72 ± 0.45%). For PFH/PFHep-ARSs (Figure 5.4C-D), US exposure at 8 MPa generated greater release on day 3 from the PFH emulsion (9.82 ± 0.65%) versus the PFHep emulsion (3.14 ± 0.39%).

5.3.5 Dual Payload Release from Single and Multiple Ultrasound Exposures

Figure 5.5A and 5B display the release profiles of PFP/PFHep-ARSs and PFH/PFHep-ARSs, respectively, following a single US exposure on day 1. PFP/PFHep-ARSs were exposed to either 2 or 8 MPa whereas PFH/PFHep-ARSs were exposed to 2.6 or 8 MPa. Figure 5.5A highlights that exposure at 8 MPa generated more payload release than 2 MPa from both PFP (10.20 ± 0.46% vs.

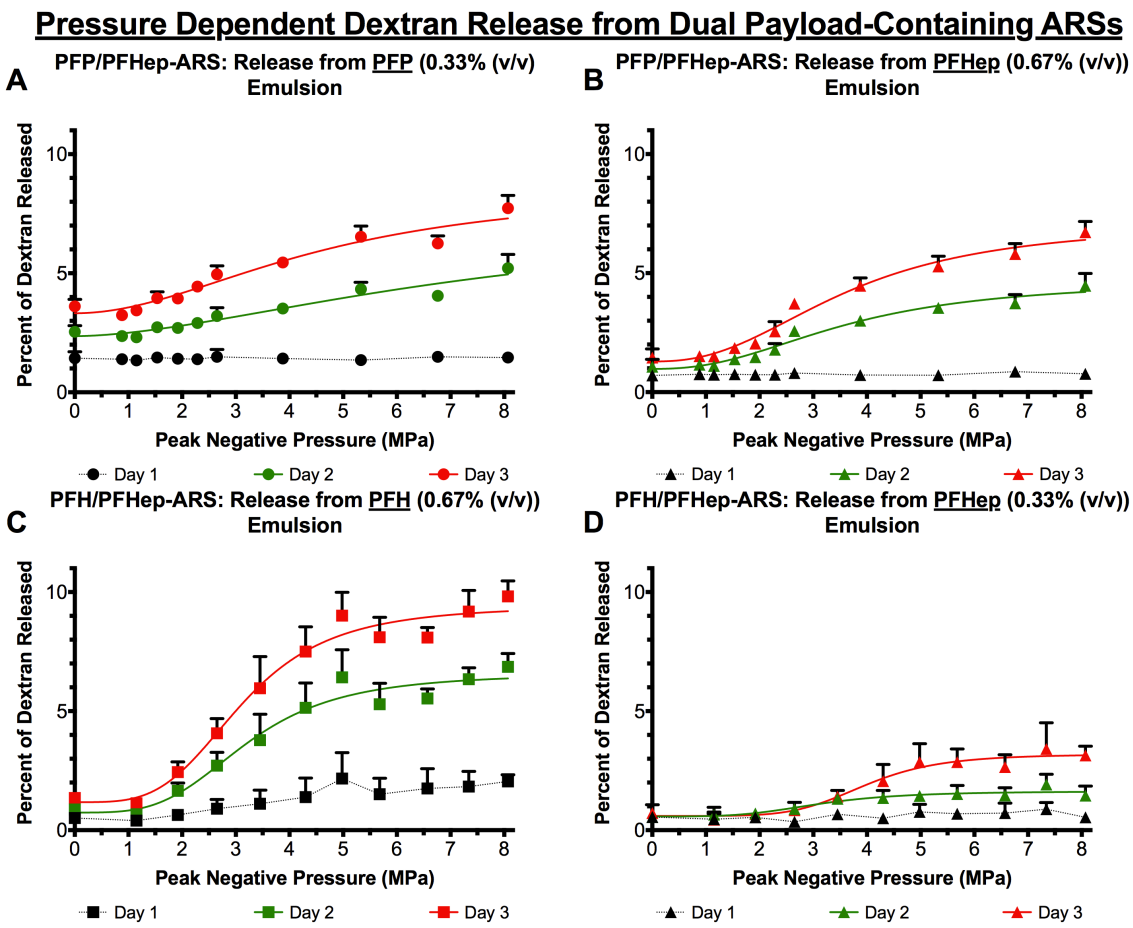

Figure 5.4: The release of dextran was longitudinally measured as a function of acoustic pressure for dual payload ARSs. The release profiles from (A) 0.33% (v/v) PFP emulsion and (B) 0.67% (v/v) PFHep emulsion within PFP/PFHep-ARSs are shown. The release profiles from (C) 0.67% (v/v) PFH emulsion and (D) 0.33% (v/v) PFHep emulsion within PFH/PFHep-ARSs are shown. PFP and PFH emulsions contained AF488 dextran while PFHep emulsion contained AF594 dextran. Statistics are based on n=5 measurements per condition. Curve fits are based on a 4 parameter sigmoidal model.

5.53 ± 0.86%) and PFHep (6.87 ± 0.86% vs. 2.47 ± 0.33%) emulsions by day 7. US exposure at 8 MPa yielded significantly greater release than 2 MPa on days 1-7 for PFP emulsion and days 2-7 for PFHep emulsion. The same trend was observed with PFH/PFHep-ARSs (Figure 5.5B), with more payload release at 8 MPa than at 2.6 MPa by day 7 for PFH (17.80 ± 2.29% vs. 9.22 ± 0.44%) and PFHep (3.71 ± 0.45% vs. 2.37 ± 0.17%) emulsions. US exposure at 8 MPa generated significantly greater release than 2.6 MPa on days 2-6 for PFH emulsion and days 3-7 for PFHep emulsion.

Figure 5.5C shows the release profiles of PFP/PFHep-ARSs following sequential US exposures on day 1 and day 3 of 2 MPa and 8 MPa, respectively. By day 7, PFP/PFHep-ARSs exposed to US (i.e., +US) had greater release than controls not exposed to US (i.e., -US), with 8.84 ± 0.45% vs. 4.66 ± 0.55% released from PFP and 9.39 ± 2.73% vs. 1.40 ± 0.04% for PFHep emulsions. Statistically significant differences were observed on days 1-7 for both emulsions. The release from PFP emulsion on day 3 (prior to the second US exposure at 8 MPa) was 3.06 ± 0.16%, which is not statistically different and consistent with the release observed in Figure 5.5A (i.e., 3.09 ± 0.53% released by day 3 at 2 MPa). A similar trend was observed from PFHep emulsions (Figure 5.5C), with 1.62 ± 0.33% released by day 3 (prior to the second US exposure at 8 MPa). This is also not statistically different and consistent with the release observed in Figure 5.5A (i.e., 1.31 ± 0.20% released by day 3 at 2 MPa). For PFP emulsion, the second US exposure at 8 MPa on day 3 yielded greater release by day 7 (8.84 ± 0.45%) compared to release observed at day 7 following a single US exposure of 2 MPa on day 1 (5.53 ± 0.86%). Analogously for PFHep emulsion, exposure to 8 MPa US on day 3 generated greater release by day 7 compared to release obtained on day 7 following a single US exposure of 2 MPa on day 1 (9.39 ± 2.73% vs. 2.47 ± 0.33%).

Figure 5.5D shows the release profiles of PFH/PFHep-ARSs following sequential

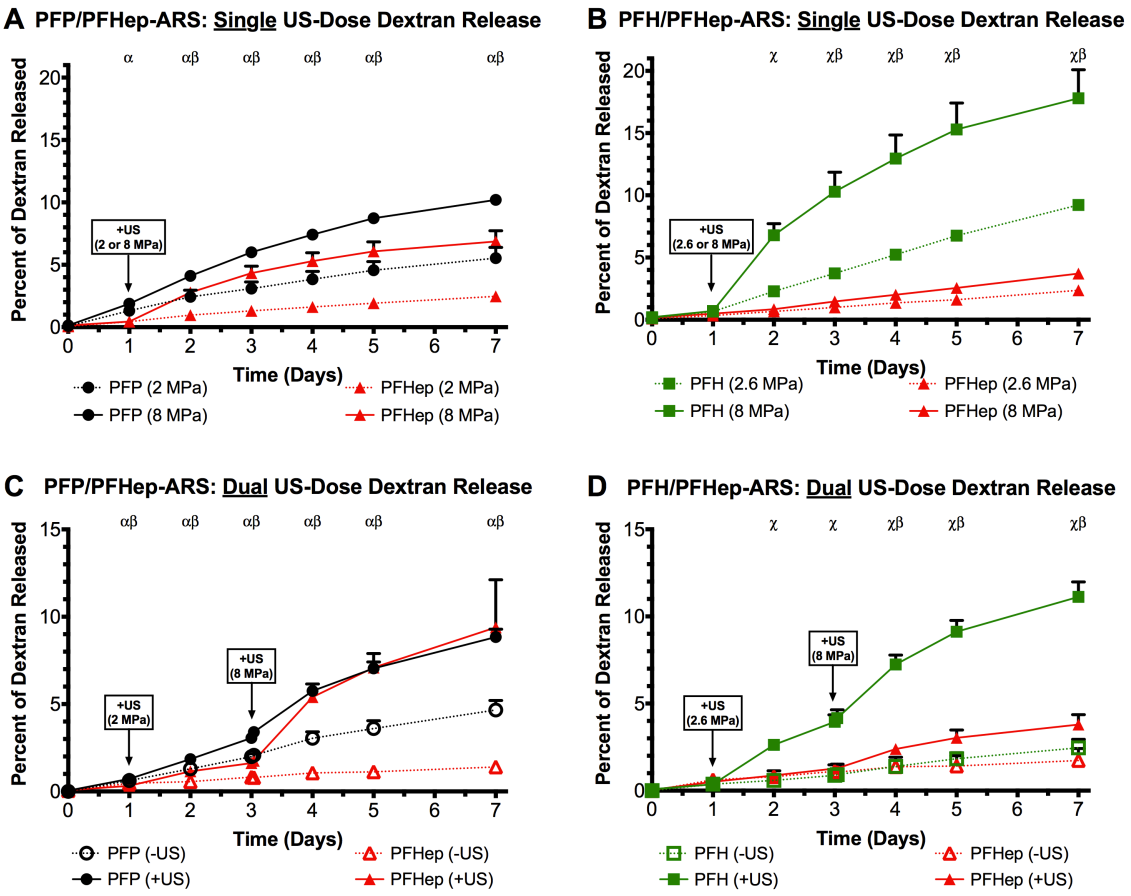

Figure 5.5: Release profiles of (A) PFP/PFHep-ARSs and (B) PFH/PFHep-ARSs are shown following a single US exposure on day 1. For PFP/PFHep-ARSs, exposure was either at 2 or 8 MPa while for PFH/PFHep-ARSs, exposure was at 2.6 or 8 MPa. The release profiles for PFP/PFHep-ARSs and PFH/PFHep-ARSs following sequential US exposures on day 1 and day 3 are shown in (C) and (D), respectively. PFP/PFHep-ARSs were exposed to 2 MPa (day 1) and 8 MPa (day 3). PFH/PFHep-ARSs were exposed to 2.6 MPa (day 1) and 8 MPa (day 3). PFP and PFH emulsions contained AF488 dextran while PFHep emulsion contained AF594 dextran. Statistically significant differences ($p < 0.05$) between AF488 and AF594 are denoted by α: PFP (+US vs. US), χ: PFH (+US vs. US), and β: PFHep (+US vs. US) for n=5 samples.

US exposures on day 1 and day 3 of 2.6 MPa and 8 MPa, respectively. The observed trends are similar to those of PFP/PFHep-ARSs (Figure 5.5C), with more release on day 7 in the +US case (PFH: 11.12 ± 0.86%; PFHep: 3.79 ± 0.57%) compared to their respective US condition (PFH: 2.46 ± 0.49%; PFHep: 1.73 ± 0.69%). For PFH emulsion, the second US exposure at 8 MPa on day 3 yielded a statistically greater release by day 7 (11.12 ± 0.86%) compared to the release observed at day 7 following a single US exposure of 2.6 MPa on day 1 (9.22 ± 0.44%). Analogously for PFHep emulsion, exposure to 8 MPa US on day 3 generated greater release by day 7 compared to release obtained on day 7 following a single US exposure of 2 MPa on day 1 (3.79 ± 0.57% vs. 2.37 ± 0.17%). Overall, greater release was observed for +US conditions, compared to US conditions, in Figure 5.5D on days 2-7 for PFH and days 4-7 for PFHep.

5.3.6 Stability of single and dual payload-containing ARSs

The macroscopic appearances of the various ARS formulations, for +US and US conditions, are displayed in Figure 5.6. For the +US condition, day 1 images were taken immediately after US exposure. For the US condition, there is qualitatively the most bubble formation in PFP-ARSs, followed by PFH-ARSs, PFH/PFHep-ARSs, and PFP/PFHep-ARSs. Qualitatively, the number and/or size of the bubbles increased from day 1 to day 2 for all of the ARS formulations, except for PFHep-ARS. There were more bubbles in the ARSs on day 1 and day 2 for the +US condition versus the matching US condition. For both +US and US conditions, there was little to no bubble formation in either ARS formulation containing PFHep emulsion.

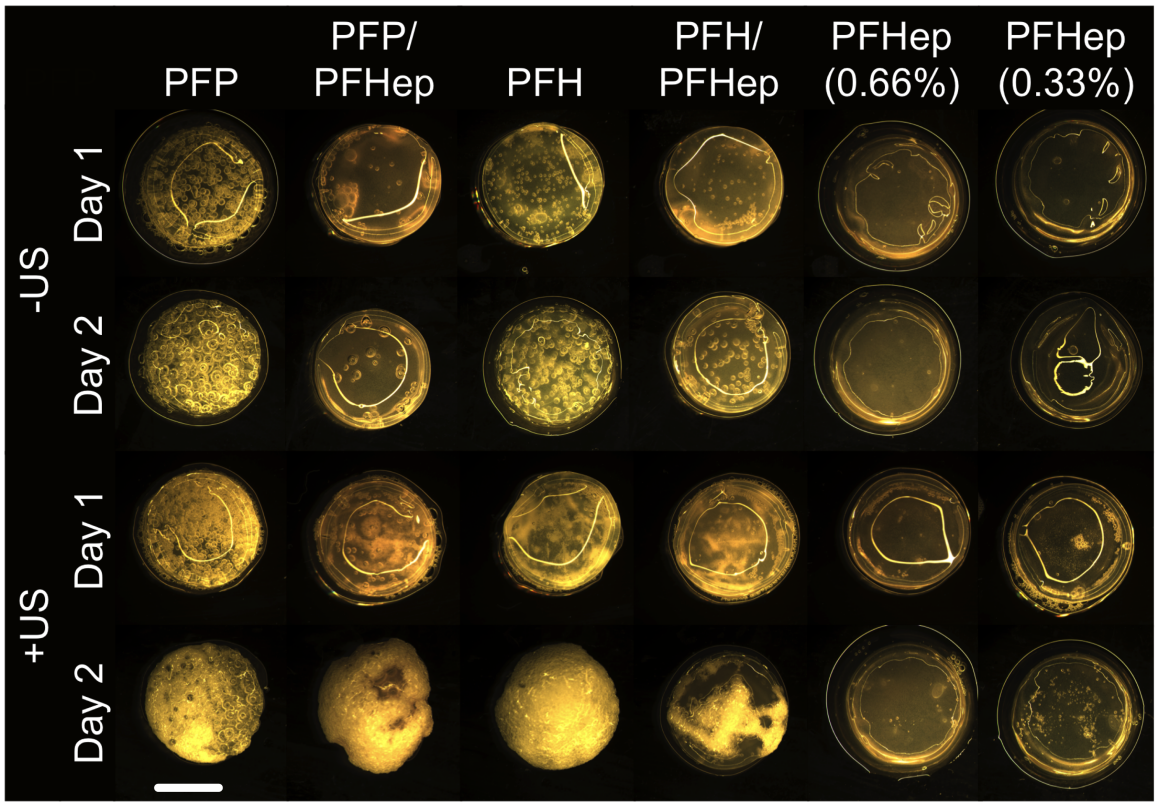

Figure 5.6: Macroscopic images of different ARS formulations as a function of time and US exposure. ARSs with a higher boiling point PFC (e.g., PFHep-ARSs) showed less bubble formation than lower boiling point ARSs (e.g., PFP-ARSs). Applying US to generated ADV in the ARSs resulted in more bubble formation on day 2 relative to the comparable condition in the absence of US. Scale bar equals 8 mm.

5.4 Discussion

In this work, sequential release of two payloads from an ARS was demonstrated by encapsulating each payload within separate sonosensitive emulsions having unique ADV thresholds. The ability to release multiple payloads from one ARS can ultimately increase the understanding of how various temporal profiles and sequences of GFs impact tissue regeneration. Overall, the highly versatile nature of ARSs, including the ability to modulate matrix (e.g., scaffold density), emulsion (e.g., droplet size) [16, 22], and US (e.g., acoustic pressure) properties provides a highly tunable approach for delivering multiple payloads in tissue engineering applications.

A critical component of ARSs is the sonosensitive emulsion containing each payload. Our work has demonstrated that monodispersed emulsions have superior stability compared to their polydispersed counterparts, and can be used for bioactive growth factor delivery [17]. In the current study, the ADV thresholds correlated with the boiling point and molecular weight of the dispersed PFC phase for similarly-sized, monodispersed emulsions. It has been hypothesized that the effective boiling point of the PFC within the emulsion is one of the factors determining the ADV threshold [22, 28, 29], with smaller droplets experiencing a higher boiling point elevation due to the Laplace pressure gained from droplet formation [24, 30]. Thus, emulsions made from low-boiling point PFCs such as PFP and perfluorobutane are stable at body temperature when formulated as submicron droplets. An alternative hypothesis is that the ADV threshold is dependent on the energy barrier for homogeneous nucleation within the PFC liquid, with the energy required to create a vapor embryo correlating with the molecular weight of the PFC [31]. Furthermore, others have shown that the droplet-to-bubble transition is dependent on the dissolved oxygen content within the PFC [28], with oxygen solubility inversely proportional to the PFC molecular weight [32].

Emulsions have been formulated using ad-mixtures of two different PFCs [23,

33, 34]. For an emulsion containing an ad-mixture of low boiling point PFCs (e.g., perfluoropropane and perfluorobutane), the vaporization threshold was close to an emulsion made solely of the higher boiling point PFC (i.e., perfluorobutane) [35]. It was determined that in an open system the lower boiling (i.e., smaller molecular weight) PFC preferentially dissolved, thereby enhancing the fraction of higher boiling point PFC within each droplet [36].This effect was not observed in our previous publication where the ADV threshold of an ARS containing emulsion with a 1:1 ad-mixture of PFP:PFH was intermediate to that of PFP and PFH [16]. In this study, each emulsion was formulated with only one PFC. However, when formulating an ARS with two different emulsions, it is possible that counterdiffusion of PFCs could occur, which may explain some of the observed differences between single and dual payload-containing ARSs.

The ADV thresholds, measured in ARSs with a single emulsion type, can be used in selecting which two emulsion formulations can be combined into a single ARS for dual payload release. For example, PFP- and PFHep-ARSs have statistically different ADV thresholds. Thus, an interval of acoustic pressures exists that will vaporize the PFP emulsion while minimally affecting the PFHep emulsion. Interestingly, this is not the case with PFH- and PFHep-ARSs, which do not have statistically different ADV thresholds. However, there was a difference when PFH and PFHep emulsions are combined in a single ARS, as seen with the release profiles for PFH-ARS (Figure 5.3C) versus PFH emulsion in a PFH/PFHep-ARS (Figure 5.4C). The P50 (Table 5.3 and 5.4) was 1.70 MPa [1.54, 1.87] and 3.12 MPa [2.84, 3.46] for PFH release from PFH-ARSs and PFH/PFHep-ARSs on day 3, respectively. A similar trend was also observed with PFHep-ARSs and PFHep emulsion in PFH/PFHep-ARSs, where the P50 was 3.23 MPa [2.99, 3.54] and 3.98 MPa [3.50, 4.73] for PFHep release from PFH-ARSs and PFH/PFHep-ARSs on day 3, respectively. However, payload release in the absence of US (indicated by the Rmin values in Tables 5.3 and 5.4)

remained unchanged, with 1.33% [0.66, 1.99] and 1.18% [0.56, 1.75]% release from PFH-ARSs and PFH emulsions in PFH/PFHep-ARSs on day 3, respectively, and 1.38% [0.70, 2.01] and 0.60% [0.28, 0.88]% release from PFHep-ARSs and PFHep emulsion in PFH/PFHep-ARSs at the same time point. However, in the absence of US, there was a significant difference when comparing PFP release from PFP-ARSs and PFP/PFHep-ARSs, with 8.75 ± 0.77% versus 3.61 ± 0.29% released by day 3, respectively. Thus, the amount of spontaneous release from the lower boiling point emulsion decreased when combined in an ARS with a higher boiling point emulsion. This is also qualitatively supported by Figure 5.6, where PFP/PFHep-ARSs contain less bubbles than PFP-ARSs and PFH/PFHep-ARSs contain less bubbles than PFH-ARSs for the US condition. The sigmoidal fit did not converge for the release from PFP-ARSs and PFP emulsions in a PFP/PFHep-ARS construct.

Table 5.3: Results of a four parameter sigmoidal curve fit of the payload release from single payload ARSs reported in Figure 5.3. The 95% confidence interval of the maximum payload release (R_{max}), minimum payload release (R_{min}), and the acoustic pressure at which half of maximum payload release was observed (P_{50}) are listed in the format S [S_L, S_H], where S is the average value, S_L is the lower bound value, and S_H is the upper bound value.

Time Point	**Variable**	**PFP-ARS (0.33% v/v) (Figure 5.3A)**	**PFHep-ARS (0.67% v/v) (Figure 5.3B)**	**PFH-ARS (0.67% v/v) (Figure 5.3C)**	**PFHep-ARS (0.33% v/v) (Figure 5.3D)**
Day 2	R_{min} (%)	4.71 [N/A, 5.3]	0.58 [0.45, 0.70]	0.97 [0.34, 1.57]	0.65 [0.06, 1.21]
Day 2	R_{max} (%)	21.75 [8.72, N/A]	3.23 [3.05, 3.49]	7.20 [6.79, 7.68]	13.90 [12.90, 15.41]
Day 2	P_{50} (MPa)	20.19 [2.88, 527.70]	3.04 [2.81, 3.36]	1.68 [1.49, 1.90]	3.29 [3.02, 3.67]
Day 3	R_{min} (%)	8.53 [N/A]	0.67 [0.47, 0.85]	1.33 [0.66, 1.99]	1.38 [0.70, 2.01]
Day 3	R_{max} (%)	79.00 [N/A]	4.94 [4.69, 5.27]	10.33 [9.86, 10.88]	17.15 [16.08, 18.66]
Day 3	P_{50} (MPa)	76.15 [N/A]	2.93 [2.73, 3.17]	1.70 [1.54, 1.87]	3.23 [2.99, 3.54]

Similar to our previous studies using a single emulsion type [16, 17, 22], the sum total of both emulsions in the dual payload ARSs was 1% (v/v). Another interesting trend was observed for the maximum payload release (indicated by Rmax in Tables 5.3 and 5.4). For example, values of Rmax for PFHep-ARSs on day 3 were 4.94% [4.69, 5.27] and 17.15% [16.08, 18.66] for single payload ARSs containing 0.67% (v/v) and 0.33% (v/v) PFHep emulsion, respectively. Rmax values for PFHep emulsion

Table 5.4: Results of a four parameter sigmoidal curve fit of the payload release from dual payload ARSs reported in Figure 5.4. The 95% confidence interval of the maximum payload release (R_{max}), minimum payload release (R_{min}), and the acoustic pressure at which half of maximum payload release was observed (P_{50}) are listed in the format S [S_L, S_H], where S is the average value, S_L is the lower bound value, and S_H is the upper bound value.

Time Point	Variable	PFP/PFHep-ARS (PFP, 0.33% v/v) (Figure 5.4A)	PFP/PFHep-ARS (PFHep, 0.67% v/v) (Figure 5.4B)	PFH/PFHep-ARS (PFH, 0.67% v/v) (Figure 5.4C)	PFH/PFHep-ARS (PFHep, 0.33% v/v) (Figure 5.4D)
Day 2	R_{min} (%)	2.36 [2.12, 2.56]	0.98 [0.75, 1.17]	0.74 [0.15, 1.27]	0.58 [0.32, 0.77]
Day 2	R_{max} (%)	7.39 [5.04, N/A]	4.69 [4.12, 6.20]	6.58 [6.00, 7.75]	1.64 [1.45, 2.85]
Day 2	P_{50} (MPa)	7.78 [3.93, 271.40]	3.61 [2.99, 5.44]	3.21 [2.83, 3.78]	3.12 [2.39, 7.40]
Day 3	R_{min} (%)	3.32 [3.02, 3.59]	1.29 [1.01, 1.54]	1.18 [0.56, 1.75]	0.60 [0.28, 0.88]
Day 3	R_{max} (%)	8.65 [7.34, 16.59]	7.12 [6.38, 8.66]	9.43 [8.82, 10.40]	3.19 [2.85, 3.98]
Day 3	P_{50} (MPa)	4.66 [3.34, 14.40]	3.62 [3.10, 4.75]	3.12 [2.84, 3.46]	3.98 [3.50, 4.73]

in a dual payload ARS were 7.12% [6.38, 8.66] and 3.19% [2.85, 3.98] for emulsion loadings of 0.67% (v/v) and 0.33% (v/v), respectively. Thus, for the higher volume fraction (i.e., 0.67% (v/v)) of PFHep emulsion, there was an increase in payload release when combined with PFP emulsion in the PFP/PFHep-ARS. Conversely, for the lower volume fraction (i.e., 0.33% (v/v)) of PFHep emulsion, there was a significant decrease in Rmax when comparing single versus dual payload ARSs. It is hypothesized that acoustic shadowing caused by the vaporization of the PFH emulsion, which was present at a 2:1 (v/v) ratio, caused the reduction in payload release from the PFHep emulsion in the PFH/PFHep-ARS. There is likely a volume fraction for the emulsion containing payload 1 below which acoustic shadowing will not be an issue for the emulsion containing payload 2. However, for therapeutic applications, this volume fraction must be balanced with respect to delivering an adequate amount of GF that can elucidate a biological response.

Sequential payload release from an ARS is dependent on sequential US exposures. A potential limitation of this approach is the generation of bubbles following the first US exposure that can remained entrapped within the scaffold, thus attenuating (e.g., shadowing) subsequent US exposures. However, when the ARS is implanted in vivo, the biodegradability of the fibrin matrix provides a means by which the host can remove the entrapped gas bubbles, or remodel the implant altogether [37].

This could reduce the extent to which bubbles affect subsequent US exposures. Additionally, as the US pressure increases, the volume of the US focus that is above the ADV threshold increases, thereby enabling the vaporization of droplets that were not previously vaporized and may be located between bubbles. This mechanism is potentially observed in Figures 5.5C and 5.5D, where the rate of payload release from the emulsion with the lower ADV threshold (i.e., PFP in PFP/PFHep-ARSs and PFH in PFH/PFHep-ARSs) increased after the second US exposure. Thus, the second US exposure either vaporized additional droplets or increased the rate of diffusion of dextran that was released from the first US exposure [16].

Most importantly, for PFH/PFHep-ARSs the release from the PFHep emulsion was not different from the US control prior to the second US exposure (Figure 5.5D). Thus, PFH/PFHep-ARS provide a more controlled dual payload release compared to PFP/PFHep-ARSs, of which the release from PFHep emulsions was not different prior to the second US exposure at 8 MPa. This lack of statistical difference, even with a lower initial US pressure exposure of the PFP/PFHep-ARSs (2 MPa) than with PFH/PFHep-ARSs (2.6 MPa), could be due to the instability of the entire ARS construct caused by the PFP emulsion.

High payload retention in the absence of US is crucial for controlled release from an ARS. Figure 5.2 shows that a significant amount of burst release occurs when the dextrans are incorporated directly into a conventional fibrin scaffold (i.e., without any emulsion), with 44.0 $\pm$ 1.0% and 40.1 $\pm$ 0.6% released for AF488 and AF594 dextrans, respectively, by day 1 Even the ARS formulation with the greatest non-selective release (i.e. PFP-ARS, Figure 5.3A) displayed better payload retention than the non-emulsified dextrans. The higher amount of release from AF488 dextran versus AF594 dextran was likely due to the higher molecular weight of the latter dextran.

There are critical differences between dextrans and regenerative GFs when

developing a scaffold-based release technology. GFs can display high affinity for fibrin, thus reducing the rate of burst release [38, 39]. Additionally, successful GF delivery requires the release of a GF that is bioactive, which is dependent on the retention of higher level protein structures that can be affected by high US pressures [40]. However, our prior work has demonstrated that 8 MPa US can be used to release bioactive bFGF with minor loss in bioactivity both in vitro and in vivo [17, 41].

Two parameters that were not explored in this study but warrant future investigation are droplet diameter and ultrasound frequency. Previous studies have shown that the ADV threshold correlates inversely with droplet diameter [24, 26, 42] and ultrasound frequency [20]. Thus, it is possible to further optimize dual payload release from an ARS by using different droplet sizes and/or different ultrasound frequencies to trigger ADV in each droplet population. Additionally, each emulsion could be incorporated anisotropically within the ARS. For example, a bilayer ARS could be generated with each layer containing a different emulsion with a unique ADV threshold and payload. The layers proximal and distal to the US transducer would contain emulsions with higher and lower thresholds, respectively. This bilayer configuration would reduce the effects of acoustic shadowing. A limitation of this bilayer approach is the difficulty in achieving in situ polymerization of the ARS for in vivo applications.

5.5 Conclusion

We have demonstrated that focused, 2.5 MHz US can sequentially release two fluorescent payloads, each encapsulated within a separate monodispersed PFC double emulsion, that are contained within a single ARS. The release strategy involved sequential US exposures, whereby the first and second payloads were released at lower and higher acoustic pressures, respectively. ADV and IC thresholds correlated

with the boiling point/molecular weight of the PFC within the emulsion. Payload release in the absence and presence of ultrasound was inversely correlated with the boiling point/molecular weight of the PFC. In general, payload release from the ARSs displayed a sigmoidal trend as a function of acoustic pressure, with increasing release over time in response to a single US exposure. Overall, PFH/PFHep-ARSs showed more controlled release when exposed to US, with release of the first payload from the PFH emulsion occurring after the initial US exposure and the release of the second payload from PFHep emulsion occurring after the second US exposure. The stability of PFP and PFH emulsions increased when combined with PFHep emulsion in one ARS. These results show that ARSs, in conjunction with focused US, have the potential of delivering two therapeutic payloads (e.g., GFs) in a temporally controlled manner. Future work will focus on optimizing the amount of selective release from the dual payload ARS, as well as demonstrating the release of two bioactive GFs for tissue regeneration.

5.6 Acknowledgements

This work was supported by NIH grant R21AR065010 (MLF) and the Basic Radiological Sciences Innovative Research Award (MLF). AM was supported by the National Science Foundation Graduate Student Research Fellowship (Grant No. DGE 1256260). ML was supported by funds from the Undergraduate Research Opportunity Program. Special thanks to Dr. Allen F. Brooks for aiding in the synthesis of the fluorosurfactant used to formulate the double emulsions.

REFERENCES

[1] Ruhrberg, C., Gerhardt, H., Golding, M., Watson, R., Ioannidou, S., Fujisawa, H., Betsholtz, C., and Shima, D.T.: Spatially restricted patterning cues provided by heparin-binding VEGF-A control blood vessel branching morphogenesis, Genes & development, 2002, 16, (20), pp. 2684-2698

[2] Akeson, A.L., Greenberg, J.M., Cameron, J.E., Thompson, F.Y., Brooks, S.K., Wiginton, D., and Whitsett, J.A.: Temporal and spatial regulation of VEGF-A controls vascular patterning in the embryonic lung, Dev Biol, 2003, 264, (2), pp. 443-455

[3] Abe, Y., Ozaki, Y., Kasuya, J., Yamamoto, K., Ando, J., Sudo, R., Ikeda, M., and Tanishita, K.: Endothelial progenitor cells promote directional three-dimensional endothelial network formation by secreting vascular endothelial growth factor, PloS one, 2013, 8, (12), pp. e82085

[4] Cao, R.H., Brakenhielm, E., Pawliuk, R., Wariaro, D., Post, M.J., Wahlberg, E., Leboulch, P., and Cao, Y.H.: Angiogenic synergism, vascular stability and improvement of hind-limb ischemia by a combination of PDGF-BB and FGF-2, Nat Med, 2003, 9, (5), pp. 604-613

[5] Li, J., Wei, Y.Q., Liu, K., Yuan, C., Tang, Y.J., Quan, Q.L., Chen, P., Wang, W., Hu, H.Z., and Yang, L.: Synergistic effects of FGF-2 and PDGF-BB on angiogenesis and muscle regeneration in rabbit hindlimb ischemia model, Microvasc Res, 2010, 80, (1), pp. 10-17

[6] Saik, J.E., Gould, D.J., Watkins, E.M., Dickinson, M.E., and West, J.L.: Covalently immobilized platelet-derived growth factor-BB promotes antiogenesis in biomirnetic poly(ethylene glycol) hydrogels, Acta Biomaterialia, 2011, 7, (1), pp. 133-143

[7] Ai-Aql, Z.S., Alagl, A.S., Graves, D.T., Gerstenfeld, L.C., and Einhorn, T.A.: Molecular mechanisms controlling bone formation during fracture healing and distraction osteogenesis, J Dent Res, 2008, 87, (2), pp. 107-118

[8] Carmeliet, P., and Jain, R.K.: Molecular mechanisms and clinical applications of angiogenesis, Nature, 2011, 473, (7347), pp. 298-307

[9] Tengood, J.E., Ridenour, R., Brodsky, R., Russell, A.J., and Little, S.R.: Sequential Delivery of Basic Fibroblast Growth Factor and Platelet-Derived Growth Factor for Angiogenesis, Tissue Eng Pt A, 2011, 17, (9-10), pp. 1181-1189

[10] Richardson, T.P., Peters, M.C., Ennett, A.B., and Mooney, D.J.: Polymeric system for dual growth factor delivery, Nat Biotechnol, 2001, 19, (11), pp. 1029-1034

[11] Basmanav, F.B., Kose, G.T., and Hasirci, V.: Sequential growth factor delivery from complexed microspheres for bone tissue engineering, Biomaterials, 2008, 29, (31), pp. 4195-4204

[12] Awada, H.K., Johnson, N.R., and Wang, Y.D.: Sequential delivery of angiogenic growth factors improves revascularization and heart function after myocardial infarction, Journal of Controlled Release, 2015, 207, pp. 7-17

[13] Lee, H.J., and Koh, W.G.: Hydrogel Micropattern-Incorporated Fibrous Scaffolds Capable of Sequential Growth Factor Delivery for Enhanced Osteogenesis of hMSCs, Acs Appl Mater Inter, 2014, 6, (12), pp. 9338-9348

[14] Kempen, D.H.R., Lu, L.C., Heijink, A., Hefferan, T.E., Creemers, L.B., Maran, A., Yaszemski, M.J., and Dhert, W.J.A.: Effect of local sequential VEGF and BMP-2 delivery on ectopic and orthotopic bone regeneration, Biomaterials, 2009, 30, (14), pp. 2816-2825

[15] Kim, S., Kang, Y.Q., Krueger, C.A., Sen, M.L., Holcomb, J.B., Chen, D., Wenke, J.C., and Yang, Y.Z.: Sequential delivery of BMP-2 and IGF-1 using a chitosan gel with gelatin microspheres enhances early osteoblastic differentiation, Acta Biomaterialia, 2012, 8, (5), pp. 1768-1777

[16] Moncion, A., Arlotta, K.J., O'Neill, E.G., Lin, M., Mohr, L.A., Franceschi, R.T., Kripfgans, O.D., Putnam, A.J., and Fabiilli, M.L.: In vitro and in vivo assessment of controlled release and degradation of acoustically responsive scaffolds, Acta Biomaterialia, 2016, 46, pp. 221-233

[17] Moncion, A., Lin, M., O'Neill, E.G., Franceschi, R.T., Kripfgans, O.D., Putnam, A.J., and Fabiilli, M.L.: Controlled release of basic fibroblast growth factor for angiogenesis using acoustically-responsive scaffolds., Biomaterials, 2017, 140, pp. 26-36

[18] Lee, K.Y., and Mooney, D.J.: Hydrogels for tissue engineering, Chemical Reviews, 2001, 101, (7), pp. 1869-1879

[19] Markert, C.D., Guo, X.Y., Skardal, A., Wang, Z., Bharadwaj, S., Zhang, Y.Y., Bonin, K., and Guthold, M.: Characterizing the micro-scale elastic modulus of hydrogels for use in regenerative medicine, Journal of the Mechanical Behavior of Biomedical Materials, 2013, 27, pp. 115-127

[20] Kripfgans, O.D., Fowlkes, J.B., Miller, D.L., Eldevik, O.P., and Carson, P.L.: Acoustic droplet vaporization for therapeutic and diagnostic applications, Ultrasound in Medicine and Biology, 2000, 26, (7), pp. 1177-1189

[21] Fabiilli, M.L., Haworth, K.J., Fakhri, N.H., Kripfgans, O.D., Carson, P.L., and Fowlkes, J.B.: The Role of Inertial Cavitation in Acoustic Droplet Vaporization, IEEE Transactions on Ultrasonics, Ferroelectrics, and Frequency Control, 2009, 56, (5), pp. 1006-1017

[22] Moncion, A., Arlotta, K.J., Kripfgans, O.D., Fowlkes, J.B., Carson, P.L., Putnam, A.J., Franceschi, R.T., and Fabiilli, M.L.: Design and Characterization of Fibrin-Based Acoustically Responsive Scaffolds for Tissue Engineering Applications, Ultrasound in Medicine and Biology, 2016, 42, (1), pp. 257-271

[23] Kawabata, K.-I., Sugita, N., Yoshikawa, H., Azuma, T., and Umemura, S.-I.: Nanoparticles with Multiple Perfluorocarbons for Controllable Ultrasonically Induced Phase Shifting, Japanese Journal of Applied Physics, 2005, 44, (6B), pp. 4548-4552

[24] Sheeran, P.S., Wong, V.P., Luois, S., McFarland, R.J., Ross, W.D., Feingold, S., Matsunaga, T.O., and Dayton, P.A.: Decafluorobutane as a Phase-Change Contrast Agent for Low-Energy Extravascular Ultrasonic Imaging, Ultrasound in Medicine and Biology, 2011, 37, (9), pp. 1518-1530

[25] Garvin, K.A., Hocking, D.C., and Dalecki, D.: Controlling the Spatial Organization of Cells and Extracellular Matrix Proteins in Engineered Tissues Using Ultrasound Standing Wave Fields, Ultrasound in Medicine and Biology, 2010, 36, (11), pp. 1919-1932

[26] Schad, K.C., and Hynynen, K.: In vitro characterization of perfluorocarbon droplets for focused ultrasound therapy, Physics in Medicine and Biology, 2010, 55, (17), pp. 4933-4947

[27] Reznik, N., Williams, R., and Burns, P.N.: Investigation of Vaporized Submicron Perfluorocarbon Droplets as an Ultrasound Contrast Agent, Ultrasound in Medicine and Biology, 2011, 37, (8), pp. 1271-1279

[28] Rapoport, N., Nam, K.H., Gupta, R., Gao, Z., Mohan, P., Payne, A., Todd, N., Liu, X., Kim, T., Shea, J., Scaife, C., Parker, D.L., Jeong, E.K., and Kennedy, A.M.: Ultrasound-mediated tumor imaging and nanotherapy using drug loaded, block copolymer stabilized perfluorocarbon nanoemulsions, Journal of controlled release : official journal of the Controlled Release Society, 2011, 153, (1), pp. 4-15

[29] Reznik, N., Shpak, O., Gelderblom, E.C., Williams, R., de Jong, N., Versluis, M., and Burns, P.N.: The efficiency and stability of bubble formation by acoustic vaporization of submicron perfluorocarbon droplets, Ultrasonics, 2013, 53, (7), pp. 1368-1376

[30] Rapoport, N.Y., Kennedy, A.M., Shea, J.E., Scaife, C.L., and Nam, K.-H.: Controlled and targeted tumor chemotherapy by ultrasound-activated nanoemulsions/microbubbles, Journal of Controlled Release, 2009, 138, (2), pp. 268-276

[31] Mountford, P.A., and Borden, M.A.: On the thermodynamics and kinetics of superheated fluorocarbon phase-change agents, Advances in Colloid and Interface Science, 2016, 237, pp. 15-27

[32] Riess, J.G.: Oxygen Carriers ("Blood Substitutes") - Raison d'Etre, Chemistry, and Some Physiology, Chemical Reviews, 2001, 101, (9), pp. 2797-2919

[33] Moncion, A., Arlotta, K.J., O'Neill, E.G., Lin, M., Mohr, L.A., Franceschi, R.T., Kripfgans, O.D., Putnam, A.J., and Fabiilli, M.L.: In vitro and in vivo assessment of controlled release and degradation of acoustically-responsive scaffolds, Acta Biomaterialia, 2016, 46, (in press), pp. 221-233

[34] Barnabe-Heider, M., Di Marco, M., Doane, P., Genest, M.H., Gornea, R., Guenette, R., Leroy, C., Lessard, L., Martin, J.P., Wichoski, U., Zacek, V., Clark, K., Krauss, C.B., Noble, A.J., Behnke, E., Feighery, W., Levine, I., Muthusi, C., Kanagalingam, S., and Noulty, R.: Response of superheated droplet detectors of the PICASSO dark matter search experiment, Nuclear Instruments & Methods in Physics Research Section a-Accelerators Spectrometers Detectors and Associated Equipment, 2005, 555, (1-2), pp. 184-204

[35] Sheeran, P.S., Luois, S.H., Mullin, L.B., Matsunaga, T.O., and Dayton, P.A.: Design of ultrasonically-activatable nanoparticles using low boiling point perfluorocarbons, Biomaterials, 2012, 33, (11), pp. 3262-3269

[36] Mountford, P.A., Smith, W.S., and Borden, M.A.: Fluorocarbon Nanodrops as Acoustic Temperature Probes, Langmuir, 2015, 31, (39), pp. 10656-10663

[37] Ceccarelli, J., and Putnam, A.J.: Sculpting the blank slate: How fibrin's support of vascularization can inspire biomaterial design, Acta Biomaterialia, 2014, 10, (4), pp. 1515-1523

[38] Jeon, O., Ryu, S.H., Chung, J.H., and Kim, B.S.: Control of basic fibroblast growth factor release from fibrin gel with heparin and concentrations of fibrinogen and thrombin, Journal of Controlled Release, 2005, 105, (3), pp. 249-259

[39] Yang, X.C., and Wang, H.J.: Electrospun Functional Nanofibrous Scaffolds for Tissue Engineering, Tissue Eng, 2010, pp. 159-177

[40] Marchioni, C., Riccardi, E., Spinelli, S., dell'Unto, F., Grimaldi, P., Bedini, A., Giliberti, C., Giuliani, L., Palomba, R., and Castellano, A.C.: Structural changes induced in proteins by therapeutic ultrasounds, Ultrasonics, 2009, 49, (6-7), pp. 569-576

[41] Fabiilli, M.L., Wilson, C.G., Padilla, F., Martin-Saavedra, F.M., Fowlkes, J.B., and Franceschi, R.T.: Acoustic droplet-hydrogel composites for spatial and temporal control of growth factor delivery and scaffold stiffness, Acta Biomaterialia, 2013

[42] Fabiilli, M.L., Haworth, K.J., Fakhri, N.H., Kripfgans, O.D., Carson, P.L., and Fowlkes, J.B.: The role of inertial cavitation in acoustic droplet vaporization, IEEE Trans Ultrason Ferroelectr Freq Control, 2009, 56, (5), pp. 1006-1017

CHAPTER VI

Conclusions and Future Work

6.0.1 Introduction

The work presented in Chapter 2 looked at the dependence between vaporization thresholds in acoustically-responsive scaffolds (ARSs) and changes to scaffold and acoustic parameters. These studies were crucial in developing the relational dependence between the acoustic droplet vaporization (ADV) threshold, the inertial cavitation (IC) threshold, and the tunable parameters of the ARS (i.e., scaffold stiffness, emulsion structure, and emulsion composition) and ultrasound (US, i.e., pulse length) in order to optimize the release process of the encapsulated payload. In addition, the physical stability of the ARSs, as well as the viability of cells co-encapsulated in an ARS and exposed to US, were determined to assess the long-term therapeutic potential of ARS and the effect of high intensity focused US on cells.

Some of the optimized parameters were used in the studies presented in Chapter 3, where ARSs in conjunction with US were used to release a surrogate, non-bioactive, payload (i.e, Alexa Fluor 680-labeled dextran) in an *in vivo* model, as well as to see the effects of sham ARSs on blood vessel formation. Chapter 4 highlights ARSs containing monodispersed emulsion with basic fibroblast growth factor (bFGF). The results of that work showed that bFGF can be released in a controlled manner from ARSs using US, subsequently producing angiogenesis as well as enhanced perfusion

in an *in vivo* model. In reality, angiogenesis - and wound healing in general - does not typically occur in response to a single growth factor. There are various growth factors that are present at different time points [1, 2]. Thus, the work presented in Chapter 5 demonstrates the use of ARSs and US to sequentially release two different payloads with temporal control. Overall, the studies presented in this dissertation have demonstrated that an ARS is a promising platform for tissue regeneration due to its potential of encapsulating biological payloads for prolonged periods of time, its biocompatibility, its tunability, its ability to hold and selectively release multiple payloads, and - as this work has shown - an effective platform for cell invasion, angiogenesis, and perfusion.

6.1 Experimental Conclusions

6.1.1 Design and Characterization of Fibrin-Based Acoustically-Responsive Scaffolds for Tissue Engineering Applications

Hydrogel scaffolds are used in tissue engineering as a delivery vehicle for regenerative GFs. Spatiotemporal patterns of GF signaling are critical for tissue regeneration, yet most scaffolds afford limited control of GF release, especially after implantation. The work presented in Chapter 2 builds on a previous study that demonstrated ADV can control the release of GF from a fibrin-based scaffold doped with PFC double emulsion [3]. The study in Chapter 2 investigated properties of the ARS critical for further optimization, and ultimately translation. Results showed that at a fundamental frequency of 2.5 MHz, ADV and IC thresholds ranged from 1.5 - 3.0 MPa and 2.0 - 7.0 MPa peak rarefactional pressure, respectively, for ARSs of varying compositions. Viability of cells, co-encapsulated in the ARS, was not impacted by pressures below 4 MPa, which is above the ADV thresholds. ARSs with higher boiling point emulsions (i.e. perfluorohexane (PFH) with a boiling point of 56°C vs. perfluoropentane (PFP) with a boiling point of 29°C) showed less payload

release in the absence of US. These results enable the selection of ARS compositions and acoustic parameters needed for optimized spatiotemporal controlled release of an encapsulated payload, while reducing concerns regarding thermal stability and cellular viability.

6.1.2 *In Vitro* and *In Vivo* Assessment of Controlled Release and Degradation of Acoustically-Responsive Scaffolds

This study investigates the impact of ARS and US properties on controlled release of Alexa Fluor 680-labeled dextran and fibrin degradation *in vitro* and *in vivo*. US exposure at 2.5 MHz generated up to 7.7 and 21.7-fold increases in dextran release from the ARSs *in vitro* and *in vivo*, respectively. The results showed that US also induced morphological changes in the ARS. Surprisingly, up to 2.9-fold greater blood vessel density was observed in ARSs compared to fibrin when implanted subcutaneously, even without delivery of pro-angiogenic GFs. These results demonstrate the potential utility of ARSs in generating controlled release for tissue regeneration.

6.1.3 Controlled Release of Basic Fibroblast Growth Factor for Angiogenesis Using Acoustically-Responsive Scaffolds

The clinical translation of pro-angiogenic GFs for treatment of vascular disease has remained a challenge due to safety and efficacy concerns. Various approaches have been used to design spatiotemporally-controlled delivery systems for GFs in order to recapitulate aspects of endogenous signaling and thus assist in translation. Payload release from ARSs can be controlled non-invasively and in an on-demand manner using focused, megahertz-range US. In this study, we investigated the *in vitro* and *in vivo* release from ARSs containing bFGF encapsulated in monodispersed emulsions generated in a two-step process utilizing a microfluidic device with a flow

focusing geometry. At 2.5 MHz, controlled release of bFGF was observed for US pressures above 2.2 ± 0.2 MPa peak rarefactional pressure. US at 8 MPa yielded a 12.6-fold increase in bFGF release *in vitro*. The bioactivity of the released bFGF was also characterized, and the released bFGF showed a minimal loss in bioactivity compared to unencapsulated bFGF. When implanted subcutaneously in mice, ARSs exposed to superthreshold US displayed up to 3.3-fold and 1.7-fold greater perfusion and blood vessel density, respectively, than ARS without US exposure. The degradation of ARSs was not impacted by US exposure. These results highlight the utility of ARSs in both basic and applied studies of therapeutic angiogenesis, and can be used as a functional delivery tool to release bioactive GF that produces functional perfused blood vessels.

6.1.4 Sequential Payload Release from Acoustically-Responsive Scaffolds Using Focused Ultrasound

Regenerative processes such as angiogenesis and osteogenesis require multiple GFs with distinct spatial and temporal patterns and sequences of expression. Payload release from ARSs can be controlled non-invasively and in an on-demand manner using focused, megahertz-rangeUS. In this *in vitro* study, we developed and characterized ARSs that enable the sequential release of two surrogate, fluorescent payloads using consecutive ultrasound exposures at different acoustic pressures. ARSs were generated with various combinations and volume fractions of PFP, PFH, and perfluorohexane (PFHep) emulsions. ADV and IC thresholds correlated with the boiling point/molecular weight of the PFC while payload release correlated inversely. Payload release was longitudinally measured and followed a sigmoidal trend versus acoustic pressure. PFP and PFH emulsions were stabilized when incorporated into ARSs with the higher boiling point PFHep emulsion. These results are important in highlighting the potential of using ARSs for sequential, dual payload release for tissue regeneration.

6.1.5 Summary of Contributions

The work presented in this dissertation has demonstrated various qualities of ARSs as well as demonstrated the therapeutic potential of ARSs when exposed to US have. The tunability of ARSs and US parameters (i.e., fibrin concentration, emulsion structure, emulsion formulation, US pulse repetition frequency, and pulse length) show that they are a versatile tool for angiogenesis and tissue engineering. The work in this dissertation ultimately demonstrates that ARSs are a promising platform for tissue regeneration, and can be used to deliver bioactive growth factors and promote the formation of perfused blood vessels - which are crucial for the health and sustainability of tissue implants.

6.2 Future Work

6.2.1 Blood Vessel Formation in the Absence of Growth Factor Delivery

Chapter 3 contains data that shows that ARSs without growth factor induced greater blood vessel formation than a conventional fibrin scaffold irrespective of US exposure to the ARS. This was a surprising finding, and serves as the foundation for future work that will determine the mechanism behind this effect. It is hypothesized that the emulsion within the ARS modulates the local oxygen concentration within the microenvironment of the ARS. The perfluorocarbon (PFC) within the emulsion could act as an oxygen sink, due to the high solubility of oxygen in PFC. This could create a local condition of hypoxia, which could stimulate angiogenesis. Some parameters that may be investigated are the effects of emulsion concentration and US exposure on the blood vessel formation within an ARS.

6.2.2 The Necessity for Multiple Payload Release

Angiogenesis requires multiple GFs with distinct spatiotemporal profiles [1, 2], and prior work has shown that passive, sequential delivery of two GFs in scaffolds has yielded enhanced angiogenesis [4]. Vessel growth must be accompanied by maturation, and this involves the suppression of endothelial cell growth to prevent the formation of disorganized and hemorrhagic vessels [5]. The timing of growth and maturation is critical since early maturation can yield an inadequate vascular network while late, or a lack of, maturation can lead to vessel regression [6]. bFGF, involved in the sprouting of new capillaries, and platelet derived growth factor (PDGF-BB), involved in vessel stabilization and functionalization by inducing anastomoses and recruiting pericytes, respectively, have key roles in the development of functional vessels [7-11]. However, bFGF and PDGF-BB can inhibit each other if present simultaneously, and studies have shown that subsequent administration of PDGF at least 24 hours after the administration of bFGF yields more than 3 times the number of blood vessels structures than the administration of bFGF alone [7, 8]. Therefore, controlling the temporal release profiles of bFGF and PDGF-BB could improve the ability to form mature, functional blood vessels, thus improving the vascularization of implanted constructs.

6.2.3 Dual Payload Release with ARSs

We have demonstrated that dual payload release can be performed with ARSs and US. One of the major characteristics for single and dual payload release is the size of the emulsion. Chapter 4 highlighted the successful delivery of bioactive GF with monodispersed emulsions. Monodispersed emulsions were used due to their temporal stability and more predictable behavior (i.e., lack of Ostwald ripening and spontaneous vaporization), and therefore provide a more controlled method of achieving payload release. Additionally, the size of the emulsion is also a

very important parameter to keep in mind when manufacturing an ARS. Smaller emulsions are more stable in the absence of US, however they have higher ADV thresholds. Droplet size is a parameter that can be exploited in dual payload release applications, where the second payload (i.e., the payload being released second) could be encapsulated in a smaller diameter emulsion with a higher ADV threshold emulsion - allowing the use of low pressure US to release the first payload. Future work will focus on optimizing dual payload release to not only provide better separation between the thresholds of the emulsions co-encapsulated within an ARS - resulting in the desired payload released at the desired time - but to also enhance the total amount of payload that gets released post-US exposure.

6.2.4 Hindlimb Ischemia and Restoration of Perfusion

In chapter 4, *in vivo* bFGF delivery was evaluated using subcutaneously implanted ARSs placed beneath the dorsal skin of mice. Subcutaneous implantation is commonly used as a first model in angiogenesis studies. As was observed in chapter 4, newly formed blood vessels ultimately regress in this model due to the lack of hypoxic markers that sustain angiogenesis. The delivery of single or multiple growth factors and their effects on vascularization is best tested in a murine model of hindlimb ischemia, which possesses many pathological markers of critical limb ischemia. The hindlimb ischemia model is generated by unilaterally ligating and excising the femoral artery, which generates severe ischemia in the hindlimb. By placing an ARS at or adjacent to the site of the excised vessel, the effects of collateral blood vessel formation can be evaluated for various experimental conditions. Thus, this model enables the study of how an ARS could restore perfusion in the ischemic hindlimb.

We have generated hindlimb ischemia according to prior methods [9, 12, 13] in the right hindlimb of BALB/c mice. In this model, the femoral artery distal to the inguinal ligament and proximal to the superficial caudal epigastric artery was ligated

using sutures and excised. Fibrin scaffolds (volume 0.1 mL) at a concentration of 10 mg/mL were polymerized *in situ* at the ligation site and then the wound was sutured closed. The experimental conditions tested were no intervention, implantation of a conventional fibrin scaffold, or a fibrin scaffold doped with free-form bFGF. The targeted GF dose for the GF containing fibrin implant was 1 μg/implant, as that concentration resulted in angiogenesis when released from an ARS [14]. The perfusion of each hindlimb was non-invasively monitored using a laser speckle perfusion system (LASCA, Perimed). Longitudinal images are show in Figure 6.1, 6.2, and 6.3 for experimental conditions in which there was no intervention, a fibrin scaffold was implanted, and a fibrin scaffold with non-encapsulated bFGF was implanted, respectively. The quantified LASCA results are shown in Figure 6.4. The LASCA images were quantified by calculating the average perfusion units within a region of interest (ROI) that was distal to the ligation site. A similar analysis was performed for the contralateral (i.e., control) limb and the normalized perfusion was calculated as the perfusion in the ligated limb versus the control limb.

The results show that the ischemia was successfully induced, as seen by the decrease in the perfusion measured with the LASCA. Longitudinal monitoring of the perfusion, however, shows that perfusion is restored within 14 day: 87.2 $\pm$ 10.4%, 94.4 $\pm$ 6.8%, and 91.0 $\pm$ 22.2% for no intervention, fibrin only, and fibrin+bFGF. None of the previously mentioned experimental conditions are different from their respective day 0 pre-surgery measurement.

Future Hindlimb Ischemia Work

There is a lot of variability in the literature regarding the spontaneous recovery of perfusion in BALB/c mice without any intervention. Prior work has shown 30% recovery 10 days after surgery [15], while others have shown 30% recovery by day 28 [16]. We believe the rapid recovery of these animals, even in the absence of intervention, is partly due to the lack of severity of the surgery. In future

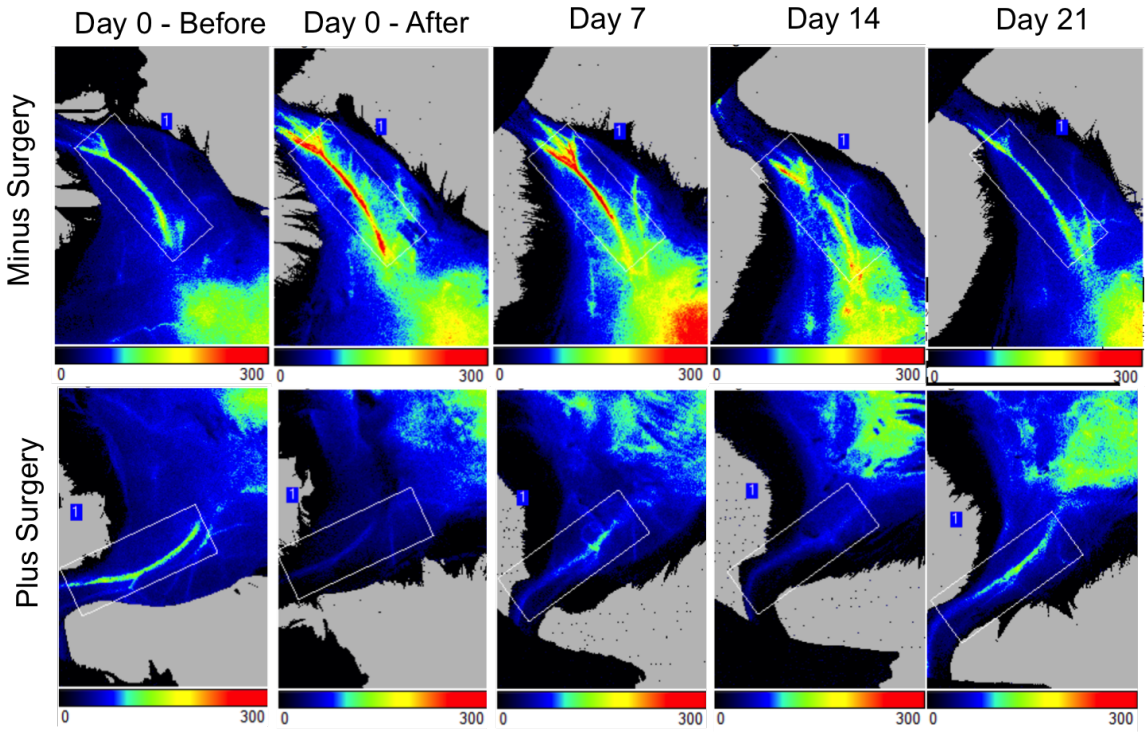

Figure 6.1: Longitudinal LASCA images showing perfusion in the control and ligated hindlimbs, with no intervention post-surgery in the ligated limb. ROIs are denoted by the white, rectangular boxes.

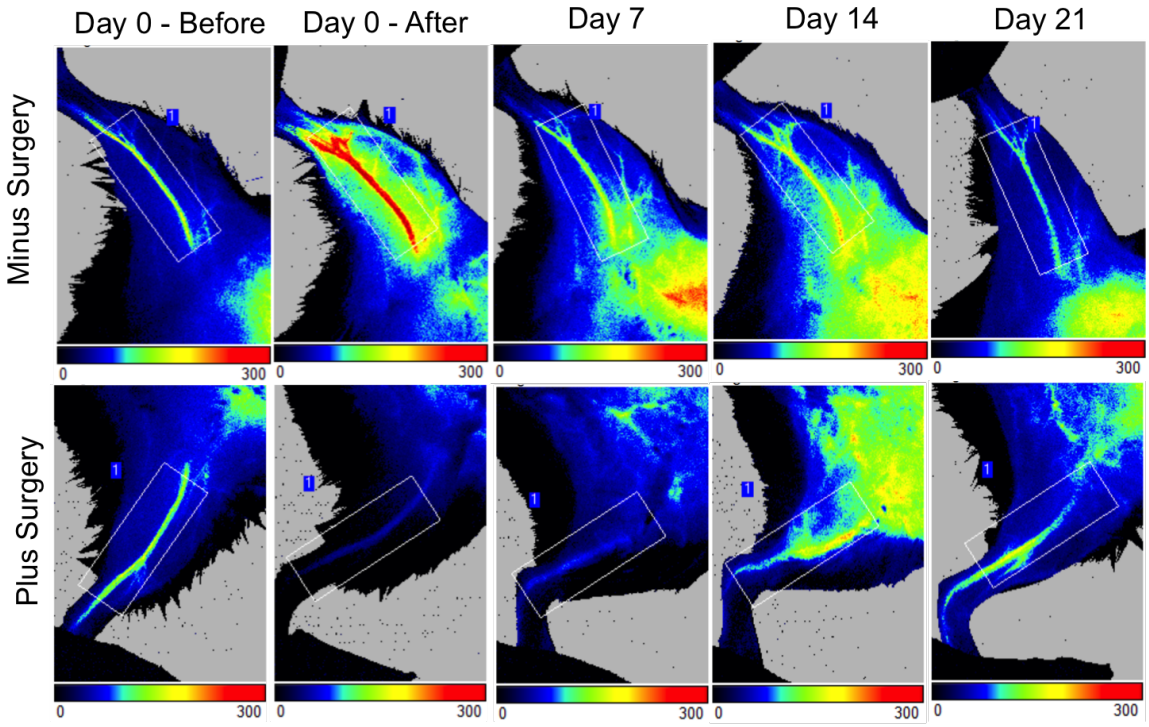

Figure 6.2: Longitudinal LASCA images showing perfusion in the control and ligated hindlimbs, with a conventional fibrin scaffold placed in the region where the femoral artery was excised. ROIs are denoted by the white, rectangular boxes.

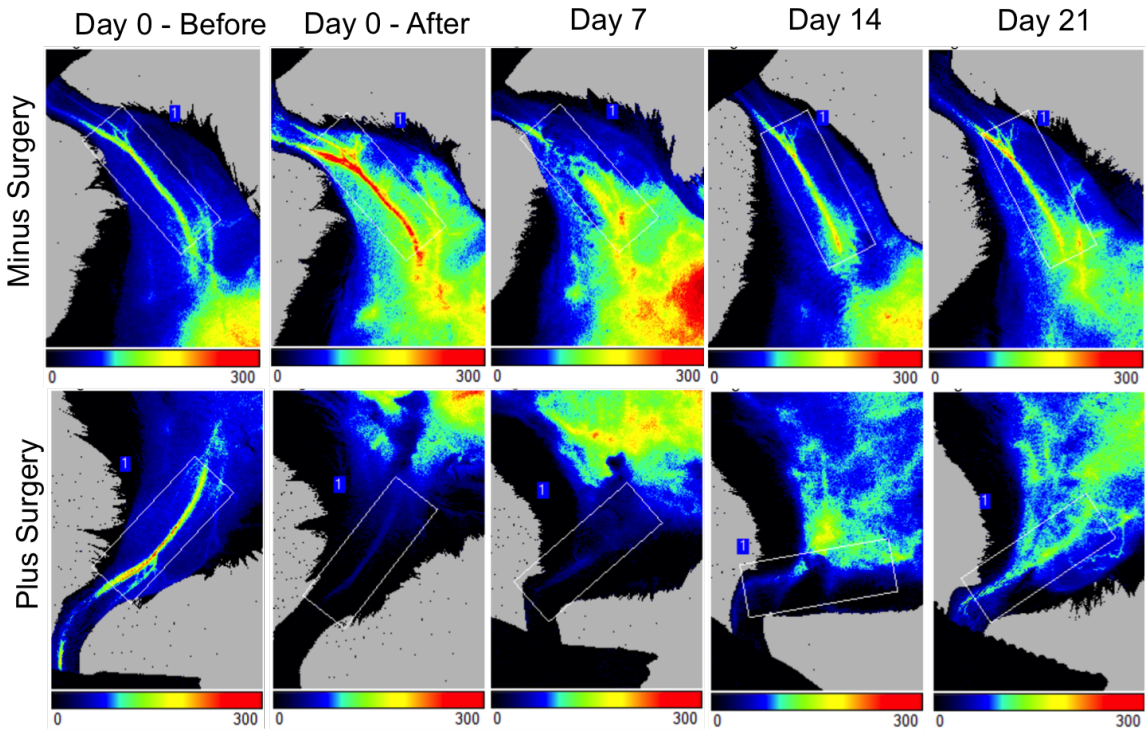

Figure 6.3: Longitudinal LASCA images showing perfusion in the control and ligated hindlimbs, with a conventional fibrin scaffold containing non-encapsulated bFGF placed in the region where the femoral artery was excised. ROIs are denoted by the white, rectangular boxes.

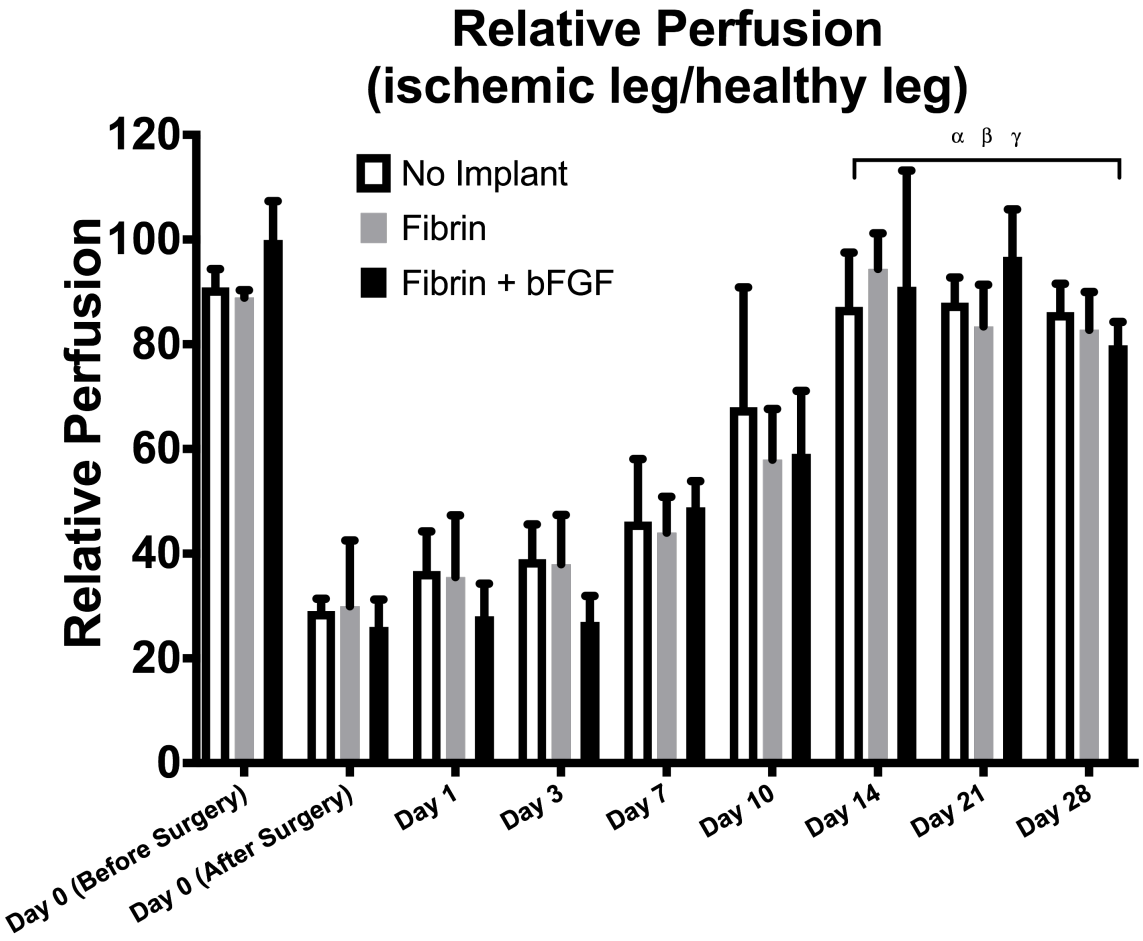

Figure 6.4: Longitudinal monitoring of hindlimb perfusion using LASCA following unilateral ligation of the femoral artery in BALB/c mice. Statistical differences are deemed significant for $p < 0.05$: α: perfusion from no intervention at any given day vs. day 0 (after surgery), β: perfusion with a fibrin scaffold at any given day vs. day 0 (after surgery), and γ: perfusion with a fibrin+bFGF scaffold at any given day vs. day 0 (after surgery). n = 3 for all experimental groups.

experiments, the ligation will be performed such that the distal ligation point is a few millimeters beyond the popliteal artery bifurcation. This larger excised region should result in a reduced rate of recovery in the absence of any intervention. Future work could also use Apolipoprotein E deficient mice that are not able to catabolize triglyceride-rich lipoproteins, thus causing plaque buildup in their arteries. This animal model would mimic intermittent claudification more closely - which is the leading cause of critical limb ischemia. Ultimately, ARSs will be evaluated in the hindlimb ischemic model to show its effect on the recovery rate from the surgery, as well as a means of delivering multiple growth factors for an accelerated rate of recovery. Based on the work presented in this dissertation, we believe that ARSs will have the greatest positive impact on the recovery, and thus restoration of perfusion, to the ligated limb.

6.3 Final Words

The studies presented in this dissertation demonstrate that ARSs are a very promising approach to tissue regeneration - primarily angiogenesis, which is crucial in all tissue regeneration applications - due to many of their proven characteristics. ARSs can encapsulate biological payloads for prolonged periods of time, they are biocompatible for *in vivo* implantation, they are highly tunable, they can hold and selectively release multiple payloads, and they are an effective platform for many tissue engineering applications.

REFERENCES

[1] Carmeliet, P.: Angiogenesis in life, disease and medicine, Nature, 2005, 438, (7070), pp. 932-936

[2] Risau, W.: Mechanisms of angiogenesis, Nature, 1997, 386, (6626), pp. 671-674

[3] Fabiilli, M.L., Wilson, C.G., Padilla, F., Martin-Saavedra, F.M., Fowlkes, J.B., and Franceschi, R.T.: Acoustic droplet-hydrogel composites for spatial and temporal control of growth factor delivery and scaffold stiffness, Acta Biomaterialia, 2013

[4] Richardson, T.P., Peters, M.C., Ennett, A.B., and Mooney, D.J.: Polymeric system for dual growth factor delivery, Nat Biotechnol, 2001, 19, (11), pp. 1029-1034

[5] Jain, R.K., Au, P., Tam, J., Duda, D.G., and Fukumura, D.: Engineering vascularized tissue, Nat Biotechnol, 2005, 23, (7), pp. 821-823

[6] Holderfield, M.T., and Hughes, C.C.W.: Crosstalk between vascular endothelial growth factor, notch, and transforming growth factor-beta in vascular morphogenesis, Circ Res, 2008, 102, (6), pp. 637-652

[7] Tengood, J.E., Ridenour, R., Brodsky, R., Russell, A.J., and Little, S.R.: Sequential Delivery of Basic Fibroblast Growth Factor and Platelet-Derived Growth Factor for Angiogenesis, Tissue Eng Pt A, 2011, 17, (9-10), pp. 1181-1189

[8] De Marchis, F., Ribatti, D., Giampietri, C., Lentini, A., Faraone, D., Scoccianti, M., Capogrossi, M.C., and Facchiano, A.: Platelet-derived growth factor inhibits basic fibroblast growth factor angiogenic properties *in vitro* and *in vivo* through its alpha receptor, Blood, 2002, 99, (6), pp. 2045-2053

[9] Cao, R.H., Brakenhielm, E., Pawliuk, R., Wariaro, D., Post, M.J., Wahlberg, E., Leboulch, P., and Cao, Y.H.: Angiogenic synergism, vascular stability and improvement of hind-limb ischemia by a combination of PDGF-BB and FGF-2, Nat Med, 2003, 9, (5), pp. 604-613

[10] Li, J., Wei, Y.Q., Liu, K., Yuan, C., Tang, Y.J., Quan, Q.L., Chen, P., Wang, W., Hu, H.Z., and Yang, L.: Synergistic effects of FGF-2 and PDGF-BB

on angiogenesis and muscle regeneration in rabbit hindlimb ischemia model, Microvasc Res, 2010, 80, (1), pp. 10-17

[11] Saik, J.E., Gould, D.J., Watkins, E.M., Dickinson, M.E., and West, J.L.: Covalently immobilized platelet-derived growth factor-BB promotes antiogenesis in biomirnetic poly(ethylene glycol) hydrogels, Acta Biomaterialia, 2011, 7, (1), pp. 133-143

[12] Horio, T., Fujita, M., Tanaka, Y., Ishihara, M., Kishimoto, S., Nakamura, S., Hase, K., and Maehara, T.: Efficacy of fragmin/protamine microparticles containing fibroblast growth factor-2 (F/P MPs/FGF-2) to induce collateral vessels in a rabbit model of hindlimb ischemia, J Vasc Surg, 2011, 54, (3), pp. 791-798

[13] Layman, H., Li, X.Y., Nagar, E., Vial, X., Pham, S.M., and Andreopoulos, F.M.: Enhanced Angiogenic Efficacy through Controlled and Sustained Delivery of FGF-2 and G-CSF from Fibrin Hydrogels Containing Ionic-Albumin Microspheres, Journal of Biomaterials Science-Polymer Edition, 2012, 23, (1-4), pp. 185-206

[14] Moncion, A., Lin, M., O'Neill, E.G., Franceschi, R.T., Kripfgans, O.D., Putnam, A.J., and Fabiilli, M.L.: Controlled release of basic fibroblast growth factor for angiogenesis using acoustically-responsive scaffolds., Biomaterials, 2017, 140, pp. 26-36

[15] Urano, T., Ito, Y., Akao, M., Sawa, T., Miyata, K., Tabata, M., Morisada, T., Hato, T., Yano, M., Kadomatsu, T., Yasunaga, K., Shibata, R., Murohara, T., Akaike, T., Tanihara, H., Suda, T., and Oike, Y.: Angiopoietin-related growth factor enhances blood flow via activation of the ERK1/2-eNOS-NO pathway in a mouse hind-limb ischemia model, Arterioscl Throm Vas, 2008, 28, (5), pp. 827-834

[16] Yang, H.N., Park, J.S., Woo, D.G., Jeon, S.Y., and Park, K.H.: Transfection of VEGF(165) genes into endothelial progenitor cells and *in vivo* imaging using quantum dots in an ischemia hind limb model, Biomaterials, 2012, 33, (33), pp. 8670-8684

APPENDICES

APPENDIX A

Immunohistochemistry Parrafin Section Protocol

NOTE: This protocol uses a DAKO Envision+ System-HRP (DAB) (K4011, Dako North America, Carpinteria, CA USA) rabbit anti mouse kit and a Dako Target Retrieval Solution 10X Concentrate (S1699, Dako North America).

A.1 Tissue Section Rehydration

1. Immerse slides in 100% Toluene for 5 minutes.
2. Immerse slides in 100% Toluene for 5 minutes.
3. Immerse slides in 100% Ethanol for 5 minutes.
4. Immerse slides in 100% Ethanol for 5 minutes.
5. Immerse slides in 95% Ethanol for 5 minutes.
6. Immerse slides in 95% Ethanol for 5 minutes.
7. Immerse slides in H_2O for 5 minutes.
8. Immerse slides in a Tris Buffered Saline (TBST) wash for 5 minutes.

A.2 Inhibition of Endogenous Peroxidase

1. Apply a layer of wax using a wax pen around each tissue section.

2. Immerse slides in a peroxidase block for 5 minutes.

3. Immerse slides in a TBST wash for 5 minutes.

A.3 Antigen Retrieval

1. Immerse slides in a 10:1 dilution of DAKO target retrieval in TBST.

2. Place slides in antigen retrieval in a food steamer for 30 minutes.

3. Immerse slides in a TBST wash for 5 minutes.

4. Immerse slides in a TBST wash for 5 minutes.

A.4 First Blocking Phase

1. If CD31 or IGG: Use 1% bovine serum albumin (BSA) for 30 minutes.

2. If NG2 or SMA: 10% goat serum with 1% BSA for 30 minutes.

3. Immerse slides in a TBST wash for 5 minutes.

A.5 Primary Antibody

1. Add primary antibody (diluted to manufacturer's recommendations) to tissue sections and incubate overnight.

2. Immerse slides in a TBST wash for 5 minutes.

3. Immerse slides in a TBST wash for 5 minutes.

A.6 Second Blocking Phase

1. If CD31 or IGG: Use 1% bovine serum albumin (BSA) for 7 minutes.

2. If NG2 or SMA: 10% goat serum with 1% BSA for 7 minutes.

3. Immerse slides in a TBST wash for 5 minutes.

A.7 Secondary Antibody

1. Add secondary antibody (from DAKO kit) to tissue sections and incubate overnight.
2. Immerse slides in a TBST wash for 5 minutes.
3. Immerse slides in a TBST wash for 5 minutes.

A.8 Revelation

1. Dilute chromagen in substrate according to manufacturer's instructions.
2. Apply DAB+ chromagen to tissues and incubate for 60 minutes.
3. Immerse slides in a H_2O for 5 minutes.
4. Immerse slides in a H_2O for 5 minutes.

A.9 Dehydration

1. Immerse slides in 95% Ethanol for 1 minute.
2. Immerse slides in 95% Ethanol for 1 minute.
3. Immerse slides in 100% Ethanol for 2 minutes.
4. Immerse slides in 100% Ethanol for 2 minutes.
5. Immerse slides in 100% Toluene for 2 minutes.
6. Immerse slides in 100% Toluene for 2 minutes.

APPENDIX B

Production of Monodispersed Double Emulsion using Dolomite Chip

B.1 Setting Up the Chip

1. Attach the chip to its mount. **Note:** Position chip assembly over inverted microscope such that junction is visible using camera.

2. Fill two 5 mL syringes with filtered 50 mg/mL Pluronic F68 (PF68) in phosphate buffered saline (or another W_2 phase) and remove air bubbles.

3. Attach the filters to the syringes and detach them from the chip by removing the fittings of the aqueous lines. **Note:** After detaching the lines with the fittings, place the fittings inside a microcentrifuge tube to prevent dust accumulation. Do not place fittings directly onto benchtop.

4. Prime the filters by running the pumps at 1000 μL/min until liquid comes out of the filters. Dont reattach the fittings yet.

5. Fill a 1 mL syringe with the primary emulsion using a pipette and remove air bubbles.

6. Attach the filter to the syringe and detach it from the chip by removing the fitting of the perfluorocarbon (PFC) line. **Note:** After detaching the line with

the fittings, place the fitting inside a microcentrifuge tube to prevent dust accumulation. Do not place fitting directly onto benchtop.

7. Make sure the diameter for the pump is set at 4.69 mm. Prime the filter by running the pump at 1000 μL/min until the primary emulsion starts to come out of the filter. Dont reattach the fittings yet.

8. Set all of the pumps to 10 μL/min.

9. Attach the fittings to the PF68 syringes, press start, and then attach the fitting to the primary emulsion syringe and press start. Turn the pump with the PFC line so that the syringe is vertical. **Note:** Make sure that all air is pushed out of the lines during the priming stage.

B.2 While the Chip is Running

1. Wait until you can see the primary emulsion in the PFC line reach the chip on the microscope, then set the pumps to desired flow rate (standard has been 2.5 μL/min outer, 0.5 μL/min inner).

2. If liquid starts flowing into the wrong channel, increase flow rate of that channel to 50 μL/min or 100 μL/min for a few ($\sim$2-5) seconds, and then switch back to the original flow rate. If liquid starts flowing backwards, do the same thing until all channels have liquids flowing toward the chip.

3. Wait until chip has equilibrated before collection of emulsions starts. This usually takes 10-15 min. Flow profile at equilibrium for 2.5 μL/min outer and 0.5 μL/min inner should look similar to this when using PFH or PFO:

4. To start collecting, pipet 5-10 μL of PF68 into a microcentrifuge tube, wipe down the collection line with ethanol, and place the line into the tube so that the tip is in the PF68.

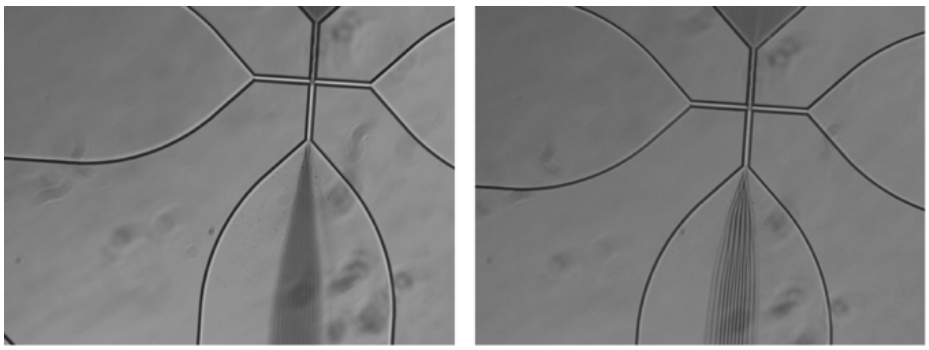

Figure B.1: Junction prior to (left) and after (right) reaching equilibrium.

5. Collect for as long as desired while timing.

6. Keep an eye out for the PFC line. There should be a continuous stream of primary emulsion with maybe occasional breaks in between. However, if you notice a long stream of clear liquid in the line and there doesnt seem to be primary emulsion coming out the syringe, stop collecting and reset the chip by increasing the flow rates of all lines to $\sim$10 μL/min (or greater for the PFC line) until you start to see primary emulsion again. Then repeat the above steps to equilibrate the chip.

7. Also keep an eye out on the collection tube. You may need to remove some of the PF68 overlying the emulsions, depending on long you run the chip.

8. If the chip gets clogged, stop collecting and increase flow rate of the channel where the block is occurring to 1000 μL/min for 1-2 seconds or until the chip gets cleared. Then return to original flow rate. (**Note:** You may have to adjust the other flow rates as well to ensure everything is flowing in the right direction. Also, when increasing flow rates to 1000 μL/min, make sure the syringes dont get bent.)

B.3 Cleaning Up

1. Stop the pumps and place the collection line back into the waste container. Put the pump with the PFC line back into its horizontal position. Wait for the flow rates to decrease.

2. Estimate the volume of double emulsions collected and size the particles using the Coulter Counter (5 μL pellet + 20 mL saline).

3. Fill up three 5 mL syringes with deionized (DI) water and fill another 5 mL syringe with hydrofluoroether (HFE).

4. Once the flow rates have started to cease, remove the primary emulsion syringe first. Before attaching the HFE syringe, the filter may be dirty, so use a pipette tip and ethanol to clean it out from both sides.

5. Set the single pump diameter back to 11.99 mm. Prime the filter by running the pump at 1000 μL/min until liquid comes out of the filter. Dont reattach the fittings yet.

6. Remove the other syringes and clean out the filters as well.

7. Prime the filters by running the pump at 1000 μL/min until liquid starts to come out of the filter. Dont reattach the fittings yet.

8. Set all pumps to 10 μL/min, attach the fittings, and press start. Wait until you can see the PFC flow profile on the chip. Wait 5 more minutes before stopping all of the pumps. Note: The flow rate of the HFE may need to be increased to 50-100 uL/min for a couple seconds to prevent backflow in the PFC/HFE line.

9. Wait another 5-10 minutes before switching out the HFE for the water syringe. Prime the filter by running the pump at 1000 μL/min until liquid starts to

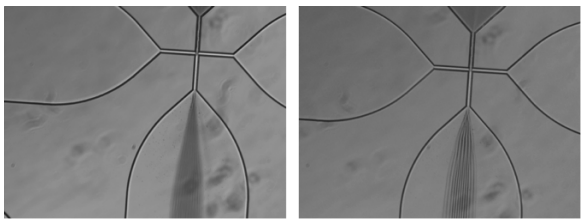

Figure B.2: Junction during cleaning with HFE.

come out of the filter. Start the double pump, attach the fitting of the PFC line, and start that pump.

10. Let the water run for about 10 minutes at 10 μL/min and then stop the pumps.

11. Store the chip back in the bag over the weekend.

B.4 Additional Notes

1. The primary emulsion consists of 225 μL W_1 phase, 0.75 g PFC, and 15 mg fluorosurfactant. The phases are sonicated on ice for 30 seconds using the QSonica (power = 20) to form the primary emulsion.

2. A stock solution of 50 mg/mL Pluronic F68 in PBS is prepared. The solution is filtered every 2 weeks with a SteriFlip (0.2 μm filter assembly)

3. Running the chip for 2 hours will yield $\sim$ 90 μL of double emulsion. Approximately 220 μL of primary emulsion will remain in the syringe after 2 hours.

4. Chip can be unclogged by pumping a dilute ($\sim$1/10x) solution of Dawn dish soap in all channels.

APPENDIX C

Hindlimb Ischemia Surgical Protocol on BALB/c mice

C.1 Before Handling the Mice

1. Weigh isoflurane scavenging filter (this can be done the day before). The maximum weight gain per filter is 50 g.
2. Make sure isoflurane vaporizer is filled with isoflurane.
3. Check oxygen level on tank.
4. Turn on water-filled heating pad and LASCA system.
5. Sterilize surgical tools with microbead sterilizer. Once tools are sterilized, allow tools to cool on a sterile tray.

C.2 Prepare Mice for Surgery

1. Place mouse in anesthesia induction chamber (5% isoflurane). When mouse is fully anesthetized, transfer mouse to microbalance and record weight.
2. Place mouse in supine position on water-filled heating pad (42°C) and continue flow of anesthesia with nose cone (1-2% isoflurane).
3. Place ophthalmic ointment in the conjunctiva of each eye to prevent eyes from drying out.

4. Clean ears with ethanol wipes and then tag ears with hole punch (if necessary). Record number/location of ear holes.

5. Shave lower ventral region of mice with clippers. Apply Nair to remove remaining hair. After 2.5-3 min, wipe off Nair/hair with 4x4 gauze pads (wet, dry).

6. Transfer mouse to imaging platform and tape down each leg. Image each leg with LASCA to assess baseline perfusion. Remove tape.

7. Wash skin with Betadine scrub and then rinse with sterile normal saline. Repeat.

8. Administer pre-emptive dose of carprofen (0.1-0.15 mL at 5 mg/kg) subcutaneously in upper ventral region.

C.3 Perform Surgery

1. Transfer mice and nose cone to sterile surgical field covered with surgical drape. Place mouse is supine position and tape down each leg.

2. Position stereomicroscope above mouse such that field of view contains lower ventral region.

3. Using surgical scissors, make an $\sim$1 cm incision from the edge of the abdominal cavity (i.e., inguinal ligament) toward the medial thigh. Use fine forceps to tent skin during incision.

4. Use fine forceps to remove overlying fascia and fat to expose femoral artery, vein, and nerve. The area to surgically expose is the segment of the femoral artery/vein where the femoral nerve diverges from the blood vessel pair (i.e., close to the inguinal ligament). If necessary make the incision slightly larger to expose this region, though overall try to keep the incision as small as possible.

5. After enough of the fascia and fat are removed, use to retractor (held down by weighted rings) to expose the vasculature. Continue removing the overlying fascia with the fine forceps to expose the vascular bundle.

6. Periodically, moisten the surgical site with a fine pointed cotton swab dipped in sterile saline.

7. Separate the femoral artery from the femoral vein and nerve using the fine forceps. The leg may twitch if the nerve is hit.

8. If bleeding occurs at any time, use a fine pointed cotton swab to absorb the blood at the surgical site and to apply gentle pressure.

9. When the artery is separated from the vein, pass silk suture underneath the proximal end of the intended ligation site by passing the suture from one set of fine pointed forceps to another. Occlude the proximal site using a set of double knots.

10. Repeat step #9 for the distal ligation site.

11. Transect the segment of femoral artery in between the proximal and distal knots.

12. Remove the retractor and close the wound using resorbable Vicryl suture. Start the running suture at the distal end of the incision and move toward the proximal end.

13. Verify that the ligation was successful using LASCA.

14. Apply Matisol to wound area.

15. Allow mouse to recover in a separate cage

C.4 Post Surgical Monitoring and Imaging

1. Complete Rodent Surgery Record for each mouse.

2. Administer carprofen subcutaneously at least for the first 48 hours post surgery (i.e., 1 dose per day). If mouse appears to be in pain, continue with daily dosing of carprofen beyond the first 48 hours.

3. Note when the sutures are absorbed on the Rodent Surgery Record. Sutures should be removed with 7-10 days post operation.

4. Note when each mouse is euthanized on the Rodent Surgery Record.

5. When the Rodent Surgery Record is closed (i.e., mouse is euthanized), submit a copy of the Record to the folder in the housing room folder.